Maryam Ghadrdan

Optimal Operation of Kaibel Columns

Doctoral thesis
for the degree of philosophiae doctor

Trondheim, October 2014

Norwegian University of Science and Technology

NTNU
Innovation and Creativity

NTNU

Norwegian University of Science and Technology

Doctoral thesis
for the degree of titulum obliviscens

ISBN N/A (printed version)
ISBN N/A (electronic version)
ISSN 1503-8181

Doctoral theses at NTNU, 2014:N/A

Printed by NTNU-trykk

دل گرچه در این بادیه بسیار شتافت

یک موی ندانست ولی موی شکافت

اندر دل من هزار خورشید بتافت

آخر به کمال ذره‌ای راه نیافت

To whom who were more solicitous about me than myself

Summary

Kaibel distillation column, which performs separation of 4 products in a dividing-wall arrangement, provides significant energy and capital savings compared to conventional distillation arrangements. In this thesis, the focus is on optimal operation and control of this type of thermally-coupled columns, which are operated with two objectives: maximizing the purities in the products with fixed boilup, minimizing energy with specified product purities.
First, the optimal operation of Kaibel column is studied. The simulation is done rigorously in HYSYS. This work demonstrates the use of the V_{min} tool [1], which can be used to visualize the minimum vapour requirement. A shortcut procedure is proposed to design a 4-product dividing-wall column. It is based on the information derived from V_{min} diagram. This has the advantage of having more meaningful guesses for energy requirements and impurity flows in the column.
Throughout the thesis, it is assumed that vapour split is a degree of freedom. The effect of vapour split is studied in detail in a separate chapter. Two methods are used to study the effect of vapour split manipulation, namely a shortcut method (V_{min} diagram) and rigorous simulations. Using a case-study, it is shown that the energy saving potential may be lost if the column is operated away from its optimal point, due to disturbances.
A control structure is designed for a 4-product dividing wall (Kaibel) distillation column, based on the plant-wide control procedure by Skogestad [2]. This is done for the case of maximizing product purities. Unlike the common approach, vapour split is considered as a degree of freedom. The exact local method is used to find the best control variables as single measurements or combination of measurements.
For the case of minimizing energy with specified product purities, a soft sensor is designed by reformulating the self-optimizing control method. The performance of the estimators depend on whether it is used for monitoring (open-loop) or for closed-loop control applications. In this work, estimators are designed to be specialized for each case. The approach is to minimize the estimation error for expected disturbances and measurement noise. The main extension compared to previous work is to include measurement noise and to provide explicit formulae for computing the optimal static estimator. The results are compared with standard existing estimators, e.g. Partial Least Squares (PLS).
One of the drawbacks of combining measurements is that measurements with slower and faster dynamics has weights with negative and positive signs and this may lead to an inverse response. Different possibilities to overcome the inverse response problem are studied in a separate chapter. In the end, control of Kaibel distillation column with the objective of minimizing the energy requirement is studied. This is done by estimating the compositions of the light and heavy keys at the ends of the prefractionator.

Acknowledgements

First and foremost, I offer my sincerest gratitude to my supervisor, Prof. Sigurd Skogestad, who has given me the opportunity to work under his supervision, and supported me throughout my thesis with his knowledge and encouragement. I also thank my co-advisor, Ivar J. Halvorsen, who has been always available for discussions, comments and further leads.
I would like to thank Prof. Bjarne Foss, Prof. Tore Haug-Warbberg and Prof. Heinz Preisig for the fruitful discussions inside and outside classrooms. I would also like to thank Dr. Vinay Kariwala for the discussions and his suggestions. The funding from Research Council of Norway through BEEDIST project is greatly acknowledged.
I also thank my colleagues in Process Systems Engineering group. I have been colleagues with Henrik Manum, Andreas Linhart, Mehdi Panahi, Johannes Jäschke, Håkon Dahl Olsen, Ivan Dones, Magnus Jakobsen, Deeptanshu Dwivedi, Ramprasad Yelchuru, Esmaeil Jahanshahi, Vinicius de Oliveira, Chriss Grimholt and Vladimoros L. Minasidis during my graduate studies. I had many enlightening discussions with my colleagues. Mehdi and his family were my first friends in Norway. They supported me from the day I got admission and onwards. I would like to acknowledge with gratitude the work of Chriss Grimholt, who contributed to this project as a Master student.
I would like to thank the Iranian community in Trondheim and my Iranian friends for the lovely events and get-togethers. I also thank the girls in 4th floor in Prof. Svendsen's group who sometimes saved me from our man-dominated group. I thank my lovely family members who have shown to me that distance is not an obstacle between hearts. And thanks to my dear husband, Hamid, who has been always very kind, understanding and helpful.

Maryam Ghadrdan

Contents

1 Introduction **1**

1.1 Motivation . . . 1
1.2 Organization of thesis . . . 1
1.3 List of Contributions . . . 2

2 A review on optimal design and control of thermally-coupled columns **5**

2.1 Introduction . . . 5
2.2 Different types of distillation column configurations . . . 5
2.2.1 Simple-column sequences . . . 5
2.2.2 Multi-effect distillation . . . 6
2.2.3 Heat Integrated Distillation Column (HIDiC) . . . 6
2.2.4 Thermally coupled arrangements . . . 7
2.3 Design of thermally-coupled columns . . . 9
2.3.1 Shortcut methods . . . 9
2.3.2 Rigorous Design . . . 11
2.4 Different Configurations and Arrangements . . . 11
2.5 Design for minimum energy . . . 13
2.5.1 Feed composition considerations . . . 14
2.6 Optimal Operation . . . 15
2.7 Controllability . . . 16
2.7.1 Controllability of thermally-coupled columns . . . 17
2.8 Control . . . 19
2.9 Conclusions . . . 21

3 Optimal Operation of Kaibel Distillation Columns **23**

3.1 Introduction . . . 23
3.2 V_{min} Diagrams . . . 25
3.2.1 V_{min} diagram basis . . . 25
3.2.2 V_{min} diagram for Conventional Column Sequences . . . 26
3.2.3 V_{min} diagram for 4-product Petlyuk arrangement . . . 27
3.2.4 V_{min} diagram for a Kaibel column . . . 28
3.2.5 V_{min} diagram for Kaibel column using Underwood equation . . . 31
3.2.6 V_{min} diagram from rigorous simulation . . . 31
3.3 Operation . . . 32
3.4 System under study . . . 32
3.5 Minimize energy requirement (mode 1) . . . 35
3.6 Maximize product purities with fixed boilup rate (mode 2) . . . 39

3.7 Conclusions . . . 43

4 A Shortcut Design for Kaibel Columns Based on Minimum Energy Diagrams 45

4.1 Introduction . . . 45
4.2 V_{min} diagrams . . . 45
4.3 Select product purities . . . 46
4.4 Minimum allowable and actual internal flows . . . 47
4.5 Conclusion . . . 50

5 Manipulation of Vapour Split in the Kaibel Distillation Arrangements 53

5.1 Introduction . . . 53
5.2 Degrees of Freedom in the Kaibel Arrangement . . . 53
5.3 Optimal Vapour split in Kaibel columns . . . 54
5.3.1 Sharp Split Separation . . . 54
5.3.2 Non-sharp Separation . . . 57
5.4 Rigorous Simulation . . . 58
5.4.1 Kaibel case-study . . . 58
5.5 Conclusion . . . 62

6 A short review on self-optimizing control 69

6.1 Control Structure Design . . . 69
6.2 Self-optimizing Control . . . 71
6.3 Solution to the CV selection problem . . . 71
6.3.1 Maximum Gain rule . . . 73
6.3.2 Null Space Method . . . 74
6.3.3 Extended Null Space Method . . . 74
6.4 Perfect Indirect Control . . . 75
6.5 Summary . . . 76

7 Economically Optimal Control of Kaibel Distillation Column: Fixed boilup rate 79

7.1 Introduction . . . 79
7.2 Steady-State Optimal Operation . . . 79
7.2.1 Process Description . . . 79
7.2.2 Definition of the Objective Function . . . 80
7.2.3 The Degrees of Freedom . . . 81
7.2.4 Control Variable Selection . . . 82
7.3 Results and Discussions . . . 83
7.3.1 Composition control in prefractionator . . . 83
7.3.2 Control structure based on Exact Local method . . . 83
7.4 Conclusions . . . 90

8 A Short Review on the steady-state estimation methods 93

8.1 Introduction . . . 93
8.2 Data-based Estimators . . . 94
8.2.1 Principal Component Regression (PCR) Method . . . 94
8.2.2 Partial Least Square (PLS) Method . . . 94
8.3 Model-based Estimation . . . 99
8.3.1 Brosilow Estimation . . . 99

8.3.2 Kalman filtering . . . 99
8.4 Our estimation method . . . 101
8.5 Summary . . . 102

9 A new class of model-based static estimators 105
9.1 Introduction . . . 105
9.2 Derivation of Model-based Static Estimators . . . 105
9.2.1 Problem definition . . . 105
9.2.2 Estimators used for monitoring (cases S1, S2 and S3) . . . 107
9.2.3 The "closed-loop" estimator (Case S4) . . . 111
9.2.4 Example 1 . . . 113
9.3 New data-based estimation . . . 114
9.3.1 Monitoring cases . . . 114
9.3.2 Closed-loop estimator . . . 114
9.4 Examples . . . 115
9.4.1 Example 2 . . . 115
9.4.2 Example 3 . . . 118
9.4.3 Further Examples . . . 119
9.5 Discussion . . . 119
9.5.1 Relationship to self-optimizing control . . . 119
9.5.2 Comparison with work of Pannocchia and Brambilla . . . 121
9.5.3 Measurement selection . . . 121
9.5.4 Comparison to standard data-based estimators . . . 121
9.6 Conclusion . . . 122

10 Control of Kaibel Column Using Estimated compositions 125
10.1 Introduction . . . 125
10.2 Estimation of impurities at prefractionator's ends . . . 125
10.3 Our estimation method . . . 127
10.4 Evaluation of Estimators . . . 128
10.4.1 Monitoring the composition ("Open-loop estimation") . . . 128
10.4.2 "Closed-loop" estimation . . . 131
10.4.3 Filtered variable controlled . . . 136
10.5 Control of Kaibel column using estimates . . . 137
10.6 Conclusion . . . 137

11 Dynamic compensation of static estimators 145
11.1 Introduction . . . 145
11.2 Motivating example . . . 146
11.2.1 No dynamic compensation . . . 146
11.3 Cascade control . . . 146
11.4 Selection of a subset of measurements . . . 148
11.5 Filtering . . . 148
11.5.1 Distillation Case-study . . . 149
11.6 Optimization of the filters . . . 150
11.6.1 Explicit solution for the optimization problem . . . 151
11.6.2 Nehari problem . . . 153

11.7 Scalar problem 154
11.7.1 Uniqueness of the solution 156
11.7.2 Example: Scalar problem 156
11.8 Matrix-valued model matching problem 157
11.9 Matrix-valued model matching problem with matrix-valued $\mathbf{R}$ 160
11.9.1 Example: Matrix valued problem 162
11.9.2 Distillation Example: 163
11.10 Discussion 163
11.11 Conclusion 164

12 Concluding Remarks **167**
12.1 Main Conclusions 167
12.2 Further work 168

A The case-study of the thesis **175**
A.1 Simulation of Kaibel column in HYSYS 175
A.2 MATLAB - HYSYS Linking 177

B Contour plots **181**
B.1 Contour plots with R_V manipulated 181
B.2 Solution plots with fixed R_V 181

C Unscented Kalman Filter **185**

Chapter 1

Introduction

1.1 Motivation

Thermally coupled distillation arrangements offer direct coupling between the prefractionator and main column which reduce mixing losses and also minimize energy requirement for a specified separation. Successful applications of the dividing-wall columns have been reported in industry (e.g. [3]), with BASF, with around 70 columns in operation, as the main user of these columns [4]. It is a promising energy-saving alternative for separating multi-component mixtures into four potentially pure products.

The focus of this thesis is to study optimal operation and control of 4-product dividing-wall columns.

1.2 Organization of thesis

Chapter 2 is a short review on Thermally coupled columns, with special focus on Kaibel columns, their design, optimal operation and control.

Chapter 3 introduces two operation modes of Kaibel distillation column which is studied in this thesis. Optimal operation of the column with the two objectives is studied. In this thesis, we have used a graphical tool, the V_{min} diagrams, developed by Halvorsen and Skogestad [1]. Therefore, the application of the V_{min} diagram for estimation of minimum energy for Kaibel distillation column is described.

Chapter 4 shows how to use the information derived from V_{min} diagram for shortcut design of a Kaibel column. This has the advantage of having meaningful guesses for energy requirements and impurity flows in the column.

Chapter 5 is on vapour split and whether it should be considered a degree of freedom or not. Two methods are used to study the effect of vapour split manipulation, namely a shortcut method and rigorous simulations.

In chapter 6, a short review of self-optimizing methods is presented. This method is used in the next chapter to find the appropriate control variables.

Chapter 7 shows the results for controlling Kaibel distillation column. The operational objective is to maximize the purities of products with fixed boilup. The control variables are derived from self-optimizing method. The results are compared with the case that the impurities coming

from top and bottom of the prefractionator are known and controlled.

Chapter 8 includes a short review on static estimators, especially the ones which were used in this thesis. In Chapter 9, a new class of static estimators in presented. The estimators were derived for four different scenarios: fully open, primary variables are controlled, secondary variables are controlled and estimation of primary variables are controlled. The results of the estimation were compared with PLS estimation on a binary and a multicomponent case. In chapter 10, the results of control of Kaibel column, which is operated with the objective of minimizing vapour consumption, are presented. This is done by controlling the estimates of key compositions in the two ends of prefractionator. chapter 11 presents some solutions to the inverse response problem which stems from combining measurements with different dynamics for estimation. In chapter 12, the main conclusions of this thesis are summarized along with some suggestions for further work.

1.3 List of Contributions

International Journals

1. **M. Ghadrdan**, S. Skogestad, I.J. Halvorsen, "Composition Estimation using Temperature Measurements: Application for Conventional and Thermally-coupled Distillation Columns", ready to submit

2. **M. Ghadrdan**, S. Skogestad, I.J. Halvorsen, "Manipulation of Vapour Split in Thermally-Coupled Distillation Arrangements", Chemical Engineering and Processing 72 (2013) 10-23

3. **M. Ghadrdan**, C. Grimholt, S. Skogestad, "A New Class of Model-Based Static Estimators", Ind. Eng. Chem. Res., 2013, 52 (35), pp 12451-12462, DOI: 10.1021/ie400542n

4. **M. Ghadrdan**, I.J. Halvorsen, S. Skogestad, "Optimal Operation of Thermally-Coupled Kaibel Distillation Columns", Chemical Engineering Research and Design, 89 (8), 2011, pp 1382-1391

Peer-reviewed Conference papers

1. **M. Ghadrdan**, S. Skogestad, I.J. Halvorsen, "Dynamic compensation of static estimators from Loss method", accepted to be presented at DYCOPS, 2013, India

2. **M. Ghadrdan**, S. Skogestad, I.J. Halvorsen, "Economically Optimal Control of Kaibel Distillation Column: Fixed boilup rate", presented at ADCHEM, 2012, Singapore

3. **M. Ghadrdan**, S. Skogestad, I.J. Halvorsen, "Estimation of Primary Variables from Combination of Secondary Measurements: Comparison of Alternative Methods for Monitoring and Control", presented at PSE, 2012, Singapore

4. **M. Ghadrdan**, I.J. Halvorsen, S. Skogestad, "A Shortcut Design for Kaibel Columns Based on Minimum Energy Diagrams", ESCAPE, 2011, Chalkidiki, Greece

5. **M. Ghadrdan**, I.J. Halvorsen, S. Skogestad, "Optimal Operation of Thermally-Coupled Kaibel Distillation Columns", Distillation & Absorption Conference, 2010, Eindhoven, The Netherlands

Conference presentations

1. **M. Ghadrdan**, S. Skogestad, I.J. Halvorsen, "Control of Kaibel Distillation Column by Estimated Compositions from temperature measurements", presented at AIChE Spring Meeting, 2012, Houston, USA

2. **M. Ghadrdan**, S. Skogestad, I.J. Halvorsen, "A New Static Estimator for Estimation of Primary Variables from Combination of Secondary Measurements", presented at 17th Nordic Process Control Workshop, 2012, Lyngby, Denmark

3. **M. Ghadrdan**, I.J. Halvorsen, S. Skogestad, "Loss method: A static estimator applied for product composition estimation from distillation column temperature profile", submitted to AIChE Annual Meeting, 2011, Minneapolis, USA

4. **M. Ghadrdan**, I.J. Halvorsen, S. Skogestad, "Manipulation of Vapour Split in Thermally-Coupled Distillation Arrangements: Is it necessary?", presented at 8th European Congress of Chemical Engineering (ECCE-8), September 2011, Berlin, Germany

5. **M. Ghadrdan**, I.J. Halvorsen, S. Skogestad, "Composition Estimation in DWC Columns Using Temperature Measurements", AIChE Spring Meeting, 2011, Chicago, USA

6. **M. Ghadrdan**, I.J. Halvorsen, S. Skogestad, "Comparison of two main approaches for operating Kaibel distillation columns", Nordic Process Control Workshop, 2010, Lund, Sweden

7. D. Dwivedi, I.J. Halvorsen, **M. Ghadrdan**, M. Shamsuzzoha, and S. Skogestad, "Basic Control of Complex Distillation Columns", Nordic Process Control Workshop, 2010, Lund, Sweden

8. I.J. Halvorsen, **M. Ghadrdan**, S. Skogestad, "Minimum Energy for the Four-Product Kaibel Distillation Column", AIChE Spring Meeting, 2009, Tampa, Florida, USA

9. I.J. Halvorsen, **M. Ghadrdan**, M. Shamsuzzoha, S. Skogestad, "Optimizing Energy- and Composition Control of Dividing Wall Columns", AIChE Spring Meeting, 2009, Tampa, Florida, USA

10. **M. Ghadrdan**, S. Skogestad, I.J. Halvorsen, "Selection of Controlled Variables for Self-Optimizing Control of Thermally-Coupled Distillation Columns", 1st Gas Conference, 2009, Trondheim, Norway

11. I.J. Halvorsen, **M. Ghadrdan**, D. Dwivedi, M. Shamsuzzoha, S. Skogestad, "Energy Efficient Distillation", 1st Gas Conference, 2009, Trondheim, Norway

12. M. Shamsuzzoha, **M. Ghadrdan**, I.J. Halvorsen, S. Skogestad, "Rigorous Dynamic Simulation of Divided-wall Columns", Nordic Process Control Workshop, 2008, Porsgrunn, Norway

Chapter 2

A review on optimal design and control of thermally-coupled columns

The thermally-coupled distillation column, which is the subject of this review, is a special distillation column that involves direct coupling between the prefractionator and the main column. This review covers from short-cut design to operation and control issues.

2.1 Introduction

Distillation is perhaps the most important and widely used separation operation that is used for about 95% of all fluid separation in the chemical industry and accounts for an estimated 3% of the world energy consumption [5]. It is notable that more than 70% of the operation costs are caused by the energy expenses [6].

At the end of 1930s, Brugma [7] first proposed a thermally coupled distillation column. This separation operation was re-introduced by Wright [8] and later analyzed by Petlyuk [9]. The energy consumption of distillation systems may be reduced by using 'coupling' of columns wherein the columns are linked directly by process streams. This technique has long been practiced in cryogenic processing where the incentive for reducing energy consumption is very great [10].

In the recent years, several groups are actively involved in research on energy efficient distillation column design and operations. Several heat integrated distillation structures have also been patented [11, 12, 13, 14].

Although several heat integration techniques are covered in this review, the main focus is placed on the dividing-wall arrangement. The main intention of this review is to focus the present status and future scope of research on these issues for columns. This chapter is organized as follows. In section 2.2, several configurations which are used for separation of the components have been presented shortly. The design and operation issues of energy-efficient separation are considered in the next section. Sections 4 and 5 include the controllability analysis and control design for dividing-wall distillation column.

2.2 Different types of distillation column configurations

2.2.1 Simple-column sequences

These consist of two or more simple columns (i.e., a column with one feed, two products, one condenser and one reboiler) connected by a single stream. For a three-product system, the following simple column sequences are possible:

Direct sequence

The first column separates the lightest product as the distillate and the rest is fed to the second column to perform the downstream separation (Figure 2.1a). The column pressures can be optimized separately or individually to perform the two splits since the two towers are independent and are connected by a liquid stream.

Indirect sequence

This setup reverses the sequence of splits by first separating out the heaviest product (Figure 2.1b). In this case, the second column is usually operated at a pressure below that of the first to ensure the natural flow of vapour without using compressor.

Distributed sequence

Unlike the other simple sequences, this one employs sloppy (or distributed) splits to minimize mixing losses in a three-column sequence (Figure 2.1c). The first column separates component a completely from c and allows b to distribute itself between the distillate and the bottoms to minimize the column's reflux ratio. The distillate of the first column feeds the second column to separate component a from b, while the third column uses the bottoms of the first to separate component b from c. The separation efficiency of this configuration is said to be the highest when a partial condenser is used on the first column [15]. However, this imposes a lower bound on the operating pressure of the column that makes the a/b split [16]. The pressure of the other column can be optimized independently. This sequence shifts part of the heating and cooling load to intermediate levels on the reboiler and the condenser of the first column. Hence, it can use lower-quality energy, a warmer cold utility or a cooler hot utility. However, distributing the split often requires a higher capital investment since it calls for a third column and additional heat exchangers.

2.2.2 Multi-effect distillation

Multi-effect distillation approach used for separating multi-component mixtures has received increasing research attention from the last decade (e.g. [17, 18]). The basic idea of this method is to use the overhead vapour of one column as the heat source in the reboiler of the next column. The columns may be heat integrated in the direction of the mass flow (forward integration) or in the opposite direction (backward integration).

2.2.3 Heat Integrated Distillation Column (HIDiC)

In the distillation technique, heat is used as a separating agent. It is conventionally supplied at the highest temperature at the bottom reboiler to evaporate a liquid mixture and is lost at the lowest temperature when liquefying the overhead vapour at the reflux condenser. So, the thermal energy recovered at the condenser cannot be reused for heating other flows in the same distillation unit. Actually, the energy is degraded over the temperature range, and this is the reason of thermodynamic inefficiency of the conventional distillation technology. A HIDiC has been developed through effectively applying heat pump principles to conventional distillation columns [19]. In contrast to other heat pump-assisted distillation columns, this process involves internal heat integration between the whole rectifying and the stripping sections and thus possesses high potential for energy savings [20, 21]. Nakaiwa et al. [22] have mentioned in their comprehensive review that a number of important issues must be considered during HIDiC design, e.g. flexibilities to operating condition changes, influences of an impurity of a third component, and process dynamics and operation. These issues impose strict constraints on the energy efficiency that can

be achieved potentially by HIDiC. Therefore, trade-off between process design economics and process operation appears to be very important and has to be carried out with great caution. In the meantime, several configurations for HIDiC have been developed and investigated up to now. So far, most of the research and development on HIDiC has primarily been confined to binary mixture separations [22]. As multi-component mixture separations represent major applications of distillation columns, development of corresponding HIDiC techniques is a very important and extremely challenging topic for future work.

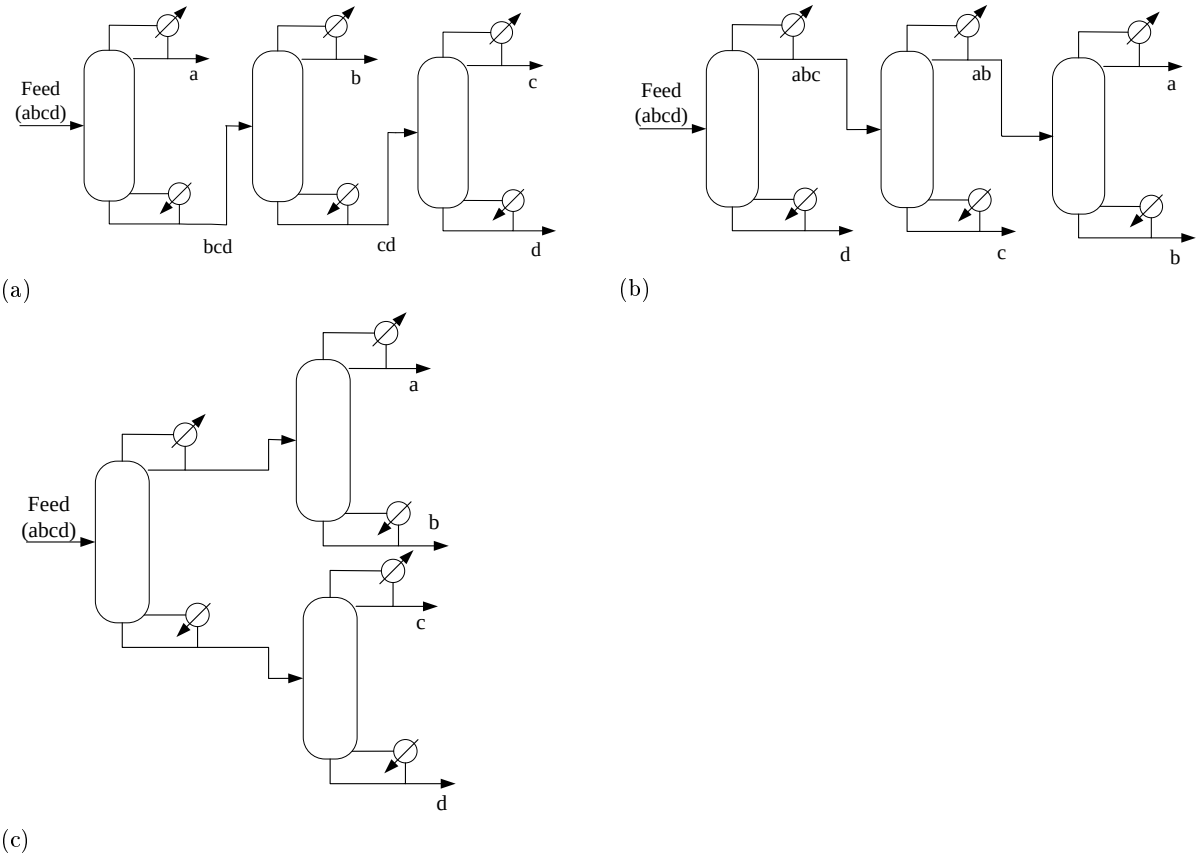

Figure 2.1: Simple column configuration for a four-component mixture. (a) Direct sequence, (b) Indirect sequence, (c) Prefractionator arrangement

2.2.4 Thermally coupled arrangements

the primary source of inefficiency in multi-component, simple distillation is due to the irreversible mixing of non-identical streams. The concentration of the middle-boiling components often reaches a maximum on intermediate trays and then decreases to satisfy the overall mass balance. This remixing inherently affects the efficiency of separation.

Employing complex column configurations can minimize these mixing losses, as well as reduce energy consumption and decrease capital costs. Such columns promote closer interaction between sections by introducing thermal coupling between different sections. They can employ additional sections (e.g., side rectifiers) to minimize remixing of components. Complex-column arrangements can also include prefractionators to minimize feed-tray mixing losses. While thermal coupling improves the separation efficiency and often reduces column duties, the pressure constraint can result in a greater temperature spread. Balancing this trade-off can be difficult.

Thermal coupling eliminates the condenser (side stripper arrangement), or the reboiler (side

Table 2.1: Criteria for using different configurations [16]

Direct sequence	when the feed contains a high concentration of a and/or the separation between b and c is relatively more difficult than that between a and b (i.e., $\alpha_{b/c} < 1.5 < \alpha_{a/b}$)
Indirect sequence	when the feed contains a large concentration of c and/or the separation between a and b is relatively more difficult than between b and c (i.e., $\alpha_{a/b} < 1.5 < \alpha_{b/c}$)
Distributed sequence	when the feed contains a high concentration of b ($x_b > 0.3$) and/or both the splits are difficult (i.e., $\alpha_{a/b} \sim \alpha_{b/c} < 1.5$)

α : Relative volatility

rectifier arrangement) or both (prefractionator arrangement) and introduces a vapour/liquid connection. Tedder and Rudd [23] showed that side rectifiers and side strippers can be cost-effective for any ternary separation where less than half of the feed leaves in the middle product or where low purity of the middle product is acceptable. Fidkowski [15] has shown that using a side stripper or side rectifier will lead to less energy requirement.

Petlyuk column

This configuration introduces additional thermal links between the first (prefractionator) and the second (main) column of the prefractionator arrangement to improve efficiency (Figure 2.2). It was named Petlyuk after presenting the detailed study which was done by Petlyuk et al. [9]. In fact, the Petlyuk design replaces the condenser and reboiler of the first (prefractionator) column with thermal couplings. This thermal integration minimizes separation losses and improves vapour /liquid interaction in all sections of both columns (i.e., yielding higher effective rectifying or stripping ratios).

The Petlyuk column requires the least amount of stripping vapour or rectifying liquid among all of the options for a three-product system. A detailed analysis of this column is found in [9] and [15]. As compared to a conventional distillation unit, the Petlyuk column has more degrees of freedom in both operation and design [24] causing difficulty in designing both the column as well as the control system.

Dividing-wall column

The dividing- wall column (DWC) is essentially a Petlyuk column in a single shell. The DWC introduces a vertical partition (wall) inside the shell to accommodates a prefractionator in the same structure [8, 25, 26]. This allows a great saving in the capital investment of the separation system and increases the separation efficiency at the same time. One difference between the DWC and the Petlyuk column is the heat transfer across the wall. Kolbe and Wenzel [27] have stated the following average savings gained by using a DWC (for an industrial case) against a conventional column system: 25% in investment cost, 35% in operating cost and 40% in space requirement. This was based on rigorous simulation of an extractive distillation pilot plant. There are also some researches for retrofitting conventional columns to dividing-wall columns because of different savings [28].

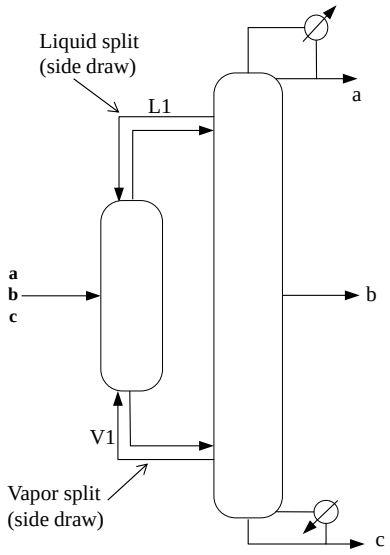

Figure 2.2: Petlyuk distillation column

The advantage offered by this partitioned column is that a ternary or 4-component mixture can be distilled into pure product streams with only one distillation structure, one reboiler and one condenser. Obviously, this reduces the cost of separation. Moreover, reduced number of equipment units leads to a low initial investment cost. To fractionate the feed mixtures containing four or more components, single tower distillation process with multiple vertical partitions was first proposed by Kaibel [25]. For multi-component mixture separation, Agrawal [29] discussed various types of partitioned columns with their advantages and disadvantages. These structures decrease the number of distillation column shells to one and the total number of reboilers and condensers by at least n - 2. Due to the lack of experience in design and control, the dividing-wall columns have not been used extensively in industry except within BASF. However, their number is growing rapidly (more than 100 units in 2007 worldwide) [30].

2.3 Design of thermally-coupled columns

2.3.1 Shortcut methods

The use of short-cut methods has been defended based on the complexity of the problem and the need to rapidly assess alternative designs, perform preliminary optimization and provide the initialization for rigorous simulation [31]. Most of the methods make two assumptions - constant molal overflow and constant relative volatility - that restrict their applicability only to non-azeotropic systems. The primary objective of the shortcut methods is to obtain estimates for the vapour /liquid traffic (i.e., reflux and reboil ratios) and the number of trays in each section of the column. For example, the minimum reflux ratio is calculated using Underwood's method [32, 33, 34], while the minimum number of theoretical stages is estimated using Winn's method [35]. It is an extension of Fenske's method and accounts for changes in the temperature of the column by introducing additional parameters that depend only on the K-values (vapour/liquid equilibrium ratios) of the key components. The actual reflux ratio and the number of stages are then determined by employing Molokanov's correlation [36] for the specified ratio of the actual to the minimum reflux ratios (R/R_{min}). This formulation provides the information about the trade-off between the reflux ratio and the number of trays [26]. The feed tray location is estimated using Kirkbride's correlation [35]. Cerda et al. [37] the proposed technique tends to

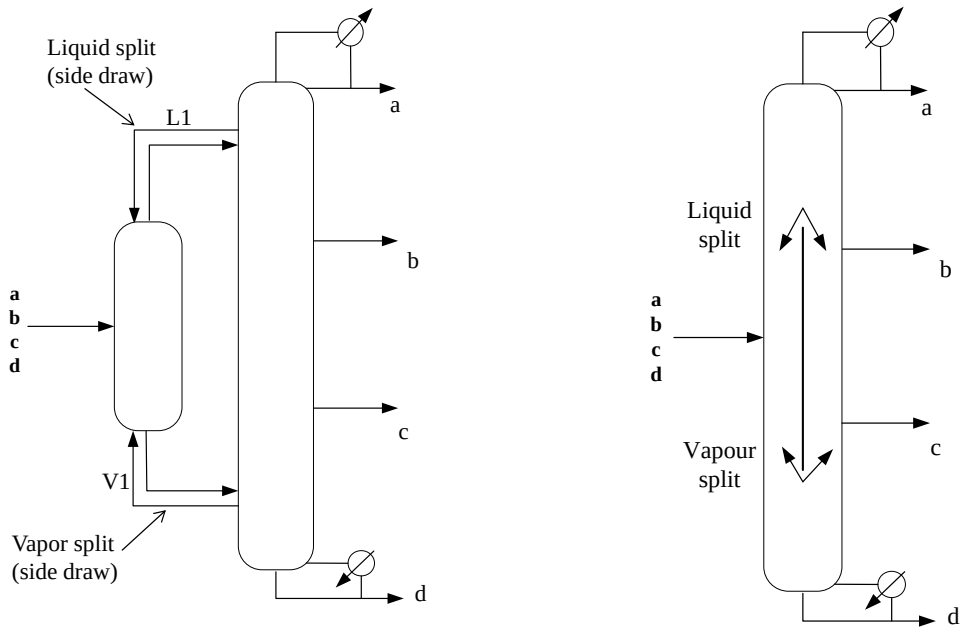

(a) (b)

Figure 2.3: Thermally coupled columns

give R values a little lower than the real ones.

Malinen and Tanskanen [38] have proposed a minimum energy method for non-ideal multi-component distillation. In their method, the actual minimum energy determination can be carried out in three steps. At first, the initial state distribution for the column sequence is calculated. Then, the state distribution of the column sequence is calculated with exact mole fraction specifications for the product flows by using the initial column profile obtained in the first phase (feasibility issues must be kept in mind). In the second step, the molar flow ratios in the ends of prefractionator, namely liquid flow entering from top / vapour flow exiting from top and vapour flow entering from bottom / liquid flow exiting from bottom, are also specified to fulfil the separation target. In the third step, the minimum energy operation point is determined based on the optimization of the the flow ratios. Optimization is based on the minimisation of the reboiler duty instead of the boilup rate or the boilup ratio. The solution obtained in the second step is used as a starting point for minimization. This method is based on the assumption of infinitely high columns and it was not considered for the case of finite number of stages. Triantafyllou and Smith [26] and Shah [39] discussed extending this method to the liquid and vapour side-draw columns. Finn [10] has redefined the net feed flow rate and feed quality in order to make use of the conventional Underwood equations for thermally coupled columns. Halvorsen et al [1, 40, 41] have presented minimum energy requirement diagrams to calculate the minimum energy required for the separation of components in the Petlyuk configuration. They have proposed to adjust the liquid and vapour splits in order to keep the boilup in its optimum point. The reboiler duty solution surface shown is reminiscent of the optimal solution surface of the Petlyuk column reported in Halvorsen and Skogestad [42]. It is worth mentioning that the energy usage, i.e., the reboiler duty, increases rapidly outside the optimal operation area. They have shown that when the column is operated at the preferred split (the minimum energy for separating components a and c in the prefractionator), the infinite-staged Petlyuk column always consumes less energy than the corresponding conventional solution. They have noted that: To operate at minimum energy, we first have to ensure that R_V is in the flat region in order to be within the solution surface $V(R_L, R_V)$ between P* and R* at all (P* and R* are the two points at two ends of the

flat region). This task seems quite easy unless the feed composition is close to the boundary curve. Second, we must find the optimal value of R_L for the particular R_V to ensure that we actually operate on P*-R* and not somewhere to the sides of P*-R*, where $V(R_L, R_V)$ may be quite steep. With both R_L and R_V constant, the probability of hitting P*-R* on a solution surface, which is moved around by changes in feed composition, quality and reflux will be very small, so this will only be a feasible strategy if the operating conditions are reasonable steady and for cases where the solution surface is not very steep. Halvorsen et al. [43] have also studied the energy consumption of a Kaibel column using shortcut analysis. This is the method which is used in this thesis.

A design procedure to utilize the three-column model was introduced by Triantafyllou and Smith [26]. Separating the main column of the fully thermally coupled distillation system makes a system of three separate continuous distillation columns to which the short-cut design equations for the multi-component distillation design can be applied. Though the design procedure easily gives the tray numbers of the three separate columns, matching the compositions of interlinking streams requires adjustment and time-consuming iterative calculation. Since the fully thermally coupled distillation column, has interlinking between a prefractionator and a main column, usual multi-component design procedures are not applicable to the design of the column when the information of the interlinking streams is not given [44].

2.3.2 Rigorous Design

The synthesis of complex distillation system is a problem of multi-hierarchy combinatorial optimization. One step is to find the optimal distillation sequence and to identify the heat integration strategy. The next step is to find the optimal operation parameters for every unit included in the flowsheet. The complexity and combinatorial explosion of this kind of problem leads to high difficulty for solving it. In this part, the major works which are done on this topic will be reviewed.

2.4 Different Configurations and Arrangements

Agrawal et al. proposes a guideline (in a diagram) to choose the most efficient configuration for different 3-component feed compositions when both splits have identical relative volatilities (α = 2) [45]. These diagrams are useful to gain insights, but it is difficult to evaluate the complicated trade-offs related to the quality and quantity of energy, or the effect of pressure constraints. Halvorsen et al. [46] have studied this matter from energy point of view. They have shown the range of feed composition in which petlyuk configuration is a good option, because of the nearly similar peaks in the minimum required energy diagram, which means that there will be no loss due to the difference of energy requirement in the upper and lower parts of the main column. For the simplicity of column construction, a dividing-wall structure is preferred and has been adopted in many studies [47]. But the structure adds the complexity in the design since the number of trays in a prefractionator has to be same or close to the tray number in the middle section of a main column. Another problem associated with the dividing-wall structure is that controlling the split of liquid and vapour flow is difficult.

There are some papers which deal with new configurations of thermally coupled columns in order to make them more operable. Agrawal and Fidkowski [48] have proposed various configurations of an FTCDC by rearranging sections in a main column and a prefractionator, which are thermodynamically equivalent. Agrawal also extended this idea to n-component systems [49, 50, 29]. These configurations are derived from the known sequential or satellite column arrangements. However, like the previous study, there is not any quantitative comparison between the proposed configurations and the conventional Petlyuk. The pressure difference between

the main column and prefractionator has a key role to determine a plausible alternative. To present the alternatives, Rong et al. [51] have formulated a procedure which makes the synthesis of the fully heat-integrated thermally coupled configuration for any n-component mixture systematically. They have [52] used a short-cut design to compare the columns for separating 5 components. The works done by Hernandez et al. [53, 54] are also with the same goal. All of the alternatives are equivalent in terms of minimum energy requirement. There are of course many differences, e.g. in how easy it is to set individual vapour and liquid flow rates in practice, how the column arrangement behaves for non-optimal operation, how easy it is to control, possibly for operation at more than one pressure level, practical construction issues.

In order to alleviate the control difficulty of a fully thermally coupled distillation column (FTCDC), the reduction of the number of interlinking streams is attempted by installing a heat exchanger at the interlinking streams [55, 56]. However, along with the conversion, a number of additional column sections as well as additional heat exchangers were added to the modified configurations. The proposed structures provide energy saving comparable to the fully thermally coupled system in some cases. Their reason of this study is that Petlyuk arrangement contains a maximum number of thermal couplings that is a disadvantage for the operability due to the harsh pressure constraints in terms of vapour transfers. The separation sequence of the Petlyuk arrangement contains all of the feasible subgroups of a multi-component mixture (i.e., n(n-1)/2 subgroups). This results in the fact that the Petlyuk arrangement contains a maximum number of thermal couplings compared to other possible thermally coupled configurations. On the one hand, at the thermally linked locations between the different columns, in order to minimize exergy losses, there need to be small pressure driving forces to facilitate the vapour transfers. At the same time, inside a column along different sections, one needs to carefully design the pressure drops in order to meet the requirements of the pressure driving forces. On the other hand, the harsh pressure constraints could cause the system to be sensitive to pressure disturbances, which would incur difficulties in the system's control.

Agrawal [57] proposed a superstructure for a certain subclass of Petlyuk arrangements by considering arrangements with n-2 satellite columns in communication with a central distillation column. Agrawal claims that this superstructure includes as substructures all previously proposed configurations giving *sharp splits*, which in fact is not quite true due to a study by Christiansen et al. [58], which is done on four-component separation in a single column. The sharp split arrangement is defined as an arrangement of columns in which any degree of separation (purity) can be obtained by increasing the number of stages (provided the internal refluxes are above certain minimum values and provided the separation is thermodynamically feasible). A Petlyuk column is then a sharp split arrangement with a single condenser and a single reboiler. In any case, Agrawal's superstructure includes Sargent's [59] superstructure and also Kaibel's and Cahn's arrangements as substructures. Agrawal derives by simple arguments that the minimum number of rectifying and stripping sections required for sharp splits using such satellite arrangements, is equal to 4n-6 (10 sections for n = 4).

Kim [60] has suggested using post-fractionator in order to decrease the energy usage even further. For examining the economical benefits from the introduction of postfractionator to the fully thermally coupled column, utility and investment costs were calculated with the formulas given in Kim and Luyben [61]. He has simulated the BTX fractionation and claimed that it's economically profitable.

Grossmann et al. [62, 63] have presented a systematic approach for generating all the thermodynamically equivalent structures for a given sequence, then, this method could be integrated in the framework of Disjunctive Programming to exact the best solution for a given objective function [64]. Afterward, a two stage decomposition procedure was described that gave a novel superstructure for designing sequences of distillation columns, which ranges from conventional to fully thermally coupled systems and goes through all the alternative intermediate possibilities

[65] and the optimal synthesis of complex distillation columns using rigorous models was given [66]. Recently, Caballero and Grossmann [67] improved a superstructure approach for synthesizing heat-integrated thermally coupled distillation sequences. The model was formulated as a Generalized Disjunctive Programming (GDP) problem and solved as a modified mixed integer non-linear programming (MINLP) model. The above works can create a large number of new distillation configurations, which has formulated a large new search space for the optimization work. Wang et al. [68] have worked on this subject using genetic programming as a stochastic tool.

2.5 Design for minimum energy

Hernandez et al [69] proposed a model which is used to detect the operating conditions under which a given design for the Petlyuk system can provide the minimum energy consumption. The approach is an extension of a model previously developed for the design of thermally coupled distillation sequences with side columns [70]; An important aspect for the design of the system is the specification of the two recycles streams. Different mixtures were analyzed in an attempt to understand the influence of the relative difficulty of the separation a/b with respect to b/c on the energy consumption and design of the system. The optimization procedure is done in the dynamic mode by changing vapour and liquid splits.

They have noted that an adjustment of the initial design might be needed if the final steady state compositions do not agree with the established set points.

The ease of separation index (ESI), as defined by Tedder and Rudd [23], was used to characterize each mixture:

$$\text{ESI} = \frac{\alpha_{ab}}{\alpha_{bc}} \tag{2.1}$$

The following recommendations were developed as a function of the mixture properties and its feed composition. For mixtures with ESI = 1:

- If the content of the intermediate component b is high (>30%), use $R_V = 0.5$ and perform an optimization search over R_L.
- If the content of the intermediate component b is low (<10%), use $R_V = 0.7$ and carry out an optimization search over R_L. For mixtures with ESI ≠ 1:
- If the content of the intermediate component is high, use $R_V = 0.7$ and optimize R_L.
- If the content of the intermediate component is low, use $R_V = 0.4$ and carry out an optimization search over R_L.
- For all cases, the optimal value of R_L is lower than that of R_V. These observed trends can provide the basis for useful heuristic design rules. It should be emphasized that these trends were obtained for separations of ideal mixtures.
- For all cases, the optimal value of R_L is lower than that of R_V.

It should be emphasized that these trends were obtained for separations of ideal mixtures. Their results show that R_V values can be correlated to an ESI, and that there is no significant deviation in the optimal solution with small changes in R_V. There is, however, a high dependency on the energy consumption with respect to R_L once a value for R_V has been specified. Therefore, the results suggest that a proper value for R_V can be set ahead of design, but a search over R_L is still required to obtain a design with minimum energy consumption. They have claimed that these observations reduce significantly the search space for the design of the Petlyuk system with minimum energy consumption.

Malinen et al. [38] have presented a rigorous minimum energy calculation method which is the extension of Tanskanen et al.'s [71] works to a fully thermally coupled distillation column system, also known as a Petlyuk column. Tanskanen et al. [71] have presented it for non-ideal multi-component distillation. The method is based on column simulation with a large number of equilibrium stages to mimic infinitely high columns .

The design method proposed by Blancarte-Palacios et al. [72] involves a search procedure on the interconnection vapour and liquid streams until a minimum energy consumption is detected. Halvorsen et al. [1, 40, 41] have sketched the solution surface in terms of the two remaining degrees of freedom. They have concluded that if the region is wide in both directions, both the remaining DOFs may be kept constant, and if it is narrow, on-line adjustment of both DOFs is required in order to achieve the potential energy savings. If the optimality region is flat in only one direction, one DOF may be kept constant, but online adjustment of the other is probably required. The degrees of freedom may be constant for the following cases:

1. A large flat region when the feed conditions (composition, liquid fraction and relative volatilities) is far from the boundary where the operating points for a preferred prefractionator split coincide with a balanced main column.

2. Low purity in the side-stream product gives a large flat region.

2.5.1 Feed composition considerations

Annakou [73] has compared three different ternary distillation schemes - the conventional schemes, the heat-integrated schemes, and the fully thermally coupled distillation column - on the basis of the total cost with four different feed compositions with different ease of separation and three different product purity specifications. He has claimed that the FTCDC can be competitive with the heat-integrated schemes only in those cases when the concentration of the middle component in the feed is high and the a/b split is harder than b/c split. The thermally coupled distillation column is not recommended when the composition of the least volatile component is the highest in the feed. Emtir et al. [74] and Mizsey et al. [75] have also reached similar results. Emtir et al. have compared heat integrated structures with thermally coupled columns and have presented some rules governing the ranks of the studied structures according to total annual cost. They have used USA and EU energy prices for their comparisons. They have also mentioned that petlyuk structure has the greatest chance to win over the energy-integrated schemes at balanced relative volatility ratio. Due to the comparisons in the work of Rév et al. [76], the advantage, in total annual costs, over energy-integrated structure is approximately 6% at low (American) utility prices; but this advantage is approximately 20% at high (European) utility prices.

Agrawal and Fidkowski [55] showed that the thermodynamic efficiency of fully thermally coupled distillation is not so high as suggested in earlier studies for some cases. The energy saving is quite dependant to feed composition. Yet the improvement of the efficiency in the coupled system is largely due to the less mixing in feed stage and remixing of middle component in a prefractionator [26], and the mixing and the remixing are not counted in the study. Two notes are worthy to mention here. First, it is important to highlight that the Petlyuk distillation column and the dividing-wall distillation column are thermodynamically equivalent, but the industrial operation is different. Recently, Suphanita et al. [77] have found that the heat transfer across the wall can improve the operation of the dividing-wall distillation column. The other difference is of course in the limitation of splits which is tight in the case of dividing-walls. Second, as mentioned previously, since a main column and a prefractionator are interlinked, more degrees of freedom than two binary distillation columns are involved. There are not enough manipulated variables to formulate control loops equivalent to the degrees of freedom, and therefore multiple steady-state solutions are obtained for a given set of product specifications [78, 79].

2.6 Optimal Operation

The degree of freedom of a the thermally-coupled column with side streams, dividing-walls and communication points is as shown below [58]:

$$\mathrm{DOF} = 2 + n_S + 2\,n_D + 4\,n_C \tag{2.2}$$

where
n_S : number of side streams
n_D : number of dividing walls
n_C : number of communication points

Due to the coupling, the number of degrees of freedom for thermally coupled columns is more than conventional columns. To design and simulate the FTCDC system, several quantities must be determined:

1. number of theoretical trays in the prefractionator,
2. number of theoretical trays in the main column,
3. internal recycle streams, liquid stream draw-off from the main column to the prefractionator, and vapour stream draw-off from the main column to the prefractionator,
4. reflux ratio in the main column,
5. tray locations for all feed streams, side draw-off streams, and side product stream.

For such a design problem two major approaches of the process syntheses are in use: the hierarchical approach (e.g., Douglas [80]) and the algorithmic approach (Grossmann [81]). The two major approaches can also be combined (Mizsey and Fonyo [82]).

Fidkowski and Krolikowski [31] have studied ideal ternary solutions and selected the fractional recovery of the middle component in the top product of the prefractionator as a decision variable. Triantafyllou and Smith [26]. They have indicated that the recovery of the middle component in the prefractionator is not an independent variable because it depends on the recoveries of the light and heavy components. Annakou et al [83] started the solution by shortcut design procedures to estimate the number of theoretical trays, location of the feed trays and draw-off trays, and the reflux ratio. In the next step of the design the system was investigated by rigorous modeling and changes made according to the desired performance. The prefractionator was designed as a separate unit. In the prefractionator it is supposed that the most volatile component of the ternary mixture is only in the top product and the heaviest component is only in the bottom product. The middle component distributes between the top and bottom products. The optimal fractional recovery of the middle component where the energy consumed by the FTCDC is minimal has been defined by Treybal [84] in terms of the relative volatilities and also used by Fidkowski and Krolikowski [31] for saturated liquid feed:

$$\beta^* = \frac{\alpha_b - \alpha_c}{\alpha_a - \alpha_c} \tag{2.3}$$

A comprehensive parametric study is performed to investigate the role of the fractional recovery on the energy consumption and the total annual cost of the FTCDC. The FTCDC is rigorously simulated at several fractional recovery values within the range of $0 < \beta < 1$ and also at the balanced fractional recovery (β^*). These results obtained by rigorous simulations show the importance of the fractional recovery and its role in determining the internal recycle streams for better economic performance of the FTCDC. The fractional recovery and as a following the internal recycle streams should not be arbitrarily selected. They are very important design parameters and should be determined to obtain the optimal economic performance of the FTCDC

2.7 Controllability

A common procedure is to design a plant based on steady-state considerations, and then add on a control system at a later stage of the project. This may be acceptable if one at the early design stage can assess whether the plant *inherent control limitations* has good *achievable control performance* and is called *controllable* or *dynamic resilient*. The controllability of a plant is determined by inherent properties of the process and not of the control system. Since a plant's dynamic resilience can not be altered by change of the control algorithm, but only by design modifications, it follows that the term dynamic resilience provides a link between process design and process control. A number of methods for evaluating controllability are described in the work of Wolff et al. [85], which are summarized shortly here. All measures are controller independent. In the next section, the researches on controllability of thermally-coupled columns will be reviewed.

Functional and state controllability

Probably the first thing that should be checked is that the plant is functional controllable. Essentially, a plant is not functional controllable if the rank of $\mathbf{G}(s)$ is for all s less than the number of outputs we want to control. For square plants the requirement is that we should have $\det \mathbf{G}(s) \neq 0$ [86].

RHP-zeros and time delays

A right half plane (RHP) transmission zero of $\mathbf{G}(s)$ limits the achievable bandwidth of the plant. This holds regardless of the type of controller used (Holt and Morari, 1985). The upper limit on the bandwidth is approximately $\omega_B < z$ where z is the location of the RHP-zero (the exact expression depends on the direction of the RHP-zero).

RHP-poles

Poles of $\mathbf{G}(s)$ in the right half plane also put limitations on the control system through stability considerations. The bandwidth of the closed-loop system must be above the frequency of the RHP-pole to ensure a stable system.

Singular Value Analysis

The singular value decomposition of any matrix $\mathbf{G}$ is $\mathbf{G} = \mathbf{U}\mathbf{\Sigma}\mathbf{V}^H$ with the matrix $\mathbf{\Sigma}$ having the singular values σ_i on the main diagonal. The singular values are directly related to the vector 2-norm. The singular values give the gain in the corresponding input and output directions (columns in $\mathbf{V}$ and rows in $\mathbf{U}$ respectively). An SVD on $\mathbf{G}$ and $\mathbf{G}_d$ is useful for examining which manipulated input combinations have the largest effect and which disturbances give the largest output variations.

Condition number

The ratio between the largest singular value ($\overline{\sigma}$) and the smallest nonzero singular value ($\underline{\sigma}$), is often denoted the condition number, $\gamma(\mathbf{G}) = \frac{\overline{\sigma}(\mathbf{G})}{\underline{\sigma}(\mathbf{G})}$. Plants with a large condition number are called ill-conditioned, and require widely different input magnitudes depending on the direction of the desired output. There is a close relationship between the optimally scaled condition number, $\gamma^*(\mathbf{G})$ (minimize $\gamma(\mathbf{G})$ with respect to input and output scaling) and the magnitude of the RGA-elements (e.g., [87]).

Relative gain array (RGA)

The most widespread controllability measure is probably the RGA which was introduced by Bristol [88]. For a square plant $\mathbf{G}(s)$ the relative gain is defined as the ratio of the "open-loop" and "closed-loop" gains between input j and output i. It is defined at each frequency as

$$\lambda_{ij}(s) = \frac{\left(\frac{\partial \mathrm{y}_i}{\partial \mathrm{u}_j}\right)_{\mathrm{u}_{i\neq j}}}{\left(\frac{\partial \mathrm{y}_i}{\partial \mathrm{u}_j}\right)_{\mathrm{y}_{i\neq j}}} = \mathrm{g}_{ij}(s)\left[\mathbf{G}^{-1}(s)\right]_{ji}$$

and a RGA-matrix is computed from $\Lambda(j\,\omega) = \mathbf{G}(j\,\omega) \times \mathbf{G}^{-1}(j\,\omega)^T$, where $\times$ denotes element-by-element multiplication. It is established that plants with large RGA-values, in particular at high frequencies, are fundamentally difficult to control. In particular, it is known that one should never use decouplers in such cases because of a strong sensitivity to (structured) input uncertainty in each channel, i.e., one should never use a controller with large RGA-values citeSkogestad1987d.

Disturbance sensitivity

The open-loop disturbance sensitivity is given by $\mathbf{G}_x^d$ whose elements are given by $\mathrm{g}_x^d = \left(\frac{\partial \mathrm{x}_i}{\partial \mathrm{d}}\right)_{\mathrm{u}_j}$. If appropriately scaling has been applied and any of the elements are larger than 1 then control is needed to get acceptable performance. Disturbance condition number: To study specifically the direction of a disturbance, Skogestad and Morari [87] introduced the disturbance condition number of the matrix $\mathbf{A}$, where $\mathbf{A}$ may be $\mathbf{G}$ or $\mathbf{L} = \mathbf{GC}$.

Relative order and phase lag

The relative order is sometimes used a controllability measure. The relative order may be defined also for nonlinear plants, and for linear plants it corresponds to the high-frequency roll-off, that is, the pole excess of the transfer function. Of course, we want the inputs to directly affect the outputs, and the relative order should be small. However, the usefulness of the concept of relative order is rather limited since it depends on the modeling details. In fact, a more useful measure to consider is the phase lag of the model at the bandwidth frequencies, for decentralized control we want to pair on variables where the phase lag is as small as possible, and it should be less than $-180°$ (see [89]).

2.7.1 Controllability of thermally-coupled columns

Mostly used indexes in papers were the Niederlinski index (NI), which must be positive, the Morari resiliency index (MRI), the larger its value, the better the control, the Relative gain array (RGA), the diagonal elements close to unity indicate weak interaction, and the condition number (CN), the smaller this number, the better the control [90]. There are of course many other indices proposed in literature. For example, He et al. [91] proposed a new loop-pairing criterion based on a new interaction measurements for the control structure configuration of the multivariable process. Decomposed relative interation array (DRIA) was defined to evaluate all possible interactions among loops, and General Interaction(GI) based on the concept of interaction energy [92]. An algorithm which combines RGA, NI, and GI rules was developed that can solve the loop configuration problem [93]. Below, some of the papers, which dealt with controllability of thermally-coupled columns, are reviewed.

Hernandez et al. [94, 95, 96] have conducted a comparison between controllability properties for three of the complex columns, namely thermally coupled distillation systems with side strippers (TCDS-SS) and side rectifiers (TCDS-SR) and Petlyuk column. Results from singular value decomposition indicate that systems with side columns offer better dynamic properties

than Petlyuk systems. Also, there is an effect, however, of the relative difficulty between the two splits of the ternary mixture. When the a/b split is more difficult than the b/c split (ESI<1), the TCDS-SS offers the best control properties; otherwise, the TCDS-SR provides the best option from a dynamic point of view. The only cases for which both economic and dynamic performance factors agree are when the feed mixture has a low composition of the intermediate component and ESI>1 (TCDS-SR) and when the mixture with low composition of intermediate component has an ESI<1 (TCDS-SS). They have also compared dynamic responses under a closed loop in thermally coupled distillation sequences with side columns or prefractionators [97]. They have mentioned that the dynamic responses in the TCDS schemes can be improved by exploring alternative control loop pairings. They have also claimed that the control properties of the nonoptimal cases are better [98]. By "optimal" they mean the minimum energy case which depends strongly on the amount of intermediate component in the three-component mixture they have studied. They have said that a reduction in the number of interconnections does not necessarily provide the operational advantages originally expected given the resulting simpler structural design [99].

Wang et al. [100] investigated the effects of liquid split and vapour split ratios on the energy efficiency and controllability of a dividing-wall column. There is a trade-off between energy efficiency and controllability of end-product composition. They have overcome such a trade-off by using a temperature + composition cascade control scheme. Liquid and vapour splits between different column sections are treated as disturbances.

Annakou et al. [73] compared the controllability of the conventional heat-integrated column sequences and the Petlyuk Column for the separation of ternary mixtures. Through degrees of freedom analysis and steady-state multivariable control synthesis tools they have shown that both investigated schemes could be controlled by conventional decentralized control structures, although interactions among control loops is smaller for the conventional heat integrated systems.

Mizsey et al. [75] have also claimed that conventional heat-integrated schemes have less interactions compared to Petlyuk column by measuring steady state control indices. The dynamic behaviour shows longer settling time and higher overshoots for the Petlyuk column comparing to conventional heat-integrated schemes, detuning is necessary due to strong interaction between its control loops. The main issue which should be considered is that the design and control part are inter-related. As Skogestad says in his book [101] that *We can not make a Ferrari out of Volkswagen.* A paper from Skogestad [102] is an example of how design affects the easiness of control. It is mentioned that it is better to have many stages. He mentioned that in terms of composition control, the best design to make feedback control easier is probably to add extra stages. This has two potential advantages:

- It makes it possible to over-purify the products with only a minor penalty in terms of energy cost; recall the expression for $V_{min} = \frac{1}{1-\alpha}F$ which is independent of the purity. The control will then be less sensitive to disturbances.

- If we do not over-purify the products, then with too many stages a pinch zone will develop around the feed stage. This pinch zone will effectively stop composition changes to spread between the top and bottom part of the column, and will therefore lead to a decoupling of the two column ends, which is good for control.

This concept is tested by Serra et al. [103]. Controllability of different optimal DWC designs with different number of trays is compared in the paper. According to controllability indices, the optimal designs have the same sets of preferred manipulated variables. It was seen that high CN is a problem associated to 'DB' inventory control (Distillate rate is used to control condensate level and Bottom flow rate is used to control reboiler level), which is improved using DWC with more trays. On the contrary, for 'LV' inventory control, addition of trays has not been found to be a good option from a control point of view. In other work, Serra et al. [104] compared the

controllability of different multi-component distillation arrangements and discussed the operation conditions that favour controllability for the DWC.

2.8 Control

The lack of widespread use of complex columns can partly be attributed to their more difficult control properties. Understanding control properties of columns with thermal couplings for the separation of ternary mixtures is an issue of extreme importance since designs with economic incentives often conflict with their operational characteristics. One issue which should be considered is the model on which the control structure is built. Cao et al. [105] have refined the model of a plant and they showed that the model affects the control structure selection.

The study on the control of the Petyluk column, which is thermodynamically equivalent to the dividing-wall column, was first reported by Wolff et al. [106, 24]. The pioneering dividing-wall control paper is the 1995 work of Wolff and Skogestad [24], where they studied the ethanol/propanol/butanol ternary system. They looked at both three-point control, in which the purities of the three products are controlled, and four-point control, in which both of the impurities in the sidestream are controlled in addition to the purities of the distillate and bottoms. The three-point structure controlled distillate purity by manipulating reflux flow rate, sidestream purity by manipulating sidestream flow rate, and bottoms purity by manipulating vapour boilup. They also tested switching the last two loop pairings but claimed this pairing is unworkable. In the four-point structure, an additional loop to control the ratio of impurities in the sidestream by manipulating the liquid split was added. They demonstrated that "holes" in the steady-state feasibility space made the four-composition control structure infeasible at some operating conditions. These authors used several linear analysis methods and nonlinear dynamic simulations to evaluate control effectiveness for feed flow rate, feed composition, and product purity set-point disturbances.

Wolff and Skogestad [24] examined possible control schemes of the column and suggested that controlling the tray temperature close to the most critical composition measurement gives better performance than the direct composition control. Temperature measurement provides a more reliable and faster means of measuring the changes that take place in the distillation column during transient conditions. However, it is well known that a temperature measurement is not an accurate method of inferring product composition. In order to overcome such limitations, techniques have been proposed by several researchers, which include over refluxing the column or using multiple temperature measurements.

Abdul et al. [107] studied the operation and control of Petlyuk Column. They suggested that both liquid and vapour splits are maintained constant at their nominal values. Two control structures are considered in their work: L-S-V and D-S-V. The steady-state Relative Disturbance Gain (RDG) of the two control structures are calculated to make an interaction analysis. According to the RDG results, that D-S-V control structure resulted in better control than L-S-V control structure.

Abdul Mutalib, Zeglam, and Smith [107] reported simulation and experimental studies of the same system using temperatures instead of compositions as the controlled variables. These authors attempted to control only two temperatures in the system. They also kept the sidestream flow rate constant. Product composition offset took place as different feed compositions entered the column. This is due to the fact that controlling temperature at the two locations does not guarantee the product compositions to be kept at specification.

Hernandez [108] presented a comparative analysis of the feedback control responses to set-point changes of three thermally-coupled distillation schemes and two conventional distillation sequences for the separation of ternary mixtures. Designs for the thermally-coupled schemes were obtained and optimized for energy consumption to link their energy characteristics to their

dynamic behaviour. For the comparison of the dynamic behaviour, responses to setpoint changes under closed loop operation with proportional-integral controllers were obtained. The effects of feed composition and of the ease of separation index were considered. The dynamic tests showed that in many cases the thermally coupled distillation schemes outperformed the dynamic responses of the conventional distillation sequences. The results indicate that there exist cases in which the energy savings provided by the thermally coupled systems do not conflict with their dynamic properties.

Serra [109] has also done the study of feedback diagonal control of DWC. Different control structures have been systematically analyzed and compared under performance and robustness considerations. In order to study the effect of the energy optimization on the controllability of the DWC, a column at optimal nominal operating conditions is compared to a column under non-optimal operation. Finally, a complete control strategy is proposed.

Adrian et al. [30] reported experimental studies of the butanol/pentanol/hexanol system in the BASF mini-plant laboratory. They used a three-temperature control scheme. One temperature was located in the prefractionator side of the wall above the feed tray to prevent the heavy boiling component from passing the upper edge of the dividing-wall. The second temperature was above the side-stream draw-off tray in the main column side of the wall to monitor the separation between the lightest and the intermediate components. The third temperature was in the stripping section to ensure that none of the intermediate component drops out the bottom of the column. At the same time, holding this temperature constant helps to keep the lightest component from passing the lower edge of the wall on the prefractionator side. They compared the conventional PID control with MPC. Their experimental results showed that stable regulatory temperature control was achieved for both feed flow rate and feed composition disturbances. However, they do not report what happened to product compositions.

Ling et al. [110] have proposed a control structure for dividing-wall column using four composition loops to control the purities of the three product streams and also achieve minimum energy consumption for both feed flow rate and feed composition disturbances. The numerical example studied the separation of benzene, toluene, and o-xylene. The four manipulated variables were reflux flow rate, side-stream flow rate, reboiler heat input, and liquid split at the top of the wall. In another paper [111], they explored the use of temperatures to avoid expensive and high-maintenance composition analyzers. Two types of temperature control structures were studied. In the first, three temperatures located in the main column and one temperature on the prefractionator side of the wall are used to adjust the four manipulated variables. Feed flow rate disturbances are well handled with this structure, but product purities start to deviate significantly from their desired values for feed composition changes greater than about 10%. In the second control structure, four differential temperature control loops are used. Performance is improved and disturbances of 20% in feed composition are well handled with only small deviations in product purities. This structure also handles large changes in column operating pressure.

The ideas related to self-optimizing control have been presented repeatedly in the process control literature, but the first quantitative treatment was that of Morari et al. [112]. Skogestad defined the problem more carefully, linked it to previous work, and also was the first to include the implementation error. As defined by Skogestad [2], self-optimizing control is when we can achieve an acceptable loss (in terms of energy or in terms of purity) with constant setpoint values for the controlled variables. In most processes there are some extra degrees of freedom that can be used for optimisation purposes. The optimal operation point can be difficult to maintain if disturbances and model uncertainty are present. Self-optimising control is an approach to solve this problem by turning the optimisation problem into a set-point problem. The key idea is to find a measurable variable with constant value at optimal operation. If this variable can be found, a feedback control loop is closed to keep the variable at the set point, and to keep indirectly the process at optimal operation. Since self-optimising control results in a feedback control loop, it

will be robust against disturbances and model uncertainties compared to any open loop model based optimisation methods. The idea of self-optimizing variables has been used several times to design the best control structure for different types of distillation columns [113][114].

The application of self-optimising control to the Petlyuk distillation column was studied by Halvorsen et al. [115, 116, 117]. Some candidate measurable feedback variables for the Petlyuk distillation column were proposed and analysed. Three output feedback variables give very good robust control of the column in a self-optimising control scheme. They are fractional recovery of the intermediate b-component leaving the prefractionator top (β), DTS (a measure of the temperature profile symmetry defined in the paper) and the c-composition of the net flow from the prefractionator distillate to the main column $y_{D1,c}$. For robustness against flow feed disturbances, β and DTS are better than the third one, because this last variable is a composition and not a recovery. For feed composition disturbances, β is the variable which maintains V closer to the minimum. However, DTS and $y_{D1,c}$ have also acceptable results. Facing feed vapour fraction disturbances, $y_{D1,c}$ is the best of the three but the other two are not far from it. Facing set point changes in the product compositions, DTS is again the best feedback variable, being β very close and $y_{D1,c}$ the worst of them. Lastly, DTS and $y_{D1,c}$ behave better in response to bad measurements of themselves than β. They have mentioned that in a real case, one of the three variables should be selected depending on the information about what are the more probable disturbances. Also technical aspects have to be considered. It has to be remarked, for example, that DTS can be calculated with only temperature measurements, which is a great advantage and on the contrary, the measurement of $y_{D1,c}$ and β involve composition measurements.

The full count of all possible combinations between potential manipulated and controlled variables may become very large especially for plant-wide control system design. Thus, the complete enumeration of all possible sets of controlled and manipulated variables would require great computational effort. There are some works on formulating this problem in the context of optimization (e.g. [118, 119, 120, 121] .

2.9 Conclusions

In this chapter, thermally-coupled columns were reviewed. A number of important issues must be considered during the design, for example, flexibilities to operating condition changes, and relation of design to process dynamics and controllability. They impose strict constraints on the energy efficiency that can be achieved. Therefore, trade-off between process design economics and process operation appears to be very important and has to be carried out with great caution.

It is important to recognize that the key to improving the design and energy efficiency of distillation systems is how their 'efficiency' is defined. If a column operates at a reflux ratio of 10% above the minimum reflux ratio it is generally considered reasonably efficient because the reboiler and condenser loads are close to the minimum for the particular separation. However, a much better indication of efficiency is found from thermodynamic considerations which take proper account of the degradation of energy in a process. When the column is operated optimally, the infinitestaged Petlyuk column always consumes less energy than the corresponding conventional solution. However, this optimal operation may be difficult to achieve in practice because the optimal operation depends strongly on the feed properties and the remaining degrees of freedom.

Chapter 3

Optimal Operation of Kaibel Distillation Columns

The objective of this chapter is to study the Kaibel distillation column from an operability point of view. Two different objectives, namely minimizing energy requirement at fixed product purities and maximizing product purities with a fixed boilup are considered. We have visualized the objective functions for the two cases as a function of operational degrees of freedom and conclude that operation with fixed product purities is the more difficult case from control point of view.

3.1 Introduction

The tight integration in the thermally-coupled columns make the design and control the column challenging, compared to the conventional sequence of simple columns. The design challenges have been mostly solved, but operation and control remains largely an open issue.

There are two main issues in terms of operation and control. First, the column, and in particular the column profile, needs to be "stabilized" to avoid drift [122]. This dynamic issue is not studied here. Second, the column needs to be operated as close to its optimum as possible in terms of minimum energy. This is mainly a steady-state issue and is our focus. It is important because a main motivation behind the Kaibel column is to save energy. Figure 3.1 and Table 3.1 show the alternatives which can be used for separating four products in conventional column arrangements and a comparison with energy requirement in the Kaibel arrangement. These are based on minimum energy requirement for the separations with 95% recovery. As an example, in the following, the V_{min} diagrams of all the columns in one of the alternatives, namely direct sequence, are presented in Figure 3.2. The idea of V_{min} diagram is presented by [123]. This will be described in detail in the next section.

Table 3.1: Energy requirements for 95% recovery with different simple column configurations and Kaibel arrangement.

	$\frac{V}{F}$ for Col.1	$\frac{V}{F}$for Col.2	$\frac{V}{F}$ for Col.3	Sum
Direct sequence	1.2109	0.6984	0.6133	2.5227
Indirect sequence	1.1021	0.9471	0.8793	2.9285
Direct-Indirect sequence	1.2109	0.8732	0.6361	2.7202
Indirect-Direct sequence	1.1021	0.9372	0.6270	2.6663
Prefractionator	1.0376	0.6137	0.8795	2.5308
Kaibel (Figure 3.12)				1.8007

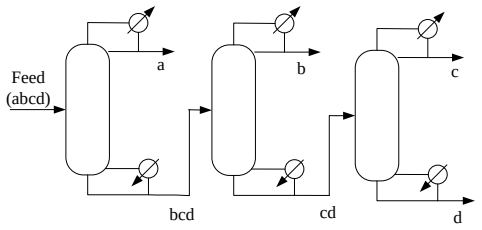

(a) Direct sequence

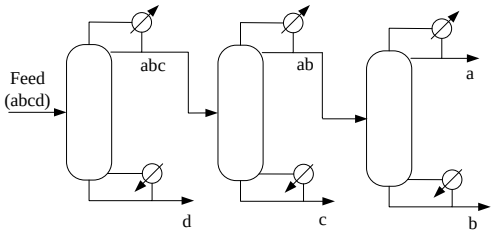

(b) Indirect sequence

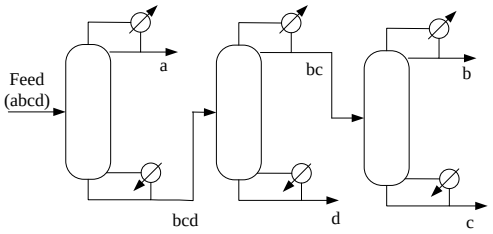

(c) Direct-Indirect sequence

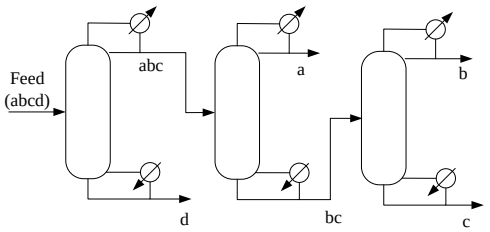

(d) Indirect-Direct sequence

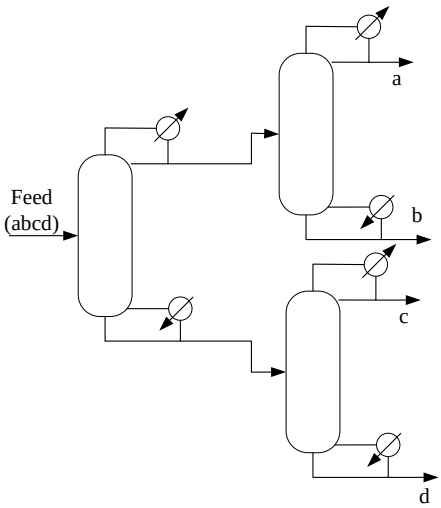

(e) Prefractionator arrangement

Figure 3.1: Simple column configuration for a four-component mixture

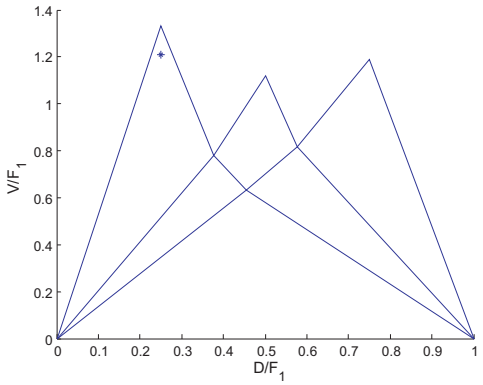

(a) V_{min} diagram of Column 1 in Direct sequence

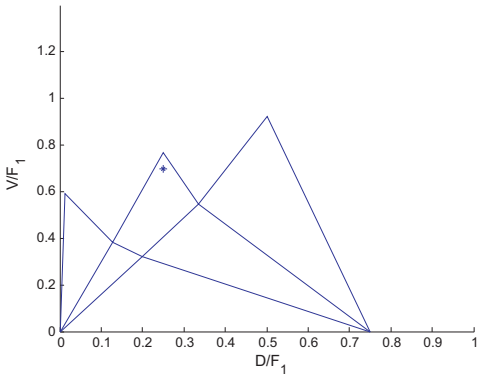

(b) V_{min} diagram of Column 2 in Direct sequence

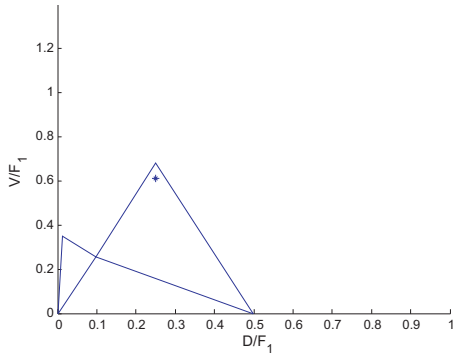

(c) V_{min} diagram of Column 3 in Direct sequence

Figure 3.2: V_{min} diagram for direct sequence of columns for separating the four components under study. The operating point for each column is shown with (*)

3.2 V_{min} Diagrams

The V_{min} diagram can be constructed for any mixture by simulating a column with a large number of stages, but it is most easily constructed for ideal mixtures based on the Underwood equations. In this section, the V_{min} diagram concept is shortly described (for more information please refer to [123], [124]). V is the vapour flow in the column, and subscript "min" is used because we consider the limiting case with infinite number of stages. The V_{min} diagram gives a lot of insight for design, operation and control of the column and has been successfully used to design thermally coupled columns (e.g. [125]).

3.2.1 V_{min} diagram basis

The basis for the V_{min} diagram is a conventional two-product distillation column with an infinite number of stages. With a given feed, such a column has two steady-state degrees of freedom. So, the entire operating range can be visualized in two dimensions, even with an arbitrary number of feed components. In the V_{min} diagram, these two dimensions are chosen to be vapour flow per unit feed (V/F) and the product split, expressed by the distillate (D/F). The choice of vapour flow rate on the ordinate provides a direct visualization of the energy consumption and column load. So, for every possible operating point given by the set of recoveries, we want to find the

normalized vapour flow rate (V/F), the overall product split (D/F or B/F), and the product distribution.

The V_{min}-diagram in Figure 3.3 illustrates how the feed components for a ternary feed (with components a, b and c) are distributed to the top and bottom products in a simple two-product "infinite stage" distillation column as a function of the product split (D/F). The "mountain-like" boundary ([0,0]-P_{ab}-P_{ac}-P_{bc}-[1,1 – q]) gives V/F when we have pure products. For values above the boundary, we are actually wasting energy. So, an important boundary is the transition from $V > V_{min}$ above boundary to $V = V_{min}$. The peak values give the vapour flow requirement for the corresponding sharp neighbour component splits. The knots (bottom of the valleys) are V_{min} for the so-called "preferred splits" where we specify sharp split between two key components (components a and c), while we allow intermediate components (component b in this example) to be freely distributed. As the vapour flow V is reduced below the boundary for a given D, we no longer have sharp splits. Note that the V_{min} diagram is as exact as the method used to calculate the internal streams. For example, if the Underwood method is used for the shortcut calculation of the internal flows, the underlying assumptions of constant relative volatilities and constant molar flows are required for the V_{min} diagram too. However, the V_{min} diagram can also be generated by simulations for real mixtures (see section 5). In a general case with N_c components, there are $N_c(N_c-1)/2$ peaks and knots: N_c-1 cases with no intermediates (e.g., a/b, b/c, c/d, ...) which are the peaks in the V_{min} diagram, N_c-2 cases with one intermediate (e.g., ac, bd, ce, ...), which are the knots between the peaks. On a first glance of Figure 3.3, we can say that the b/c split is the most difficult separation, since it is the highest peak.

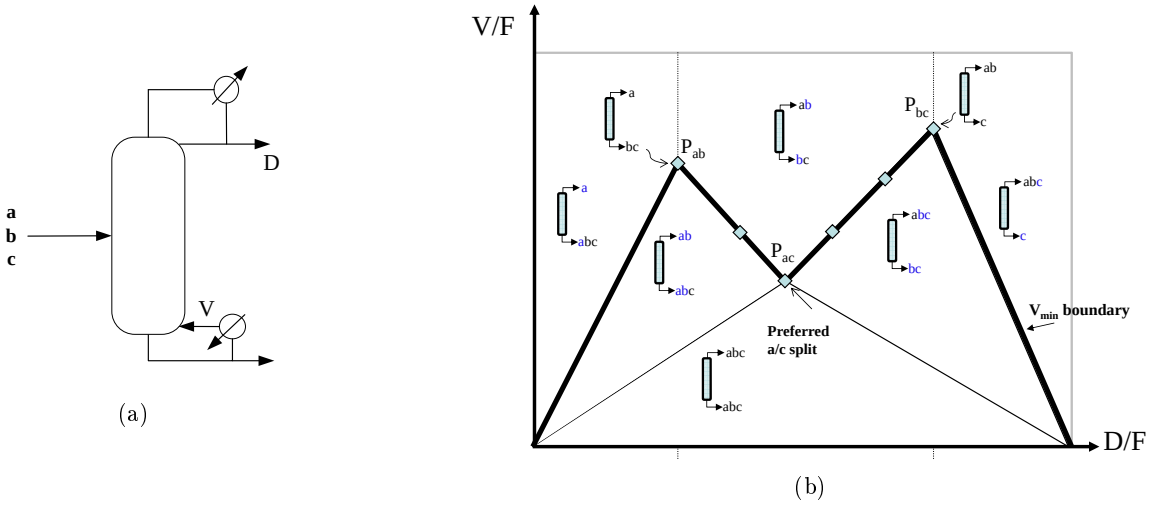

Figure 3.3: V_{min} diagram for a ternary feed

3.2.2 V_{min} diagram for Conventional Column Sequences

The peaks show the energy needed for the sharp split of two consequent components, e.g. a/b, b/c and c/d from the right for four-component system, and the valleys show the energy needed for non-consequent components, i.e. a/c and b/d for four-component system. The down-most valley is for the so-called "preferred split" ([126]), that is the minimum energy operating point for the a/d split. The diagrams are based on sharp splits and the operating point for each column is shown by a star (∗), which is 95% recovery in our study. Figure 3.2(a) shows the V_{min} diagram for the first column. Here, we have a separation between components a and b with 95% recovery. So, the star shows the operating point for column 1. The distillate flow of column 1 is around 25% of the original feed. The next column has a feed of 75% of the original feed and

different feed composition. The task of second column is to separate components b and c with 95% recovery. The first peak in Figure 3.2(b) is because of the non-sharp split in the previous column. In the case of sharp splits, we will have only two peaks for the second column and 1 for the third column. The energy demand for separating the four components will be the sum of $\frac{V}{F1}$ in all the columns. The minimum energy requirement for a full extended Petlyuk arrangement is simply given by the highest peak in the V_{min} diagram in Figure 3.2(a). Since we have to add the contributions from the peaks in Figures 3.2(b) and 3.2(c) for obtaining the direct split sequence, we clearly see that it is outperformed by the Petlyuk arrangement. For the Kaibel column, the resulting V_{min} diagram is shown in Figure 3.11. The dashed peaks are obtained by computing a new V_{min} diagram for the upper and lower part of the product columns in the prefractionator arrangement shown in Figure 3.1(e), assuming the equivalent liquid fraction obtained with a fully thermally coupled connection from the prefractionator when it performs the sharp ab/cd split.

3.2.3 V_{min} diagram for 4-product Petlyuk arrangement

Here, we consider the separation of four components. Before deriving the overall minimum vapour flow for the Kaibel column, let us consider the more complex but more energy-efficient extended Petlyuk arrangement for separating four products shown in Figure 3.4. The feed specifications and relative volatilities used to sketch the minimum energy diagram in Figure 3.4 are:

$$\begin{aligned} z_F &= [\ 0.25 \quad 0.25 \quad 0.25 \quad 0.25\ ] \\ q &= 1, \text{ (Liquid feed)} \\ \alpha &= [\ 6.704 \quad 4.438 \quad 2.255 \quad 1\ ] \end{aligned}$$

The minimum total vapour flow requirement in a Petlyuk arrangement is given by the highest peak in the V_{min} diagram [123]. For example, the minimum vapour requirement for a 4-component feed (abcd), which is separated into 3 products (a/b/cd) will be

$$V_{T,min,Petlyuk}\left(a/b/cd\right) = \max\left(V_{min,2P}\left(a/b\right), V_{min,2P}\left(b/cd\right)\right)$$

where the subscript T refers to the vapour flow in the top of the Petlyuk column, and the subscript $2P$ refers to conventional columns with two products (Figure 3.3a). This expression requires that every internal column in the arrangement is operated at its preferred split [126]. All the internal flows can also be obtained from V_{min} diagram [41]. Note that the minimum energy which should be provided by the reboiler for the case with constant molar flows is

$$V_{B,Petlyuk} = V_{T,Petlyuk} - (1-q)F$$

where q is the liquid feed fraction.

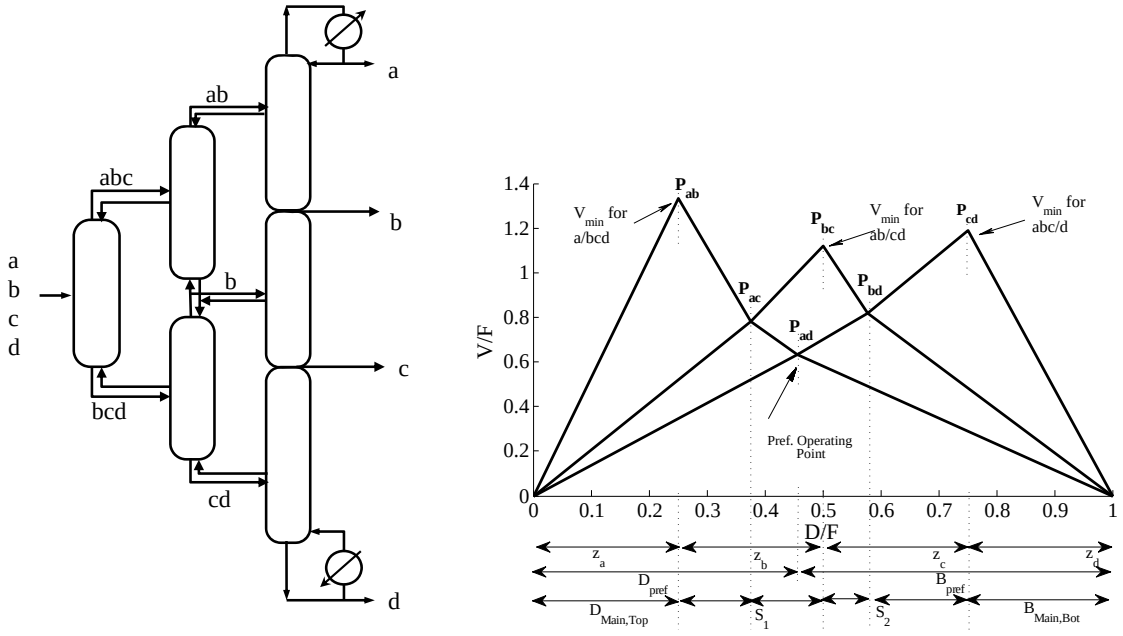

Figure 3.4: V_{min} diagram for a 4-product Petlyuk column

3.2.4 V_{min} diagram for a Kaibel column

In the Kaibel-arrangement, the prefractionator is not operated at the preferred split, but performs a sharp ab/cd split. The succeeding "main column" performs the a/b split in the top and the c/d split in the bottom. The middle section between the b and c outlet should be operated at full reflux ($V \approx L$) without any net transport of components, since the b/c split is already obtained in the prefractionator. The minimum vapour flow requirement in the main column is given by the highest requirement from the a/b or the c/d split. The minimum vapour flow requirement in the Kaibel column is always outperformed by the full Petlyuk arrangement. This difference can be high or small depending on feed properties [43].

The V_{min} diagram in Figure 3.5 (which is identical to the one in Figure 3.4) is the V_{min} diagram for the prefractionator of the Kaibel column. As mentioned earlier, the task of the prefractionator is to perform a sharp b/c split. So, the important information to be obtained from the V_{min} diagram in Figure 3.5 is the vapour flow V_{1t}, and the net flow D_1 associated with the peak P'_{bc}.

While for the Petlyuk arrangement, all information can be obtained from the standard V_{min} diagram, the Kaibel column requires additional computations for the main column, from which we obtain the corresponding vapour flows V_{2t} and V_{3b} (see Figures 3.6 and 3.7). These are obtained using the approach explained in [43] (see Appendix).

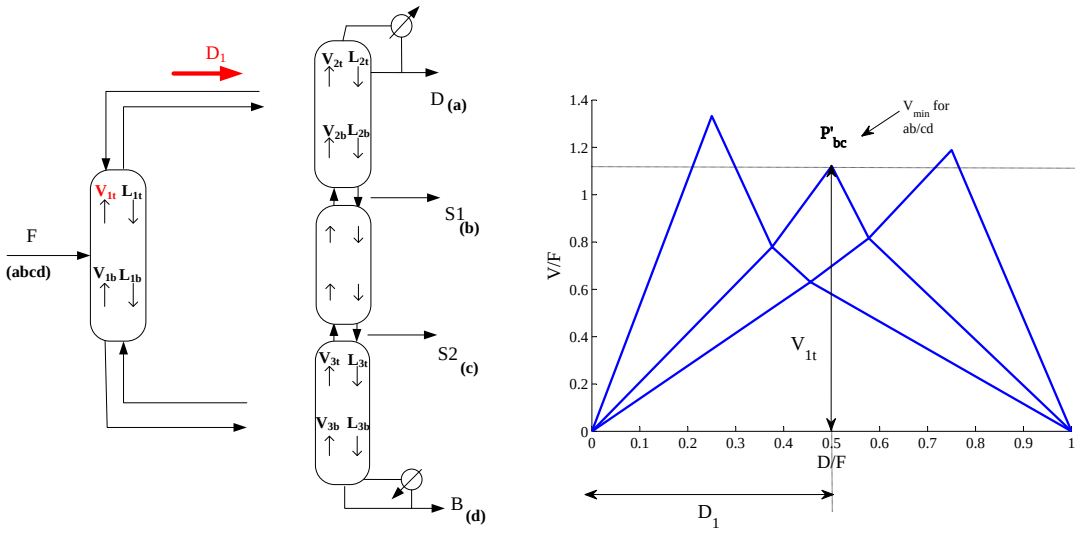

Figure 3.5: V_{min} diagram for the prefractionator of Kaibel distillation column (b/c split)

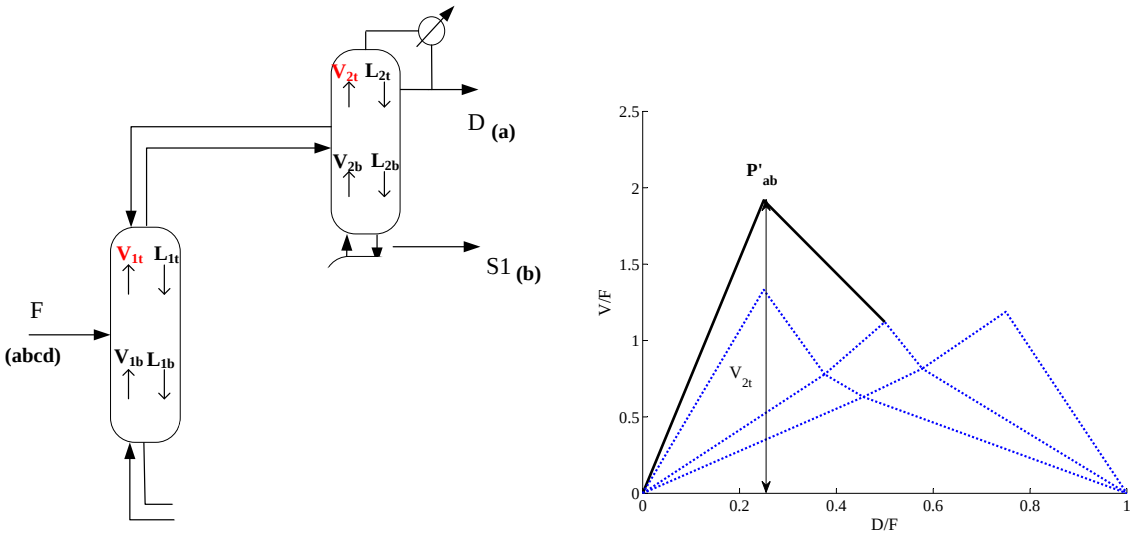

Figure 3.6: V_{min} diagram for the top main section of Kaibel distillation column (a/b split)

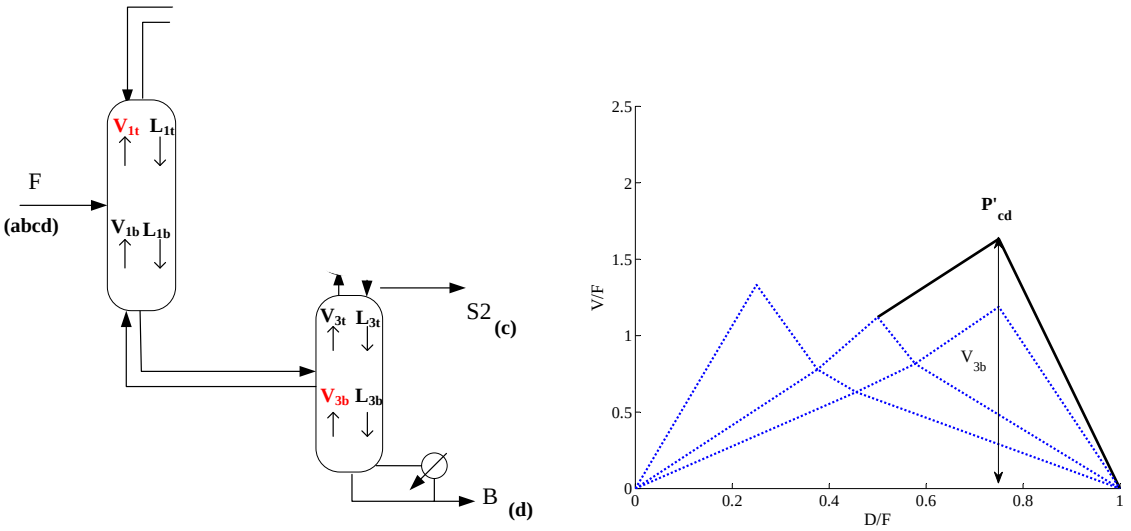

Figure 3.7: V_{min} diagram for the bottom main section of Kaibel distillation column (c/d split)

Figure 3.8 shows the final V_{min} diagram for a 4-product Kaibel column made by combining Figures 3.5, 3.6 and 3.7. As it is seen from the figure, the most difficult split is taking place in the top main section where we perform the a/b split. So, the total vapour requirement of the column is dictated by the peak P'_{ab} and we have $V_{min} = V_{2t}$. This will lead to excess energy in the other section of the column. Note that from this point on, for the sake of simplicity, we have kept only those parts of the diagram which are specific for the Kaibel distillation column, which correspond to the upper solid line in Figure 3.8.

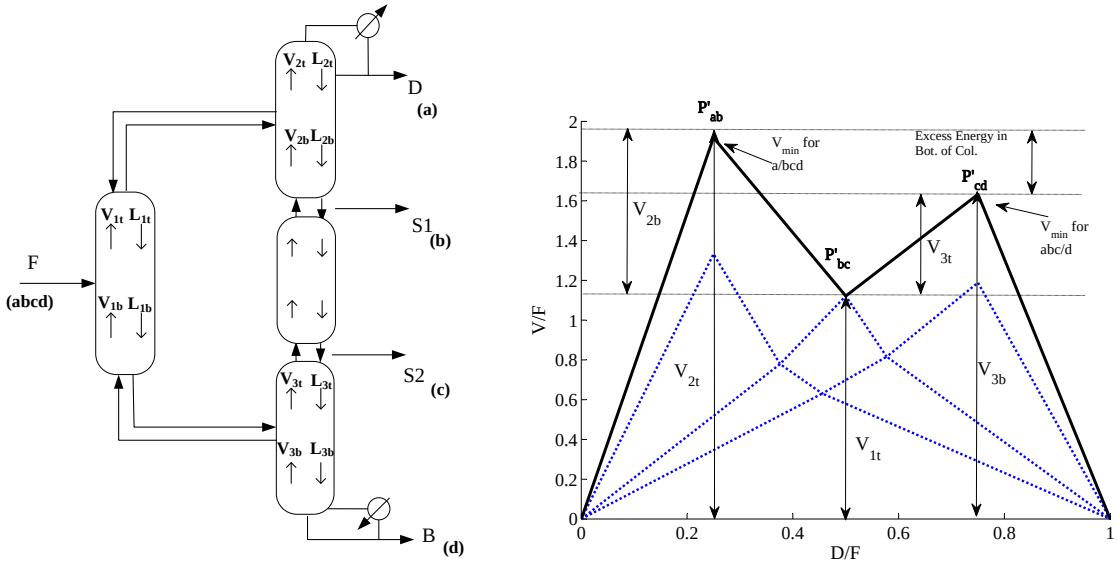

Figure 3.8: V_{min} diagram for Kaibel distillation column

As it is reported in Table 3.1, Kaibel column is the winner of all the alternatives from energy requirement point of view. The value reported in the table for Kaibel column comes from the assumption of sharp split between b and c in the prefractionator. In practice, there will be some allowance for the impurities of the key components b and c in top and bottom of prefractionator, which leads to even less amount of vapour requirement for the whole column. This can simply be checked by sketching the objective function (here: total amount of vapour fed to the Kaibel

column) as a function of impurities in the top and bottom of the prefractionator from a rigorous simulation.

3.2.5 V_{min} diagram for Kaibel column using Underwood equation

In this section, we show how to obtain the minimum vapour flow requirements for Kaibel distillation column from the Underwood equation. This assumes constant relative volatility (α) and constant molar flows. The minimum vapour flow rate at the top of the prefractionator is expressed analytically by the Underwood expression [127]:

$$\frac{V_{1t}^{b/c}}{F} = \frac{\alpha_a z_a}{\alpha_a - \theta_b} + \frac{\alpha_b z_b}{\alpha_b - \theta_b}$$

Here θ_b is the middle common Underwood root found from the feed equation:

$$\frac{\alpha_a z_a}{\alpha_a - \theta} + \frac{\alpha_b z_b}{\alpha_b - \theta} + \frac{\alpha_c z_c}{\alpha_c - \theta} + \frac{\alpha_d z_d}{\alpha_d - \theta} = 1 - q$$

The actual roots of the prefractionator will be the common roots for the next section. The following equations show the minimum requirements in the top and bottom of the main column [43].

$$\frac{V_{2t}^{a/b}}{F} = \frac{\alpha_a z_a}{\alpha_a - \theta_a^{2t}} = \frac{\alpha_a z_a}{\alpha_a - \phi_a}$$
$$\frac{V_{3b}^{c/d}}{F} = \frac{\alpha_d z_d}{\alpha_d - \theta_a^{3b}} = \frac{\alpha_d z_d}{\alpha_d - \psi_c}$$

3.2.6 V_{min} diagram from rigorous simulation

In this section, we study the minimum energy diagram with a finite (but large) number of stages using rigorous simulations. This is to check the validity of the V_{min} diagrams which are obtained by ideality assumptions.

Table 3.2 shows the procedure for obtaining the V_{min} diagram using rigorous simulations. Each row in Table 3.2 corresponds to one line in the V_{min} diagram. For each line, one recovery is fixed. The simulations are done for a conventional column with four components. The recovery can be used as one of the two specifications which are needed to specify the column using the simulator ([128]). The other specification is chosen to be the distillate flow rate. So, by keeping a recovery constant and increasing the distillate flow rate, the points on each line are obtained. When the recovery specifications for the peaks or valleys are reached, the recovery specifications for the next line should become active to continue the simulation (see Table 3.2).

In the ideal V_{min} diagram, it is only the peaks and valleys which are calculated. The boundary lines to separate different regions come from connecting these points. This is why the lines go to the origin. For a real column, we should start with a feasible point. This is because it may not be possible to get a certain recovery with any amount of distillate flow. We need to start from higher distillate flow rates if the recovery specification is high. The first boundary line is made by specifying the recovery of component b in the bottom ($R_{b,bot}$) at the upper bound (UB). The distillate flow rate is increased until the point where the recovery of component a in the top ($R_{a,top}$) reaches the specified value. The specifications for other boundary lines are given in Table 3.2.

The infeasible area should be avoided. The area below the line $V = D$ is infeasible since all liquid and vapour streams above and below the feed have to be positive. So, in every step, we

Table 3.2: Procedure of constructing the V_{min} diagrams using rigorous simulations

Line	Specifications
0 - a/b,	$R_{b,bot} = UB$, Increase D while $R_{a,top} < UB$
a/b - a/c,	$R_{a,top} = UB$, Increase D while $R_{c,top} < LB$
a/c - b/c,	$R_{c,bot} = UB$, Increase D while $R_{b,top} < UB$
b/c - b/d,	$R_{b,top} = UB$, Increase D while $R_{d,top} < LB$
b/d - c/d,	$R_{d,top} = UB$, Increase D while $R_{c,top} < UB$
c/d - end,	$R_{c,top} = LB$, Increase D while $R_{a,bot} < LB$

R =Recovery UB =Upper bound LB =Lower bound

should check if the operating point hits the infeasible region or not. The net liquid molar flow in the top section (second stage) is the criterium and it should not become negative. When the $V = D$ line is crossed, we discontinue the current line and the line $V = D$ is followed up to the point where the criterium of the next line is met.

Figure 3.9 shows the V_{min} diagrams for a four-component column with fifty stages for different recoveries. It is shown that the difficult split changes depending on the product recoveries. Figure 3.10 shows the V_{min} diagrams for 99% recovery for all the main products and with different numbers of stages. As the number of stages become larger, the V_{min} diagram becomes more similar to the ideal V_{min} diagram. As expected, when the number of stages gets relatively low, the peak V increases sharply. It would go to infinity as we reach N_{min} for the section in question.

3.3 Operation

In terms of optimal operation, it is usually assumed that the objective is to make products of given purity using the minimum energy. However, in practical operation this is often not the issue, but rather to make the purest possible products with a given energy, especially when there is a bottleneck in the plant. Both these cases are discussed here. We are going to study how the mode of operation is going to affect the behaviour of the column and as a result the ease of operating the column. Controllability has been studied by some researchers ([129];[111];[104]) for a three-product dividing wall column. The four-product Kaibel column is more complex and the analysis in this chapter addresses the more basic problem of understanding the column behaviour at and around the optimal operating point. The insight gained can be used to select a suitable operation target and optimizing control strategy.

So, the two modes of operation which are studied here are as below:

- Mode 1: minimize energy requirement for fixed product purities.
- Mode 2: maximize the product purities with constant boilup (i.e., minimize impurity sum).

3.4 System under study

The system under study is shown in Figure 3.12 and is considered for separation of the first four simple alcohols (methanol, ethanol, 1-propanol, 1-butanol) and the feed is equi-molar. Figure 3.12(b) shows the schematic of the Kaibel column built in NTNU ([130]). This process is simulated as a 4-column model in HYSYS. It allows flexibility regarding the specifications in different column sections. The pumps and valves are placed to compensate the pressure difference between two column sections in two sides of the wall. In reality different packing structures are used for this purpose. As it is clear from Figure 3.12(c), there are twelve stages in each subsection in the main column. The number of stages in the prefractionator is equal to the number of stages in

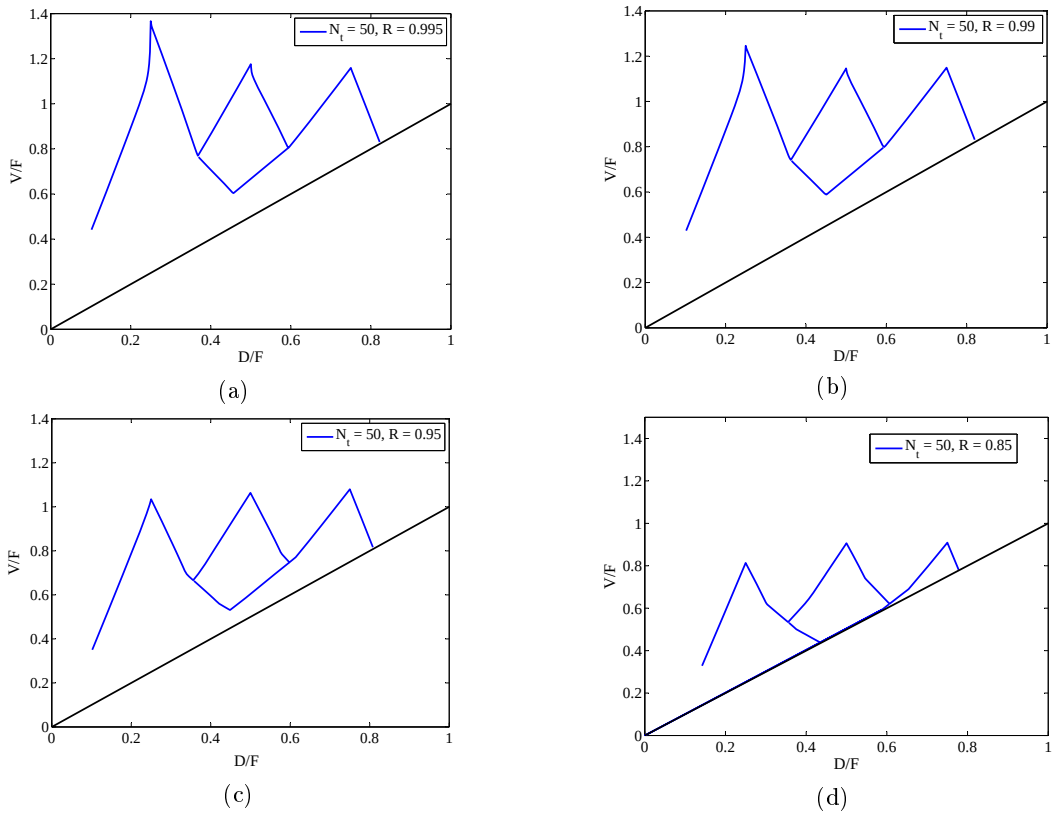

Figure 3.9: V_{min} diagrams for different recoveries using rigorous simulations

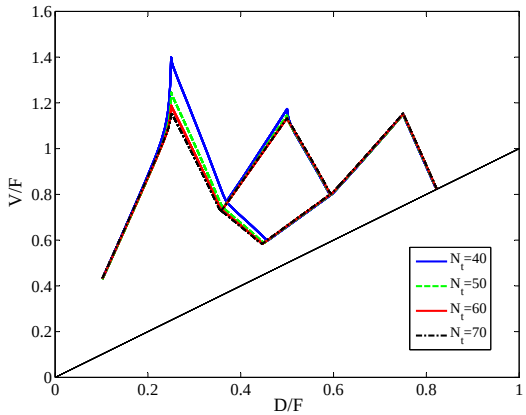

Figure 3.10: V_{min} diagrams for 99% recovery with different numbers of trays from rigorous simulations

the other side of the wall. It is assumed that the number of stages in all sections are fixed and they are not included in optimization.

To achieve the liquid split, a practical solution would be to draw off all liquid above the partitioning wall and transfer it to an intermediate holdup-tank before pumping and metering the liquid back to the column on either side of the dividing wall. Some alternative methods have been reported by the industrial manufacturers ([131]). Note that liquid split (R_L) is defined as the ratio of the liquid entering the top of the prefractionator to the liquid coming from the top of the main column to the liquid splitter and vapour split (R_V) is defined as the ratio of the vapour entering the bottom of the prefractionator to the vapour entering the vapour splitter from bottom of the main column.

In the case of the vapour split, the situation is quite different. Except for [130], there are no reports of adjustable vapour splits in the literature, nor has it been reported in any industrial implementations. Usually the detailed design will determine the best position of the wall and the pressure drop either side of the partitioning will determine the vapour split ratio. One can argue that if the desired vapour split ratio is not achieved it can be compensated by adjusting the liquid split. This is true up to a point, but if the ratio is too far off from the optimal value the product purities or at least the column efficiency will suffer. However, in case of manipulating vapour split, we have an extra degree of freedom for control that could be used to increase purities or make the separation more energy efficient in the face of process disturbances ([131]). Figure 3.11 shows the minimum energy diagram for the case under study. For every possible operating point, the normalized vapour flow rate (V/F), the overall product split (D/F or B/F), and the distribution (given by a set of recoveries) is shown. Note that the peaks and valleys are only valid. They are calculated based on the Underwood equations.

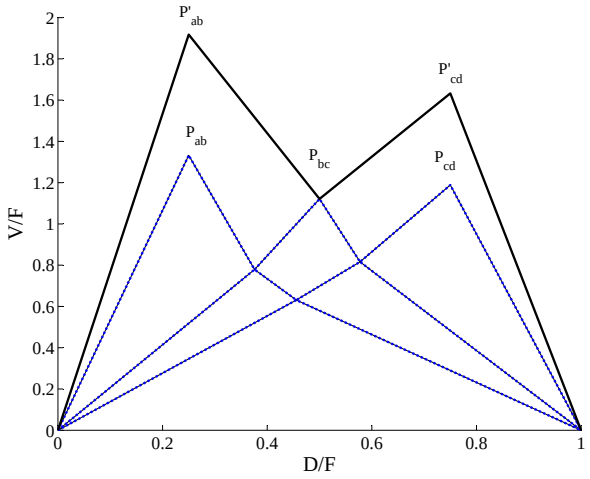

Figure 3.11: Minimum energy diagram (solid lines) for the equimolar mixture of methanol, ethanol, 1-propanol, 1-butanol. The highest peak (P_{ab}) gives the minimum boilup for petlyuk arrangement. The dotted line is for the Kaibel column and the highest peak (P'_{ab}) gives the minimum biolup.

The peaks at the dashed lines in Figure 3.11 give the vapour flow rate requirement to separate a/b and c/d in a Kaibel column, when the prefractionator does a sharp ab/cd split. The highest peak (here P_{ab}) determines the overall energy requirement of the Kaibel column, so the lower part of the column has more energy available than required. This can be utilized to obtain somewhat higher purity in the other section of the column or to reduce the number of stages. The other point is that unlike Petlyuk configuration where we normally have a certain slack in the prefractionator operation regarding distribution of the intermediate components (b and c),

the Kaibel-column prefractionator must perform a relatively sharp split between streams ab and cd, given by the P_{bc} in the V_{min}-diagram. We can find a certain slack if we allow nonsharp split in the Kaibel configuration, but this is limited by the product specifications. Prefractionator operation with higher vapour rate than at P_{bc} could give us some slack also for sharp ab/cd split, but this will lead to higher vapour requirement to split a/b and c/d in the succeeding sections.

Figure 3.13 shows an alternative structure which could be used for obtaining good estimates for flows as initial values using the information from V_{min}-diagram. The number of degrees of freedom in this structure is again six and all of them are for the main column (four product compositions and two flowrates of the streams going back to the prefractionator). We use the minimum rates from minimum energy diagram together with the pinch point compositions [123] at the ends of the prefractionator from the ideal model as an initial guess. The flow rates and compositions of the returning streams (R2 and VB2) to the prefractionator should match the ones entering the prefractionator column (R1 and VB1). So, by setting the compositions of the entering streams (R1 and VB1) from pinch point calculations, and the flow rates of the returning streams from the V_{min} diagram, we will have some iteration to adjust the flow rates of the entering streams, so that the compositions of the returning streams match the ones of the entering streams. The split values from this simulation are used in the original model to find the minimum energy required for the separation. This model is mainly used for the cases where we had problem in convergence, especially for the mode of minimizing energy requirement.

3.5 Minimize energy requirement (mode 1)

The objective is here to minimize the energy requirement with given purities of the four products. The cost function J to be minimized is therefore selected to be the boilup rate

$$J = V$$

For mode 1 where the products purities are fixed, there remain two degrees of freedom (vapour and liquid splits) which should be used to minimize energy requirement. The other degrees of freedom are used to satisfy the product purities specifications. Since the product purities are constraints, the splits are inter-related and cannot be changed independently as optimization variables to get to the minimum energy requirement. So, it is difficult to run the optimization program as it is done for the other mode. Therefore, to get a feeling about where the optimum is, the minimum vapour rates is found from the V_{min}-diagram ([43]). Figure 3.14 shows the optimal composition and temperature profiles for the nominal case and different disturbances. We will discuss about Figure 3.14(b) more in the next section.

Visualization of the cost function gives a qualitative insight into the problem at hand. Since there are two optimization variables, the solution surfaces can be shown in two-dimensional plots. The contours of the objective value are shown in Figure 3.15. In the 3-dimensional graph, they are like thin bended cones. The cross-sectional area of the cone will increase as boilup flow rate increases. This figure also shows that for the case which feed quality is zero, R_L is greater than R_V, especially near the optimal point. The opposite is seen for the case of q = 1. The reason is quite obvious (e.g. for q = 0, since a part of vapour needed for separation is provided by the feed itself, so it needs more liquid than vapour to contact). Note that this cannot be generalized. For other feed compositions or relative volatilities, this is not followed.

There exists multiplicity in the solution. This can be seen in Figure 3.16(a) as we get two different boilups when all the specifications are set and the system is defined. This is due to two different ways for impurity flows to go to products ([24]), namely from top or bottom of the prefractionator (see Figure 3.16(b)).

Figure 3.17 shows the dependency of boilup rate on the vapour split as the liquid split changes over a wide range. It shows the general trend of change of the minimum vapour as the splits are

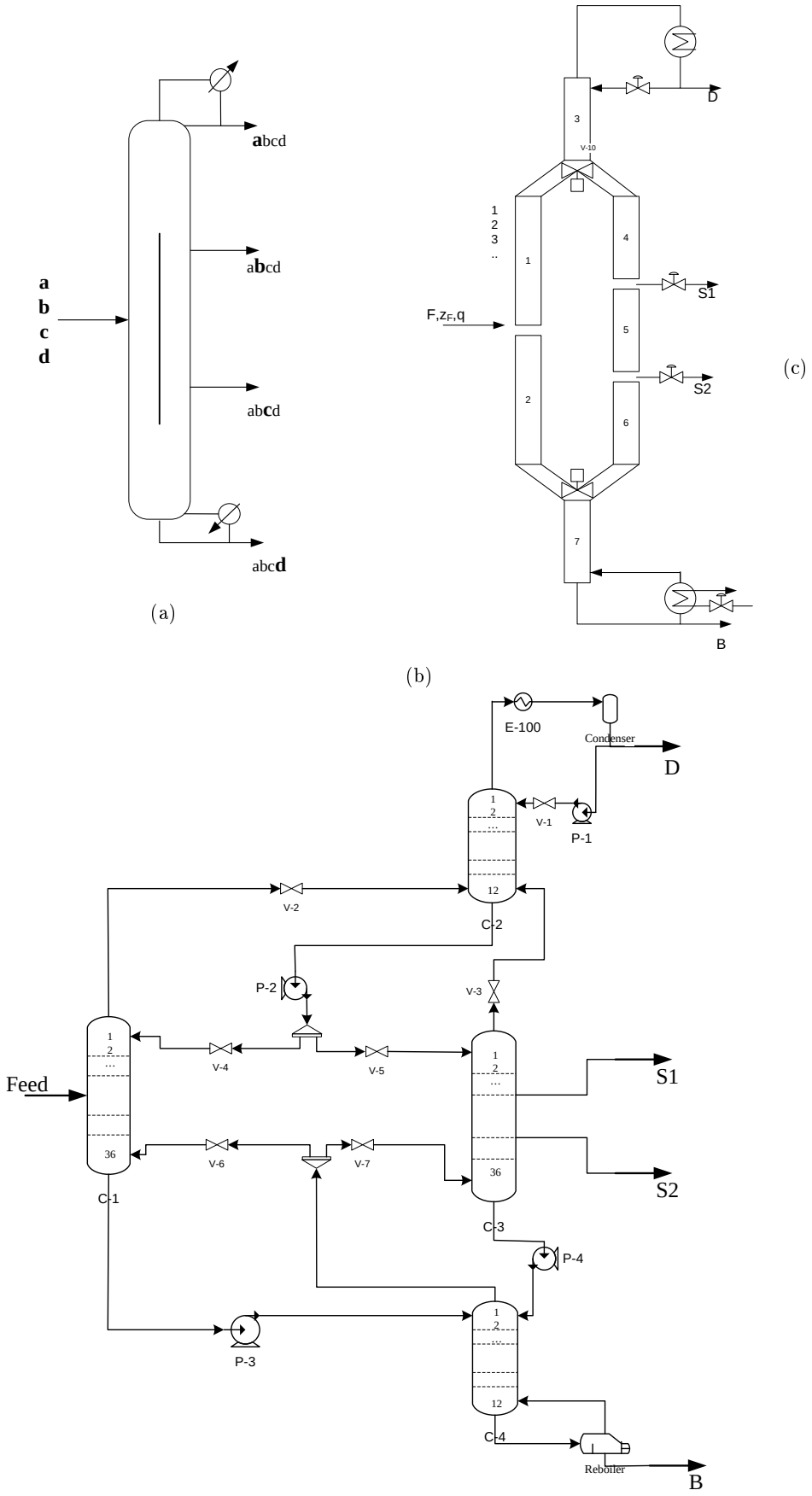

Figure 3.12: (a) 4-Product dividing-wall column schematic, (b) schematic of the lab Kaibel column at NTNU, and (c) HYSYS simulation

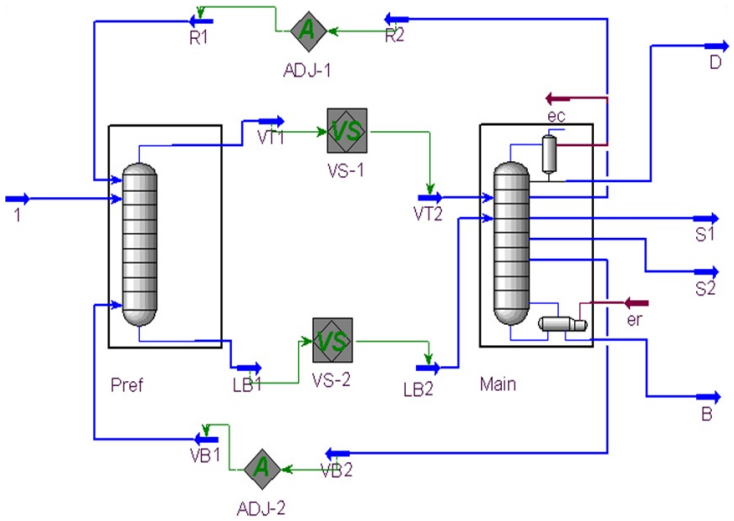

Figure 3.13: HYSYS simulation that uses the information from V_{min} diagram to obtain initial estimates for the detailed simulation.

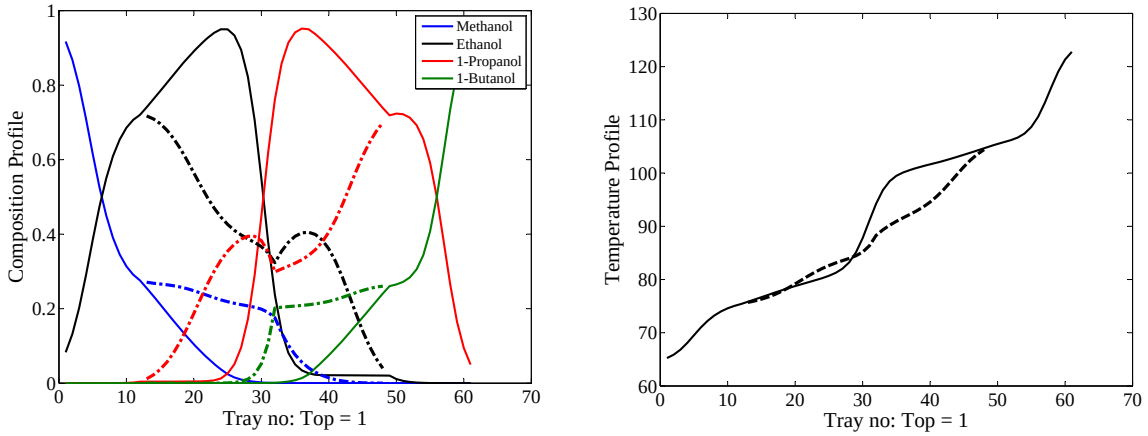

(a) (b)

Figure 3.14: Mode 1: optimal composition and temperature profiles. (a) Optimal composition profile for nominal case, prefractionator: dashed lines; main column: solid lines (feed liquid fraction = 1). (b) Optimal temperature profiles for nominal case and various disturbances in feed compositions (5%), liquid fraction (10%) and feed flowrate 10%), prefractionator: blue lines; main column: black lines (feed liquid fraction = 1).

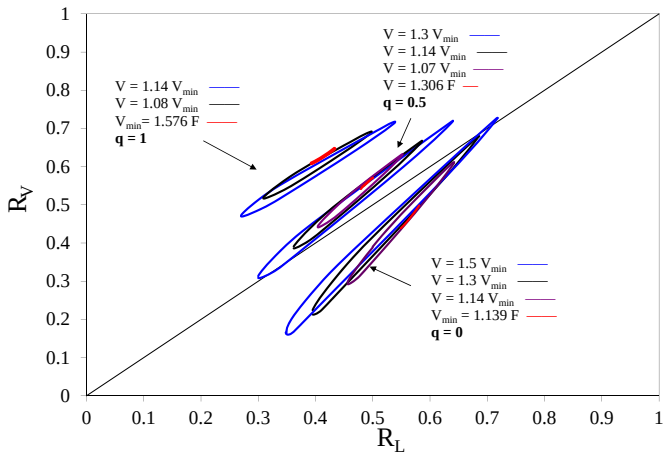

Figure 3.15: Mode 1 (fixed purities of 95% for all products): contours of boilup as a function of liquid and vapour splits for liquid feed (q = 1), two-phase feed (q = 0.5) and vapour feed (q = 0).

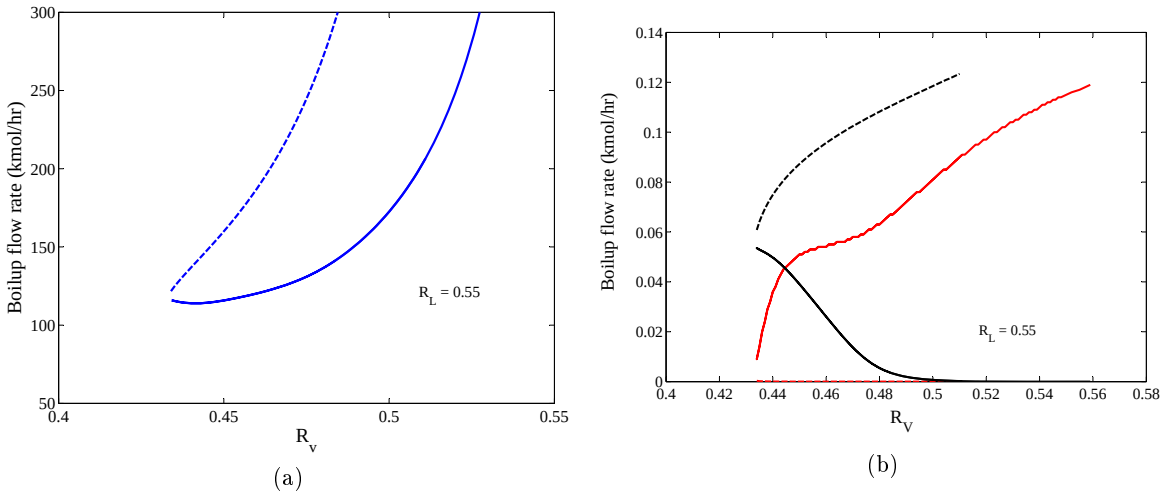

Figure 3.16: Mode 1 (fixed purities of 95% for all products): (a) boilup rate as a function of vapour split (Rv) with fixed liquid split. (b) Impurities of C2 and C3 in the ends of prefractionator, red for C3 and black for C2 respectively. The solid lines in figure (a) correspond to the solid line in figure (b) (feed liquid fraction = 0).

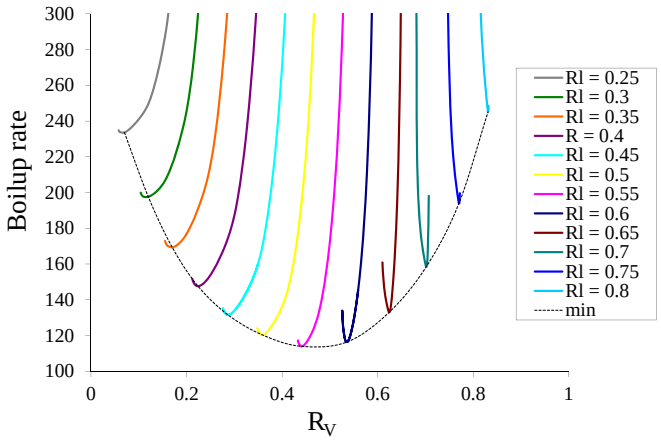

Figure 3.17: Mode 1 (fixed purities of 95% for all products): boilup rate versus vapour split (Rv) at different values of liquid split (feed liquid fraction = 0).

changing and the span for one split value in which there is a feasible solution as the other one is fixed. Also, the location of minimum is clearer in this figure.

As mentioned previously, in industrial practice it is not common to adjust the vapour split online. It will normally be given by the dividing wall placement and flow/pressure characteristics of the packings and the liquid load on each side. The results show that the optimal operating region (somewhat close to minimum energy point) is narrow and we are actually forcing the process to go through a very restricted area to reach the purity specifications. So, the liquid split has to be adjusted carefully to obtain minimum energy.

3.6 Maximize product purities with fixed boilup rate (mode 2)

The objective function is here to maximize the purity of the products with a given energy, that is, with fixed boilup (V). The cost function J to be minimized can be defined as the sum of the impurities in the products,

$$J = D(1 - x_D) + S1(1 - x_{S1}) + S2(1 - x_{S2}) + B(1 - x_B)$$

Two different cases that will lead to this mode are ([131]:

1. If all the prices for the products are equal, but we get paid for the main component only in each product.

2. If products S1 (upper side stream) and B (bottom product) have zero value (or same value as the feed) and for the valuable products S2 and D we only get paid for the main component. In this case all impurities give losses.

The optimal steady state solution is reached with a specified boilup rate and with the other degrees of freedom optimized such that the products will be as pure as possible. Table 3.3 shows the results of optimization for the two cases studied. The numbers in bold in each column are fixed during the optimization. The optimal composition and temperature profiles for the nominal case and different disturbances are shown in Figure 3.18. It is seen that the temperatures in the middle stages (stages 15-33) of main column and middle of the prefractionator remain constant after optimizing for different disturbances. So, these temperatures are good candidates as controlled

Table 3.3: Optimal steady-state solution (equimolar feed of 100 kmol/h which is saturated liquid).

	Mode 1	Mode 2
R_L	0.42	0.4009
R_V	0.635	0.6179
Reflux ratio	6.127	6.375
D flow rate (kmol/h)	25.33	24.43
B flow rate (kmol/h)	25.68	24.41
S1 flow rate (kmol/h)	24.32	24.93
S2 flow rate (kmol/h)	24.67	26.22
V (kmol/h)	157	157
Q (kW	1842	1842
Objective value	157	157
Purity of methanol in D	95 %	97.66 %
Purity of ethanol in S1	95 %	94.19 %
Purity of 1-propanol in S2	95 %	93.48 %
Purity of 1-butanol in B	95 %	99.28 %

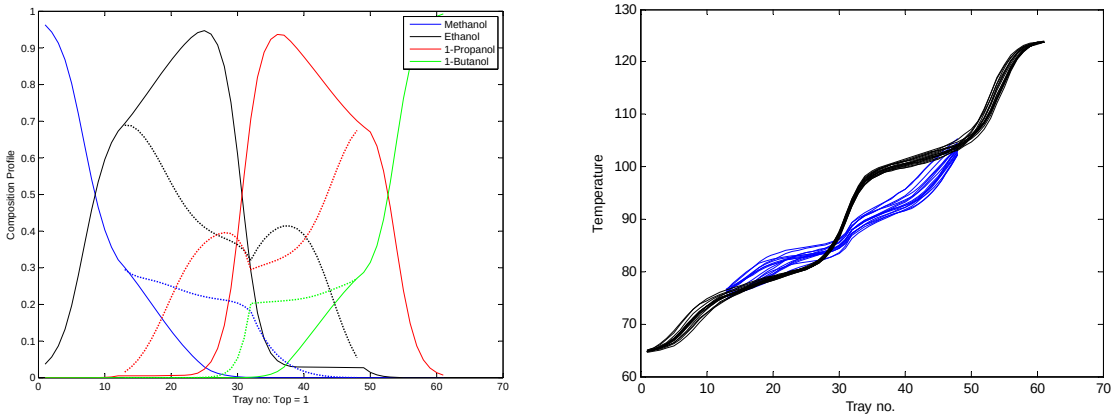

(a) (b)

Figure 3.18: Mode 2: optimal composition and temperature profiles for nominal case. (a) Optimal composition profile for nominal case, prefractionator: dashed lines, main column: solid lines (feed quality = 1). (b) Optimal temperature profiles for nominal case and various disturbances in feed compositions (5%), liquid fraction (10%), boilup flow setpoint (10%) and feed flowrate 10%), prefractionator: blue lines; main column: black lines (feed quality = 1).

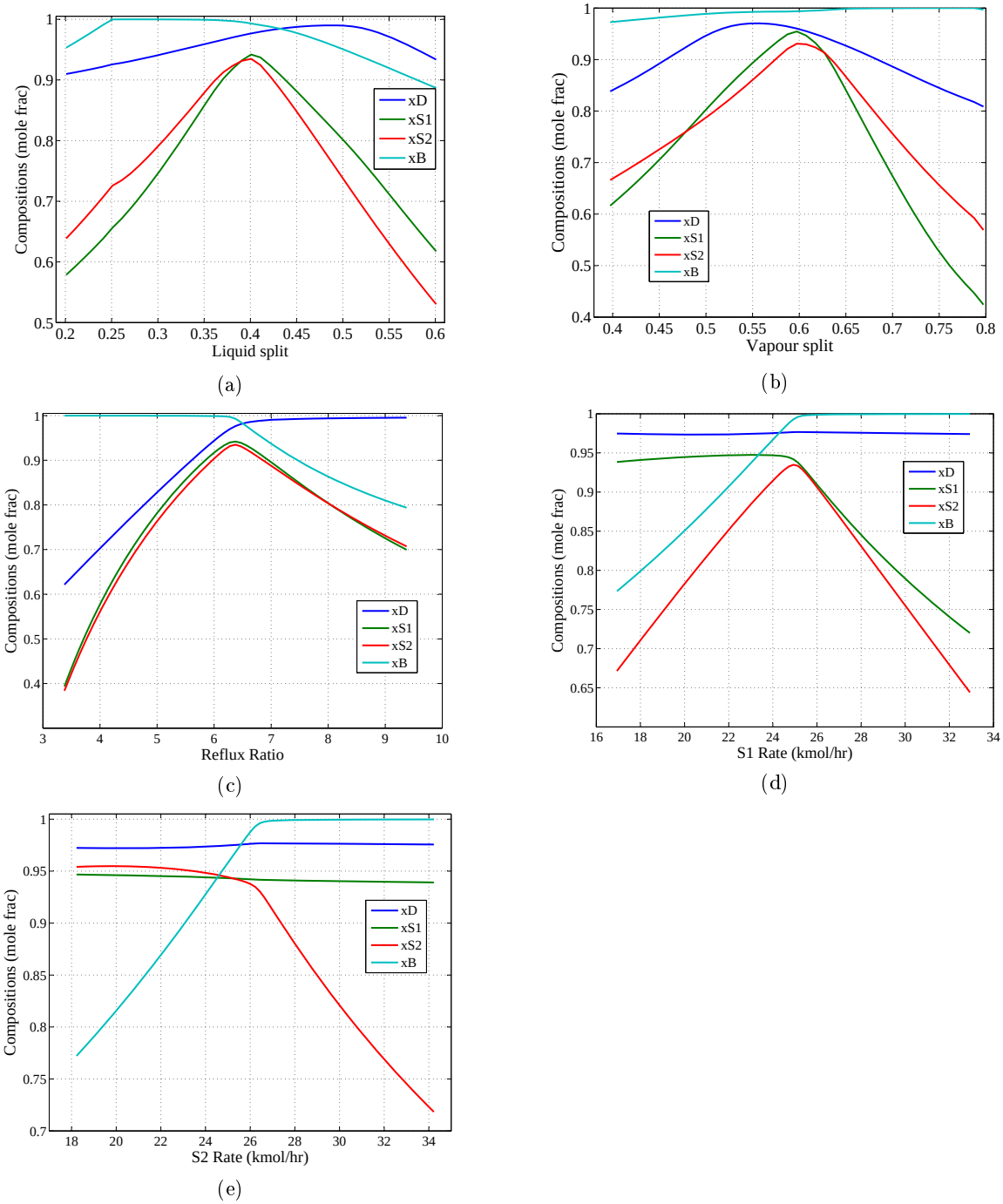

Figure 3.19: Mode 2 with fixed boilup: Impurities in each product and sum (cost J) as a function of the degrees of freedom (vapour split, liquid split, reflux, side stream flow rates) with the other variables kept constant at their original optimal values.

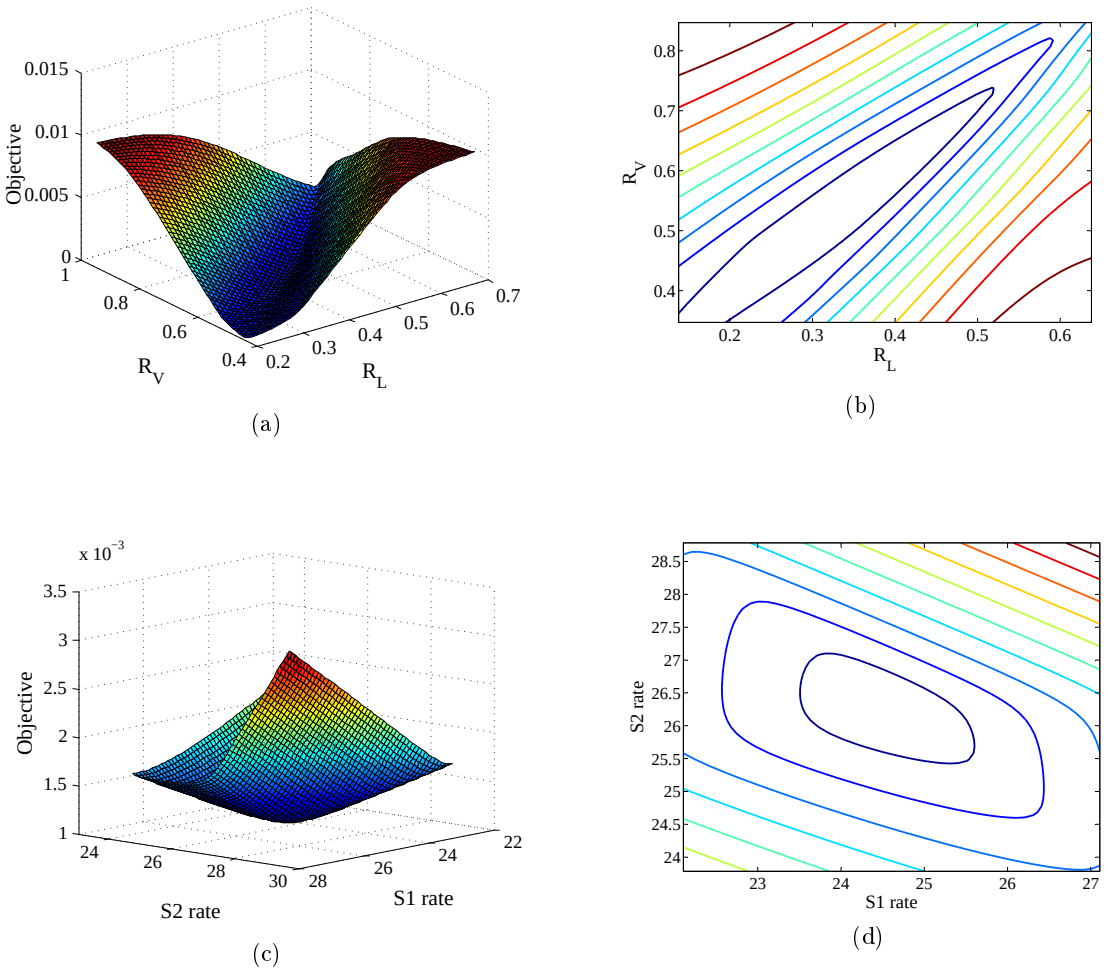

Figure 3.20: Mode 2 with fixed boilup: 3-D surfaces and contour plot of impurity sum (cost J) as a function of degrees of freedom with the other variables fixed at their optimal values.

variables. Combinations of measurements which show self-optimizing properties can also be considered as controlled variables [121].

Note that it is possible to increase some of the products purities with the same amount of energy (vapour). Some of the products will easier obtain higher purity than the other, which is due to both the actual selected number of stages and to the extra energy available in the parts of the column related to the lowest peak in the V_{min}-diagram (here the bottom split related to P_{cd}). Thus, this should be considered when specifying the individual product purities with the minimum energy objective since only the most difficult split is actually setting the energy requirement.

For control purposes it is interesting to know how the manipulated variables affect the process. Figure 3.19 shows the dependency of product compositions and the objective value on each of the five degrees of freedom while all the others are kept constant at their nominal point. The objective value shows a linear dependency on the variables away from the optimum. The degree of effect of a change in each variable on the objective value is clear in these figures. For example, the deviation of S1 from the optimal point has more effect on the objective value than S2. It can be seen that any change in reflux (L) and side streams flow rates (S1, and S2) affect mainly the purities below. For example a change in the S1 flow rate does not have any effect on the purity of the distillate stream. Likewise, the change in S2 flow rate does not have any effect on the purity of the distillate and S1 streams. By considering each of the four parts as separate columns, we can easily confirm the results by analyzing the amounts of internal flows in each part and how they affect separation. Often in distillation, the internal flows, reflux and boilup, are used as control degrees of freedom.

Since there are five degrees of freedom, it is difficult to sketch the solution surface in this case. Figure 3.20 includes 3-dimensional surfaces which show how the objective value is affected by splits and side stream flow changes. Like the previous case, there is "bad" direction for both of them, along which a small change in one of the variables will result in a large change in the objective value.

3.7 Conclusions

In this chapter, two modes of operating a Kaibel column are studied. The first mode, which is minimizing vapour flow rate at given product purities, is more difficult to handle. This difficulty is due to the very narrow solution surface and also multiplicity problem. However, the second mode, where the product purities are free, seems to be easier to operate. This case is not as common as the first objective, but can be relevant for refineries where the product purities do not play a vital role or when there is a bottleneck in the process.

Chapter 4

A Shortcut Design for Kaibel Columns Based on Minimum Energy Diagrams

In this chapter, a shortcut procedure is proposed to design a 4-product dividing-wall column. It is based on the information derived from V_{min} diagram. This has the advantage of having more meaningful guesses for energy requirements and impurity flows in the column. An example is used for illustration.

4.1 Introduction

The dividing-wall column is a single-shell column, divided into two parts with a prefractionator and a main section with a side-stream product, which is capable of separating mixtures into three high-purity products. Compared to conventional schemes with two columns in sequence, it needs less energy, capital and space. We study the Kaibel column, which has been modified to have two side-stream products and can separate the feed into four high-purity products using a single shell.

In terms of design, there are twelve degrees of freedom for the Kaibel column. These are the number of theoretical stages in each of the six sections plus the 6 operational DOFs. This is for a given feed rate (e.g. F=1 mol/s) and the column diameter will depend on the chosen feed rate.

Some shortcut methods have been proposed for design of 3-product columns ([26]; [132]). One approach is to extend the existing methods of conventional columns to dividing wall columns by representing the Petlyuk column by three conventional columns. Another approach is to use more direct insight into the properties of the Petlyuk column and make use of the V_{min} diagram [1]. We use this approach.The method consists of the following steps: First, the V_{min} diagram is sketched. The advantages of using V_{min} diagram in design are discussed in detail in section 3. In section 4, the minimum flowrates in all parts of the column will be calculated. Assuming that actual vapour flow is somewhat higher (around 10%) than the minimum value, the actual flows will be calculated. N_{min} will be calculated based on Underwood equation, except for the section between two side streams for which the Fenske equation is used.

4.2 V_{min} diagrams

Figure 4.1 shows the V_{min} diagram for the methanol-ethanol-propanol-butanol system ($abcd$) which is the example considered here. The peaks P_{ab}, P_{bc} and P_{cd} represent minimum energy for sharp product splits of the original mixture in the Petlyuk configuration. Each peak is related to each of the common Underwood roots (θ_a, θ_b, θ_c). For a Petlyuk arrangement, the prefractionator performs the "easy" split between components a and d (P_{ad}). However, in a Kaibel-arrangement

the prefractionator performs the more difficult split between components b and c. For the Kaibel column we must compute the new peaks P'_{ab} and P'_{cd} (determined by the actual Underwood roots (ϕ_a, ψ_c)). The minimum energy in the Kaibel arrangement is given by the highest of the new peaks (here P'_{ab}). It is obvious from this diagram that the Kaibel arrangement always consumes more energy than the full Petlyuk arrangement since $P'_{ab} > P_{ab}$, $P'_{cd} > P_{cd}$ and trivially: $P'_{ab} > P_{bc}$ and $P'_{cd} > P_{bc}$. It is also simple to see that the difference between Kaibel- and Petlyuk-arrangements can become small when peak P_{bc} is quite low [43]. In case of unequal peaks in the Petlyuk configuration, there will be an optimality region which is a line from preferred split point to the point where the two peaks become equal [123]. The optimality region will be like a square below b/c peak, which is impurity allowance in prefractionator. We assume that the recovery of component a in the top of prefractionator and the recovery of c4 in the bottom of prefractionator are 1 and 0 respectively ($r_{a,T} = 1$, $r_{b,T} = \beta_1$, $r_{c,T} = \beta_2$, $r_{d,T} = 0$). The net flow rates which enter the main column for the top and bottom will be calculated from $\sum z_i F \beta_i$ and $\sum z_i F(1-\beta_i)$ respectively. The common underwood roots in the prefractionator are calculated from

$$1 - q = \sum \left(\frac{\alpha_i z_i}{\alpha_i - \theta} \right) \tag{4.1}$$

$$V_{min,F} = \sum \left(\frac{\alpha_i z_i F}{\alpha_i - \theta} \right) \times \beta_i \tag{4.2}$$

The vapour flow rate which corresponds to θ_2 will be the minimum requirement for prefractionator.

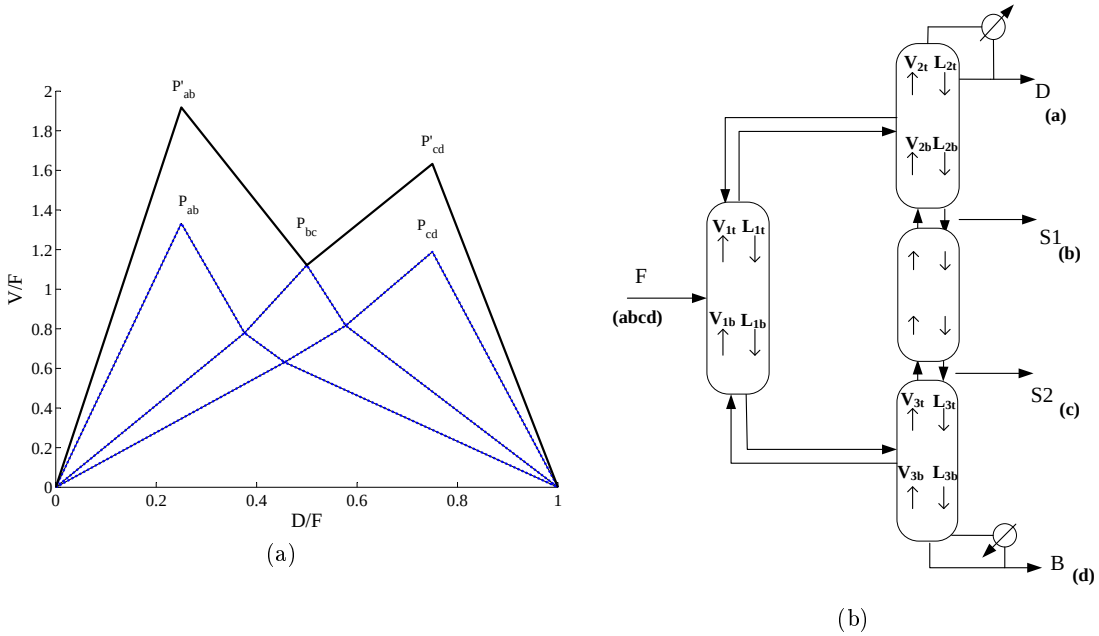

Figure 4.1: HYSYS simulation that uses the information from V_{min} diagram to obtain initial estimates for the detailed simulation.

4.3 Select product purities

Selection of product purities is based on the economical analysis and customer needs. Note that the minimum vapour flow for the Kaibel column is the same as the maximum of the minimum energy required for any pair of product splits, and the highest peak shows the most difficult split. It is clear that we can think of extra energy in one section and then talk about either increasing

the product recovery or designing with lower number of trays. It is shown that overfractionating one of the products makes it possible to bypass some of the feed and mixing it into the product while retaining the constraints on the products [133]. In addition, the impurities in products can be guessed from V_{min} diagram. For example, the highest peak in the V_{min} diagram determines the component that may appear as impurity in the side stream during optimal operation. So, care should be taken in specifying the product impurities.

Figure 4.2 shows the trends of changes in side-stream impurity ratios as functions of splits and impurities coming from the prefractionator for the example studied. This proves the fact about the impurity flows which go to the side-stream and also helps to put some feasible values in mass balance equations. By writing the total and component mass balances for the whole column to get the minimum allowable flows inside each section we will have eight equations (component balances) and twenty unknowns, which means that twelve variables should be set in order to solve the mass balance equations.

$$Fz_{c_i} = Dx_{c_i,D} + S_1x_{c_i,S_1} + S_2x_{c_i,S_2} + Bx_{c_i,B} \quad \sum x_{i,Str_j} = 1$$

where $x_{m,n}$ means mole fraction of component m in Product N. We assume that the composition of the component in two sections away from which it is the main product, is nearly zero, e.g. the compositions of the lightest component in side stream S2 and bottom stream. By doing so and also specifying the composition of the main product in each product stream, there remains two DOF to be specified. It is shown that specifying two composition specifications in a product stream may lead to problems [24]. This means that the impurity can not be chosen as an arbitrary value. Figure **??** shows the contours of the ratios of impurities in side streams around the optimum as functions of vapour and liquid split. It can be read from the figures that for example the specifying two ratios as 1 is not possible. So, one important issue is the allowable variables which can be set for product impurities so that the mass balance equations lead to feasible solution.

4.4 Minimum allowable and actual internal flows

The other internal flow rates for the prefractionator section and main column will be calculated easily from balances around different junctions. The common roots in the prefractionator section, will be the active roots in the main section. The minimum vapour flow rate value for each section in the main column can be calculated from equation (2), by simply substituting the proper feed flow, feed composition and recovery values for each section (for example $z_{i,2} = (F/D_1) \times \beta_i z_{i,F}$, $q_2 = -L_{min,p}/D_1$, $\beta_i(sec2) = Dz_D/D_1z_{D_1}$ for top section of the main column). Now, we can continue with assuming the actual vapour flow needed for the whole column to some extent (we assume 10%) higher than the minimum value and then calculate the actual internal flows.

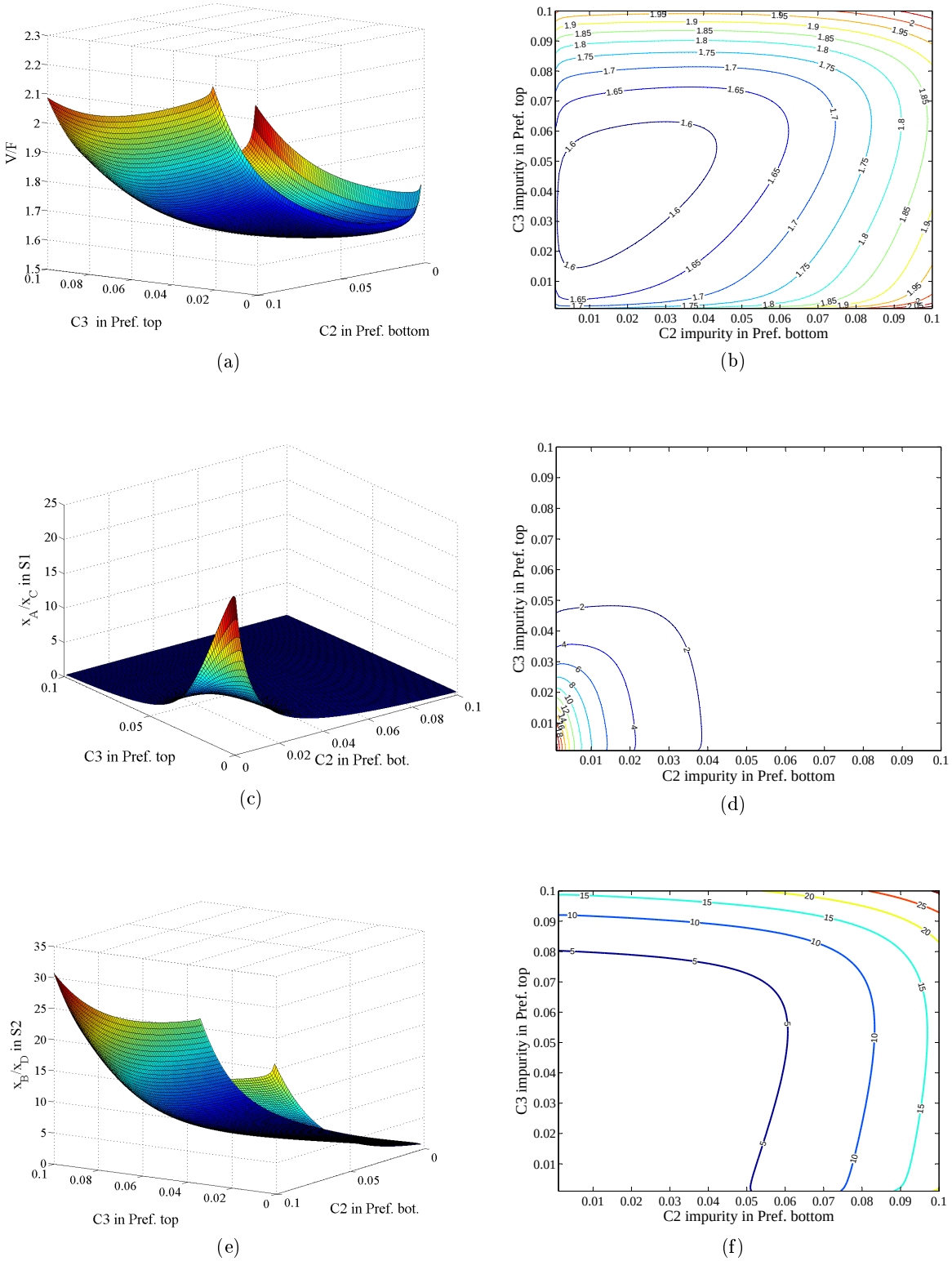

Figure 4.2: Objective value and side streams impurities as functions of impurities of C2 and C3 from bottom and top of the prefractionator respectively

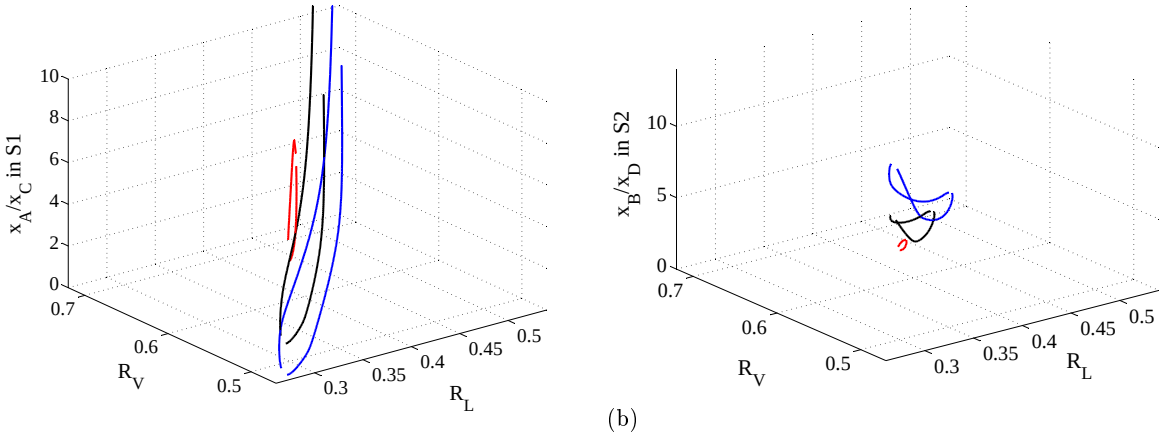

(a) (b)

Figure 4.3: Contours of the impurity ratios in side streams as functions of liquid and vapour split

The liquid and vapour splits are defined as the ratio of the streams going to the prefractionator to the amount coming to the joint.

$$R_L = \frac{L_1}{L_2}$$

$$R_V = \frac{\bar{V}_1}{\bar{V}_3}$$

The other internal flows on two sides of the wall will be calculated based on the splits. Since the internal flows should be greater than the minimum flows, there are some constraints which should be met. Otherwise, the equations will not have proper roots related to relative volatilities.

$$R_L < \frac{L_2 - \bar{L}_{min,2}}{L_2}$$

$$R_L > max(\frac{L_{min,1}}{L_2}, \frac{(\bar{L}_{min,1} - qF)}{L_2})$$

$$R_V > max(\frac{\bar{V}_{min,1}}{\bar{V}_3}, \frac{(V_{min,1} - (1-q)F)}{\bar{V}_3})$$

$$R_V < \frac{\bar{V}_3 - V_{3,min}}{\bar{V}_3}$$

Section four is the section between two side-streams and it is considered to have total reflux and the number of trays will be calculated directly from Fenske equation. Since Fenske equation is based on assuming equal compositions of liquid and vapour streams at top and bottom of prefractionator, -which is not the case for DWC-, we derive the minimum number of trays from Underwood equation. A few iterations are done to reach a desired value for number of trays and energy requirement. The equation below is used for calculating the number of trays in each section. $x_{i,L}$ is the composition of the entering stream to prefractionator, which is calculated from pinch point equations [123].

$$N = \log\Big(\Big(\Sigma \frac{\alpha_i x_{i,D}}{\alpha_i - \phi_2} / \Sigma \frac{\alpha_i x_{i,D}}{\alpha_i - \phi_1}\Big) / \Big(\Sigma \frac{\alpha_i x_{i,L}}{\alpha_i - \phi_2} / \Sigma \frac{\alpha_i x_{i,L}}{\alpha_i - \phi_1}\Big)\Big) / \log\Big(\frac{\phi_2}{\phi_1}\Big) \tag{4.3}$$

4.5 Conclusion

Designing the complex columns is not as straightforward as the conventional columns. In this chapter, we have presented a method for shortcut design of Kaibel column based on V_{min} diagram. The next step is to start simulating the model using the data from shortcut design as first guess. By plotting the contours of the objective value as a function of the two operational DOFs, we can get more information about the behaviour of the column close to the optimum and do the optimal design based on the rigorous model.

Chapter 5

Manipulation of Vapour Split in the Kaibel Distillation Arrangements

In this chapter, we want to show how we can gain more from a Kaibel distillation column by considering a degree of freedom which is normally not used. Two methods are used to study the effect of vapour split manipulation, namely a shortcut method and rigorous simulations. Using a case-study, we show that we may not be able to operate close to minimum energy requirement for some feed disturbances as we have the vapour split fixed.

5.1 Introduction

The vapour split ratio (see Figure 5.1) is one of the degrees of freedom in a dividing-wall column. It is usually set at the design phase by determining the location of the wall and the pressure drop in the divided sections, but it is not adjustable during operation (e.g. [134]). There is no report from industry of an adjustable vapour split and a degree of freedom is lost. However, to reduce energy usage, several authors including Wolff et al. [24], Halvorsen et al. [117] and Ghadrdan et al. [135] have shown that it is important to set the liquid and vapour splits at their right values.

The Kaibel laboratory setup at NTNU [130] is probably the only implementation of active manipulation of the vapour split. Figure 5.2 shows a picture of the lab column with manipulatable vapour and liquid splits. The vapour split valve in this implementation is rudimentary and not very precise, but Dviwedi et al. [136] showed that this can be corrected with a simple temperature feedback action, and the column can be operated and stabilized using the vapour split[136]. The issue of this chapter is to further study the potential savings of manipulating the vapour split in the Kaibel arrangements. We study two approaches: First, the V_{min} diagram [123] is used to study the effect of vapour split on the energy requirement. Then, we have confirmed the results by rigorous simulations in HYSYS.

5.2 Degrees of Freedom in the Kaibel Arrangement

Figure 5.1 shows a schematic of a Kaibel dividing-wall distillation column and its thermodynamic equivalent with separate sections. Assuming that the distillate (D) and bottom (B) flows are used for level control, there are six remaining degrees of freedom (u) in a Kaibel distillation column: boilup rate (V), reflux (L), side stream flows (S1, S2), liquid split (R_L) and vapour split (R_V).

$$u = \begin{bmatrix} R_L & R_V & L & V & S_1 & S_2 \end{bmatrix}$$

Table 5.1: The optimal values of R_V for different composition disturbances in three main directions

Disturbance	Feed composition				V_{1t}	V_{2t}	V_{3b}	Optimal R_V
a/b change	0.20	0.30	0.25	0.25	1.160	1.995	1.670	0.5815
	0.25	0.25	0.25	0.25	1.121	1.918	1.633	0.5846
	0.30	0.20	0.25	0.25	1.081	1.838	1.594	0.5882
b/c change	0.20	0.30	0.25	0.25	1.059	1.7399	1.671	0.6086
	0.25	0.25	0.25	0.25	1.121	1.918	1.633	0.5846
	0.30	0.20	0.25	0.25	1.180	2.089	1.591	0.5649
c/d change	0.20	0.30	0.25	0.25	1.081	1.886	1.508	0.5733
	0.25	0.25	0.25	0.25	1.121	1.918	1.633	0.5846
	0.30	0.20	0.25	0.25	1.160	1.949	1.753	0.5952

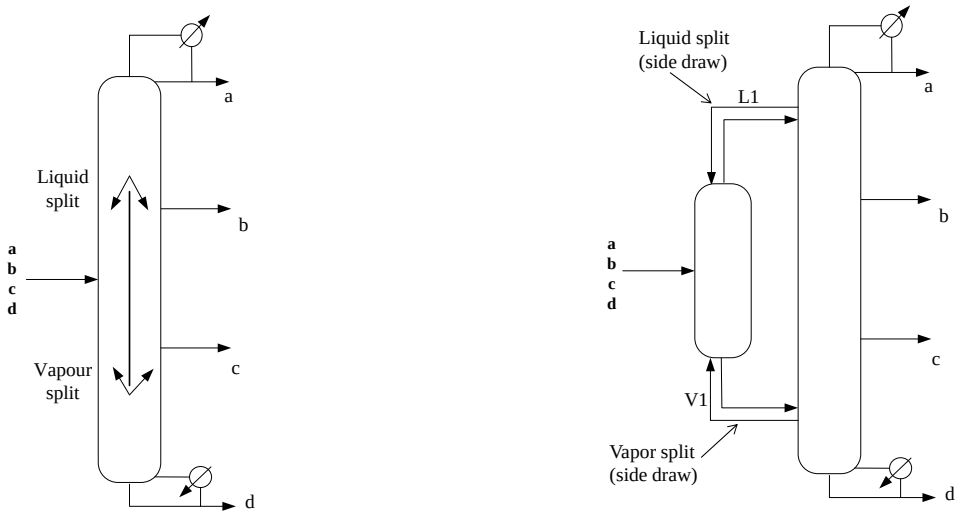

(a) (b)

Figure 5.1: A schematic of Kaibel dividing-wall distillation column (left) and its thermodynamic equivalent (right)

Note that liquid split (R_L) is defined as the ratio of the liquid entering the top of the prefractionator (L1) to the overall liquid (L) coming from the top of the main column and the vapour split (R_V) is defined as the ratio of the vapour entering the bottom (V1) of the prefractionator to the overall vapour (V) from the bottom of the main column. Assuming that the objective of the separation is to reach specific product purities, four of the degrees of freedom are used to satisfy the product purity specifications: Top ($x_{D,a}$), side-stream 1 $\left(x_{S1,b}\right)$, side-stream 2 ($x_{S2,c}$), bottom $\left(x_{B,d}\right)$. The two remaining degrees of freedom can be used for optimization, e.g. for minimizing energy consumption.

5.3 Optimal Vapour split in Kaibel columns

5.3.1 Sharp Split Separation

We first consider the case of a sharp split separation, which means that the lines in V_{min} diagram are for 100% recovery of a component. The following equation is used to calculate the optimal

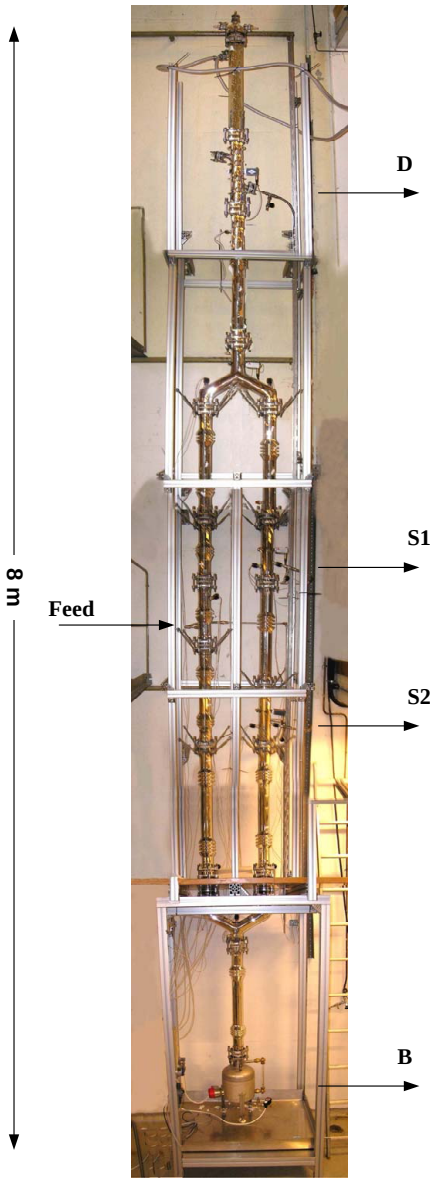

Figure 5.2: Laboratory Kaibel distillation column at the chemical Engineering department at NTNU, Norway [130]

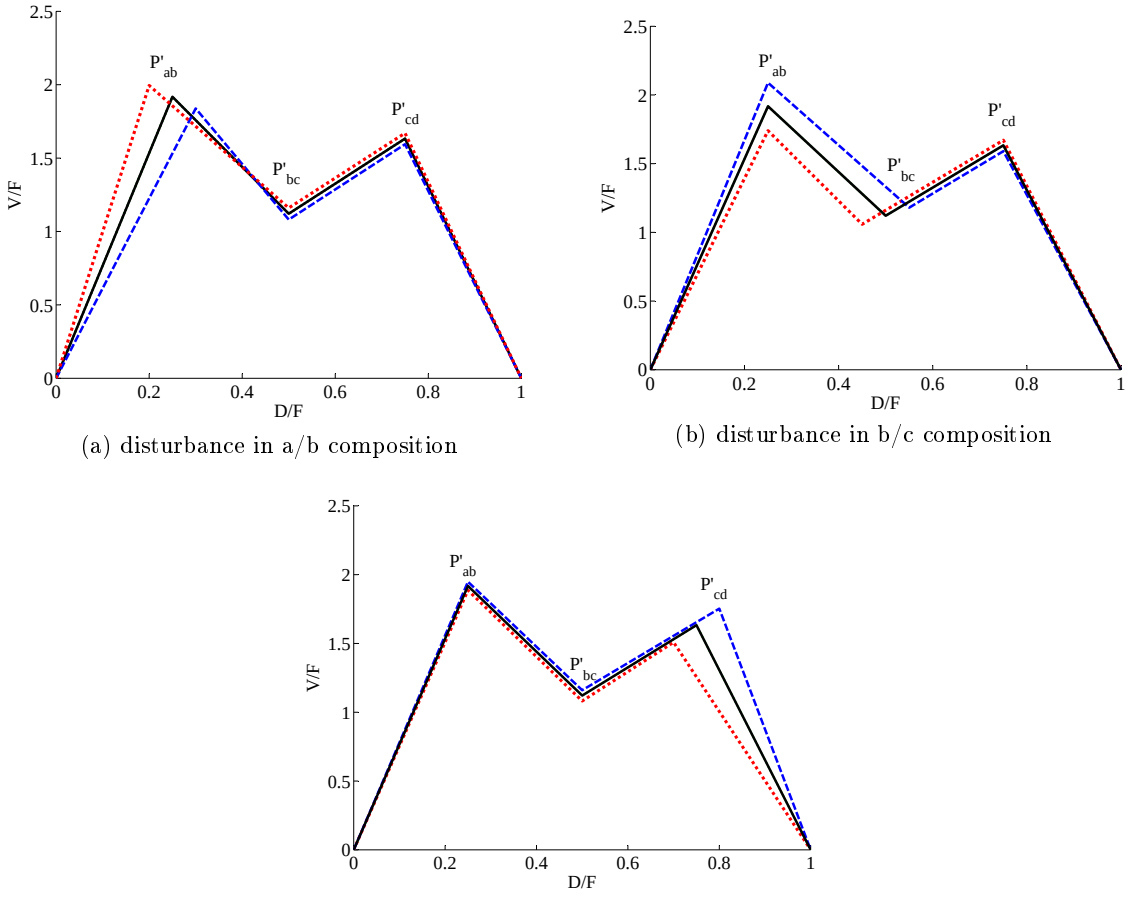

(a) disturbance in a/b composition

(b) disturbance in b/c composition

(c) disturbance in c/d composition

Figure 5.3: V_{min} diagram for the Kaibel distillation columns for different feed disturbances. red: z_i/z_j = 0.20/0.30, Black: z_i/z_j = 0.25/0.25, Blue: z_i/z_j = 0.30/0.20

vapour split.

$$R_V = \frac{V_{1t}/F}{V_M/F} \tag{5.1}$$

where

$$V_M/F = \max\left(V_{2t}/F, V_{3b}/F\right)$$

The values of V_{1t}/F (P'_{bc}), V_{2t}/F (P'_{ab}) and V_{3b}/F (P'_{cd}) can be obtained from V_{min} diagram. Figure 5.3 shows the V_{min} diagram for three feed composition disturbances, and the corresponding optimal R_V for each case is given in Table 5.1. It seems that a constant R_V may work fine for a/b feed composition changes, since the vapour requirement in both the prefractionator and main column (peaks P'_{bc} and P'_{ab}) seem to change with about the same ratio. This is shown more clearly in Table 5.1, where we see that the R_V value is mostly affected by the composition disturbance in the direction of b/c.

In the case when we have a fixed R_V, we need to make sure that the minimum vapour requirement for a b/c sharp separation in the prefractionator is guaranteed. Since the V_{min} diagram is for the optimal R_V, having a fixed R_V means that the vapour requirement for the prefractionator should increase, so that the the ratio of V_{1t} and the corresponding requirement

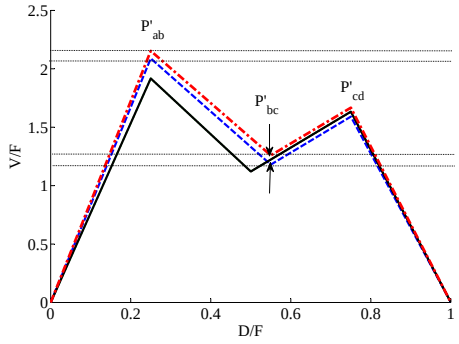

Figure 5.4: V_{min} diagram for the nominal feed properties (black, R_V = 0.5649) and new feed composition (b/c composition change to 0.30/0.20) with optimal (blue, R_V = 0.5846) and fixed R_V(red, R_V = 0.5649)

for the main section of the column (V_M) equals the fixed value which is set for R_V. Figure 5.4 is an example which shows the vapour requirement for the column for a change in feed composition. The optimal R_V for the new feed composition leads to less requirement (In this case: $V_{M,R_{V,opt}}$ = 2.089), compared to fixed R_V scenario ($V_{M,R_{V,fixed}}$ = 2.1535). This is done by increasing the vapour in the prefractionator (V_{1t}). This in turn will affect the actual Underwood roots and so the vapour requirements in the top and bottom sections of the column (see Appendix).

5.3.2 Non-sharp Separation

The analysis becomes more difficult for non-sharp separations. Here, the compositions of component b in the top and c in the bottom of the prefractionator are not zero. We can find a certain slack if we allow non-sharp split in the Kaibel configuration, but this is limited by the product specifications. So, there will be a small region below P_{bc} from which any point could be chosen as the prefractionator's operating point. An optimization can be done to find the best operating point of the prefractionator. Figure 5.5 shows an example of non-sharp separation with 95% recoveries for the main products.

The recoveries of the components in all products should be specified in order to sketch the V_{min} diagram. For example, a recovery of 95% for component a in the distillate flow rate does not give any information about the possible existence and the amount of b in this stream. The recoveries of the main products are usually set by the customer needs. By writing the component mass balances around the column and assuming that at optimal operation, the component which is to be drawn at a product stream will only appear in the adjacent product streams and not in the ones away from it (for example, component b which is the main product of S1 stream, will appear as impurity in streams D and S2), we need to estimate two variables to get a feasible solution for mass balance equations. The impurities in products can be guessed from the V_{min} diagram. These issues are dealt in [137]. The highest peak in the V_{min} diagram determines the component that may appear as impurity in the side stream during optimal operation.

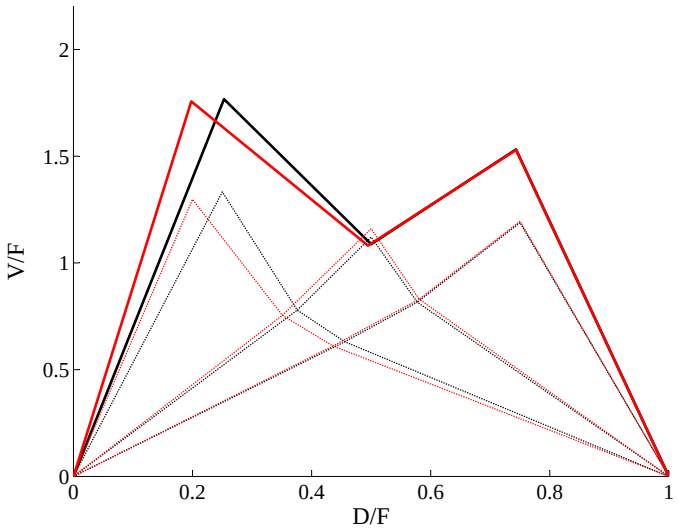

Figure 5.5: Nonsharp separation with recovery of 95% for products: Equimolar (black) and feed composition of [0.20 0.30 0.25 0.25] (red)

5.4 Rigorous Simulation

5.4.1 Kaibel case-study

Figure 5.6 shows the HYSYS simulation flowsheet of a Kaibel column separating four simple alcohols (methanol, ethanol, 1-propanol, 1-butanol). Pumps and valves are needed in the simulations to compensate for the pressure difference between the column sections on the two sides of the wall. In reality, these are not required. With a given feed, there are six steady-state degrees of freedom. In our case, four degrees of freedom are used to satisfy the four product purities specifications. The remaining two degrees of freedom, here selected as vapour and liquid splits, are used to minimize the energy requirement. Figure 5.7 shows contours of constant boilup (V) as a function of the vapour and liquid splits. In a 3-dimensional figure, this looks like a thin bended cone.

Note that the contours for $V > V_{min}$ do not encircle the optimal point for R_L and R_V corresponding to $V = V_{min}$. This is surprising, and implies that there are two solutions for R_L and R_V, where one is undesirable. In Figure 5.7 the lower parts of each contour will be undesirable. This may be understood from Figure 5.8, which shows a cut of the solution surface at fixed vapour split.

From Figure 5.8a, we see that the optimal value for R_L is obtained at a minimum value. We also see the multiplicity in the solution, where the upper branch is the undesirable solution. This is further described by Figure 5.8(b) and Figure 5.9, which shows that there are two different ways for the components to go to the side-streams and satisfy the product specifications.

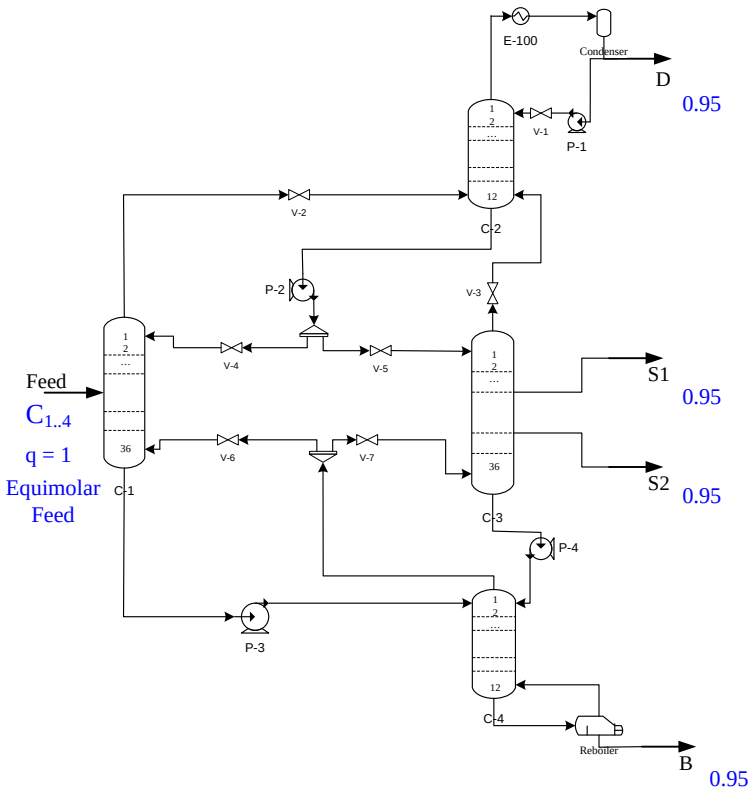

Figure 5.6: Simulation flowsheet of Kaibel distillation column

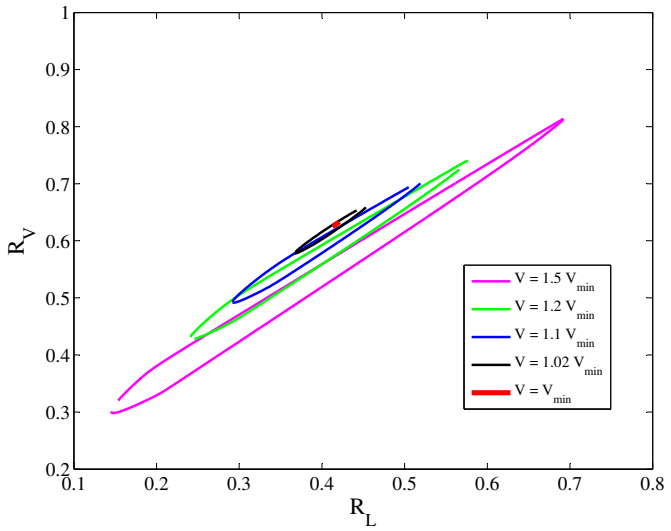

Figure 5.7: Contours of constant boilup as a function of vapour and liquid splits at constant product purities

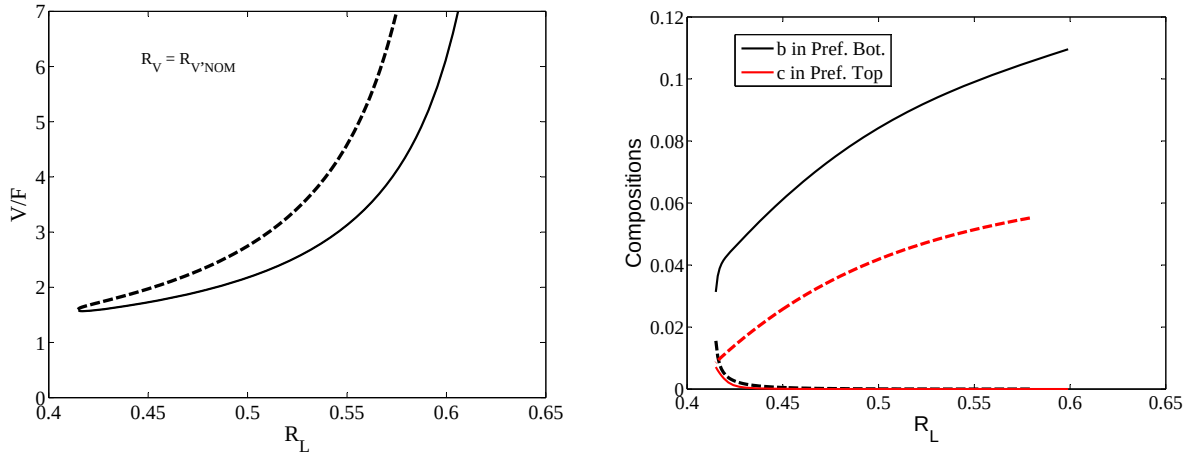

(a) (b)

Figure 5.8: (a) Boilup rate as a function of liquid split at constant vapour split (R_V = 0.6295) and constant product purities, (b) Corresponding impurities in the top and bottom of prefractionator

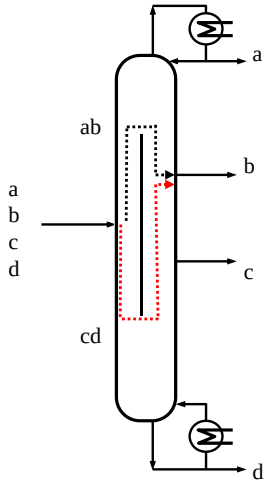

Figure 5.9: Paths of component b flow to upper side streams

In Figure 5.10, we study one of the contours and show how the impurities in the top and bottom of the prefractionator and the impurity ratios in the side streams change along the contour. By impurity ratios, we mean $\frac{x_a}{x_c}$ in the $S1$ stream and $\frac{x_b}{x_d}$ in the $S2$ stream. That a/b is the most difficult split can also be seen here, so that impurities of b in the bottom of prefractionator are greater than the impurity of c in the top. This leads to larger ratios of impurities in side stream 1 compared to the impurity ratio in side stream 2. This information could also be obtained from the V_{min} diagram, by finding the column section where we have energy surplus (see Figure 3.8). Figure 5.10b actually shows many different points that could be picked as the prefractionator's operating point. This was discussed in section 5.3.2 and is shown schematically in Figure 5.11.

An important point to investigate is to check how much we may lose by keeping R_V constant. To study this, we have plotted in Figure 5.12 contours of boilup +2% above the optimal point corresponding to each set of feed compositions for three main directions of composition change. We assume that operating within 2% of minimum energy is still acceptable. The red dots in this figure show the optimum point for each set of feed composition. From Figure 5.12, we find that with R_V constant at its nominal value R_V = 0.6295, it is possible to operate within 2% of

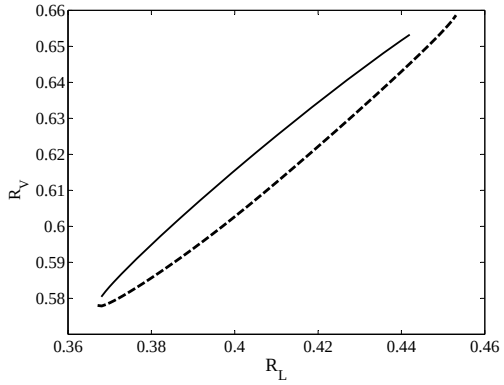

(a) $R_L - R_V$ solution contour for $V = 1.02V_{min}$

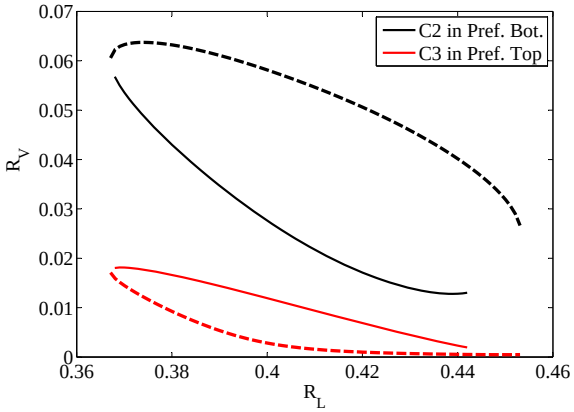

(b) Corresponding impurities in prefractionator's ends

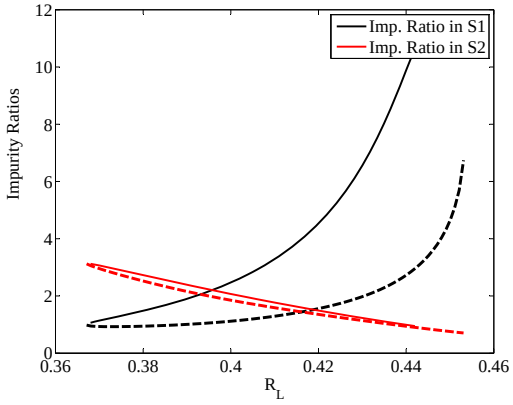

(c) Impurity ratios (light/heavy) in side streams

Figure 5.10: Solution properties along a contour of constant vapour boilup ($V = 1.02V_{min}$)

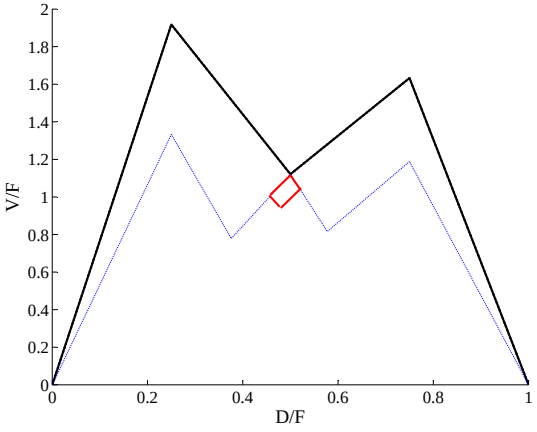

Figure 5.11: Degree of freedom for prefractionator operation

the minimum energy requirement when there are disturbances in the a/b direction and almost possible in the c/d direction. However, as seen from Figure 5.12C, this is not the case for a disturbance in the b/c direction. In the figures, we have shown the ranges for R_V that keeps V inside +2% of V_{min} for the disturbances, and for the c/d and b/c disturbances the nominal value of R_V is not in this range.

These figures also show that the value of a constant vapour split should be chosen carefully so that it covers most of the expected disturbances. As we go further from the minimum requirement, a wider range of disturbances is covered by a fixed R_V, as is shown in Figure 5.13, and in this case, the c/d disturbance can be handled by keeping R_V at its nominal value, when we allow for V vary 10% above the minimum.

Figure 5.15 shows the comparison between three values of vapour splits: one is the optimal value for the nominal case and the others are some lower and higher value which is chosen by the insight obtained from Figures 5.12 and 5.13. The values in the Figure show the percentage of loss compared to the case that we re-optimize and R_V is a manipulatable variable. It is confirmed that if some lower value is chosen for the constant R_V, the disturbances in b/c direction are handled better.

The analysis we have done in Figures 5.12 and 5.13 is with the assumption of using additional energy and check if this is sufficient. Another approach would be to check how much additional energy is needed to handle a given a disturbance. Figure 5.14 shows plots of boilup (V) versus R_L with fixed R_V. For various feed disturbances, as shown in Figure 5.15, the difference in minimum energy consumption is relatively small for the disturbances in a/b ($V + 0.8\%$) and c/d directions ($V + 2.8\%$). However, the loss is larger if we fix R_V when there are large disturbances in b/c direction ($V + 16.4\%$). A large adjustment for R_L is needed to stay at V_{min} (see Figure 5.14 C). However, this may be easy by controlling the composition in the prefractionator.

5.5 Conclusion

We have shown that the realization of the energy saving potential of thermally coupled columns may require on-line adjustment of the vapour split in order to handle expected feed property variations and still maintain minimum energy operation. In particular, this applies to cases where the optimal operating window with a fixed vapour split is narrow, like in a 4-product Kaibel column, and also in some 3-product dividing-wall columns with high purity in the side product. We should pay special attention to disturbances that make the peaks sequence change from one section of the column to the other.

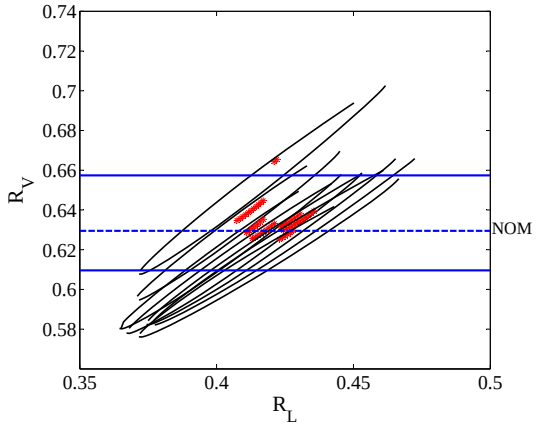

(a) Change in a/b composition (from 0.1/0.4 to 0.4/0.1)

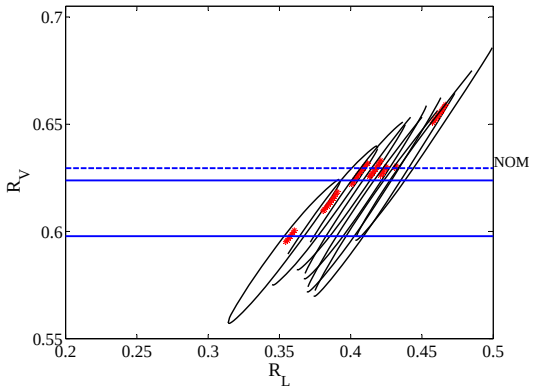

(b) Change in c/d composition (from 0.1/0.4 to 0.4/0.1)

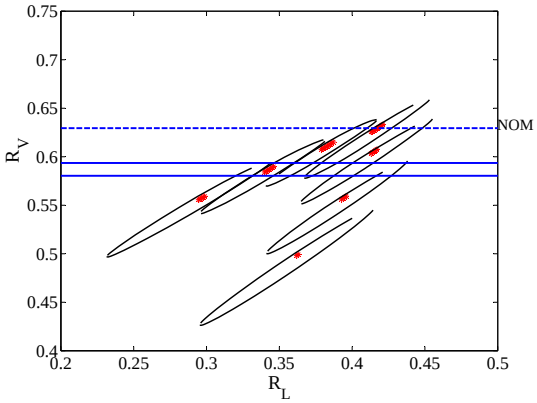

(c) Change in b/c composition (from 0.1/0.4 to 0.4/0.1)

Figure 5.12: Contours for boilup +2% above optimal value for different feed composition disturbances. Optimum points for each feed composition in red

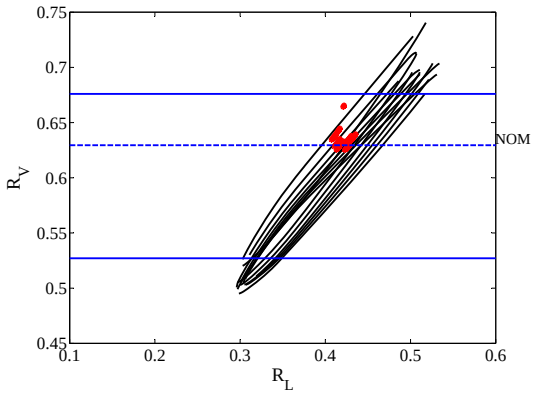

(a) Change in a/b composition (from 0.1/0.4 to 0.4/0.1)

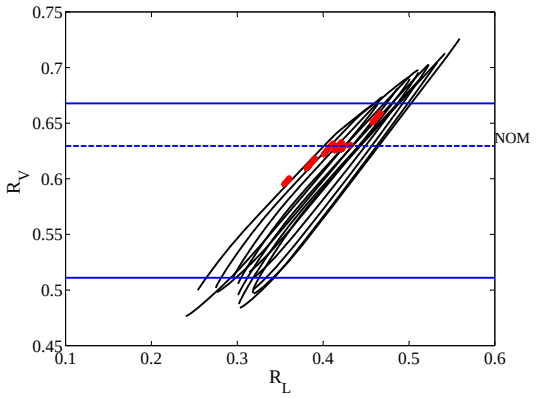

(b) Change in c/d composition (from 0.1/0.4 to 0.4/0.1)

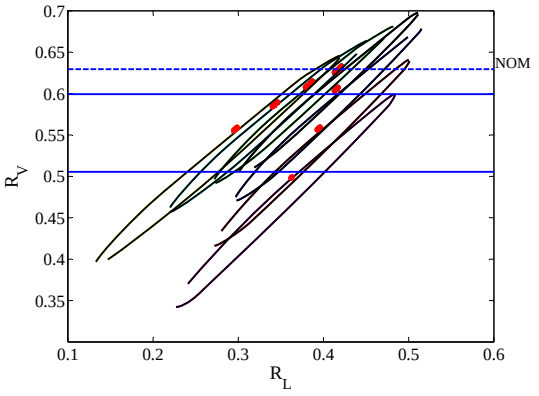

(c) Change in b/c composition (from 0.1/0.4 to 0.4/0.1)

Figure 5.13: Contours for boilup +10% above optimal value for different feed composition disturbances. Optimum points for each feed composition in red

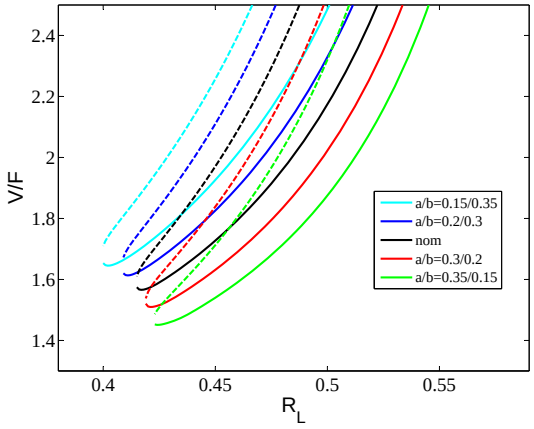

(a) Change in a/b composition

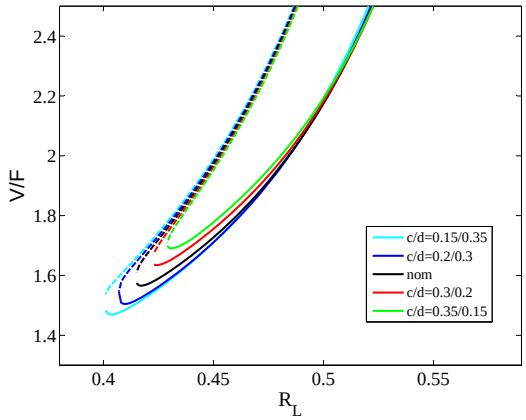

(b) Change in c/d composition

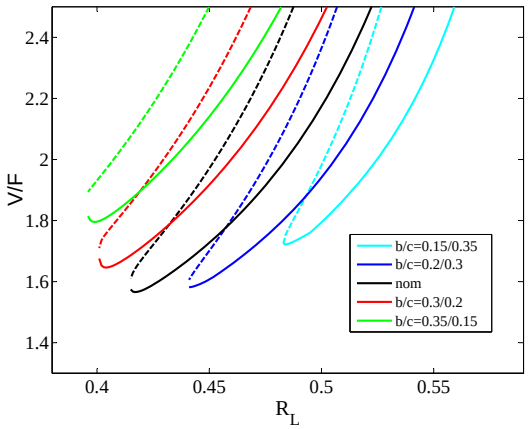

(c) Change in b/c composition

Figure 5.14: Solution boundaries for different feed disturbances with fixed R_V ($R_V = 0.6295$)

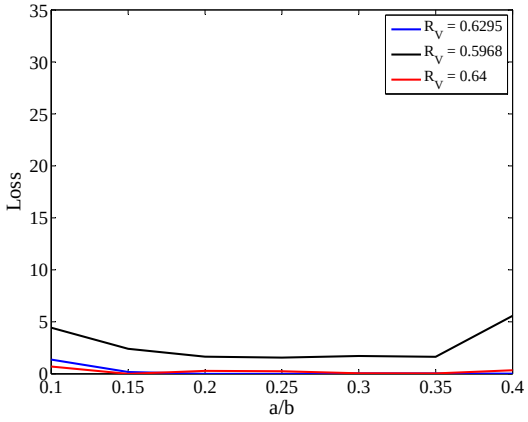

(a) Change in a/b composition

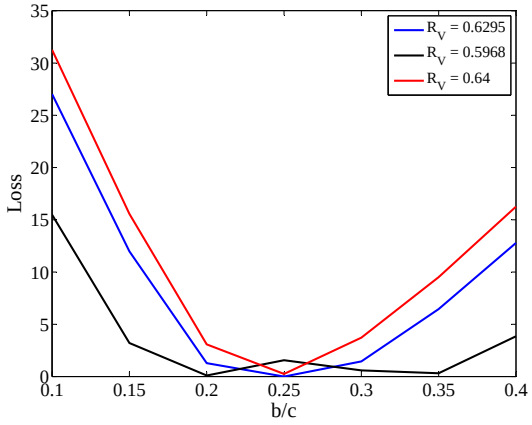

(b) Change in c/d composition

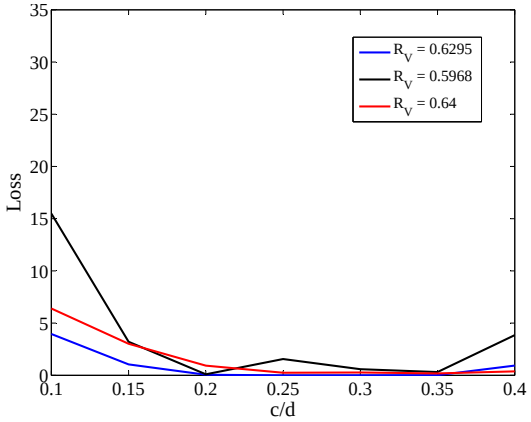

(c) Change in b/c composition

Figure 5.15: Loss in energy (V) for different fixed values of R_V: Nominal $R_V = 0.6295$ (blue), lower "optimally" adjusted $R_V = 0.5968$ (black), higher $R_V = 0.64$ (red)

Chapter 6

A short review on self-optimizing control

6.1 Control Structure Design

Implementation of a control system is necessary to operate chemical plants economically optimal, safe and stable in the presence of disturbances which may frequently occur during operation. Control structure design includes the design of controllers as well as selecting the potential control variables, manipulated variables and the way they should be connected. There is generally a time scale separation between different control layers which are connected through control variables [138] (see Figure 6.1). At each layer, the setpoint for controlled variables is given by the upper layer and implemented by the lower layer.

The following procedure includes a top-down analysis to optimize the process for various disturbances and identify primary self-optimizing controlled variables and a bottom-up analysis to identify secondary controlled variables and find the structure of the control system (pairing). Self-optimizing control is when we can achieve an acceptable loss with constant setpoint values, for the controlled variables ([2]). The procedure is as follows:

I Top-down (focus on steady-state economics)

(a) Define operational objectives (optimal operation):

-i- Scalar cost function J (to be minimized)

-ii- Constraints

(b) Objective: Find regions of active constraints

-i- Identify steady-state degrees of freedom and

-ii- expected disturbances.

-iii- Optimize the operation with respect to the degrees of freedom for the expected disturbances (off-line analysis)

(c) Select location of throughput manipulator (TPM) (Decision 3)

- Some plants, e.g., with parallel units, may have more than one TPM
- One may consider moving the TPM depending on the constraint region

II Bottom-up (focus on dynamics)

(d) Select structure of regulatory control layer (including inventory control):

-i- Select 'stabilizing' controlled variables CV2 (Decision 2)

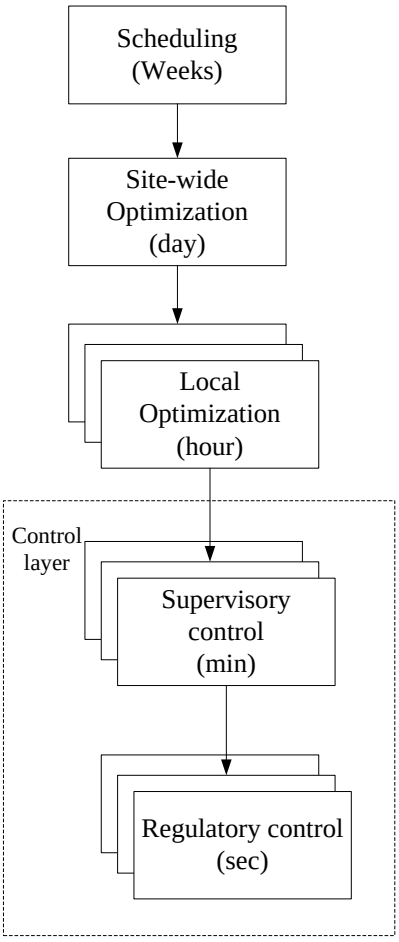

Figure 6.1: Typical control system hierarchy in a chemical plant [138]

-ii- Select inputs (valves) and 'pairings' for controlling CV2 (Decision 4)
- Stabilizes the process and avoids drift
- If possible, use same regulatory layer for all regions

(e) Select structure of supervisory control
-i- Controls primary CV1's
-ii- Supervises regulatory layer
-iii- Performs switching between CV1s for different regions

(f) Select structure of (or need for) optimization layer (RTO)
- Updates setpoints for CV1 (if necessary)

The Top-down analysis focuses on steady-state economics where an economical optimization problem is formulated. Optimization is performed both at nominal point and for important disturbances. Based on the optimization results, a self-optimizing analysis is done for finding the active constraint regions and selecting the best controlled variables in different operational regions. The Bottom-up analysis focuses on dynamic control of the process. Dynamic model of the process is necessary to validate implementation of the proposed controlled variables from the top-down analysis. In this part, first stabilizing controlled variables (secondary CVs) are selected and paired with the proper manipulated variables and then the structure of the supervisory control layer (pairing of the primary CVs with the remained manipulated variables) is determined.

6.2 Self-optimizing Control

A key step in the design of control systems is to find the appropriate set of control variables (CVs). A collection of methods dealing with CV selection is available in the survey article by van de Wal [139]. Self-optimizing control is a useful method for finding the appropriate set of controlled variables. It is assumed that the economics of the plant are characterized by the scalar objective function $J(u,d)$, where u and d represent the inputs (or unconstrained degrees of freedom) and the disturbances, respectively. For the nominal disturbances d^*, let $u_{opt}(d^*)$ denote the optimal inputs. When the disturbances change from d^*, the optimal operation policy is to update $u_{opt}(d)$ according to d. This usually requires using an online optimizer, which provides the optimal value of the objective functional denoted as $J_{opt}(d)$ [140]. A simpler strategy results when u can be indirectly adjusted using a feedback controller. In this case, the feedback controller manipulates u to hold the CVs close to their specified setpoints.

6.3 Solution to the CV selection problem

To present the local method, let the linearized model of the process, obtained around the nominally optimal operating point, be given as

$$x = \mathbf{G}_x u + \mathbf{G}_x^d \mathbf{W}_d + \mathbf{W}_n n \tag{6.1}$$

Figure 6.3 shows the feedback diagram for the linearized model. The diagonal matrices $\mathbf{W}_d$ and $\mathbf{W}_n$ contain the magnitudes of expected disturbances and implementation errors associated with the individual measurements, respectively. The matrices $\mathbf{G}_x$ and $\mathbf{G}_x^d$ are the steady-state gains from inputs and disturbances to measurements, which are obtained by linearizing the system around the operating point.

The objective function J around $u_{opt}(d)$ is

$$J(u,d) = J(u_{opt}(d),d) + J_u(u - u_{opt}) + \frac{1}{2}(u - u_{opt})^T J_{uu}(u - u_{opt}) \tag{6.2}$$

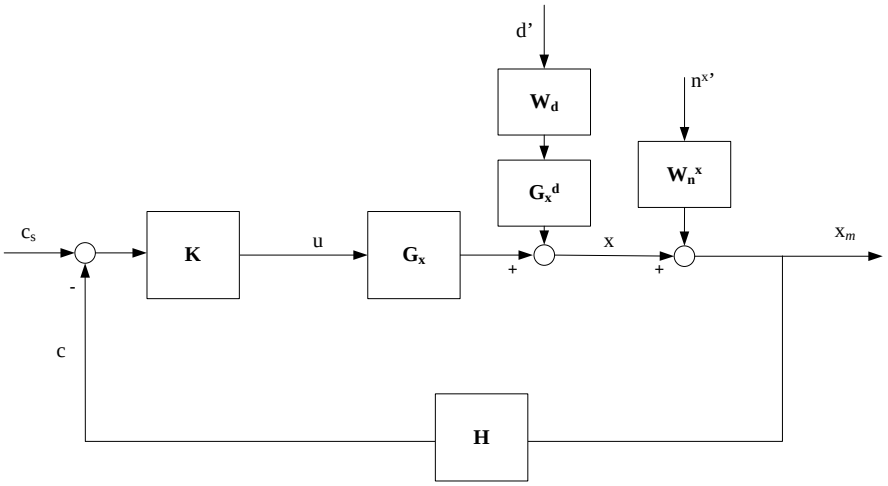

Figure 6.2: Feedback diagram

By defining loss as $L(\mathrm{u},\mathrm{d}) = \mathrm{J}(\mathrm{u},\mathrm{d}) - \mathrm{J}_{opt}(\mathrm{d})$, and knowing that the derivative of the objective function is zero at optimum, we will have

$$L(\mathrm{u},\mathrm{d}) = \mathrm{J}(\mathrm{u},\mathrm{d}) - \mathrm{J}_{opt}(\mathrm{d}) = \frac{1}{2}z^T z = \frac{1}{2}\|z\|_2^2 \tag{6.3}$$

where

$$z = \mathrm{J}_{uu}^{1/2}\left(\mathrm{u} - \mathrm{u}_{opt}(\mathrm{d})\right) \tag{6.4}$$

$\mathrm{u}_{opt}(\mathrm{d})$ is obtained by expanding the gradient around the nominal point

$$\mathrm{J}_\mathrm{u} = \mathrm{J}_\mathrm{u}^* + \mathrm{J}_{uu}^*\mathrm{u} + \mathrm{J}_{ud}^*\mathrm{d} = \underbrace{\mathrm{J}_\mathrm{u}^*}_{=0} + \begin{bmatrix} \mathrm{J}_{uu}^* & \mathrm{J}_{ud}^* \end{bmatrix}\begin{bmatrix} \mathrm{u} \\ \mathrm{d} \end{bmatrix}$$

To remain optimal, we must have $\mathrm{J}_\mathrm{u} = 0$, so

$$\mathrm{u}_{opt} = -\mathrm{J}_{uu}^{-1}\mathrm{J}_{ud}\mathrm{d} \tag{6.5}$$

We have assumed a linear relation between inputs and outputs. So,

$$\mathrm{x}_{opt} = \mathbf{G}_x\mathrm{u}_{opt} + \mathbf{G}_x^d\mathrm{d} = \underbrace{\left(-\mathbf{G}_x\mathrm{J}_{uu}^{-1}\mathrm{J}_{ud} + \mathbf{G}_x^d\right)}_{\mathbf{F}}\mathrm{d}$$

F is defined as the optimal sensitivity matrix. The main objective in self-optimizing control is to find a linear combination of measurements, $\mathrm{c} = \mathbf{H}\mathrm{x}$, such that control of these indirectly leads to close-to-optimal operation with a small loss, in spite of unknown disturbances and measurement noise.

$$\mathrm{c} = \mathbf{H}\mathrm{x} = \mathbf{H}\mathbf{G}_x\mathrm{u} + \mathbf{H}\mathbf{G}_x^d\mathrm{d}$$

$$\mathrm{c}_{opt} = \mathbf{H}\mathrm{x}_{opt} = \mathbf{H}\mathbf{G}_x\mathrm{u}_{opt} + \mathbf{H}\mathbf{G}_x^d\mathrm{d}$$

So,

$$\mathrm{u} - \mathrm{u}_{opt} = \left(\underbrace{\mathbf{H}\mathbf{G}_x}_{\mathbf{G}}\right)^{-1}\left(\mathrm{c} - \mathrm{c}_{opt}\right)$$

We need to write $c - c_{opt}$ as a function of d and n^x.

$$\mathbf{H}(x + n^x) = \underbrace{c_s}_{0}$$

We also have $c_{opt} = \mathbf{HF}d$. So,

$$c - c_{opt} = \mathbf{H}(\mathbf{F}d + n^x) = \mathbf{H}\left(\mathbf{F}\mathbf{W}_d d' + \mathbf{W}_{n^x} n^{x'}\right) = \mathbf{H}\begin{bmatrix} \mathbf{F}\mathbf{W}_d & \mathbf{W}_{n^x} \end{bmatrix}\begin{bmatrix} d' \\ n^{x'} \end{bmatrix}$$

So, the final loss term will be

$$L = \frac{1}{2} J_{uu}^{1/2} (\mathbf{H}\mathbf{G}_x)^{-1} \mathbf{H}\underbrace{\begin{bmatrix} \mathbf{F}\mathbf{W}_d & \mathbf{W}_{n^x} \end{bmatrix}}_{\tilde{\mathbf{F}}}\begin{bmatrix} d' \\ n^{x'} \end{bmatrix} \tag{6.6}$$

By assuming that $\begin{bmatrix} d' \\ n^{x'} \end{bmatrix} \leq 1$, the focus is on minimizing the rest. This method is called "Exact Local Method" and was introduced first by Halvorsen et al. [141].

Steady state control error is assumed to be zero, because it is assumed that all controllers have integral action. So, the implementation error is caused by measurement error. The other assumption is that the set of active constraints for the nonlinear optimization problem does not change with d. In general, the use of an online optimizer may be advantageous in case of frequent changes in the active constraint set. It is also assumed that there are at least as many measurements as degrees of freedom. Plus, the number of control variables is equal to the number of inputs.

Alstad et al. [121] have reformulated the exact local method problem to make it convex. They have defined $\mathbf{M}_n \equiv J_{uu}^{1/2} (\mathbf{H}\mathbf{G}_x)^{-1}$, which may be viewed as the effect of implementation error on z. Using the fact that the solution to the original loss problem is not unique, so that if $\mathbf{H}$ is an optimal solution, then another optimal solution is $\mathbf{H}_1 = \mathbf{D}\mathbf{H}$, where $\mathbf{D}$ is a nonsingular matrix of $n_u \times n_u$. They have used the degree of freedom to choose $\mathbf{M}_n$ freely. By setting $\mathbf{M}_n = \mathbf{I}$, it can be reformulated as $\min_{\mathbf{H}} \|\mathbf{H}\tilde{\mathbf{F}}\|$ subject to $\mathbf{H}\mathbf{G}_x = J_{uu}^{1/2}$. They provided a explicit solution to this problem.

$$\mathbf{H}^T = \left(\tilde{\mathbf{F}}\tilde{\mathbf{F}}^T\right)^{-1} \mathbf{G}_x \left(\mathbf{G}_x^T \left(\tilde{\mathbf{F}}\tilde{\mathbf{F}}^T\right)^{-1} \mathbf{G}_x\right)^{-1} J_{uu}^{1/2}$$

As the minimum singular value has the monotonic property, we can use a branch and bound algorithm to search for the configuration with largest minimum singular value, avoiding the evaluation of all possible configurations [105]

6.3.1 Maximum Gain rule

The Maximum Gain Rule (or Minimum Singular Value) is a criterion for the selection of controlled variables, which is based on the scaled steady-state input-output gain [141]. To derive the maximum gain rule, we return to the loss expression

$$J = \frac{1}{2} z^T z \tag{6.7}$$

where

$$z = J_{uu}^{1/2} (u - u_{opt}) = J_{uu}^{1/2} \mathbf{G}^{-1} (c - c_{opt}) \tag{6.8}$$

and

$$\mathbf{G} = \mathbf{H}\mathbf{G}_x \tag{6.9}$$

It is assumed that $c - c_{opt} = \mathbf{W}_c c'$, where $\mathbf{W}_c$ is the expected optimal variation matrix. It is assumed that $\|c'\|^2 \leq 1$ are allowed. It is required to make $u - u_{opt}$ small. The largest value of $\|z\|_2$ for any allowed $\|e'_c\|^2 \leq 1$ is equal to $\underline{\sigma}\left(J_{uu}^{1/2}\mathbf{G}^{-1}\mathbf{W}_c\right)$. Loss is defined to be [141]

$$L_{max} = \max_{\left\|\begin{bmatrix} d' & n^{x'} \end{bmatrix}^T\right\| \leq 1} L = \frac{1}{2\left(\underline{\sigma}\left(S_1\mathbf{G}S_2\right)\right)^2} \tag{6.10}$$

where $S_1 = \mathbf{W}_c^{-1} = diag\left(\frac{1}{|c_i - c_{opt,i}|}\right)$and $S_2 = J_{uu}^{-1/2}$. S_1 includes the sum of optimal variation (as given by $\mathbf{F}$ matrix) and the expected measurement error.

In the simplified maximum gain rule, we do not need to evaluate Hessian. This is done by choosing the input variables in a way that J_{uu} is close to unity. Maximum gain rule gives considerable insight when we want to compare different alternatives of individual measurements.

6.3.2 Null Space Method

The null-space method, which was proposed by Alstad et al. [142], focuses on minimizing the loss caused by disturbances. If we assume that there is no implementation error, i.e. $\mathbf{W}_{n^x} = 0$, then $\tilde{\mathbf{F}} = \mathbf{F}$ (see equation 6.6), then it is possible to find $\mathbf{H}$ such that $\mathbf{H}\tilde{\mathbf{F}} = 0$. The null space method can be applied if

$$n_x \geq n_u + n_d \tag{6.11}$$

6.3.3 Extended Null Space Method

The concept of Extended Null Space method is to first minimize the loss with respect to disturbances, and then, if there is any remaining degrees of freedom, minimize the loss with respect to measurement error [121]. Two reason which are mentioned for doing this are:

- Disturbances are the reason for introducing optimization and feedback in the first place
- It may be easier later to reduce measurement errors than to reduce disturbances.

An error term is defined as below

$$E = \mathbf{M}_n\mathbf{H}\tilde{\mathbf{G}}_x - \tilde{J} \tag{6.12}$$

where $\tilde{J} = \begin{bmatrix} \mathbf{J}_{uu}^{\frac{1}{2}} & \mathbf{J}_{uu}^{\frac{1}{2}}\mathbf{J}_{uu}^{-1}\mathbf{J}_{ud} \end{bmatrix}$ and $\tilde{\mathbf{G}}_x = \begin{bmatrix} \mathbf{G}_x & \mathbf{G}_x^d \end{bmatrix}$

By writing the optimal sensitivity as $\mathbf{F} = -\tilde{\mathbf{G}}_x \begin{bmatrix} J_{uu}^{-1}J_{ud} \\ -I \end{bmatrix}$ and combining with $\mathbf{M} \triangleq \begin{bmatrix} \mathbf{M}_d & \mathbf{M}_{n^x} \end{bmatrix} = \mathbf{M}_n\mathbf{H}\begin{bmatrix} \mathbf{F}\mathbf{W}_d & \mathbf{W}_{n^x} \end{bmatrix}$, the following expression is obtained.

$$\mathbf{M}_d = \mathbf{M}_n\mathbf{H}\tilde{\mathbf{G}}_x \begin{bmatrix} J_{uu}^{-1}J_{ud} \\ -I \end{bmatrix}\mathbf{W}_d = \left(E + \tilde{J}\right)\begin{bmatrix} J_{uu}^{-1}J_{ud} \\ -I \end{bmatrix}\mathbf{W}_d$$

Since $\tilde{J}\begin{bmatrix} J_{uu}^{-1}J_{ud} \\ -I \end{bmatrix} = 0$,

$$\mathbf{M}_d = E\begin{bmatrix} J_{uu}^{-1}J_{ud} \\ -I \end{bmatrix}\mathbf{W}_d \tag{6.13}$$

The explicit equation for $\mathbf{H}$ is derived which is by minimizing E ,which in turn minimizes $\mathbf{M}_d$, is as below

$$\mathbf{H} = \mathbf{M}_n^{-1}\tilde{J}\left(\mathbf{W}_{n^x}^{-1}\tilde{\mathbf{G}}_x\right)^{\dagger}\mathbf{W}_{n^x}^{-1} \tag{6.14}$$

- For just-enough measurements, $\tilde{\mathbf{G}}_x$ is invertible and $\mathbf{H}$ will be the same as original null-space method.
- For Extra measurements:
  - Select just-enough subset: use $n_x = n_u + n_d$ before forming c and obtain $\mathbf{H}$ to achieve $\mathbf{M}_d = 0$ and use the rest to minimize $L_{wc} = \underset{\|n'^x\|_2 \le 1}{max}\ L = \frac{1}{2}\overline{\sigma}\left(\mathbf{M}_{n^x}\right)^2$
  - Use all measurements: will give solution that minimizes measurement noise subject to zero disturbance loss. († for $\mathbf{H}$ in equation 6.14 is left inverse)
- For too few measurements: The optimal $\mathbf{H}$ is not affected by noise weight. To minimize E, solve $\mathbf{H} = \mathbf{M}_n^{-1}\tilde{\mathrm{J}}\left(\tilde{\mathbf{G}}_x\right)^{\dagger}$, where † is right inverse. However, the objective is to minimize $\|\mathbf{M}_d\|_{\mathbf{F}}$. So, the problem is formulated as below:

$$\mathbf{H} = \arg\min_{\mathbf{H}} \|\mathbf{H}\mathbf{F}\mathbf{W}_d\|_2$$

$$\mathbf{H}\mathbf{G}_x = \mathrm{J}_{uu}^{1/2}$$

6.4 Perfect Indirect Control

Indirect control is when we control a combination of measurements such that there is no effect of disturbances on the primary outputs at steady-state[143]. In indirect control, the loss is deviation from setpoint of the primary variables (instead of an economical loss). It is a special case of self-optimizing control. The control error including measurement noise is ignored in their work. The linear models for measurements x and primary variables y are

$$\mathrm{x} = \mathbf{G}_x\mathrm{u} + \mathbf{G}_x^d\mathrm{d} \tag{6.15}$$

$$\mathrm{y} = \mathbf{G}_y\mathrm{u} + \mathbf{G}_y^d\mathrm{d} \tag{6.16}$$

substituting the above equations in $\mathrm{c} = \mathbf{H}\mathrm{x}$ and rearranging for u, we will have

$$\mathrm{u} = \left(\mathbf{H}\mathbf{G}_x\right)^{-1}\mathrm{c} - \left(\mathbf{H}\mathbf{G}_x\right)^{-1}\mathbf{H}\mathbf{G}_x^d\mathrm{d} \tag{6.17}$$

So,

$$\mathrm{y} = \underbrace{\mathbf{G}_y\left(\mathbf{H}\mathbf{G}_x\right)^{-1}}_{\mathbf{P}_c}\mathrm{c} + \underbrace{\left(\mathbf{G}_y^d - \mathbf{G}_y\left(\mathbf{H}\mathbf{G}_x\right)^{-1}\mathbf{H}\mathbf{G}_x^d\right)}_{\mathbf{P}_d}\mathrm{d} \tag{6.18}$$

$\mathbf{P}_c$ gives the effect of changes in control variables c on primary variables y , and $\mathbf{P}_d$ gives the effect of disturbances on the primary variables. Acceptable indirect control is achieved if $\mathbf{P}_d$ is sufficiently small. There are some assumptions included:

- $n_c = n_u$
- linear models
- control error is ignored (we achieve $\mathrm{c} = \mathrm{c}_s$ at steady state)
- Nominal operating point is optimal (at nominal point: $\mathrm{y} = \mathrm{y}_s$)
- $n_y = n_c$

Based on the number of measurements, there are three cases considered by Hori et al. [143]:

1. For just-enough measurements (if $n_x = n_u + n_d$): We want to find $\mathbf{H}$ such that $\mathbf{P}_d = 0$ ($\mathbf{P}_c = \mathbf{P}_{c0}$). So,

$$\mathrm{y} = \underbrace{\begin{bmatrix} \mathbf{G}_y & \mathbf{G}_y^d \end{bmatrix}}_{\tilde{\mathbf{G}}_y} \begin{bmatrix} \mathrm{u} \\ \mathrm{d} \end{bmatrix} = \mathbf{P}_{c0}\mathbf{H}\tilde{\mathbf{G}}_x \begin{bmatrix} \mathrm{u} \\ \mathrm{d} \end{bmatrix}$$

   So $\mathbf{H} = \mathbf{P}_{c0}^{-1}\tilde{\mathbf{G}}_y\tilde{\mathbf{G}_x^{-1}}$.
   Note: Since $\mathrm{c} = \mathbf{H}\mathrm{x}$, the effect of measurement error on controlled variables c is $n^c = \mathbf{H}n^x$. The corresponding error in the primary variables will be $\mathrm{y} = \mathbf{P}_c\mathbf{H}n^x$. So, the effect of measurement error will be large if the norm of $\mathbf{P}_c\mathbf{H}$ is large. With indirect control, $\mathbf{P}_c\mathbf{H} = \tilde{\mathbf{G}}_y\tilde{\mathbf{G}}_x^{-1}$, which is large if the measurements are closely correlated and $\tilde{\mathbf{G}}_x$ is close to singular.

2. For extra measurements:

   - Select just-enough subset ($n_x = n_u + n_d$): Measurements should be selected such that the effect of measurement noise be minimized. Solve $\max_{\|n^x\|_2 \le 1} \|\mathrm{y}\|_2 = \overline{\sigma}\left(\tilde{\mathbf{G}}_y\tilde{\mathbf{G}}_x^{-1}\right)$. Note that measurements should be scaled.
   - Use all measurements: this will average out the measurement error effect. With $\mathbf{P}_c = \mathbf{I}$, $\mathbf{H} = \tilde{\mathbf{G}}_y\tilde{\mathbf{G}}_x^{\dagger}$, where $\dagger$ is left inverse.

3. For too few measurements: Prefect indirect control is impossible. To minimize $E = \mathbf{P}_{c0}^{-1}\tilde{\mathbf{G}}_y - \mathbf{H}\tilde{\mathbf{G}}_x$, solve $\mathbf{H} = \tilde{\mathbf{G}}_y\tilde{\mathbf{G}}_x^{\dagger}$, where $\dagger$ is right inverse.

Relation to Self-optimizing

The objective function is defined as $\mathrm{J} = \frac{1}{2}(\mathrm{y} - \mathrm{y}_s)^T(\mathrm{y} - \mathrm{y}_s)$. By differentiation, we will have

$$\begin{aligned} \mathrm{J}_u &= \left(\mathbf{G}_y\mathrm{u} + \mathbf{G}_y^d\mathrm{d}\right)^T\mathbf{G}_y \\ \mathrm{J}_{uu} &= \mathbf{G}_y^T\mathbf{G}_y \\ \mathrm{J}_{ud} &= \mathbf{G}_y^T\mathbf{G}_y^d \end{aligned}$$

6.5 Summary

In this chapter, a short review of self-optimizing methods are given. They are based on local analysis of loss and linearized steady state model at an operating point with an assumption that the plant economics are governed by the plant pseudo/steady state behavior. An explicit solution is presented for loss method. This method is used in the next chapter to find the appropriate control variables for Kaibel distillation column.

Chapter 7

Economically Optimal Control of Kaibel Distillation Column: Fixed boilup rate

In this chapter, a control structure is designed for a 4-product dividing wall (Kaibel) distillation column, based on the plant-wide control procedure by [2]. Unlike the common approach, vapour split is considered as a degree of freedom. The exact local method is used to find the best control variables as single measurements or combination of measurements.

7.1 Introduction

The choice of control structures for thermally-coupled columns is an important issue for practical industrial operation. There are some literature on controllability study and control of dividing-wall columns, which were mostly on 3-product columns (e.g. [144], [116], [145] and [110]). In this work, we have presented the approach of self-optimizing control for selecting the appropriate control variables for 4-product divided-wall distillation column. In addition, we have considered the vapour split as a degree of freedom which can be used for control. As it was shown earlier, the ability of the column to handle disturbances will be enhanced by having R_V manipulated ([146]). The performance of the controlled system is shown by dynamic simulations in face of various process disturbances.

7.2 Steady-State Optimal Operation

The idea behind self-optimizing control is to find a variable which characterizes operation at the optimum, and the value of this variable at the optimum should be less sensitive to variations in disturbances than the optimal value of the remaining degrees of freedom.

7.2.1 Process Description

The model used for this study is simulated in HYSYS. The feed stream is an equimolar mixture of methanol, ethanol, 1-Propanol, 1-butanol and saturated liquid. The constant value assigned to boilup rate is obtained from the minimum energy diagram (see [43]). The nominal optimal solution is found as it is shown in Table 7.1. All the optimal operating points for different sets of the disturbances are found by applying an optimization solver in MATLAB with the full non-linear model in HYSYS. The nominal values for inputs are shown in bold numbers. In this study,

Table 7.1: Optimal values for the variables

Var.		Nominal value	Unit
RR	Reflux Ratio	6.375	ratio
V	Vapor boilup	157	kmol/h
Q	Reboiler duty	1842	kW
D	D flow rate	24.43	kmol/h
B	B flow rate	24.41	kmol/h
$S1$	S1 flow rate	24.93	kmol/h
$S2$	S2 flow rate	26.22	kmol/h
Rl	Liquid split	0.388	ratio
Rv	Vapor split	0.597	ratio
F	Feed flow	**100.0**	kmol/h
z_F	Feed composition	$\begin{bmatrix} \mathbf{1} & \mathbf{1} & \mathbf{1} & \mathbf{1} \end{bmatrix}/\mathbf{4}$	mol/mol
q	Feed quality	**1.0**	-
x_D	C1 composition in D	97.66	mol%
x_{S1}	C2 composition in B	94.19	mol%
x_{S2}	C3 composition in S2	93.48	mol%
x_B	C4 composition in B	99.28	mol%
J	Objective value	0.0011	

we assume that the design is fixed and we only consider the operational degrees of freedom to optimize the process.

7.2.2 Definition of the Objective Function

Defining an objective function for optimal operation depends on the purpose of the process. In terms of operation of Kaibel distillation column, there are two different ways to operate a distillation column. One approach is to specify the product purities and use the remaining degrees of freedom for minimizing the vapor consumption, which is the motivation to introduce thermally-coupled columns. The other approach is to fix the column boilup at the maximum and try to get the most out of the column. This case happens in the situations when energy is relatively cheap. So, in this case the objective is to make the purest products possible with a given energy. It is shown that the first option is the more difficult case to handle, which is due to the very narrow solution surface and also multiplicity problem ([135]). By multiplicity we mean that there are two values for boilup flow as all the degrees of freedom are kept constant. The physical interpretation of multiplicity in this case is that there are two ways for the internal flow streams to get to the outlet streams and to satisfy the specifications.

In this chapter, we focus on the second objective. The Objective function is defined as the summation of impurities in the product streams (Eq. 7.1). Two different cases will lead to this definition ([130]).

1. If all the prices for the products are equal and we only get paid for the main component. J is then the loss compared to the pure products.

2. If products 2 (first side stream) and 4 (the bottom product) are as valuable as feed and the distillate and second side stream are the valuable products. In this case, loss compared to the ideal profit (pure products) is defined as the previous case.

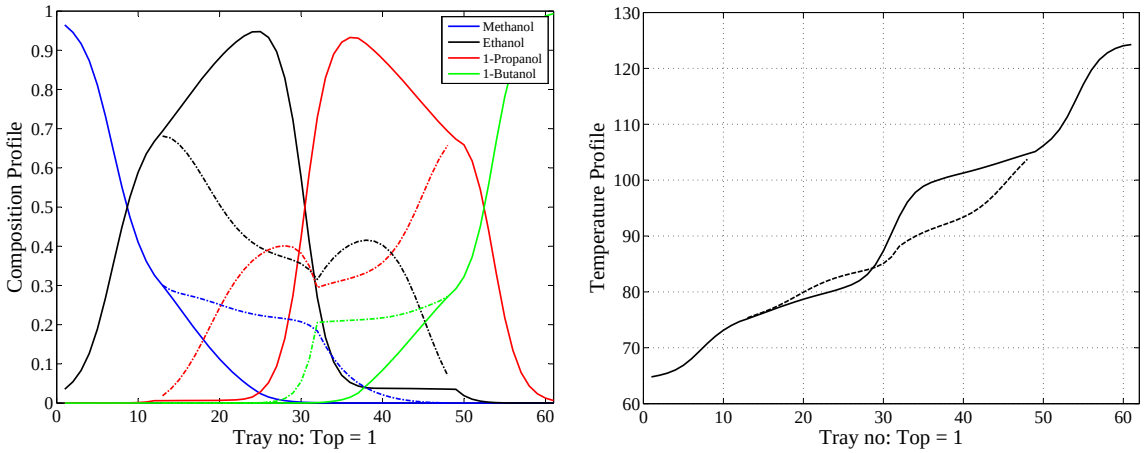

Figure 7.1: Optimal composition and temperature profiles for Kaibel column

$$\begin{aligned}\mathbf{J} = \mathrm{D}\,(1 - x_D) + \mathrm{S}_1\,(1 - x_{S1}) \\ + \mathrm{S}_2\,(1 - x_{S2}) + \mathrm{B}\,(1 - x_B)\end{aligned} \tag{7.1}$$

7.2.3 The Degrees of Freedom

Degrees of freedom used for stabilization

Before talking about the steady-state degrees of freedom, we should make sure that a consistent inventory control is applied and hence remove the manipulated variables which are used in this layer (see the guidelines proposed by Aske et al [147]). The Throughput Manipulator (TPM) is the feed to the column. TPM is a degree of freedom that affects the network flow and is not directly or indirectly determined by the control of the individual units, including their inventory control. The common LV configuration is used here, where D and B are used for level control and L and V remain as degrees of freedom. Pressure in the top of the column is controlled by the heating duty of the condenser. An additional inventory issue for distillation columns is related to the split between light and heavy components (component inventory). One is not really free to set the split between D and B, and to avoid a 'drifting' composition profile (with possible 'breakthrough' of light component in the bottom or of heavy component in the top). A quality (e.g., temperature) loop should be closed to achieve component local consistency ([147]). In this work, we have tried to use the same temperature loops in the upper layer as for stabilization. So, it is important that the single measurements are chosen from different sections of the column.

Remaining degrees of freedom

We are left with six degrees of freedom: boilup duty, reflux rate, side stream flows, liquid split and vapor split. Since boilup rate is assumed to be constant by manipulating the reboiler heat duty (and since we do not have any constraint on product composition specification), there will remain 5 variables for optimization purposes. Changes in the setpoints of controllers, feed flow rate (F), feed composition (z_F) and feed liquid fraction (q) are considered as disturbances. In this work, the vapor split is used as a manipulated variable.

Table 7.2: Expected disturbances

Disturbances	$\mathbf{W}_d$
Feed flow rate	10%
Feed quality	0.1
Boilup flow rate	10%
Feed composition (for each component)	0.05

7.2.4 Control Variable Selection

Control variable (CV) selection is based on the exact local method ([141]; [120]; [121]). This method is based on 2nd order approximation of the objective function around the operating point. So the cost function behaviour should be quadratic around the optimal point, which is the case for our process if the steps are small enough. Table 7.2 shows the expected values for disturbances in the process.

The controlled variables are considered to be a combination of measurements:

$$\mathrm{c} = \mathbf{H}\mathrm{x} \tag{7.2}$$

Since we want to use single measurements, matrix $\mathbf{H}$ contains n_c number of columns with a single 1 and rest of the columns are zero. Note that we have also tried the combination of all the measurements, which means that the measurements from all the temperature sensors in the column are combined to be controlled by the manipulated variables. The matrix $\mathbf{H}$ is full and the rows are the measurements from those specific trays on which we have sensors let's say every fourth tray in the column. $\mathbf{H}$ is found by minimizing the frobenius norm of the loss:

$$\min_{\mathbf{H}} \|\mathbf{J}_{uu}^{1/2} \left(\mathbf{H}\mathbf{G}_x\right)^{-1} \mathbf{H}\tilde{\mathbf{F}}\|_F^2 \tag{7.3}$$

where $\tilde{\mathbf{F}} = \begin{bmatrix} \mathbf{F}\mathbf{W}_d & \mathbf{W}_{\mathrm{n}^x} \end{bmatrix}$. $\mathbf{F}$ is the optimal sensitivity matrix. It can be found numerically from its definition or using

$$\mathbf{F} = -\mathbf{G}_x\mathbf{J}_{uu}^{-1}\mathbf{J}_{ud} + \mathbf{G}_x^d$$

The second derivatives can be difficult to obtain, especially if one relies on numerical methods, and also taking the difference can introduce numerical inaccuracy. Therefor we obtained $\mathbf{F}$ from its definition (shown below), by numerically re-optimizing the model for the disturbances.

$$\mathbf{F} = d\mathrm{x}_{opt}/d\mathrm{d} \tag{7.4}$$

It is most common that distillation columns are controlled using temperatures as measurements. The temperature at a stage in a distillation column is a good indication of its composition. Skogestad et al. [101] present some benefits of using temperature loops for controlling the composition:

1. Stabilizes the column composition profile along the column
2. Gives indirect level control: Reduces the need of level control
3. Gives indirect composition control: Strongly reduces disturbance sensitivity
4. Makes the remaining composition problem less interactive and thus makes it possible to have good two-point composition control
5. Makes the column behave more linearly

In this work, we have used the column temperatures as candidate control variables. Note that the implementation error is considered to be 0.1 degree centigrade for the temperature sensors.

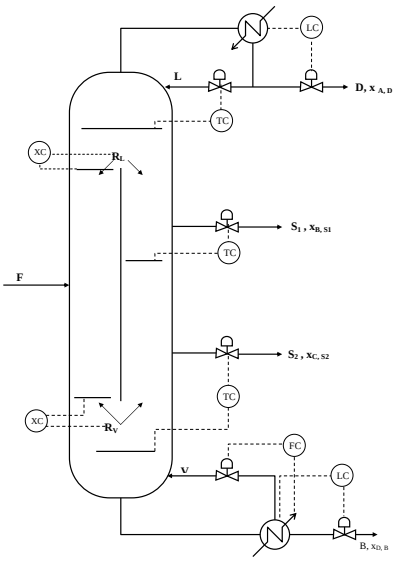

Figure 7.2: Kaibel column control configuration with controlling compositions at prefractionator's ends

7.3 Results and Discussions

The required matrices are obtained by linearizing the plant around the operating point. Calculation of **F** matrix is done by re-optimizing the process for different disturbances. The Genetic Algorithm toolbox in MATLAB has been used for this purpose.

7.3.1 Composition control in prefractionator

Before going to the results of control variable selection by systematically combining the temperature measurements, we would like to comment about the selection of appropriate control variables from engineering point of view. As mentioned earlier, the task of the prefractionator in Kaibel column is to separate the two middle components. The impurities from top and bottom of prefractionator will end up in the side streams and will lead to less pure side products. So, it is wise to limit the impurity flows from prefractionator to the main column. To avoid this, we need to control the composition of the heavy impurity in the top and the light impurity in the bottom of the prefractionator (see Figure 7.2). It is assumed that the compositions are directly controlled with the composition controllers. Figures 7.3 and 7.4 show the dynamic response of the closed-loop system to some of the disturbances. However, composition measurement is always with delay and of course composition of the internal trays are not accessible. A soft-sensor should be designed to give the estimate of the required compositions.

7.3.2 Control structure based on Exact Local method

Single measurements

Figure 7.5 shows the temperature profiles after re-optimizing when different disturbances happen. This gives us some insight about where is the proper place to pick the measurements from. The points with less sensitivity to disturbances and more sensitivity to changes in manipulated variables are preferred. This means that the temperature measurements in the range of top part in the main column are among the best options for this process. This argument is true when our goal is to select single measurements to be controlled by the manipulated variables.

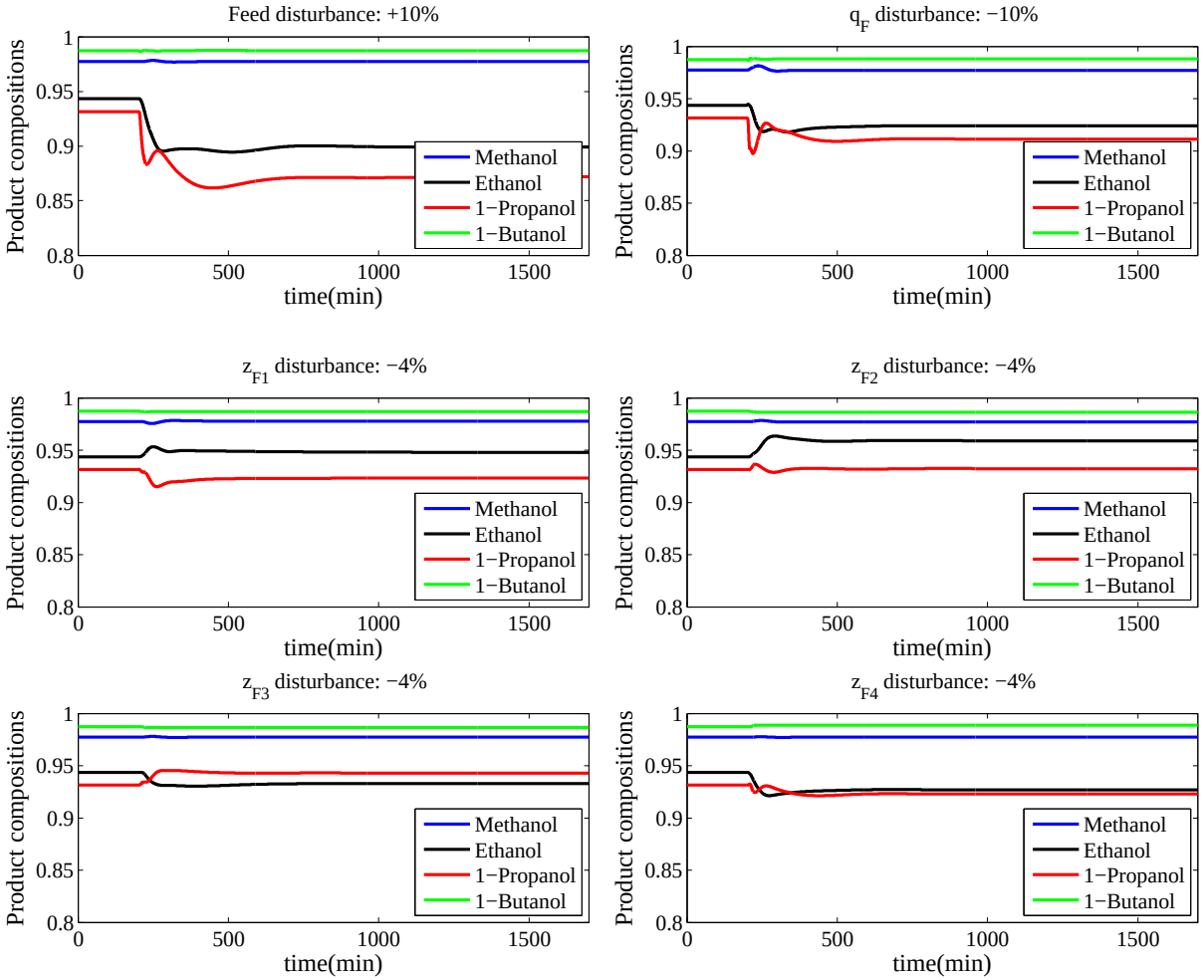

Figure 7.3: Product compositions of Kaibel column; Impurities estimation in the ends of pre-fractionator are controlled

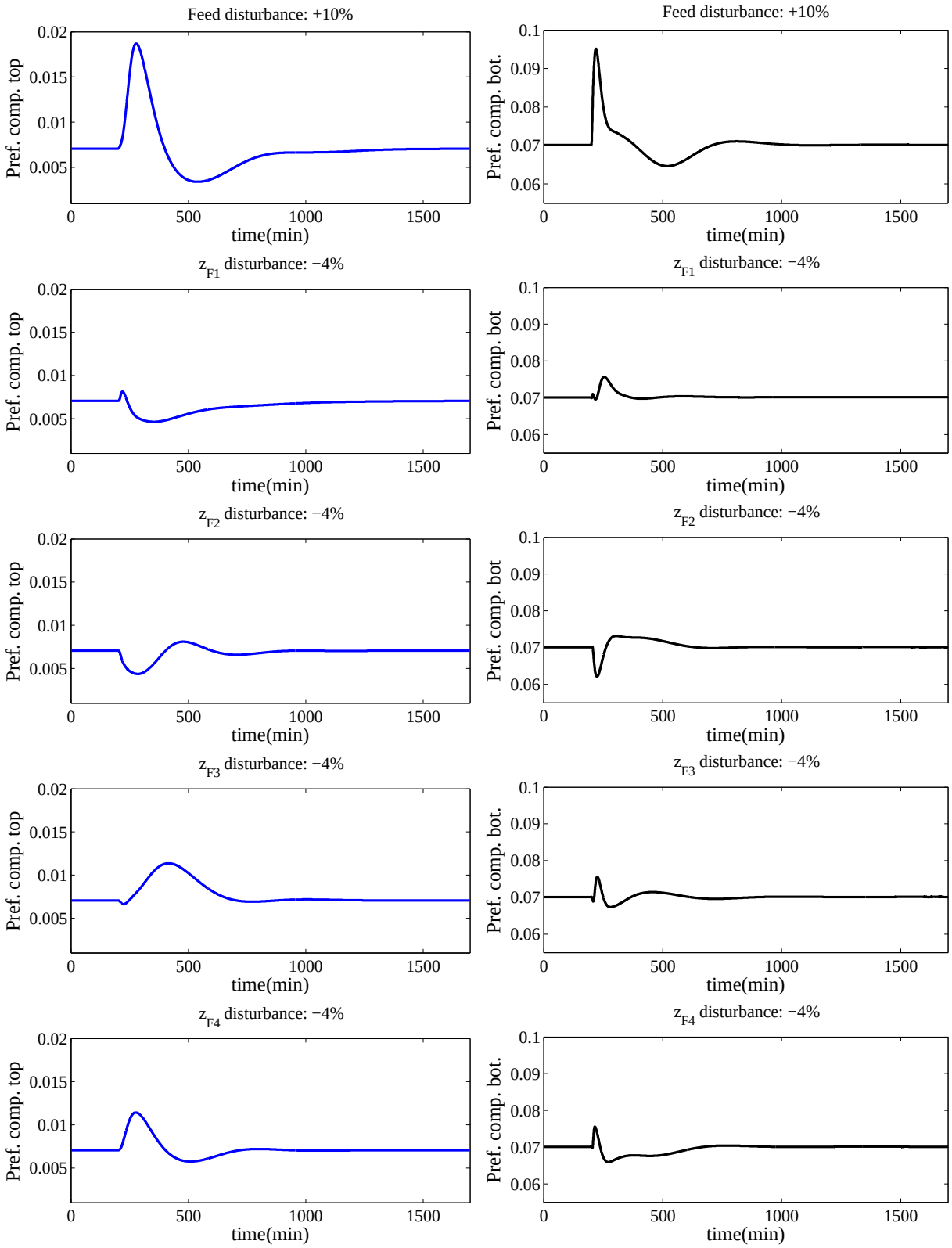

Figure 7.4: Responses of controlled estimated compositions of prefractionator ends

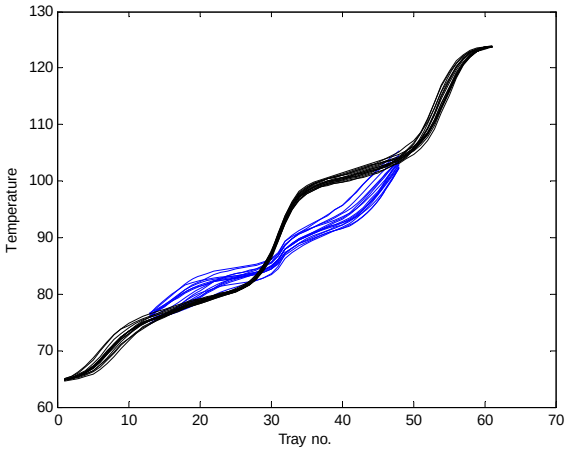

Figure 7.5: Optimal temperature profiles for disturbances in feed compositions, liquid fraction and boilup flow setpoint

Table 7.3: Proposed control structure

MV	CV	Setpoints
Liquid split (R_L)	T15	83.63
Vapour split (R_V)	T36	103.7
Reflux	T39	65.46
S1 flow	T54	77.76
S2 flow	T75	100.9

However, it is not clear from the temperature profiles that what will be the case for combination of measurements.

Table 7.3 shows the set of measurements selected by the exact local method as best control variables and their nominal values.

RGA is a measure of interactions between the loops. RGA elements larger than one means that the corresponding loop will have a smaller gain by closing other loops, and vise versa. One should select pairings such that RGA $\approx \mathbf{I}$ at the crossover for the rearranged system. In addition the steady-state RGA should be considered. We found the steady state 5×5 matrix of RGA:

$$\begin{array}{c} \\ T15 \\ T36 \\ T39 \\ T54 \\ T75 \end{array} \begin{array}{c} \begin{array}{ccccc} R_l & R_v & RR & Side_1 & Side_2 \end{array} \\ \begin{bmatrix} 0.31 & 0.72 & 0.49 & -0.06 & -0.47 \\ -0.74 & 0.42 & 10.37 & 0.33 & -9.38 \\ 2.18 & -0.78 & 4.16 & -1.50 & -3.07 \\ -1.13 & 0.77 & -4.22 & 2.31 & 3.27 \\ 0.38 & -0.13 & -9.81 & -0.08 & 10.64 \end{bmatrix} \end{array}$$

where steady-state RGA is calculated as

$$RGA(\mathbf{G}) = \mathbf{G} \times (\mathbf{G}^{-1})^T \tag{7.5}$$

The pairing is done based on the RGA rules

- Avoid pairing on negative steady-state relative gain, otherwise you get instability if one of the loops become inactive.
- Choose pairings corresponding to RGA-elements close to 1 (actually only at bandwidth frequency).

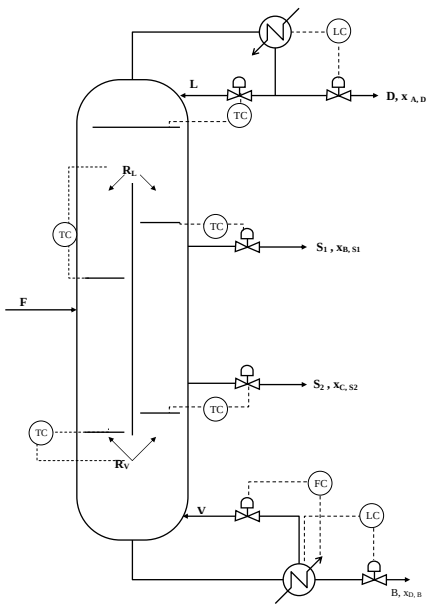

Figure 7.6: Control structure of Kaibel column with single measurements

- Prefer pairing on variables with good controllability (=small effective delay).

  From this we see that the pairing given in Table 7.3 and shown in Figure 7.6 is acceptable and the final control structure and the dynamic response to some disturbances are shown in Figures 7.7 and 7.8. The temperature controller on S2 had to be detuned. One of the drawbacks of using HYSYS as the simulation tool is that the steady-state and dynamics environments are separated from each other. When converting to dynamic mode, the steady-state specifications will be deactivated and controllers should do the task of stabilization and keeping variables at their specifications. Choosing the right control structure to get to the same profiles as the steady-state model in important. This is done by closing composition loops at the ends of the prefractionator (x_{C3} in top and x_{C2} in bottom of prefractionator), the distillate product composition (x_{C1}) and ratios of impurities in side streams ($\frac{x_{C1}}{x_{C3}}$ in side stream 1 and $\frac{x_{C2}}{x_{C4}}$ in side stream 2).

  As mentioned previously, we would like to use the same control loops in the supervisory layer as the stabilizing layer. So, the measurements should be picked from all sections of the column. In addition, it would be interesting to control a controlled variable with a manipulated variable in the same part of the process. So, we need to exert structural constraint in the **H** matrix ([148]).

Combination of measurements

Figure 7.9 shows the trend of **H** values along the column. We assume we have temperature sensors in every 4th tray. From this figure, we can get idea about which temperatures in the column play more important role and how we can use structured **H**. For example, a section of a column which does not have a major effect can be removed. The loss will be larger when all the measurements are not used, but the dynamic properties are better. The calculated average loss in this case is 2.34e-4 compared to 0.1791 which is the loss for single temperature measurements. This shows that the effect of measurement error is averaged out.

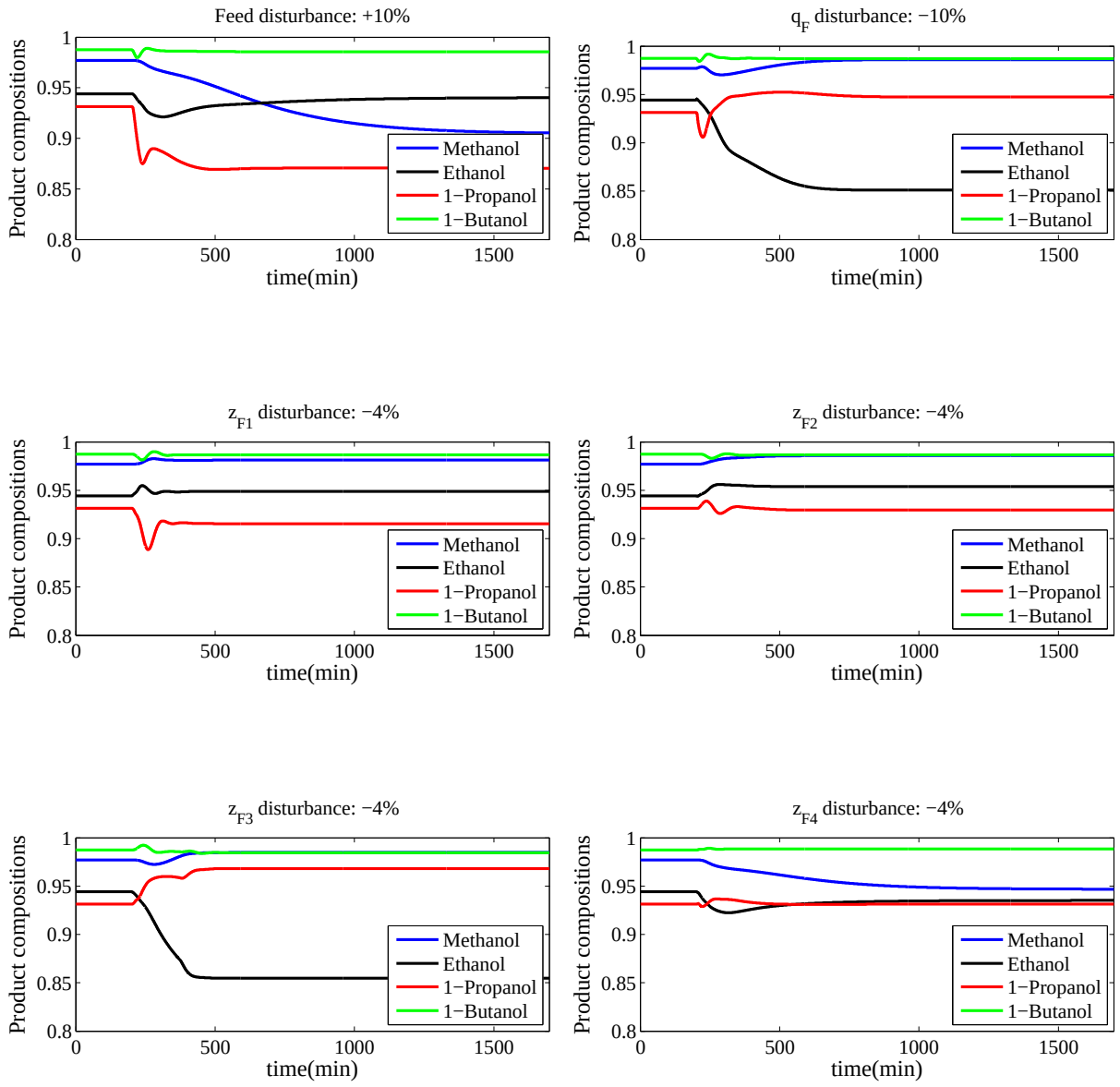

Figure 7.7: Product compositions of Kaibel column; Responses of control structure by self-optimizing method

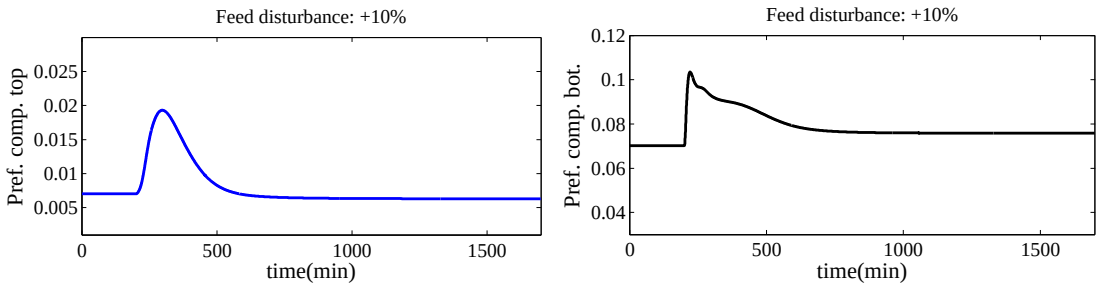

(a) Change in feed flow

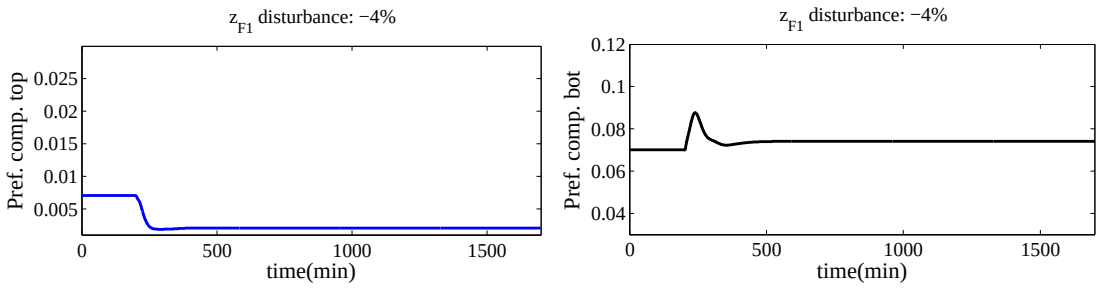

(b) Change in zF1

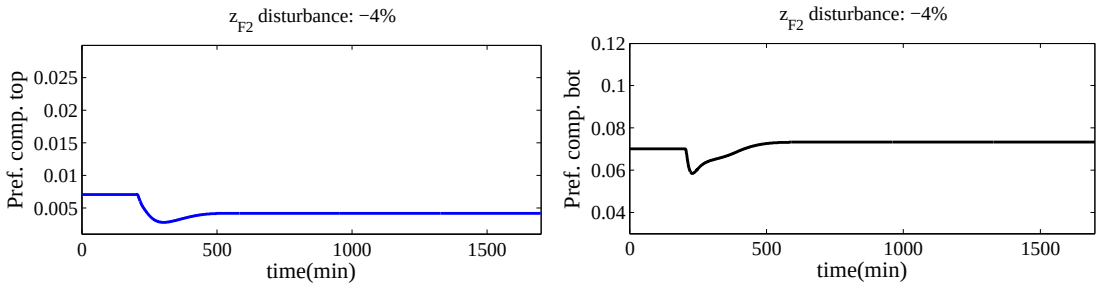

(c) Change in zF2

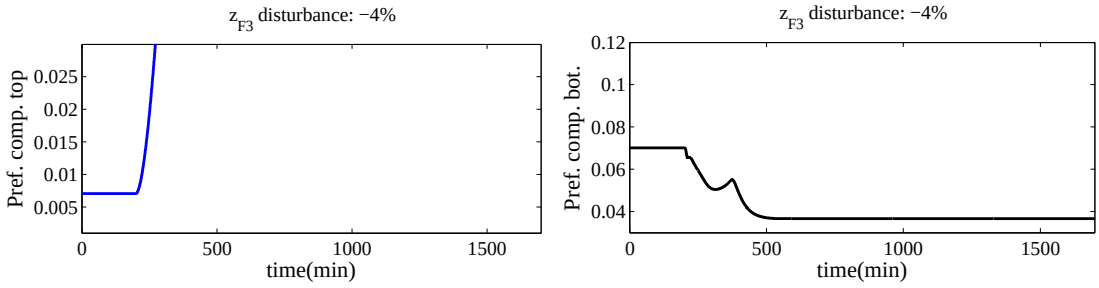

(d) Change in zF3

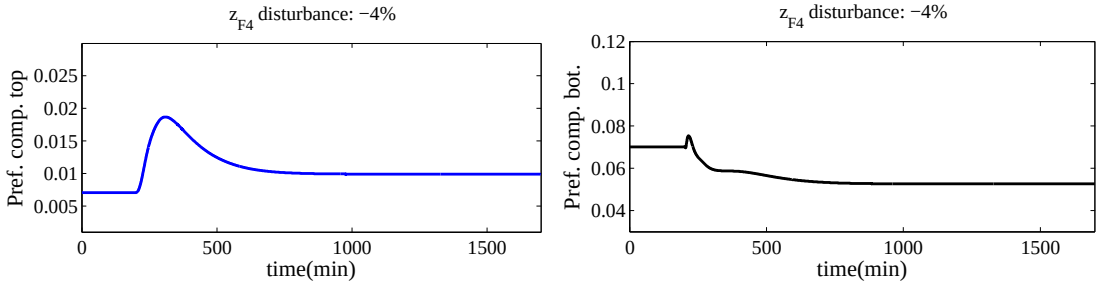

(e) Change in zF4

Figure 7.8: Responses of control structure by self-optimizing method

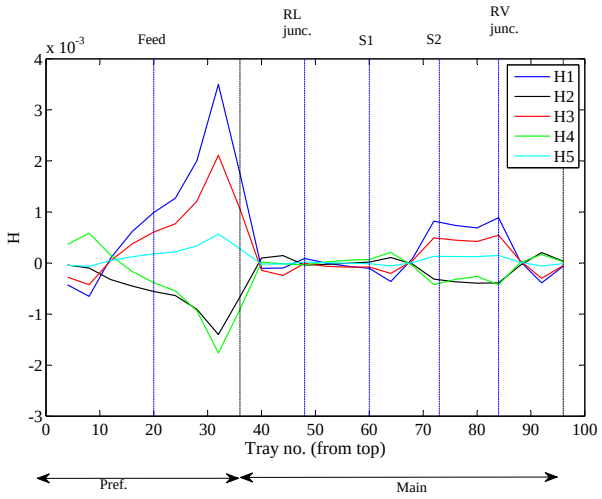

Figure 7.9: **H** values for combination of measurements (every 4th tray)

7.4 Conclusions

In this work, we applied a systematic method to select the control variables for a Kaibel distillation column. The objective was to maximize the product purities with fixed boilup rate. This is when there are some limitations for the boilup flowrate in some plants because of the utility limitations or bottlenecks. For better performance, it's better to use a combination of measurement as control variables.

Chapter 8

A Short Review on the steady-state estimation methods

In this chapter, a short review of steady-state estimation methods is presented. The focus is more on the methods that has been used in this thesis

8.1 Introduction

It happens frequently in process control that some important variables are not measurable. Sometimes they are expensive to measure and include delay. The value of primary variable can be inferred by using some secondary variable measurements. The task of soft sensors is the maximal exploitation of transforming the information of secondary measurements into more useful process knowledge. They provide frequent on-line estimates of quality variables on the basis of their correlation with real-time process measurements. Such predictive models devoted to producing real-time estimates of desired plant variables can help to reduce the need for measuring devices, improve system reliability, and develop tight control policies.

There are several advantages of inferential sensors in comparison with traditional instrumentation, including easy implementation, no capital cost and more information from the existing data. At a very general level, these fields can be divided into three broad categories [149]:

1. Process monitoring
   - Substituting/complimenting on-line instrumentation
   - Predicting process quality variables or key performance indicators
   - Monitoring and analysis of process trends
   - Fault detection
2. Process control
   - Development of advanced control strategies, such as model predictive control
   - Heuristics and logic in planning and scheduling of process operations
3. Off-line operation assistance
   - Diagnosis of process operations
   - Knowledge based engineering design
   - Development of plant simulator

Both dynamic and static estimators may be used, but the simpler static estimators are most common in the process industry. Since our method is a static estimator, our literature survey is limited to this group. There are many approaches that have been used to obtain the static estimators, including multivariate regression [150, 151], artificial neural networks [152], support vector machine regression [153], etc. At a very general level one can distinguish two different classes of Soft Sensors, namely model-driven and data-driven. In the next section, we will shortly describe these two categories.

8.2 Data-based Estimators

Process data analysis is the initial step in the design of inferential sensors. The careful investigation of laboratory and operational data enables us to extract relevant information contained in historical data, select influential variables, and assess data quality (e.g. reliability, accuracy, completeness, and representativeness).

The collected process data is often divided into two subsets: the calibration data-set and the validation data-set. The calibration data-set is used for inferential model identification purposes, while the validation data-set is used for evaluating the performance of the developed inferential sensor. It is noteworthy that the distribution of calibration data within the process operating region is crucial to ensure the quality of inferential sensors. This will be seen in the next chapter's example.

Principle Component Regression (PCR) [154] and Partial Least Squares (PLS) [155] are two of the most used data analysis tools in chemometrics. These methods are based on projecting the solution to a lower-dimensional subspace. These methods are discussed in the following sections. Here, we start from the observations collected in the matrices $\mathbf{X}$ and $\mathbf{Y}$. We want to obtain a linear relationship between the data sets.

$$\mathbf{Y} = \mathbf{XB} + \mathbf{B}_0 \tag{8.1}$$

where $\mathbf{B}$ and $\mathbf{B}_0$ as optimization variables. $\mathbf{B}_0$ is normally zero if the data are centered. The least-square solution to this problem is

$$\mathbf{B} = \mathbf{YX}^{\dagger} \tag{8.2}$$

8.2.1 Principal Component Regression (PCR) Method

It starts with a principal component singular value analysis of the data matrix $\mathbf{X}$, to remove directions in $\mathbf{X}$ data with little information. The matrix is truncated to rank a, where a is the number of principal components, and gives $\tilde{\mathbf{X}} = \tilde{\mathbf{U}}_a \tilde{\Sigma}_a \tilde{\mathbf{V}}_a^T$. The optimal estimator is then

$$\mathbf{B}_{PCR} = \mathbf{Y}\tilde{\mathbf{X}}^{\dagger}$$

where $\tilde{\mathbf{X}}^{\dagger}$ is the inverse of the truncated SVD of the matrix $\mathbf{X}$.

8.2.2 Partial Least Square (PLS) Method

This method is used to compress the predictor data matrix X, into a set of latent variable or factor scores. The orthogonal factor scores are used to fit a set of observations to dependent variables Y. The main attraction of the method is that it finds a parsimonious model even when the predictors are highly collinear or linearly dependent.

In its general form, PLS creates orthogonal score vectors (called latent vectors or components) by maximizing the covariance between different sets of variables. There are several different algorithms generating bases which all give the same predictor, when there is one $\mathbf{Y}$ variable. Rosipal et al. present a review of the different forms [156]. Some of them are described in more detail below.

Nonlinear Iterative Partial Least Squares (NIPALS)

The first PLS approach was nonlinear iterative partial least squares (NIPALS), which was proposed by Wold et al. [157]. The first step is to center the data matrices $\mathbf{X}$ and $\mathbf{Y}$. The predictor data matrix $\mathbf{X} = [\mathrm{x}_1, \mathrm{x}_2, \ldots, \mathrm{x}_r]$, containing the values of r predictors for N samples is compressed into a set of a orthogonal factor scores $\mathbf{T} = [\mathrm{t}_1, \mathrm{t}_2, \ldots, \mathrm{t}_a]$, where $A \leq r$. The factor scores $\mathbf{U} = [\mathrm{u}_1, \mathrm{u}_2, \ldots, \mathrm{u}_a]$ are calculated from companion matrix $\mathbf{Y} = [\mathrm{y}_1, \mathrm{y}_2, \ldots, \mathrm{y}_m]$. The first factors t_1 and u_1 are weighted sums of the centered variables: $\mathrm{t}_1 = \mathbf{X}\mathrm{w}_1$ and $\mathrm{u}_1 = \mathbf{Y}\mathrm{q}_1$. The next factors are determined sequentially using NIPALS. The sequence is as below

$$\mathrm{w}_1 \propto \mathbf{X}'\mathrm{u}_1 \tag{8.3}$$

$$\mathrm{t}_1 = \mathbf{X}\mathrm{w}_1 \tag{8.4}$$

$$\mathrm{q}_1 \propto \mathbf{Y}'\mathrm{t}_1 \tag{8.5}$$

$$\mathrm{u}_1 = \mathbf{Y}\mathrm{q}_1 \tag{8.6}$$

Here, the symbol $\propto$ not only indicates proportionality, but it also implies the subsequent normalization of the resultant vector. Thus, the weight vectors w_1 and q_1 have length 1. The iteration sequence starts by choosing for u_1 some columns of $\mathbf{Y}$, e.g. the one having maximum variance. Once the first $\mathbf{X}$ block factor t_1 is obtained, the matrices $\mathbf{X}$ and $\mathbf{Y}$ are deflated

$$\mathbf{X}_1 = \mathbf{X}_0 - \mathrm{t}_1\mathrm{p}_1' \tag{8.7}$$

$$\mathbf{Y}_1 = \mathbf{Y}_0 - \mathrm{b}_1\mathrm{t}_1\mathrm{q}_1' \tag{8.8}$$

where

$$\mathrm{p}_1 = \frac{\mathbf{X}_0'\mathrm{t}_1}{\mathrm{t}_1'\mathrm{t}_1} \tag{8.9}$$

The scalar b_1 is the estimated regression coefficient for the inner relation between the two datasets. There are some assumptions which are inherent in the problem definition or some in the solution procedure, which are as follows [158]:

1. Assume centered data generated according to the latent variable model
2. Weight matrices should have orthonormal column vectors
3. The number of y variables is less than the number of components ($m \leq A$)
4. Components of measurement variables and response variables are independent, i.e. diagonal expectations $\mathrm{E}\left(\mathrm{x}_k, \mathrm{x}_k^T\right) = 0$ and $\mathrm{E}\left(\mathrm{y}_k, \mathrm{y}_k^T\right) = 0$
5. The most important assumption is that the outputs and the input data have linear relationship.

The NIPALS method includes various iterative orthogonalization (deflation) processes. In addition, since the weight vectors used for defining the associated factor scores are applied to a residual matrix, the interpretation of the factors is difficult. It is also possible that the method does not converge to a solution. The NIPALS does not converge if two or more of the eigenvectors of the matrix $\mathbf{X}$ are almost identical.

SIMPLS

To avoid deflation steps at each iteration of PLS1 and PLS2, de Jong [159] has introduced another form of PLS denoted SIMPLS. They have put this name on their algorithm, since it is a straightforward implementation of a Statistically Inspired Modification of the PLS method according to the simple concept given in Table 1. The SIMPLS approach directly finds the weight vectors which are applied to the original not deflated matrix $\mathbf{X}$. It has been shown that SIMPLS is equal to PLS1 but differs from PLS2 when applied to the multidimensional matrix $\mathbf{Y}$ [159]. It is shown that upon convergence the weight vectors w_1 and q_1 correspond to the first pair of left and right singular vectors obtained from singular vector decomposition of the matrix $\mathbf{X}'\mathbf{Y}$ [160]. SIMPLS starts with computing the matrix $\mathbf{S} = \mathbf{X}'\mathbf{Y}$ and computing the SVD of this product. We will have the scores and loadings as below

$$t = \mathbf{X}r$$
$$p = \frac{\mathbf{X}t}{t't}$$

where r is the first left singular vector. The loadings and scores in the next rounds are obtained by calculating the SVD of $\mathbf{S} - \mathbf{P}\left(\mathbf{P}'\mathbf{P}\right)^{-1}\mathbf{P}'\mathbf{S}$.

So,

$$\mathbf{B}_{PLS} = \mathbf{R}\mathbf{T}^{\dagger}\mathbf{Y} \tag{8.10}$$

where, $\mathbf{R} = [r_1, r_2, \ldots, r_a]$.

In the context of process industry, measurement noise, missing measurements, outlying observations, multi-rate data, measurement delay, and drifting data are the common factors affecting the quality of process data. The satisfactory performance of inferential sensors can be achieved only if such challenging issues are addressed. As a preliminary step, thus, data pre-processing is often required in order to obtain a data-set which adequately represents the characteristic properties of process under investigation [161].

Non-iterative PLS

Di Ruscio et al. have presented a new interpretation and description of the basic PLS solution which is non-iterative, which is more interesting for control community [162]. This solution can be expressed in terms of some weighting vectors only. The equivalence between this method and the NIPALS version of the PLS method is demonstrated by Elden et al. by proving that they give the same sequence of orthogonal basis vectors [163]. The weight matrix $\mathbf{W}_a$ is of size $r \times a$ (so the number of components, a, should of course first be specified). They have first calculated the weight vectors by an orthogonalization process. The solution is parameterized as $\mathbf{B} = \mathbf{W}_a p$, where the vector p is chosen to minimize the Frobenius norm of $\mathbf{Y} - \mathbf{X} \times \mathbf{B} = \mathbf{Y} - \mathbf{X} \times \mathbf{W}_a \times p$ for some specified weighting matrix $\mathbf{W}_a$.

The orthogonalization process for calculating the weight vectors is not unique. It is evident that any weighting matrix defined as $\mathbf{W}_a := \mathbf{W}_a\mathbf{D}$ (where $\mathbf{D} \in \mathbb{R}^{a \times a}$ is defined as a non-singular transformation matrix) can be a solution for this problem, as mentioned by Di Ruscio et al. [162]. So, by taking the weights $\mathbf{W}_a$ from the Krylov subspace or from the space which span the Krylov subspace, the optimal weights will be found in the sense that an iterative Ordinary Least square (OLS) converges the fastest to the OLS solution, i.e. in a minimum number of iterations [162].

Theorem 1. *(PLS1: a non-iterative solution). [162]: Given data matrix* $\mathbf{X} \in \mathbb{R}^{N\times r}$ *and* $\mathbf{Y} \in \mathbb{R}^{N}$*, the PLS solution is given by*

$$\mathbf{B}_{PLS} = \mathbf{K}_a \mathrm{p}^* r \tag{8.11}$$

where $\mathbf{K}_a \in \mathbb{R}^{r\times a}$ *is the reduced controllability (Krylov) matrix for the pair* $\left(\mathbf{X}^T\mathbf{X}, \mathbf{X}^T\mathbf{Y}\right)$ *defined as*

$$\mathbf{K}_a = \left[\begin{array}{cccc} \mathbf{X}^T\mathbf{Y} & \mathbf{X}^T\mathbf{X}\mathbf{X}^T\mathbf{Y} & \left(\mathbf{X}^T\mathbf{X}\right)^2\mathbf{X}^T\mathbf{Y} & \ldots \quad \left(\mathbf{X}^T\mathbf{X}\right)^{a-1}\mathbf{X}^T\mathbf{Y} \end{array}\right]$$

where $1 \le a \le r$*, and the polynomial coefficient vector* $\mathrm{p}^* \in \mathbb{R}^a$ *is determined as the LS solution to*

$$\mathrm{p}^* = \arg\min \|\mathrm{V}(\mathrm{p})\|_F^2 \tag{8.12}$$

where

$$\mathrm{V}(\mathrm{p}) = \|\mathbf{Y} - \mathbf{X}\mathbf{K}_a\mathrm{p}\|_p^2 \tag{8.13}$$

Hence

$$\mathrm{p}^* = \left(\mathbf{K}_a^T\mathbf{X}^T\mathbf{X}\mathbf{K}_a\right)^{-1}\mathbf{K}_a^T\mathbf{X}^T\mathbf{Y} \tag{8.14}$$

which gives the PLS solution

$$\mathbf{B}_{PLS} = \mathbf{K}_a\left(\mathbf{K}_a^T\mathbf{X}^T\mathbf{X}\mathbf{K}_a\right)^{-1}\mathbf{K}_a^T\mathbf{X}^T\mathbf{Y} \tag{8.15}$$

with the assumption that $\left(\mathbf{K}_a^T\mathbf{X}^T\mathbf{X}\mathbf{K}_a\right)^{-1}$ *is non-singular for some* $1 \le a \le r$*. The PLS prediction of* $\mathbf{Y}$ *is given by*

$$\mathbf{Y}_{PLS} = \mathbf{X}\mathbf{K}_a\mathrm{p}^* \tag{8.16}$$

where p^* *is given by (8.14). Furthermore, the minimum is*

$$\mathrm{V}(\mathrm{p}^*) = trace\left(\mathbf{Y}^T\mathbf{Y}\right) - trace\left(\mathbf{Y}^T\mathbf{X}\mathbf{K}_a\left(\mathbf{K}_a^T\mathbf{X}^T\mathbf{X}\mathbf{K}_a\right)^{-1}\mathbf{K}_a^T\mathbf{X}^T\mathbf{Y}\right) \tag{8.17}$$

Proof. From Cayley-Hamilton Theorem we have that $\mathbf{X}^T\mathbf{X}$ satisfies its own characteristic equation, i.e.

$$\left(\mathbf{X}^T\mathbf{X}\right)^r + \mathrm{p}_2\left(\mathbf{X}^T\mathbf{X}\right)^{r-1} + \ldots + \mathrm{p}_r\mathbf{X}^T\mathbf{X} + \mathrm{p}_{r+1}\mathbf{I}_r = 0 \tag{8.18}$$

where $p_2, \ldots, p_{r+1}$are the coefficients of the characteristic polynomial $\det(\lambda\mathbf{I}_r - \mathbf{X}^T\mathbf{X})$. This can be used to form the matrix inverse

$$\left(\mathbf{X}^T\mathbf{X}\right)^{-1} = -\frac{1}{\mathrm{p}_{r+1}}\left(\mathrm{p}_r\mathbf{I}_r + \mathrm{p}_{r-1}\mathbf{X}^T\mathbf{X} + \ldots + \mathrm{p}_2\left(\mathbf{X}^T\mathbf{X}\right)^{r-2} + \left(\mathbf{X}^T\mathbf{X}\right)^{r-1}\right) \tag{8.19}$$

which is derived by post-multiplying (8.18) with $\left(\mathbf{X}^T\mathbf{X}\right)^{-1}$and then solving for the inverse. When this equation is substituted into the OLS solution $\left(\mathbf{X}^T\mathbf{X}\right)^{-1}\mathbf{X}^T\mathbf{Y}$ gives the truncated solution

$$\mathbf{B}(\mathrm{p}) = \mathbf{K}_a\mathrm{p} \tag{8.20}$$

where $\mathbf{K}_a$ is the controllability matrix and $\mathrm{p} \in \mathbb{R}^a$ is the coefficient vector. We know that $\|\mathbf{A}\|_F^2 = trace\left(\mathbf{A}^T\mathbf{A}\right) = \sum_{i=1}^m\sum_{j=1}^n a_{ij}^2$, So

$$\mathrm{V}(\mathrm{p}) = trace\left(\mathbf{Y}^T\mathbf{Y}\right) - 2trace\left(\mathrm{p}^T\mathbf{K}_a\mathbf{X}^T\mathbf{Y}\right) + trace\left(\mathrm{p}^T\mathbf{K}_a^T\mathbf{X}^T\mathbf{X}\mathbf{K}_a\mathrm{p}\right) \tag{8.21}$$

Letting the gradient

$$\frac{d\mathrm{V}(\mathrm{p})}{d\mathrm{p}} = -2\mathbf{K}_a^T\mathbf{X}^T\mathbf{Y} + 2\mathbf{K}_a^T\mathbf{X}^T\mathbf{X}\mathbf{K}_a\mathrm{p} \tag{8.22}$$

equal to zero gives the optimal solution (8.14), which when substituted into (8.11) gives (8.15). Furthermore, the minimum value (8.17) can be found by substituting the optimal truncated polynomial coefficient into (8.21). □

By "Non-iterative" they meant that there is no need for any deflation (rank one reduction) process in computing the PLS solution. The following theorem is an extension of PLS1 to incorporate multivariate Y data.

Theorem 2. *(CPLS: Controllability PLS solution). [162] . Given data matrix* $\mathbf{X} \in \mathbb{R}^{N\times r}$ *and* $\mathbf{Y} \in \mathbb{R}^{N\times m}$*, the PLS solution is given by*

$$\begin{aligned}\mathbf{B}_{CPLS} &= \begin{bmatrix} \mathbf{X}^T\mathbf{Y} & \left(\mathbf{X}^T\mathbf{X}\right)\mathbf{X}^T\mathbf{Y} & \dots & \left(\mathbf{X}^T\mathbf{X}\right)^{a-1}\mathbf{X}^T\mathbf{Y} \end{bmatrix} \times \begin{bmatrix} \mathrm{p}_1\mathbf{I}_m \\ \mathrm{p}_2\mathbf{I}_m \\ \vdots \\ \mathrm{p}_a\mathbf{I}_m \end{bmatrix} \\ &= \left(\mathrm{p}_1\mathbf{I}_r + \mathrm{p}_2\mathbf{X}^T\mathbf{X} + \mathrm{p}_3\left(\mathbf{X}^T\mathbf{X}\right)^2 + \ldots + \mathrm{p}_a\left(\mathbf{X}^T\mathbf{X}\right)^{a-1}\right)\mathbf{X}^T\mathbf{Y} \\ &= \textstyle\sum_{i=1}^{a} \mathrm{p}_i\left(\mathbf{X}^T\mathbf{X}\right)^{i-1}\mathbf{X}^T\mathbf{Y}\end{aligned} \tag{8.23}$$

where the vector of polynomial coefficients

$$\mathrm{p}^* = \begin{bmatrix} \mathrm{p}_1 & \mathrm{p}_2 & \dots & \mathrm{p}_a \end{bmatrix}^T \in \mathbb{R}^a \tag{8.24}$$

is found from the solution to the LS problem

$$\mathrm{p}^* = \arg\min_{\mathrm{p}} \|vec\left(\mathbf{Y}\right) - \mathbf{X}_{\mathrm{p}}\mathrm{p}\|_F^2 \tag{8.25}$$

where $vec\left(\mathbf{Y}\right)$ *is the vectorization of the matrix* $\mathbf{Y}$*. The minimizing solution is given by*

$$\mathrm{p}^* = \left(\mathbf{X}_p^T\mathbf{X}_p\right)^{-1}\mathbf{X}_p vec\left(\mathbf{Y}\right) \tag{8.26}$$

where

$$\mathbf{X}_p = \underset{\in\,\mathbb{R}^{Nm\times a}}{\begin{bmatrix} vec\left(\mathbf{X}\mathbf{X}^T\mathbf{Y}\right) & vec\left(\mathbf{X}\mathbf{X}^T\mathbf{X}\mathbf{X}^T\mathbf{Y}\right) & \dots & vec\left(\mathbf{X}\left(\mathbf{X}^T\mathbf{X}\right)^{a-1}\mathbf{X}^T\mathbf{Y}\right) \end{bmatrix}} \tag{8.27}$$

Proof. Using that $\mathrm{V}\left(\mathrm{p}\right) = \|\epsilon\|_F^2$, where ϵ is the prediction error, gives the optimal LS solution (8.26) by letting the gradient $\frac{d\mathrm{V}}{d\mathrm{p}} = 0$. □

Remarks

The literature review by Wenzell et al. [164] compared PCR and PLS methods, covering both experimental and simulation studies. In short, the advantage of PLS is that the method obtains a small prediction error with fewer principal components compared to PCR.

The main drawback of this method is that there are several realization of the same method which do not lead to the same result for a specific problem for the case of multivariate set of dependent variables.

In SIMPLS and Di Ruscio's methods, it's not necessary to deflate the data matrices as in NIPALS, which may result in faster computation. All factors are equally easy to interpret, namely as simple linear combinations of the original variables.

8.3 Model-based Estimation

8.3.1 Brosilow Estimation

The simplest model-based static estimator is the "inferential estimator" of Brosilow and coworkers [165]. Let $\tilde{u} = \begin{bmatrix} u & d \end{bmatrix}$ represent the vector of independent variables, including the inputs u and the disturbances d. Let x represent the process measurements and y the variables we want to estimate. Let the linear static model in deviation variables be

$$x = \mathbf{X}\tilde{u} \tag{8.28}$$

$$y = \mathbf{Y}\tilde{u} \tag{8.29}$$

The "Brosilow" estimator is then simply the following least squares estimate of y

$$\hat{y} = \mathbf{H}x_m \tag{8.30}$$

where

$$\mathbf{H} = \mathbf{Y}\mathbf{X}^{\dagger} \tag{8.31}$$

and $\mathbf{X}^{\dagger}$ is the pseudo inverse of the matrix $\mathbf{X}$.

Joseph and Brosilow [165] discuss some of the weaknesses of this estimator. For "ill-conditioned" plants with large condition number of $\mathbf{X}$, they find that the estimate may be improved in some cases by removing measurements, because this reduces the condition number. Intuitively, removing measurements cannot be the optimal way of dealing with these problems, because we are throwing away information. This is also clear when we consider the popular "data-based" regression estimators, like Partial Least Squares (PLS) regression, where one does not remove measurements, but instead removes weak "directions" in the data.

A fundamental problem with the Brosilow inferential estimator is that it fails to take into account measurement noise in an explicit manner. The main goal of our estimation method is to include the effect of measurement noise in the derivation of the optimal model-based static estimator. This means that we handle in an optimal manner the "high condition number problem", which has been a major concern in previous work[165, 150, 143, 166, 167]. The derivation is straightforward, but surprisingly it seems it has not been presented before.

Another issue is that the Brosilow least squares estimator does not take into account whether the estimator is used only for monitoring or for closed-loop operation. Actually, the latter is a shortcoming of most existing data-based estimators.

8.3.2 Kalman filtering

The Kalman filter estimates process states by using a form of feedback control. The linearity of state dynamics and observation process, as well as the normal distribution of noise in state dynamics and measurements are the assumptions of kalman filter. A linear difference equation $x_k = Ax_{k-1} + Bu_{k-1} + w_{k-1}$ with a measurement that is $z_k = \mathbf{C}x_k + v_k$, define the linearized process. The random variables w_k and v_k represent the process and measurement noise respectively. They are assumed to be independent of each other and with normal distributions.

$$p(w) \sim \mathcal{N}(0, Q) \tag{8.32}$$

$$p(v) \sim \mathcal{N}(0, R) \tag{8.33}$$

The objective is to minimize the estimation error. By writing a posteriori state estimate as a linear combination of an a priori estimate and the difference between actual measurement and measurement prediction weighted by kalman gain, K is calculated to minimize the a posteriori estimation error covariance. Since the focus of our work is on chemical processes, the time scales at which the sensor noise characteristics change are much larger than the time scale at which we study the system. Thus we assume the system and noise covariances are time-invariant. In addition, as mentioned previously, our proposed estimator is categorized as static estimator. So, the steady-state of kalman filter is interesting. The steady-state kalman gain is calculated as

$$K_{\infty} = P_{\infty}^{-} H^T \left(H P_{\infty}^{-} H^T + R \right) \tag{8.34}$$

Figure 8.1 shows the block diagram of kalman filter estimation.

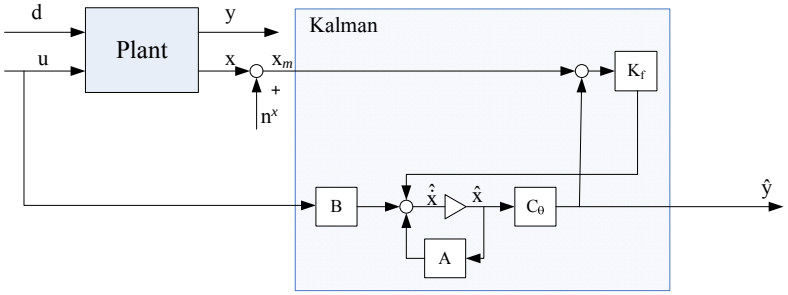

Figure 8.1: Block diagram of Kalman filter

The algorithm of Kalman filter requires knowledge of the process noise variance W and the measurement noise variance V [168]. If state-feedback control is used, the overall controller is optimal because of the separation principle. If an output-feedback controller ($u = \mathbf{K}y$) is used, then it is generally not optimal to use the $\hat{y} = \mathbf{C}\hat{x}$ estimated by Kalman filter. In our estimation method, the primary variable comes directly from combination of measurements ($c = \mathbf{H}x$). Since the measurements do not contribute similarly in the estimation of primary variable, it is expected that by putting weights on the state error terms, the estimation of primary variable will be improved. Another point is that we should think of what to use the estimation for. Kalman Filter is said to be used for control, but if R approaches infinity, then it means that there is no control. Mejdell et al. [169] have shown that the kalman-filter might be better than a simple PCR in open-loop performance, which is because of the recursive nature of the filter, but PCR performs similarly if it is used for closed loop. We can model slowly-varying disturbances by adding states of the noise model. This gives the augmented kalman filter [170]. Here, we use non-stationary noise. So zero steady-state is not reached.

It is noteworthy that all conclusions drawn from the evaluation of posterior distributions depend on the quality and extent of the prior information included in Bayesian inference processing. In the limit of the large data-set and non-informative priors (e.g. uniform), the MAP estimates are identical to the Maximum Likelihood (ML) estimators which can be expressed as follows:

$$X^{ML} = \text{argmax } p(D|X)X$$

from review paper shima sepehr

8.4 Our estimation method

In the next chapter, we derive optimal estimators for four cases. Case S1 is the direct extension of the Brosilow inferential estimator to include measurement noise. In case S2, the inputs u are used to control the variables y at given setpoint y_s. It is similar to case S1, except that the setpoint y_s takes the role of the inputs. Case S3 is a generalization where we control the variables z. Cases S1, S2 and S3 are practically relevant if the estimator is used for monitoring only, because the estimate $\hat{y}$ is not used for control. Finally, case S4 is the relevant case when we use the estimator in closed loop (for control purposes). Whereas the optimal estimators for cases S1, S2 and S3 are least-square estimators with a similar structure to the Brosilow estimator in (8.31), the structure for case S4 is quite different and the mathematics to derive it are more complex. The derivation is based on results for optimal measurement combination for self-optimizing control [121] and is the main new contribution of the next chapter.

For data preparation we have two ways: If we have data, small directions in the measurement space should be deleted by SVD. We should ensure that all important directions are sufficiently exposed. We can also use exactly the same data that we get in loss method. $\mathbf{X}$ and $\mathbf{Y}$ in PLS method are the first and second row of $\mathbf{Y}_{all}$ matrix respectively.

$$\mathbf{Y}_{all} = \begin{bmatrix} \mathbf{Y} \\ \mathbf{X} \end{bmatrix} = \begin{bmatrix} \mathbf{G}_y & 0 \\ \mathbf{G}_x & \mathbf{X}_{opt} \end{bmatrix} \tag{8.35}$$

where $\mathbf{X_{opt}} = \begin{bmatrix} \mathbf{F}\mathbf{W}_d & \mathbf{W}_{n^x} \end{bmatrix}$.

We need to know the expected "optimal variation" in $\mathbf{X}$ as given by the matrix $\mathbf{X}_{opt}$. Here "optimal" means that y is constant (see the second column in $\mathbf{Y}_{all}$). In addition, we also need to obtain $\mathbf{G}_x$ and $\mathbf{G}_y$ from the data, which means that the data must contain "non-optimal" variations in u, and not only contain optimal data where $u = u_{opt}(d)$- see the first column in $\mathbf{Y}_{all}$. This is called Closed-Loop Regressor (CLR) [171]. CLR suffers from the same weakness as LS, giving poor results for ill-conditioned matrices and underdetermined systems. Performing a principal component analysis on the $\mathbf{X}$ data will remove the weaker directions containing noise resulting in a well-conditioned matrix. Then, CLR can be applied to the data. We call this "truncated CLR".

outliers should be removed. This is the thing which does not exist in our method. We get just enough data from the model to calculate the estimator parameters.

In the paper, we derive optimal estimators for four cases as illustrated in Figure 9.1. Case S1 is the direct extension of the Brosilow inferential estimator to include measurement noise. In case S2, the inputs u are used to control the variables y at given setpoint y_s. It is similar to case S1, except that the setpoint y_s takes the role of the inputs. Case S3 is a generalization where we control the variables z. Cases S1, S2 and S3 are practically relevant if the estimator is used for monitoring only, because the estimate $\hat{y}$ is not used for control. Finally, case S4 is the relevant case when we use the estimator in closed loop (for control purposes). Whereas the optimal estimators for cases for cases S1, S2 and S3 are least-square estimators with a similar structure to the Brosilow estimator in (8.31), the structure for case S4 is quite different and the mathematics to derive it are more complex. The derivation is based on results for optimal measurement combination for self-optimizing control [121] and is the main new contribution of this paper.

8.5 Summary

In this chapter, a short review of the static estimation methods which are used in this thesis are given. In the next chapter, four estimators will be derived for different applications and will be compared with other well-known estimators. Four scenarios are used to get the calibration data. Our emphasis is on the fact that we should be aware of what we want to use the estimator for.

Chapter 9

A new class of model-based static estimators

Static estimators are commonly used as "soft-sensors" in the process industry. The performance of the estimators depend on whether it is used for monitoring (open-loop) or for closed-loop control applications. In this work, we propose to design estimators specialized for each case. The approach is to minimize the estimation error for expected disturbances and measurement noise. The main extension compared to previous work is to include measurement noise and to provide explicit formulae for computing the optimal static estimator. We also compare the results with standard existing estimators, e.g. PLS. The approach is applied to estimation of product composition in a distillation column from combination of temperature measurements.

9.1 Introduction

The derivation of the new static estimators is presented in section 2. The concept of some well-known data-based estimators are described in section 3. In section 4 we discuss how we can use our new ideas for optimal model-based to derive new data-based estimator. Finally, in section 5, we compare the new static estimators with previous work, including the Brosilow estimator and regression based estimators on distillation case-studies.

9.2 Derivation of Model-based Static Estimators

9.2.1 Problem definition

We define the following variables:

- u: inputs (degrees of freedom); these may include setpoints to lower-layer controllers
- d: disturbances, including parameter changes.
- x: all available measured variables.
- n^x: measurement noise (error) for x.
- y: primary variables that we want to estimate
- z: secondary variables, which we may control, $\dim(\mathrm{z}) = \dim(\mathrm{u})$

All variables are assumed to be deviation variables (away from the nominal or centered values). In this section, we derive optimal "open-loop" and "closed-loop" static estimators. By "optimal", it is meant that we for a linear estimator of the form

$$\hat{\mathrm{y}} = \mathbf{H}\mathrm{x}_m \tag{9.1}$$

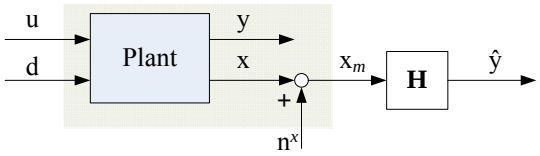

(a) S1: Monitoring case where u is a free variable

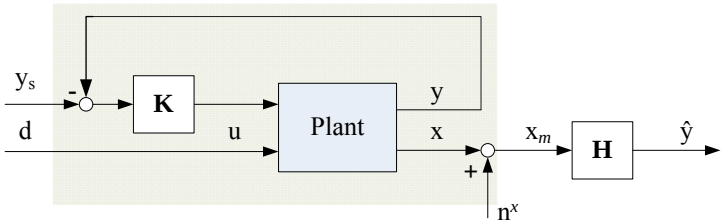

(b) S2: Monitoring case where u is used to control the primary variable y

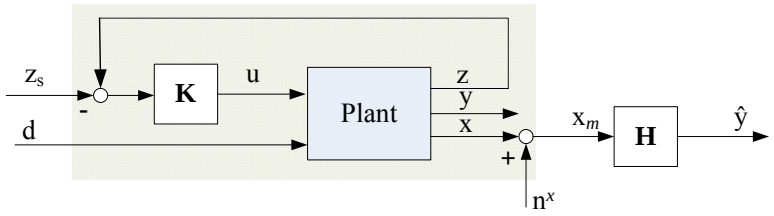

(c) S3: Monitoring case where u is used to control the secondary variable z

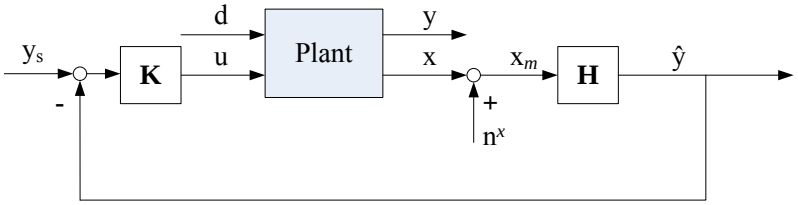

(d) S4= CL: "closed-loop" case where u is used to control the predicted variable ŷ

Figure 9.1: Block diagrams for different cases

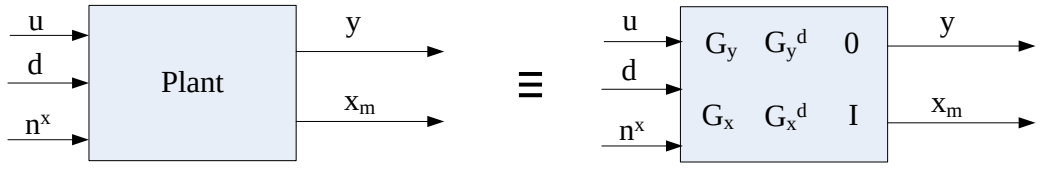

Figure 9.2: Block diagram for the linearized plant

want to minimize the expected prediction error

$$e = y - \hat{y} \tag{9.2}$$

The measurement signals x_m, corrupted by measurement noise n^x, are

$$x_m = x + n^x \tag{9.3}$$

We use linear static models for the primary variables y, measurements x, and secondary variables z (see Figure 9.2)

$$y = \mathbf{G}_y u + \mathbf{G}_y^d d \tag{9.4}$$

$$x = \mathbf{G}_x u + \mathbf{G}_x^d d \tag{9.5}$$

$$z = \mathbf{G}_z u + \mathbf{G}_z^d d \tag{9.6}$$

In terms of the notation used for the Brosilow inferential estimator in (8.28) we have

$$\mathbf{X} = \begin{bmatrix} \mathbf{G}_x & \mathbf{G}_x^d \end{bmatrix} \tag{9.7}$$

$$\mathbf{Y} = \begin{bmatrix} \mathbf{G}_y & \mathbf{G}_y^d \end{bmatrix} \tag{9.8}$$

In addition, the expected magnitude variables of the independent variables for each case (see Figure 9.1) is quantified by weighting matrices ($\mathbf{W}_u$, $\mathbf{W}_d$, $\mathbf{W}_{n^x}$,$\mathbf{W}_{y_s}$, $\mathbf{W}_{z_s}$), as explained in detail below.

9.2.2 Estimators used for monitoring (cases S1, S2 and S3)

With the term "open-loop", it is implied that the predicted variables $\hat{y} = \mathbf{H}x_m$ are used for monitoring, that is, they are not used for control purposes. It should be noted that this is not the same as implying that the variables in a given system are uncontrolled. We can think of three main types of open-loop monitoring estimators are illustrated in Figure 9.1:

Case S1. Predicting primary variables from a system with no control, i.e. the inputs u are free variables.

Case S2. Predicting primary variables from a system where the primary variables y are measured and controlled, i.e. the inputs u are used to keep $y = y_s$.

Case S3. Predicting primary variables from a system where the inputs u are used to control the secondary variables z, i.e. $z = z_s$.

We first consider case S1 in detail. Cases S2 and S3 are then straightforward extensions.

Case S1

Case S1 is the direct extension of the Brosilow estimator to include noise. To find the optimal estimator for open-loop operation, the prediction error has to be expressed as a function of the system and the estimator.

Lemma 1. *For a given linear estimator , when applied to the system defined in equations (9.1)-(9.5), and considering that* u *is a free variable, the prediction error can be expressed as*

$$e(\mathbf{H}) = \begin{bmatrix} (\mathbf{G}_y - \mathbf{H}\mathbf{G}_x) & \left(\mathbf{G}_y^d - \mathbf{H}\mathbf{G}_x^d\right) & -\mathbf{H} \end{bmatrix} \begin{bmatrix} \mathrm{u} \\ \mathrm{d} \\ \mathrm{n}^x \end{bmatrix} \tag{9.9}$$

Proof. An expression of $\hat{\mathrm{y}}$ as a function of u, d and n^x can be obtained by substituting equations (9.3) and (9.5) into equation (9.1).

$$\hat{\mathrm{y}} = \mathbf{H}\left(\mathbf{G}_x\mathrm{u} + \mathbf{G}_x^d\mathrm{d} + \mathrm{n}^x\right)$$

Using the definition of prediction error and substituting the expression for $\hat{\mathrm{y}}$, we will have

$$\mathrm{e}(\mathbf{H}) = (\mathbf{G}_y - \mathbf{H}\mathbf{G}_x)\,\mathrm{u} + \left(\mathbf{G}_y^d - \mathbf{H}\mathbf{G}_x^d\right)\mathrm{d} - \mathbf{H}\mathrm{n}^x$$

which is the same as equation (9.9). Q.E.D.

Next, we derive an expression for the expected prediction error, assuming that u, d, n^x are normally distributed with given weight matrices.

Lemma 2. ***Expected prediction error***. *Let the disturbance and noise be normalized on the form*

$$\mathrm{u} = \mathbf{W}_u\mathrm{u}'$$
$$\mathrm{d} = \mathbf{W}_d\mathrm{d}'$$
$$\mathrm{n}^x = \mathbf{W}_{n^x}\mathrm{n}^{x'}$$

where the elements u', d' and $n^{x'}$ of the normalized vectors u′, d′ *are assumed to be normally distributed with zero mean and unit standard deviation;*

$$u' \sim \mathcal{N}(0,1)$$
$$d' \sim \mathcal{N}(0,1)$$
$$n^{x'} \sim \mathcal{N}(0,1)$$

The diagonal scaling matrices $\mathbf{W}_u$, $\mathbf{W}_d$ and $\mathbf{W}_{n^x}$ contain the standard deviations of the elements in u, d *and* n^x *respectively.*

From Lemma 1 the prediction error can be expressed as

$$e = \underbrace{\begin{bmatrix} (\mathbf{G}_y - \mathbf{H}\mathbf{G}_x)\mathbf{W}_u & \left(\mathbf{G}_y^d - \mathbf{H}\mathbf{G}_x^d\right)\mathbf{W}_d & -\mathbf{H}\mathbf{W}_{n^x} \end{bmatrix}}_{\mathbf{M}(\mathbf{H})} \begin{bmatrix} \mathrm{u}' \\ \mathrm{d}' \\ \mathrm{n}^{x'} \end{bmatrix}$$

The expected value of the 2-norm of the prediction error (variance) then becomes

$$\mathrm{E}(\|e\|_2) = \|\mathbf{M}(\mathbf{H})\|_F^2$$

Proof. Let $\tilde{\mathrm{d}} = \begin{bmatrix} \mathrm{u}' \\ \mathrm{d}' \\ \mathrm{n}^{x'} \end{bmatrix}$. Then, $\mathrm{e} = \mathbf{M}\tilde{\mathrm{d}}$, and noting that $\|\mathrm{e}\|_2 = \mathrm{tr}\left(\mathrm{e}\mathrm{e}^T\right)$, the expected value of the 2-norm of the prediction error can be written as

$$\begin{aligned} \mathrm{E}(\|\mathrm{e}\|_2) &= \mathrm{E}\left[\mathrm{tr}\left(\mathbf{M}\tilde{\mathrm{d}}\tilde{\mathrm{d}}^T\mathbf{M}^T\right)\right] \\ &= \mathrm{E}\left[\mathrm{tr}\left(\mathbf{M}^T\mathbf{M}\tilde{\mathrm{d}}\tilde{\mathrm{d}}^T\right)\right] \\ &= \mathrm{tr}\left(\mathbf{M}^T\mathbf{M}\,\mathrm{E}\left[\tilde{\mathrm{d}}\tilde{\mathrm{d}}^T\right]\right) \end{aligned}$$

where $\mathrm{tr}(.)$ denotes the trace of the matrix and $E[.]$ is the expectation operator.

Since $\left\| \begin{bmatrix} \mathrm{u}' \\ \mathrm{d}' \\ \mathrm{n}^{x'} \end{bmatrix} \right\| \sim \mathcal{N}(0, \mathbf{I}_{n_u+n_d+n_x})$, by substituting the normal distribution in the definition of expected value we have

$$\mathrm{E}\left[\tilde{\mathrm{d}}\tilde{\mathrm{d}}^T\right] = \mathrm{Var}\left(\tilde{\mathrm{d}}\right)$$

In addition, we know that the square root of the trace of the matrix $\mathbf{M}^T\mathbf{M}$ is actually the definition of Frobenius norm of matrix $\mathbf{M}$. So,

$$\mathrm{E}\left(\|\mathrm{e}\|_2\right) = \mathrm{tr}\left(\mathbf{M}^T\mathbf{M}\right) = \|\mathbf{M}\|_F^2$$

Q.E.D.

From Lemma 2, the expected value of the 2-norm prediction error (variance) is minimized by selecting $\mathbf{H}$ to minimize $\|\mathbf{M}\|_F$. This leads to the following theorem

Theorem 3. *The optimal "open-loop" estimator following the linear relationship*

$$\hat{\mathrm{y}} = \mathbf{H}\mathrm{x}_m$$

that minimizes the variance of the prediction error (Lemma 1 and 2)

$$\mathrm{e} = \mathrm{y} - \hat{\mathrm{y}}$$

when u is a free variable, is

$$\mathbf{H}_1 = \mathbf{Y}_1\mathbf{X}_1^{\dagger} \tag{9.10}$$

where $\mathbf{X}^{\dagger}$ is the pseudo-inverse of $\mathbf{X}$, and

$$\begin{aligned} \mathbf{Y}_1 &= \begin{bmatrix} \mathbf{G}_y\mathbf{W}_u & \mathbf{G}_y^d\mathbf{W}_d & 0 \end{bmatrix} \\ \mathbf{X}_1 &= \begin{bmatrix} \mathbf{G}_x\mathbf{W}_u & \mathbf{G}_x^d\mathbf{W}_d & \mathbf{W}_{n^x} \end{bmatrix} \end{aligned} \tag{9.11}$$

If $\mathbf{X}_1$ has full column rank, we have $\mathbf{X}_1^{\dagger} = \left(\mathbf{X}_1^T\mathbf{X}_1\right)^{-1}\mathbf{X}_1^T$. If $\mathbf{X}_1$ has full row rank, we have $\mathbf{X}_1^{\dagger} = \mathbf{X}_1^T\left(\mathbf{X}_1^T\mathbf{X}_1\right)^{-1}$. For the general case, where $\mathbf{X}_1$ has neither full row nor column rank, the pseudo-inverse may be obtained using the singular value decomposition

Proof. In Lemma 2, we showed that minimizing $\|\mathrm{e}(\mathbf{H})\|_2$ is equivalent to minimizing $\|\mathbf{M}(\mathbf{H})\|_F^2$ for the expected prediction error. $\mathbf{M}(\mathbf{H})$ can be rewritten as

$$\mathbf{M} = \mathbf{Y}_1 - \mathbf{H}\mathbf{X}_1$$

The optimization problem then becomes

$$\min_{\mathbf{H}} \|\mathbf{Y}_1 - \mathbf{H}\mathbf{X}_1\|$$

and we recognize that this is the least squares problem with the known optimal solution.

$$\mathbf{H}_1 = \mathbf{Y}_1\mathbf{X}_1^{\dagger}$$

Q.E.D.

Figure 9.3 shows an interpretation of Theorem 1, which is a direct generalization of the Brosilow estimator, when we also include noise. Note that the elements in $\mathbf{Y}_1$ corresponding to $\mathrm{n}^{x'}$ is zero.

This estimator is optimal for the case where the process input u are truly independent variables, that is, when we have no control (case S1 in Figure 9.1).

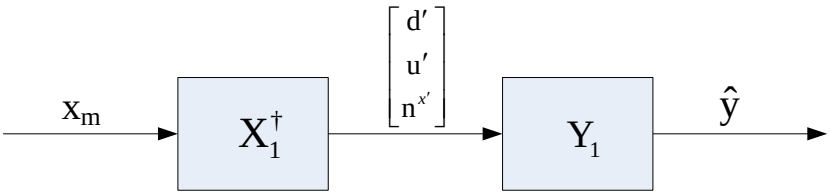

Figure 9.3: Interpretation of Theorem 1

Case S2

We now consider the case where the inputs u are used to keep the outputs y at given setpoints y_s. This means that y_s replaces u as independent variables. It is assumed that $\dim(y) = \dim(u)$.

Theorem 4. *The optimal "open-loop" estimator* $\mathbf{H}$ *for closed-loop operation, where the degrees of freedom* u *are adjusted such that the primary variables* y *are kept at the setpoints* y_s*, that minimizes the variance of the prediction error* $y - \hat{y}$ *for normally distributed setpoint changes, disturbances and noise (of magnitudes* $\mathbf{W}_{y_s}$*,* $\mathbf{W}_d$ *and* $\mathbf{W}_{n^x}$ *respectively) is*

$$\mathbf{H}_2 = \mathbf{Y}_2 \mathbf{X}_2^\dagger$$

where

$$\begin{aligned} \mathbf{Y}_2 &= \begin{bmatrix} \mathbf{W}_{y_s} & 0 & 0 \end{bmatrix} \\ \mathbf{X}_2 &= \begin{bmatrix} \mathbf{G}_x^{cl}\mathbf{W}_{y_s} & \mathbf{F}\mathbf{W}_d & \mathbf{W}_{n^x} \end{bmatrix} \end{aligned} \tag{9.12}$$

where $\mathbf{G}_x^{cl} = \mathbf{G}_x \mathbf{G}_y^{-1}$ *and* $\mathbf{F} = \mathbf{G}_x^d - \mathbf{G}_x \mathbf{G}_y^{-1} \mathbf{G}_y^d$

Proof. We assume that u is used to keep $y = y_s$ (with no control error). Solving equation (9.4) with respect to u when $y = y_s$ gives

$$u = \mathbf{G}_y^{-1} y_s - \mathbf{G}_y^{-1} \mathbf{G}_y^d d$$

By combining equations (9.5), (9.3) and (9.1) with the above equation, the following expression for $\hat{y}$ as an explicit function of y_s, d and n^x is obtained,

$$\hat{y} = \mathbf{H}\left[\mathbf{G}_x \mathbf{G}_y^{-1} y_s + \left(\mathbf{G}_x^d - \mathbf{G}_x \mathbf{G}_y^{-1} \mathbf{G}_y^d\right) d + n^x\right]$$

Here, $\left(\mathbf{G}_x^d - \mathbf{G}_x \mathbf{G}_y^{-1} \mathbf{G}_y^d\right) = \left(\frac{\partial x}{\partial d}\right)_{y=y_s}$ is the optimal sensitivity $\mathbf{F}$ [121], and $\mathbf{G}_x \mathbf{G}_y^{-1} = \left(\frac{\partial x}{\partial y_s}\right)_d$ is known as the closed-loop gain $\mathbf{G}_x^{cl}$. So, the above equation becomes

$$\hat{y} = \mathbf{H}\left[\mathbf{G}_x^{cl} y_s + \mathbf{F} d + n^x\right]$$

With the assumption that $y = y_s$, the prediction error becomes

$$e = y - \hat{y} = \begin{bmatrix} \left(\mathbf{I} - \mathbf{H}\mathbf{G}_x^{cl}\right) & -\mathbf{H}\mathbf{F} & -\mathbf{H} \end{bmatrix} \begin{bmatrix} y_s \\ d \\ n^x \end{bmatrix}$$

Proceeding analogous to Lemmas 1 and 2 and Theorem 1, using $y_s = \mathbf{W}_s y_s'$ results in the given preposition. Q.E.D.

Case S3

The following theorem generalizes theorems 1 and 2.

Theorem 5. *The optimal "open-loop" estimator* $\mathbf{H}$ *for closed-loop operation where the degrees of freedom* u *are adjusted such that the secondary variables* z *are kept at the setpoints* z_s*, that minimizes the variance of the prediction error* $y - \hat{y}$ *for normally distributed setpoint changes, disturbances and noise (of magnitudes* $\mathbf{W}_{z_s}$*,* $\mathbf{W}_d$ *and* $\mathbf{W}_{n^x}$ *respectively) is*

$$\mathbf{H}_3 = \mathbf{Y}_3 \mathbf{X}_3^{\dagger}$$

where

$$\mathbf{Y}_3 = \begin{bmatrix} \mathbf{G}_y^{cl}\mathbf{W}_{z_s} & \mathbf{F}'_y\mathbf{W}_d & 0 \end{bmatrix}$$

$$\mathbf{X}_3 = \begin{bmatrix} \mathbf{G}_x^{cl}\mathbf{W}_{z_s} & \mathbf{F}'_x\mathbf{W}_d & \mathbf{W}_{n^x} \end{bmatrix}$$

where $\mathbf{G}_y^{cl} = \mathbf{G}_y\mathbf{G}_z^{-1}$, $\mathbf{G}_x^{cl} = \mathbf{G}_x\mathbf{G}_z^{-1}$, $\mathbf{F}'_y = \mathbf{G}_y^d - \mathbf{G}_y\mathbf{G}_z^{-1}\mathbf{G}_z^d$ *and* $\mathbf{F}'_x = \mathbf{G}_x^d - \mathbf{G}_x\mathbf{G}_z^{-1}\mathbf{G}_z^d$

Proof. We assume that u is used to keep $z = z_s$ (with no control error). Solving equation (9.6) with respect to u when $z = z_s$ gives

$$u = \mathbf{G}_z^{-1} z_s - \mathbf{G}_z^{-1}\mathbf{G}_z^d d$$

By combining equations (9.4) and the above expression for u, we have

$$y = \underbrace{\mathbf{G}_y\mathbf{G}_z^{-1}}_{G_y^{cl}} z_s + \left(\underbrace{\mathbf{G}_y^d - \mathbf{G}_y\mathbf{G}_z^{-1}\mathbf{G}_z^d}_{F'_y}\right) d$$

Introducing the optimal sensitivity $\mathbf{F}'_y$ and the closed-loop gain $\mathbf{G}_y^{cl}$ we get

$$y = \mathbf{G}_y^{cl} z_s + \mathbf{F}'_y d$$

By combining equations (9.5), (9.3) and (9.1), the following expression for $\hat{y}$ as an explicit function of y_s, d and n^x is obtained.

$$\hat{y} = \mathbf{H}\left[\underbrace{\mathbf{G}_x\mathbf{G}_z^{-1}}_{G_x^{cl}} z_s + \left(\underbrace{\mathbf{G}_x^d - \mathbf{G}_x\mathbf{G}_z^{-1}\mathbf{G}_z^d}_{F'_x}\right) d + n^x\right]$$

Using the definition of prediction error with the expression for $\hat{y}$ and y gives

$$e(\mathbf{H}) = \begin{bmatrix} \left(\mathbf{G}_y^{cl} - \mathbf{H}\mathbf{G}_x^{cl}\right) & \left(\mathbf{F}'_y - \mathbf{H}\mathbf{F}'_x\right) & -\mathbf{H} \end{bmatrix} \begin{bmatrix} z_s \\ d \\ n^x \end{bmatrix}$$

Proceeding analogous to Lemma 2 and Theorem 1, will result in the given proposition. Q.E.D.

Note that Theorem 3 is a generalization of Theorems 1 and 2, since setting z = u gives Theorem 1 and setting z = y gives Theorem 2.

9.2.3 The "closed-loop" estimator (Case S4)

In this section, we derive an expression for the optimal estimator under the assumption that the prediction $\hat{y} = \mathbf{H}x_m$ is used for controlling the primary variables, that is, we have $\hat{y} = y_s$ (assuming integral action in the controller). It is assumed that $\dim(y) = \dim(u)$.

Theorem 6. *The optimal "closed-loop" estimator* $\mathbf{H}$ *(denoted* $\mathbf{H}_{CL}$*) following the linear relationship*

$$\hat{\mathrm{y}} = \mathbf{H}\mathrm{x}_m \tag{9.13}$$

that minimizes the variance of the prediction error

$$e = \mathrm{y} - \hat{\mathrm{y}}$$

for normally distributed sets of d, n^x *and* y_s *(of magnitudes* $\mathbf{W}_d$*,* $\mathbf{W}_{n^x}$ *and* $\mathbf{W}_{y_s}$*, respectively) assuming that the degrees of freedom* u *are adjusted to keep the prediction at the setpoint (*$\hat{\mathrm{y}} = \mathrm{y}_s$ *), is*

$$\mathbf{H}_{CL} = \arg\left(\min_{\mathbf{H}} \left\| \mathbf{H} \begin{bmatrix} \mathbf{F}\mathbf{W}_d & \mathbf{W}_{n^x} \end{bmatrix} \right\|_F\right) \tag{9.14a}$$

$$s.t.\ \mathbf{H}\mathbf{G}_x = \mathbf{G}_y \tag{9.14b}$$

where the sensitivity matrix $\mathbf{F}$ *is defined as*

$$\mathbf{F} = \left(\frac{\partial \mathrm{x}}{\partial \mathrm{d}}\right)_{\mathrm{y}=0} = \mathbf{G}_x^d - \mathbf{G}_x\mathbf{G}_y^{-1}\mathbf{G}_y^d \tag{9.14c}$$

Comment: Note that (9.14b) is equivalent to $\mathbf{H}\mathbf{G}_x^{cl} = \mathbf{I}$

Proof. An expression for the prediction as an explicit function of u, d and n^x is achieved by combining Equations (9.5), (9.3) and (9.1) to get

$$\hat{\mathrm{y}} = \mathbf{H}\left(\mathbf{G}_x\mathrm{u} + \mathbf{G}_x^d\mathrm{d} + \mathrm{n}^x\right) \tag{9.15}$$

Using a controller with integral action, the prediction $\hat{\mathrm{y}}$ is held at the setpoints y_s by manipulating u. Solving equation (9.15) with respect to u when $\hat{\mathrm{y}} = \mathrm{y}_s$, gives

$$\mathrm{u} = -\left(\mathbf{H}\mathbf{G}_x\right)^{-1}\mathbf{H}\left(\mathbf{G}_x^d\mathrm{d} + \mathrm{n}^x\right) + \left(\mathbf{H}\mathbf{G}_x\right)^{-1}\mathrm{y}_s \tag{9.16}$$

and inserting this into (9.4) yields

$$\mathrm{y} = -\mathbf{G}_y\left(\mathbf{H}\mathbf{G}_x\right)^{-1}\mathbf{H}\left[\mathbf{F}\mathrm{d} + \mathrm{n}^x\right] + \mathbf{G}_y\left(\mathbf{H}\mathbf{G}_x\right)^{-1}\mathrm{y}_s \tag{9.17}$$

where $\mathbf{F} = \left(\mathbf{G}_x^d - \mathbf{G}_x\mathbf{G}_y^{-1}\mathbf{G}_y^d\right)$ is the optimal sensitivity. Inserting the expression for y into the prediction error e, remembering that the prediction is kept at the setpoint ($\hat{\mathrm{y}} = \mathrm{y}_s$), gives

$$\mathrm{e} = \mathrm{y} - \hat{\mathrm{y}} = \mathrm{y} - \mathrm{y}_s = -\mathbf{G}_y\left(\mathbf{H}\mathbf{G}_x\right)^{-1}\mathbf{H}\left(\mathbf{F}\mathrm{d} + \mathrm{n}^x\right) + \left[\mathbf{G}_y\left(\mathbf{H}\mathbf{G}_x\right)^{-1} - \mathbf{I}\right]\mathrm{y}_s \tag{9.18}$$

Introducing normalized (weighted) variables, gives

$$\mathrm{e} = \underbrace{-\mathbf{G}_y\left(\mathbf{H}\mathbf{G}_x\right)^{-1}\mathbf{H}\begin{bmatrix} \mathbf{F}\mathbf{W}_d & \mathbf{W}_{n^x} \end{bmatrix}\begin{bmatrix} \mathrm{d}' \\ \mathrm{n}^{x'} \end{bmatrix}}_{\mathrm{e}_1(\mathbf{H})} + \underbrace{\left[\mathbf{G}_y\left(\mathbf{H}\mathbf{G}_x\right)^{-1} - \mathbf{I}\right]\mathrm{y}_s}_{\mathrm{e}_2(\mathbf{H})} \tag{9.19}$$

In the first term of equation (9.19), we have extra degree of freedom, because if we pre-multiply $\mathbf{H}$ by a matrix $\mathbf{D}$, we will have

$$\mathrm{e}_1(\mathbf{H}) = \mathrm{e}_1(\mathbf{D}\mathbf{H})$$

where $\mathbf{D}$ is any nonsingular square matrix. This follows because

$$\left(\mathbf{D}\mathbf{H}\mathbf{G}_x\right)^{-1}\mathbf{D}\mathbf{H} = \left(\mathbf{H}\mathbf{G}_x\right)^{-1}\mathbf{D}^{-1}\mathbf{D}\mathbf{H} = \left(\mathbf{H}\mathbf{G}_x\right)^{-1}\mathbf{H}$$

Since $\mathbf{D}$ can be chosen freely without affecting $\mathrm{e}_1(\mathbf{H})$, we may choose it such that the last term is zero, $\mathrm{e}_2(\mathbf{H}) = 0$, corresponding to having $\mathbf{H}\mathbf{G}_x = \mathbf{G}_y$. This means that the optimal $\mathbf{H}$ can be found by minimizing the first term (e_1) in equation (9.19), subject to the constraint $\mathbf{H}\mathbf{G}_x = \mathbf{G}_y$. This problem is equivalent to solving the constrained minimization problem (9.14) which is convex [121]. Q.E.D.

Comment: The optimization problem in equation (9.14) is expressed with open-loop gains ($\mathbf{G}_x$ and $\mathbf{G}_y$), but can also be expressed with closed-loop gains by just substituting the open-loop gains for the closed-loop gains. This can easily be shown by postmultiplying the constraint $\mathbf{HG}_x = \mathbf{G}_y$ with $\mathbf{G}_y^{-1}$ on both sides of the equality, to get $\mathbf{HG}_x\mathbf{G}_y^{-1} = \mathbf{HG}_x^{cl} = \mathbf{I}$.

Analytical Solution for H

If $\tilde{\mathbf{F}} \triangleq \begin{bmatrix} \mathbf{FW}_d & \mathbf{W_{n^x}} \end{bmatrix}$ is full rank, which is always the case if we include independent measurement noise (so that $\mathbf{W}_{n^x}$ is full rank), then we may alternatively use the analytic expression in Theorem 7.

Theorem 7. *Under the assumption that $\tilde{\mathbf{F}}\tilde{\mathbf{F}}^T$ is full rank, an analytical solution for the problem (9.14) is*

$$\mathbf{H}_{CL}^T = \left(\tilde{\mathbf{F}}\tilde{\mathbf{F}}^T\right)^{-1}\mathbf{G}_x\left(\mathbf{G}_x^T\left(\tilde{\mathbf{F}}\tilde{\mathbf{F}}^T\right)^{-1}\mathbf{G}_x\right)^{-1}\mathbf{G}_y \tag{9.20}$$

Proof. The proof is in the paper written by Alstad et al.[121] and is based on first vectorizing the problem and then using standard results from constrained quadratic optimization. Q.E.D.

Remark 1. One special case, when the expression for $\mathbf{H}$ in equation (9.20) applies also for $\mathbf{W}_{n^x} = 0$, is when there are more independent than measurements, because $\tilde{\mathbf{F}}\tilde{\mathbf{F}}^T$ then remains full rank [121].

Remark 2. The solution (9.20) is equivalent to the following [171]

$$\mathbf{H}_{CL} = \mathbf{D}\left(\left(\tilde{\mathbf{F}}\tilde{\mathbf{F}}^T\right)^{-1}\mathbf{G}_x\right)^T \tag{9.21}$$

where

$$\mathbf{D} = \mathbf{G}_y\left(\mathbf{G}_x^T\left(\tilde{\mathbf{F}}\tilde{\mathbf{F}}^T\right)^{-1}\mathbf{G}_x\right)^{-1} \tag{9.22}$$

The following example shows the effect of noise for various cases.

9.2.4 Example 1

We consider a scalar case with one input (u), one disturbance (d), one measurement (x), one output y, and with the following model matrices

$$\mathbf{G}_x = \mathbf{G}_x^d = 1$$
$$\mathbf{G}_y = \mathbf{G}_y^d = 1$$
$$\mathbf{W}_u = \mathbf{W}_d = \mathbf{W}_{y_s} = 1$$

This corresponds to the case where y = x and we have $\mathbf{F} = 0$.

For case S1, Theorem 1 gives

$$\mathbf{Y}_1 = \begin{bmatrix} 1 & 1 & 0 \end{bmatrix}$$
$$\mathbf{X}_1 = \begin{bmatrix} 1 & 1 & \mathbf{W}_{n^x} \end{bmatrix}$$

and we find

$$\mathbf{H}_1 = \frac{2}{\mathbf{W}_{n^x}^2 + 2}$$

For case S2, Theorem 2 gives

$$\mathbf{Y}_2 = \begin{bmatrix} 1 & 0 & 0 \end{bmatrix}$$
$$\mathbf{X}_2 = \begin{bmatrix} 1 & 0 & \mathbf{W}_{n^x} \end{bmatrix}$$

Table 9.1: Optimal $\mathbf{H}$ matrix for different values of the measurement noise in Example 1

$\mathbf{W}_{n^x}$	$\mathbf{H}_1$	$\mathbf{H}_2$	$\mathbf{H}_{CL}$
0	1	1	1
1	0.67	0.5	1
5	0.074	0.038	1
∞	0	0	1

and we find

$$\mathbf{H}_2 = \frac{1}{\mathbf{W}_{n^x}^2 + 1}$$

For case S4, Equation 9.20 gives

$$\tilde{\mathbf{F}}\tilde{\mathbf{F}}^T = (\mathbf{W}_{n^x})^2$$

and we have $\mathbf{H}_{CL} = 1$ for all values of the measurement noise $\mathbf{W}_{n^x}$.

Table 9.1 shows the optimal $\mathbf{H}$ for the three cases for some values of the measurement noise. For the "monitoring" cases ($\mathbf{H}_1$ and $\mathbf{H}_2$), the optimal estimator gain $\mathbf{H}$ approaches zero when the measurement noise goes to infinity, but this does not occur for the closed-loop estimator ($\mathbf{H}_{CL}$). The reason is that the estimate $\hat{y} = \mathbf{H}_{CL}x_m$ is used for control, that is, u is changed such that $\hat{y}$ is equal to y_s. If we used an estimator where $\mathbf{H}_{CL} \to 0$ then we would need u to go to infinity, which is not optimal.

9.3 New data-based estimation

We want to use our results for the optimal model-based estimators, to derive data-based estimators. The first step is to obtain the required model to use for cases S1-S4 in Theorems 1-4.

9.3.1 Monitoring cases

For cases S1-S3, all the optimal estimators are on the form $\mathbf{H} = \mathbf{Y}\mathbf{X}^\dagger$, so we may use the data directly. The result will be identical to the conventional least squares solution, which from our derivation should be the optimal estimator for the case when there is no measurement noise for y.

9.3.2 Closed-loop estimator

Let us now consider the more interesting case S4, where we want to find the optimal estimator to be used for closed-loop operation. To use Theorem 4, we need to have information about $\tilde{\mathbf{F}} = \begin{bmatrix} \mathbf{F}\mathbf{W}_d & \mathbf{W}_{\mathbf{n^x}} \end{bmatrix}$ and $\mathbf{G}_x\mathbf{G}_y^{-1} = \mathbf{G}_x^{cl}$.

This information can be obtained by transforming the original data in $\mathbf{Y}$ and $\mathbf{X}$, to match the "closed-loop" form as given by the matrices $\mathbf{Y}_2$ and $\mathbf{X}_2$ in (9.12):

$$\mathbf{Y}_2 = \begin{bmatrix} \mathbf{W}_{y_s} & 0 \end{bmatrix}$$
$$\mathbf{X}_2 = \begin{bmatrix} \mathbf{G}_x^{cl}\mathbf{W}_{y_s} & \tilde{\mathbf{F}} \end{bmatrix}$$

This may be done as follows. Collect all the experimental data in the big matrix $\mathbf{Y}_{all}$.

$$\mathbf{Y}_{all} = \begin{bmatrix} \mathbf{Y} \\ \mathbf{X} \end{bmatrix} \tag{9.23}$$

Then

1. Perform a singular value decomposition on the data matrix $\mathbf{Y} = \mathbf{U}\Sigma\mathbf{V}^T$
2. Multiply the data matrix $\mathbf{Y}_{all}$ with the unitary matrix $\mathbf{V}$ to get $\mathbf{Y}_{all}\mathbf{V}$ on the desired form

$$\mathbf{Y}_{all}\mathbf{V} = \begin{bmatrix} \mathbf{W}_{y_s} & 0 \\ \mathbf{G}_x^{cl}\mathbf{W}_{\mathbf{y_s}} & \tilde{\mathbf{F}} \end{bmatrix} \tag{9.24}$$

where $\tilde{\mathbf{F}} = \begin{bmatrix} \mathbf{F}\mathbf{W}_d & \mathbf{W}_{n^x} \end{bmatrix}$. $\tilde{\mathbf{F}}$ is denoted $\mathbf{X}_{opt}$ in the following.

Note that $\mathbf{F}$ is defined as $\left(\frac{\partial \mathrm{x}}{\partial \mathrm{d}}\right)_{\mathrm{y}=0}$. Since $\mathbf{V}$ is a unitary matrix, the magnitude of the prediction error does not change when it is multiplied by $\mathbf{V}$, so $\|\mathbf{YV} - \mathbf{HXV}\|_F = \|\mathbf{Y} - \mathbf{HX}\|_F$. This follows because the singular vectors satisfy $\mathbf{V}^T = \mathbf{V}^{-1}$, so we have

$$\mathbf{YV} = \mathbf{U}\Sigma = \begin{bmatrix} \mathbf{U}_1 & \mathbf{U}_2 \end{bmatrix}\begin{bmatrix} \Sigma_1 \\ 0 \end{bmatrix} = \begin{bmatrix} \mathbf{U}_1\Sigma_1 & 0 \end{bmatrix}$$

$\mathbf{G}_x^{cl}$ can be easily calculated. To find $\mathbf{G_x}$ and $\mathbf{G_y}$, which are needed to calculate the optimal $\mathbf{H}$ matrix (denoted by $\mathbf{B}_{CL}$ in the following), we assume that the degrees of freedom are chosen to be the primary variables. This will result in $\mathbf{G}_y = \mathbf{I}$.

The closed-loop data-based estimator ($\mathbf{B}_{CL}$) suffers from the same weakness as ordinary least-squares, giving poor results for ill-conditioned matrices and underdetermined systems. Performing a principal component analysis on the $\mathbf{X}$ data will remove the weaker directions containing noise resulting in a well-conditioned matrix. Then, closed-loop data-based estimator can be applied to the data. We call this "truncated closed-loop estimator" ($\mathbf{B}_{CL}^{\dagger}$).

9.4 Examples

9.4.1 Example 2

To investigate the performance of the estimators, they were applied to a linear approximation of a binary distillation column model - Column A [172] - subjected to different control cases. Full information about the model and the source codes are online. There are two inputs, namely the reflux flow and the boilup, and one disturbance, which is the change in feed composition. The linearized model for open-loop system for the two primary variables is

$$\mathrm{y} = \begin{bmatrix} 0.8754 & -0.8618 \\ 1.0846 & -1.0982 \end{bmatrix}\mathrm{u} + \begin{bmatrix} 0.8812 \\ 1.1188 \end{bmatrix}\mathrm{d} \tag{9.25}$$

where the primary variables are compositions of the two main components in the top and bottom products. The model for the eight measurements (temperatures) is

$$\mathrm{x}_m = \begin{bmatrix} -64.665 & 65.413 \\ -171.884 & 173.569 \\ -226.276 & 227.842 \\ -130.878 & 130.911 \\ -195.132 & 193.623 \\ -142.092 & 140.419 \\ -55.816 & 55.013 \\ -11.818 & 11.634 \end{bmatrix}\mathrm{u} + \begin{bmatrix} -67.174 \\ -180.728 \\ -242.622 \\ -146.618 \\ -207.430 \\ -146.928 \\ -56.667 \\ -11.897 \end{bmatrix}\mathrm{d} + \mathrm{n}^x \tag{9.26}$$

These measurements are chosen from the top and bottom sections in the column. The two secondary variables, which are reflux flow and a temperature measurement from 25th tray of column, are given by

$$\mathrm{z} = \begin{bmatrix} 1 & 0 \\ -195.132 & 193.623 \end{bmatrix}\mathrm{u} + \begin{bmatrix} 0 \\ -207.4297 \end{bmatrix}\mathrm{d} \tag{9.27}$$

This means that the reflux flow rate and the temperature measurement from 25th tray are controlled and their setpoints are the degrees of freedom. The disturbance and noise variances are as below for all cases:

$$\mathrm{d} \sim \mathcal{N}\left(0, 0.05^2\mathbf{I}_2\right)$$

$$\mathrm{n}^x \sim \mathcal{N}\left(0, 0.5^2\mathbf{I}_8\right)$$

Since there is no control in the first case, the standard deviation in u ($\sigma \approx 0.05$) was selected to give a small standard deviation in y. The resulting standard deviations in the primary variables for all cases are the same.

Table 9.2: Four operation cases

Operation	Estimator	Input variables	Variable distribution
Open-loop	$\mathbf{H}_1$	u	$\mathrm{u} \sim \mathcal{N}\left(0, 0.08^2\mathbf{I}_2\right)$
$\mathrm{y} = \mathrm{y}_s$	$\mathbf{H}_2$	$\mathbf{G}_y^{-1}\left(\mathrm{y}_s - \mathbf{G}_y^d\mathrm{d}\right)$	$\mathrm{y}_s \sim \mathcal{N}\left(0, 0.005^2\mathbf{I}_2\right)$
$\mathrm{z} = \mathrm{z}_s$	$\mathbf{H}_3$	$\mathbf{G}_z^{-1}\left(\mathrm{z}_s - \mathbf{G}_z^d\mathrm{d}\right)$	$z_s \sim \mathcal{N}\left(0, \begin{bmatrix} 0.05^2 & 2^2 \end{bmatrix}\mathbf{I}_2\right)$
$\hat{\mathrm{y}} = \mathrm{y}_s$	$\mathbf{H}_{CL}$	$(\mathbf{H}\mathbf{G}_x)^{-1}\left[\mathbf{H}\left(\mathbf{G}_x^d\mathrm{d} + \mathrm{n}^x\right) + \mathrm{y}_s\right]$	$\mathrm{y}_s \sim \mathcal{N}\left(0, 0.005^2\mathbf{I}_2\right)$

For the data-based estimators, calibration data was generated by drawing 32 random values for u, d, y_s and z_s with the distributions given in Table 9.2, and calculating the corresponding output variables x_m and y for the respective cases (except case 4). This gave one set of calibration data with 32 experiments: $\mathbf{X}$ (8 × 32) and $\mathbf{Y}$ (2 × 32). The median of the prediction error for 150 runs are used to assess the estimators' performances because noise and variation in input variables resulted in a distorted picture of estimator performance by outliers.

Model-based estimators

Table 9.3 shows the results of validation for model-based for different cases. For each case (S1, S2, S3 and S4), the matrix $\mathbf{H}$ is obtained first, using theorems 1-4. For example for case S4 we obtain

$$\mathbf{H}_{CL} = \begin{bmatrix} -0.0024 & 0.0008 \\ 0.0004 & -0.0041 \\ -0.0001 & -0.0017 \\ -0.0025 & -0.0001 \\ 0.0011 & 0.0004 \\ 0.0003 & 0.0013 \\ 0.0007 & -0.0026 \\ -0.0037 & 0.0005 \end{bmatrix}$$

Then, they were validated on the data generated randomly for each case (S1, S2, S3, S4), with the given standard deviations for n^x, u, z_s, y_s (see Table 9.2). The validation is done by first calculating u for the given case and then substituting into the model. The reported data in Table 9.3 shows the median of the prediction errors. In Table 9.3, the diagonal elements correspond to the optimal estimators for the intended cases, and, as expected, the prediction error is smallest along the diagonal. Note that the cases are not comparable along the rows because of different variances for different cases. Calibrating with one case and validating with another is mostly applicable to the last case. So, the shaded cells are actually showing the more interesting data.

The prediction errors are equal for all the cases for S4 due to the constraint $\mathbf{G}_y = \mathbf{H}\mathbf{G}_x$. The closed-loop estimator generally gives the best performance.

Data-based estimators

Table 9.4 shows the results of validation for data-based estimators. As mentioned in the previous section, the dashed cells are the more interesting data.

Table 9.3: The mean prediction error of the model-based estimators applied to four operation cases

	Cases			
Estimator	S1	S2	S3	S4
S1	0.0168	0.0248	0.0177	0.1972
S2	0.271	0.0156	0.035	0.0221
S3	0.0207	0.0224	0.0176	0.1021
S4= CL	0.0187	0.0187	0.0187	0.0187

Table 9.4: The mean prediction error of the data-based estimators applied to four operation scenarios

		Loss			
Calibration Data					
Operation	Estimator	S1	S2	S3	S4
S1	$\mathbf{B}_{LS,1}$	0.017	0.019	0.018	0.02
S2	$\mathbf{B}_{LS,2}$	0.316	0.016	0.061	0.173
S3	$\mathbf{B}_{LS,3}$	0.077	0.022	0.017	0.054
S1	$\mathbf{B}_{PCR,1}$	0.017	0.018	0.017	0.018
S2	$\mathbf{B}_{PCR,2}$	0.379	0.015	0.069	0.192
S3	$\mathbf{B}_{PCR,3}$	0.091	0.023	0.016	0.065
S1	$\mathbf{B}_{PLS,1}$	0.016	0.018	0.017	0.018
S2	$\mathbf{B}_{PLS,2}$	0.352	0.014	0.067	0.192
S3	$\mathbf{B}_{PLS,3}$	0.077	0.021	0.016	0.055
S1	$\mathbf{B}_{CL,1}$	0.018	0.02	0.018	0.020
S2	$\mathbf{B}_{CL,2}$	0.132	0.018	0.028	0.067
S3	$\mathbf{B}_{CL,3}$	0.077	0.022	0.017	0.053
S1	$\mathbf{B}^{\dagger}_{CL,1}$	0.017	0.019	0.017	0.019
S2	$\mathbf{B}^{\dagger}_{CL,2}$	0.130	0.016	0.028	0.066
S3	$\mathbf{B}^{\dagger}_{CL,3}$	0.088	0.024	0.016	0.061

Figure 9.4 shows the "closed-loop" performance with two different data sets. The number of measurements is increased from 8 to 41 (the total number of stages). All estimators are trained on calibration data from case 2 and validated on case 4. The performance of new closed-loop estimator (shown with $\mathbf{B}_{CL}$ in Figure 9.4) and the ordinary least square estimator (shown with $\mathbf{B}_{LS}$ in Figure 9.4) was deteriorated when then the system was over-determined with low number of data. This is because they were forced to use the weak directions and assimilate noise and collinearity. Since the truncated closed-loop estimator ($\mathbf{B}^{\dagger}_{CL}$ in Figure 9.4) filters out the noise, it results in better performance. Comparing the two figures in Figure 9.4, we will see that if the data-based estimators are given enough data they will approach their model-based counterparts.

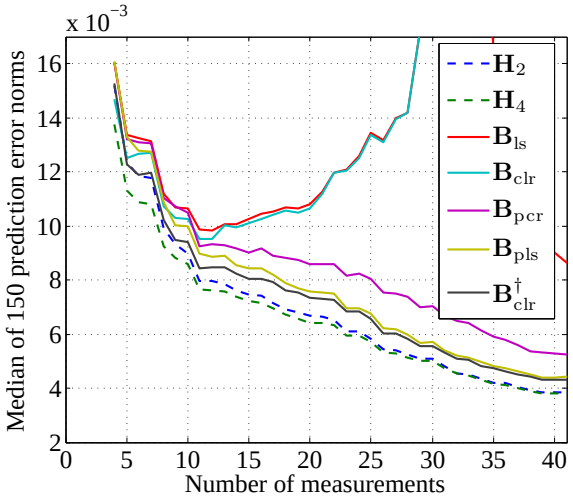

(a) Median prediction error for 150 data set with 32 samples

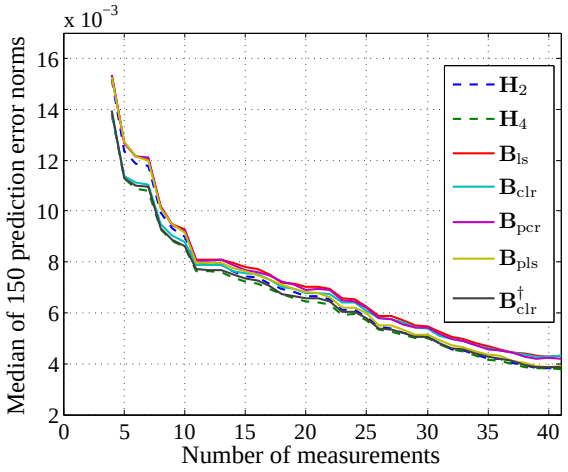

(b) Median prediction error for 150 data set with 200 samples

Figure 9.4: Median prediction error for two sample sizes (validated for S4)

9.4.2 Example 3

The next example is from a multi-component distillation column (4 components) which is simulated rigorously. The schematic of the distillation process with estimator is shown in Figure 9.5.

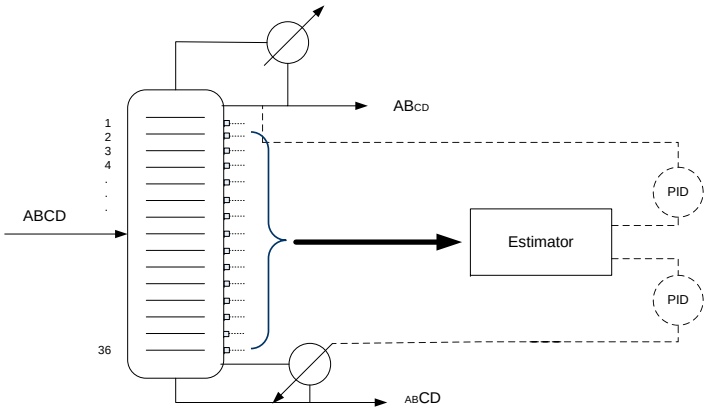

Figure 9.5: Schematic of the distillation process with estimator

The two lightest and the two heaviest products are supposed to be separated in the column. The feed stream is a saturated liquid mixture of methanol, ethanol, 1-propanol, 1-butanol. Disturbances are composition, flow rate, quality, Pressure in the feed stream and also condenser pressure.The composition setpoints for 1-propanol in the top ($x_{C_3\,in\,D}$) and ethanol in the bottom ($x_{C_2\,in\,B}$) of prefractionator are 0.0095 and 0.038 respectively.

Here we show how simple the closed-loop model-based estimator can be derived by choosing the right variables as manipulated variable. We can actually consider u to be any two variables from the process. For the sake of simplicity and because we can use the close-loop information of the system, we select the inputs to the estimation model to be equal to the product compositions, in our case

$$\mathrm{u} = \mathrm{y} = \begin{bmatrix} x_{C_3 in\,D} & x_{C_2 in\,B} \end{bmatrix}$$

This will make the case easier and the matrices will be as below:

$$\mathbf{G}_y = \mathbf{I}$$
$$\mathbf{G}_x^d = \mathbf{F}$$
$$\mathbf{G}_y^d = 0$$

We use exactly the same information for PLS method. $\mathbf{X}$ and $\mathbf{Y}$ in PLS method are the first and second row of $\mathbf{Y}_{all}$ matrix (Equation (9.23)) respectively. We have assumed that we have temperature sensors in every 4th tray. The matrices in the following show the fitting matrices for the two methods ($\mathbf{B}$ for PLS and $\mathbf{H}_{CL}$ is from equation 9.20).

$$\mathbf{B} = \begin{bmatrix} -0.0045 & 0.0075 \\ 0.0113 & -0.0076 \\ -0.0036 & 0.0037 \\ -0.0038 & -0.0013 \\ 0.0074 & -0.0092 \\ -0.0055 & 0.0152 \\ -0.0022 & 0.0057 \\ 0.0011 & -0.0140 \end{bmatrix}$$

$$\mathbf{H}_{CL} = \begin{bmatrix} -0.0038 & 0.0080 \\ 0.0104 & -0.0082 \\ -0.0028 & 0.0041 \\ -0.0035 & -0.0011 \\ 0.0059 & -0.0101 \\ -0.0049 & 0.0156 \\ -0.0019 & 0.0059 \\ 0.0010 & -0.0141 \end{bmatrix}$$

Figure 9.6 shows the dynamic behaviour of the model as disturbances happen and also of the estimators. It is shown that the estimated values can track the real composition very well. It should be noted that the steady state value is more in focus since the methods under study are static estimators. The dynamic behaviour can be corrected by feedback.

9.4.3 Further Examples

Some additional examples are provided by Skogestad et al. [171], where the new closed-loop estimator is compared with PCR and PLS. It is also suggested that adding "artificial noise" may provide additional degrees of freedom for our method. This is particularly relevant when there are a large number of measurement (x), but relatively few samples, for example, for spectroscopic data, because it is then difficult to obtain a good estimate of $\mathbf{W}_{n^x}$ using equation (30). The idea is to add an extra diagonal matrix $\mathbf{W}'_{n^x}$ to the end of $\mathbf{X}_{opt} = \tilde{\mathbf{F}}$, which contains the expected noise for each measurement x along its diagonal.

9.5 Discussion

9.5.1 Relationship to self-optimizing control

This work originated from considering the "indirect control problem" [143] using the "exact local method" in self-optimizing control. In "indirect control" the objective is to find a set of controlled variables c = $\mathbf{H}$x such that by keeping c constant, we indirectly keep the primary variables y constant (or more specifically, at their desired setpoints y_s), in spite of disturbances d and measurement noise n^x. This can be viewed as a special case of "self-optimizing control" with cost function $J = \|y - \hat{y}\|_2$. We can then apply the theory that has been developed for "self-optimizing" control,

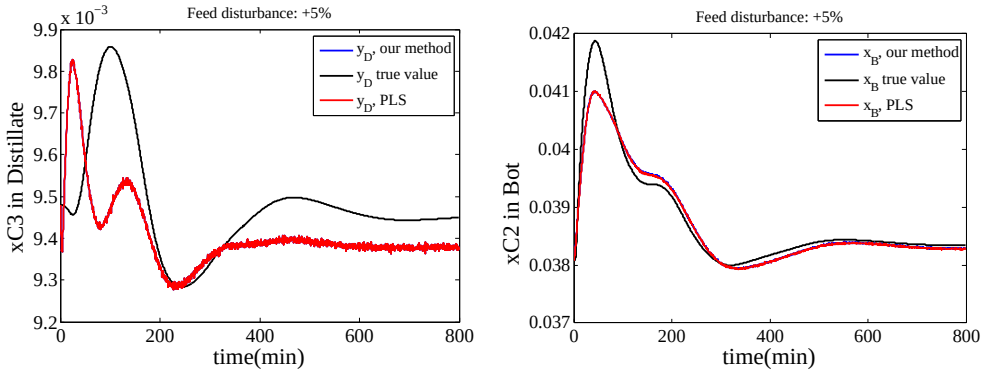

(a) $+5\%$ disturbance in feed flow

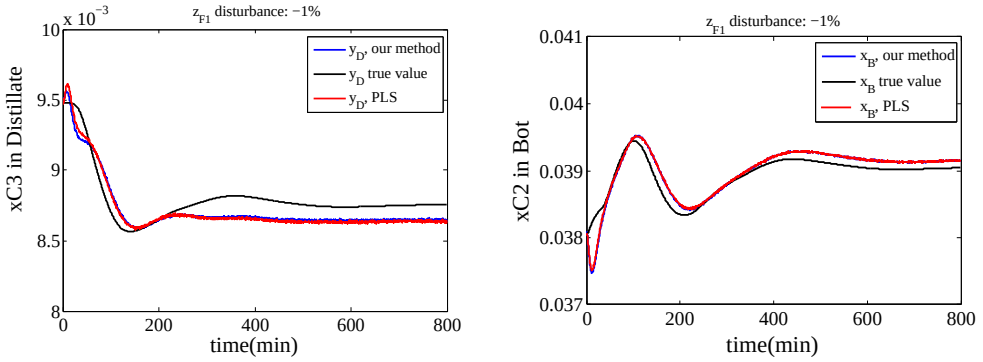

(b) -1% disturbance in Feed composition $z_{1,F}$

Figure 9.6: Estimated and model Composition values for the case with two temperature controls and with the consideration of 8 measurements

which includes the "exact local method". This directly leads to the result in Theorem 4, when the "extra degrees of freedom" in $\mathbf{H}$ are selected such that c = ŷ. This requires some explanation. In indirect control, we adjust the inputs u by feedback to keep c = $\mathbf{H}$x = 0 (constant). Note that we will generate the same inputs u (for a given d and n^x), also if we keep c′ = $\mathbf{D}$c = 0 where $\mathbf{D}$ is any invertible matrix. The matrix $\mathbf{D}$ is the so-called "extra degrees of freedom" in $\mathbf{H}$.

It is clear that one good variable c = $\mathbf{H}$x to use for indirect control of y is the estimate ŷ. However, if we look the other way around, then the optimal c will not necessarily correspond to an estimate of y (ŷ). However, there are extra degrees of freedom in selecting c = $\mathbf{H}$x, we can use these extra degrees of freedom (i.e., the $\mathbf{D}$-matrix), to make c = $\mathbf{H}$x equal to ŷ, which is in fact done when we select $\mathbf{H}$ such that $\mathbf{HG}_x = \mathbf{G}_y$ (see Theorem 4).

9.5.2 Comparison with work of Pannocchia and Brambilla

Our paper provides an extension of the results of Pannocchia and Brambilla [166] on "steady-state closed-loop consistency" to include also measurement noise. In addition, we have shown, in agreement with the results in the paper by Hori et al. [143], that we can always achieve "perfect consistency" for setpoint changes, that is, the use of the "extra degrees of freedom" in $\mathbf{H}$, makes it possible to always have the norm from y_s to the prediction error (y − ŷ) equal to zero, without sacrificing the norm from disturbances (d) to the prediction error. In the notation of Pannocchia and Brambilla [166] this means that we can always make $\epsilon_r = 0$ without sacrificing the norm of ϵ_d.

The inclusion of measurement noise is important, because this is often a critical factor. As an example, consider the estimation of the two product compositions in a distillation column (y = $\begin{bmatrix} x_D & x_B \end{bmatrix}$) based on temperature measurements (x = T). For a binary distillation column with constant pressure, temperature and compositions are uniquely related. So, if there were no measurement noise ($n^x = 0$), one could in theory have a perfect estimate of y by measuring the temperature at the two columns ends (x = $\begin{bmatrix} T_D & T_B \end{bmatrix}$), irrespective of any disturbances in feed composition or feed rate (which may affect stage efficiency). However, in practice, the estimate will be poor because of measurement error, especially for high-purity columns. For example, assume the bottom product of a methanol/water distillation column should be about 99.99% water. At 1 atm, the boiling point of this mixture will be approximately (0.9999×100 °C + 0.0001× 65 °C = 99.9965 °C, whereas the boiling point of 100% water is 100.00 °C. Thus, if we have a measurement error of more than 0.0035 °C (which we certainly will have), then the temperature measurement will be useless to infer composition as it would lead to predicting negative compositions. Thus, due to measurement error (n^x), we need to locate the temperature sensor away from the column end, and the optimal location can be found using the methods presented in this chapter which include measurement noise.

9.5.3 Measurement selection

The results presented in this chapter also provide the basis for optimal measurement selection, which extends Algorithm 1 in Pannocchia and Brambilla [166] to include measurement noise. For example, assume there are 10 candidate measurements, and there are 2 outputs that we want to estimate (i.e, we have 2 y's and 2 u's). Assume that we want to use 4 out of these 10 measurements. There are then 210 candidate measurement sets, and we find the best set by computing for each set the prediction error using Theorem 4. To avoid checking all sets, we can also use the branch and bound method developed by Kariwala and Cao[173].

9.5.4 Comparison to standard data-based estimators

1. In least squares regression (LS), one gets $\mathbf{B} = \mathbf{YX}^{-1}$, or more generally $\mathbf{B} = \mathbf{YX}^{\dagger}$, where $\mathbf{X}^{\dagger}$ denotes the pseudo inverse of $\mathbf{X}$. In principal component regression (PCR), one uses $\mathbf{B} = \mathbf{YX}_a^{\dagger}$ where $\mathbf{X}_a^{\dagger} = \sum_{i=1}^{a} \frac{1}{\sigma_i} \nu_i u_i^H$ denotes the pseudo inverse of $\mathbf{X} = \mathbf{U\Sigma V}^H$ with only a principal components included. Thus, in both LS and PCR one inverts the $\mathbf{X}$-matrix, while with the new estimation method, see equation (9.21) in Theorem 3, one considers only a part $\mathbf{X}_{opt} = \tilde{\mathbf{F}}$ of the

transformed $\mathbf{X}$-matrix. It is optimal because the corresponding $\mathbf{Y}$ data are zero. The proposed method seems a bit similar to PLS in that we use the data for $\mathbf{Y}$ to affect the $\mathbf{X}$-data (we get $\mathbf{X}_{opt}$ from $\mathbf{X}$ by using the SVD of $\mathbf{Y}$).

2. Comparing the regression equations of our new estimator and PLS, we realize that the PLS method has one more degree of freedom ($\mathbf{B}_0$), which provides an optimal centering of the data. We may include this degree of freedom into our method as follows: By assuming deviation variables, we may write

$$\mathbf{Y} - \mathbf{Y}_0 = \mathbf{H}(\mathbf{X} - \mathbf{X}_0) \tag{9.28}$$

or

$$\mathbf{Y} = \mathbf{H}\mathbf{X} + \mathbf{H}_0 \tag{9.29}$$

where $\mathbf{H}_0 = \mathbf{Y}_0 - \mathbf{H}\mathbf{X}_0$. By writing

$$\mathbf{H}_0 = diag(\mathbf{H}_0) \times 1 - vector \tag{9.30}$$

Equation (9.29) then can be written as

$$\mathbf{Y}' = \mathbf{H}'\mathbf{X}' \tag{9.31}$$

where $\mathbf{H}' = \begin{bmatrix} \mathbf{H} & diag(\mathbf{H}_0) \end{bmatrix}$ and $\mathbf{X}' = \begin{bmatrix} \mathbf{X} & 1 - vector \end{bmatrix}$.

Thus, by just adding 1's to the end of the $\mathbf{X}$-data, one can optimize to find $\mathbf{H}'$, and then find $\mathbf{H}$ and $\mathbf{H}_0$.

3. The general equation for $\mathbf{B}$ in PLS is [174]

$$\mathbf{B}_{PLS} = \mathbf{W}_a \left(\mathbf{W}_a^T \mathbf{X}^T \mathbf{X} \mathbf{W}_a\right)^{-1} \mathbf{W}_a^T w_1 \tag{9.32}$$

Comparing this with $\mathbf{H}$ for our closed-loop estimator in equation (9.21), we see that $\mathbf{X}_{opt} = \tilde{\mathbf{F}}$ is a variation of $\mathbf{W}_a\mathbf{X}$. $\mathbf{X}_{opt}$ is actually $\mathbf{X}\mathbf{V}$ in our method, where $\mathbf{V}$ is the right singular vector. It acts as some sort of $\mathbf{W}_a$.

We must assume that $\mathbf{X}_{opt} = \tilde{\mathbf{F}}$ is full rank (invertible) to use the analytic expression in equation (9.21). If $\tilde{\mathbf{F}}$ does not have full rank one may use some pseudo-inverse of $\tilde{\mathbf{F}}$ (similar to PCR). This adds degrees of freedom to the method, which in PLS is the size of the matrix $\mathbf{W}_a$ and is specified in the first step (the number of components in PLS). The problem of invertibility is solved by manipulating $\mathbf{W}_a$ matrix.

4. The PLS method for univariate data is optimal in the prediction error sense [162]. However, the PLS algorithm for multivariate data is not optimal in the same way as the PLS algorithm for univariate data. There are reports that from the literature that the PLS solution using different approaches are not equivalent. For example de Jong's SIMPLS [159] is not equivalent to Herman Wold's NIPALS.

5. As mentioned before, the reports from different studies showed that PLS always give a higher coefficient of determination (denoted R^2 in statistics) than PCR (Table 1 in the paper by Wentzell et al. [164]). However, some authors [175, 176, 177] have taken a closer look on the shrinkage properties of PLS and have shown that PLS nearly always can be improved in principle, so the regression method as such is not optimal.

9.6 Conclusion

In this chapter, we have introduced a new class of static estimators based on minimizing the prediction error. We have considered four different cases, where the first three (S1-S3) correspond to cases where the estimator is used for monitoring, and the fourth case (S4) is when the estimator is used in closed-loop. The new estimators (Theorems 1-5) are derived based on the assumption that we have available a linear process model. If only we have data available, then these may directly be used for the three monitoring estimators (S1-S3). For the closed-loop estimator (S4), we have proposed a method to extract the data, see equations (9.23) and (9.24). For the data-based

case, the new estimators have been compared with the established PCR and PLS estimators, and the results were found to be comparable (see Figure 9.4). For a specific case, our new estimators should be better as they are optimal in terms of minimizing the prediction error, but PCR and PLS are found to generally give good predictions.

Chapter 10

Control of Kaibel Column Using Estimated compositions

In this chapter, control of Kaibel distillation column with the objective of minimizing the energy requirement is studied. This is done by estimating the compositions of the light and heavy keys at the ends of the prefractionator. The static estimator which we have developed previously [178] is used for this purpose.

10.1 Introduction

It is discussed in the previous chapters that it is important to control compositions of the streams coming from top and bottom of the prefractionator. This is because the impurities coming from top and bottom of the prefractionator will end up in the side streams and will lead to less pure side products. In this chapter, the compositions of heavy key in the top and light key in the bottom of the prefractionator are estimated and controlled at their optimal nominal values. These values are estimated from a simpler case which is a conventional column with the same specifications and profiles (excluding the stages at both ends) as the prefractionator. The resulting values are applied to the Kaibel column.

A schematic of the Kaibel column is shown in Figure 10.1. The two lightest and the two heaviest products are separated in the prefractionator and the products are separated further and drained in the main column. As it is obvious, the most difficult separation is taking place in the prefractionator and the other sections are performing close to binary separation with small light or heavy impurity.

10.2 Estimation of impurities at prefractionator's ends

Impurities from top and bottom of prefractionator end up in sidestreams making them off-spec. This is the reason that we need to keep track of what is going out from the prefractionator's ends. Our idea is to estimate the compositions of the impurities at the ends of the prefractionator and control them. Figure 10.2 shows the temperature and composition profiles for the prefractionator of the Kaibel column and a conventional column that is made with the same feed properties and the same compositions. Due to mixing effects by the condenser and the reboiler in the conventional column, the final product purities of the two cases should not be the same because they don't refer to the same internal profiles. The simplified problem which will be solved is shown in Figure 10.3.

Degrees of Freedom

Considering a Kaibel arrangement, four of the degrees of freedom, namely boilup rate (V), reflux (L), side stream flows (S1, S2), are used for controlling product compositions. The two remaining

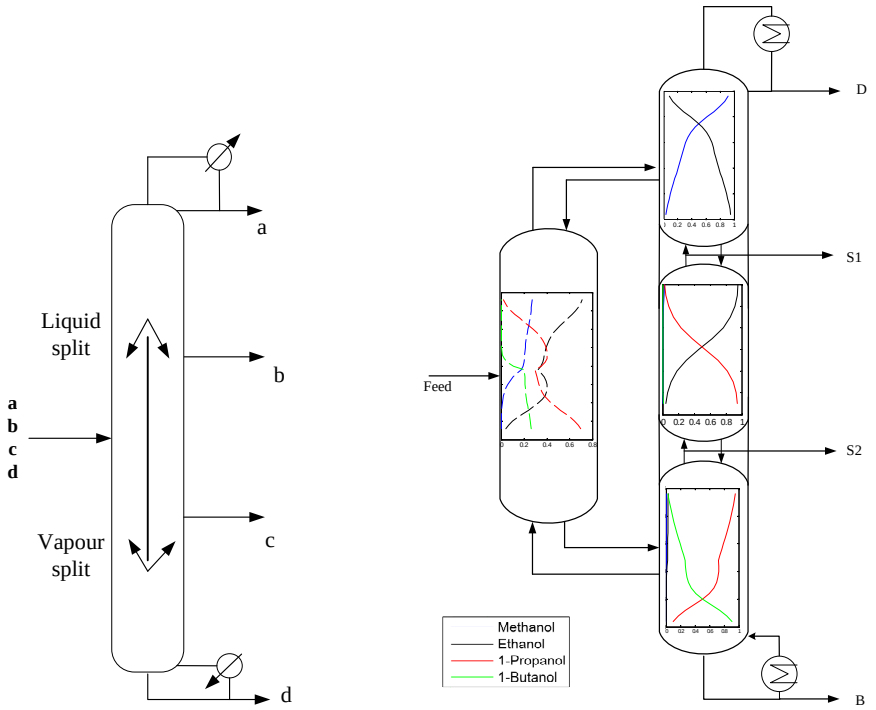

Figure 10.1: Schematic of Kaibel distillation column with composition profiles in different sections

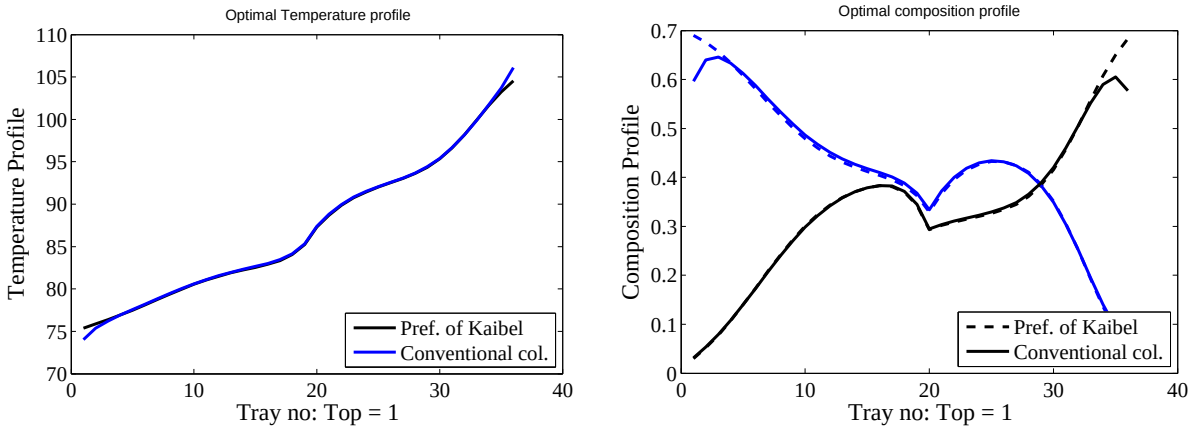

Figure 10.2: Temperature and composition profiles

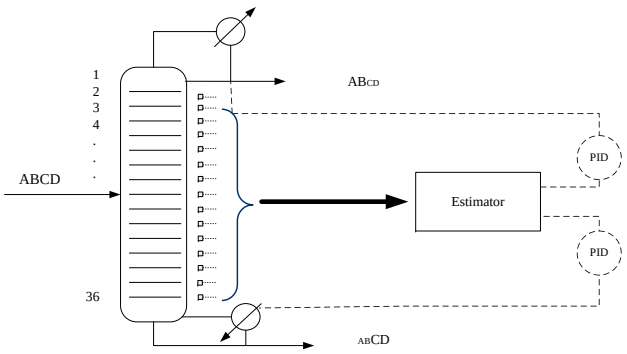

Figure 10.3: Schematic of the estimation problem structure

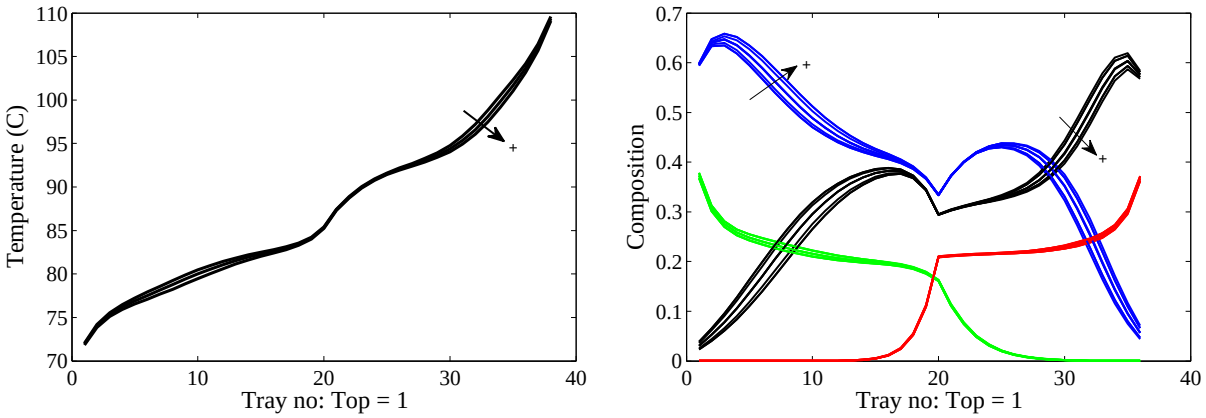

(a) Change in Reflux rate

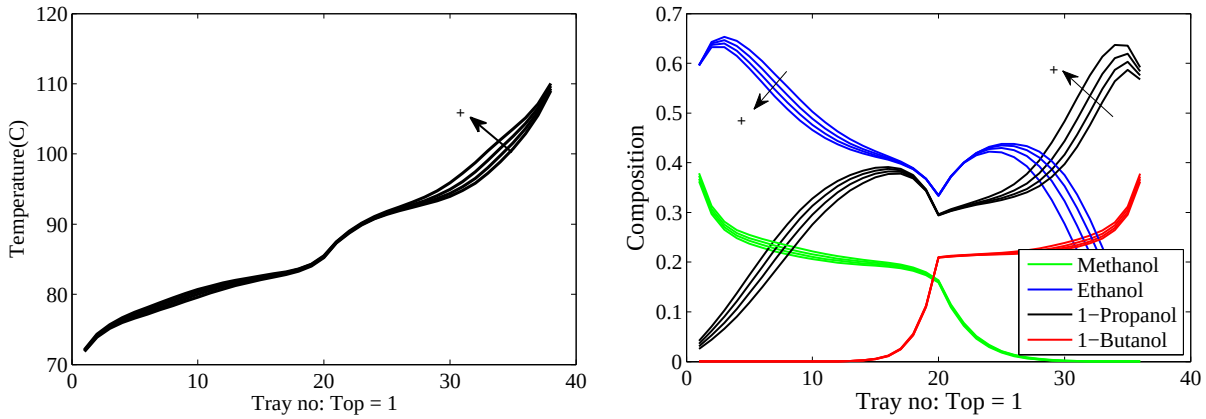

(b) Change in Boilup rate

Figure 10.4: Temperature and composition profiles for changes in the degrees of freedom reflux and boilup by ±1%

degrees of freedom (liquid split (R_L) and vapour split (R_V)) can be considered as inputs for the estimation problem. Expected ranges for disturbances in feed flow rate, feed and product compositions, feed quality and boilup flow should be considered. The problem will become smaller by focusing on prefractionator section. Reflux and boilup in the conventional column, which represent Kaibel prefractionator, function as splits in the Kaibel column. Figure 10.4 shows the temperature profiles for the column when Reflux and boilup are varied ±1% away from nominal values. We note that the variation of the temperatures towards the ends of the column are small. Also, changes in feed composition have a large effect on the temperatures inside the column even though the product compositions are constant. Figures 10.5 and 10.6 show the profiles as a result of disturbance variations.

10.3 Our estimation method

Figure 10.7 shows a general structure for loss minimization (irrespective to what **H** is used for), which is a simple presentation of the linear matrices needed from the plant to do the calculations, and not the specific application. Details of deriving 4 scenarios are given in Chapter 9. In this chapter, **H** is derived from scenario 4. The validation is done for the fully open-loop, closed-loop (the estimates are controlled) and the case were the stabilization loops are closed.

The optimal sensitivity matrix **F**, which is defined as $\mathbf{F} = \frac{\partial \mathbf{y}_{opt}}{\partial \mathbf{d}}$, is simply obtained numerically by

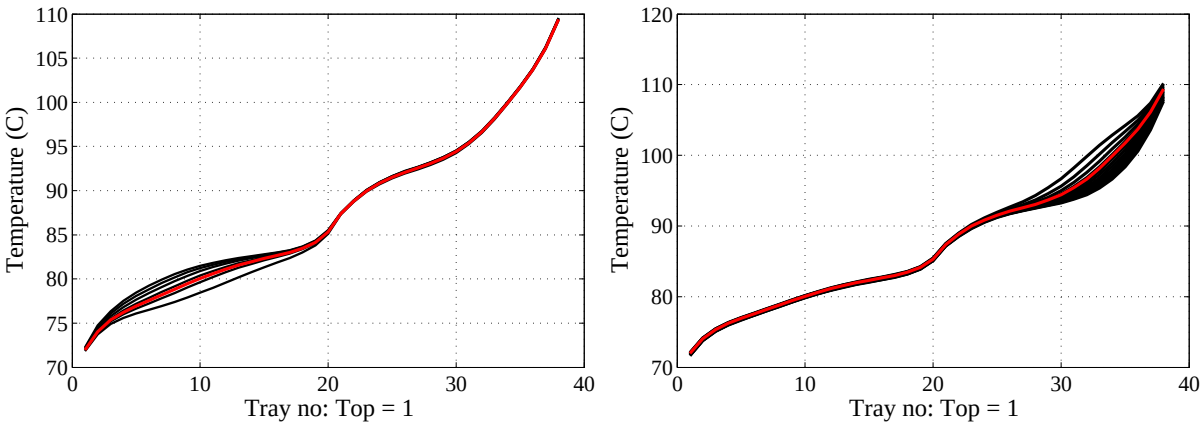

(a) Change in product composition x_{C3t} (b) Change in product composition x_{C2b}

Figure 10.5: Temperature profiles of the conventional column for changes in the light and heavy keys in products

re-optimizing the model for different disturbances. We have assumed 0.1 °C as the expected noise.

As mentioned earlier, it is scenario four which is under our focus. We assume first that we use a controller to set the manipulated variables that brings the real product compositions y to the specified values y_s. In the steady state model of HYSYS, this can be obtained simply by specifying product compositions. The manipulated variables, here reflux and boilup, do normally not enter the estimation scheme, but these may actually be treated as measurement along with temperatures and possibly column pressure. Mejdell [179] has shown that they are not good choices for measurements.

We can consider u to be any two variables from the process. For the sake of simplicity and because we can use the closed-loop information of the system, we select the inputs to the estimation model to be equal to the product compositions. The matrices will become simpler as shown below:

$$\mathbf{G}_y = \mathbf{I}$$
$$\mathbf{G}_x^d = \mathbf{F}$$
$$\mathbf{G}_y^d = 0$$

Note the trivial $\mathbf{G}_y$ and $\mathbf{G}_y^d$ since we have chosen u = y. Figure 10.8 shows the calculated $\mathbf{H}$ values for this case. The end temperatures were not considered as measurements.

$$\begin{bmatrix} \Delta\hat{y}_1 \\ \Delta\hat{y}_2 \end{bmatrix} = \begin{bmatrix} \mathbf{H}_1 & \mathbf{H}_2 \end{bmatrix} \times \begin{bmatrix} \Delta T_5 \\ \Delta T_6 \\ \vdots \\ \Delta T_{32} \end{bmatrix} \tag{10.1}$$

10.4 Evaluation of Estimators

The estimators are tested for three cases: "Open-loop" case (Scenario 1), where the input variables are free, "Open-loop" case (Scenario 3), where the secondary variables are controlled and "Close-loop" case (S4), where the estimates are controlled. The SIMC tuning rules are used [180].

10.4.1 Monitoring the composition ("Open-loop estimation")

Figure 10.9 shows the response of the primary variables and their estimates to a change in an input (boilup). In Figure 10.10, the response of the primary variables and their estimates to different disturbances for the case where two temperature loops are closed, are shown.

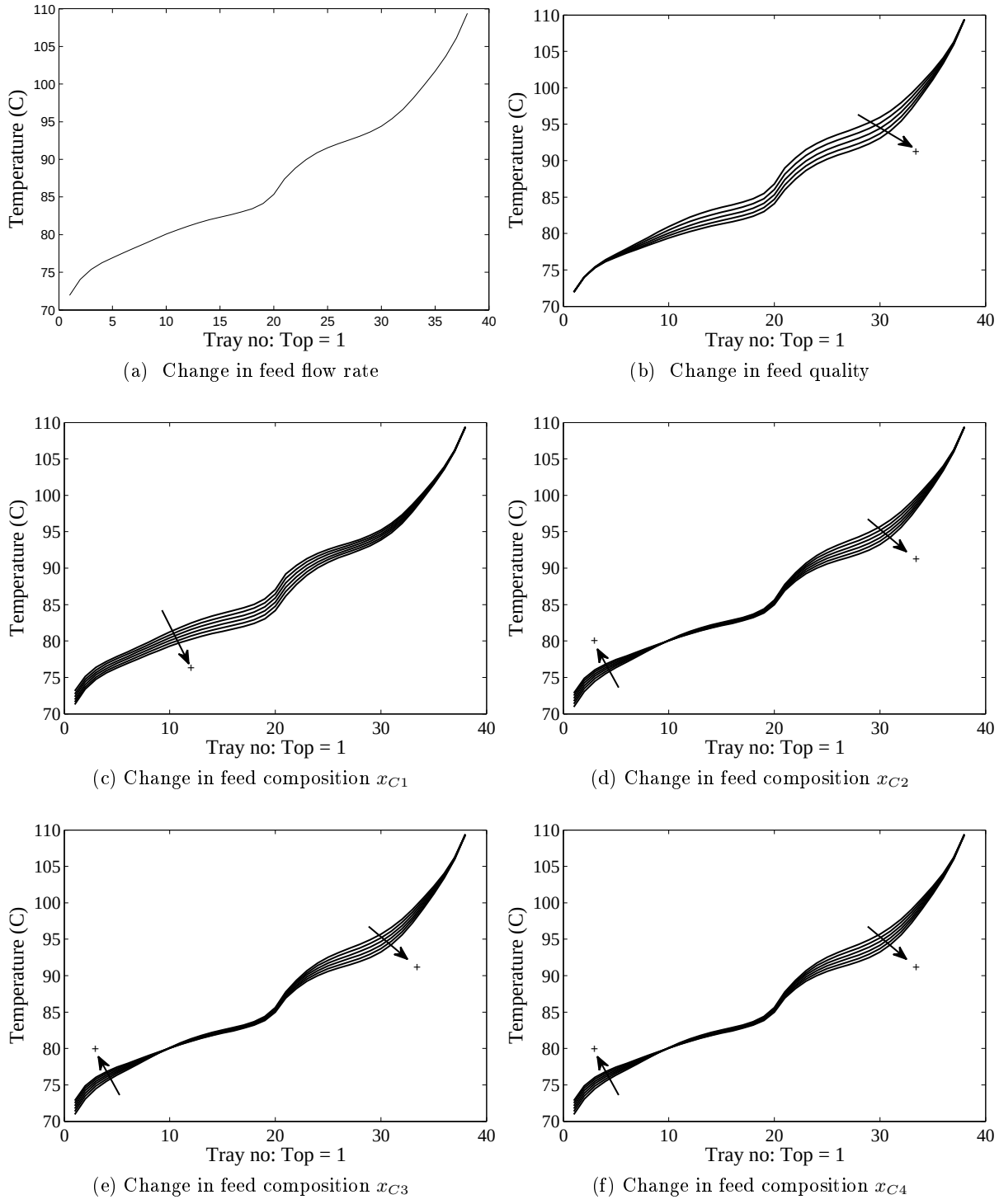

(a) Change in feed flow rate

(b) Change in feed quality

(c) Change in feed composition x_{C1}

(d) Change in feed composition x_{C2}

(e) Change in feed composition x_{C3}

(f) Change in feed composition x_{C4}

Figure 10.6: Temperature profiles of column as a result of disturbance variations; ±5% change in feed compositions, ±20% change in feed vapour fraction

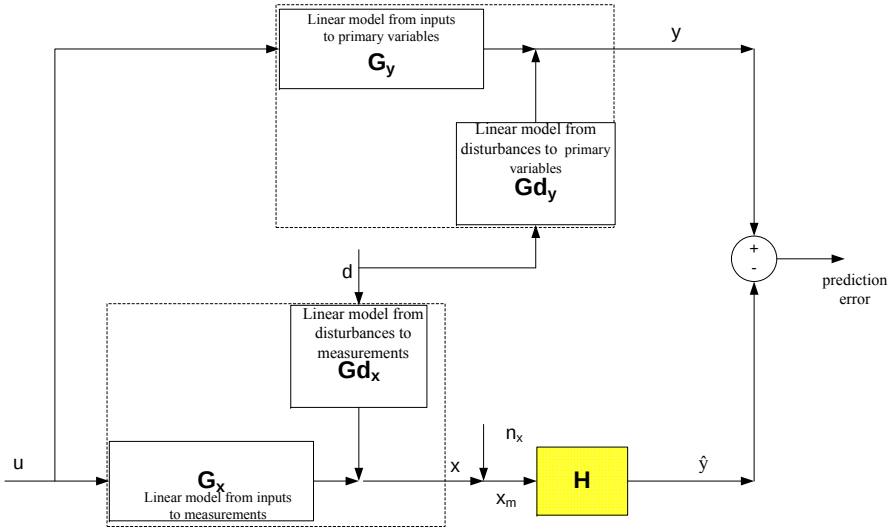

Figure 10.7: A general structure for loss minimization

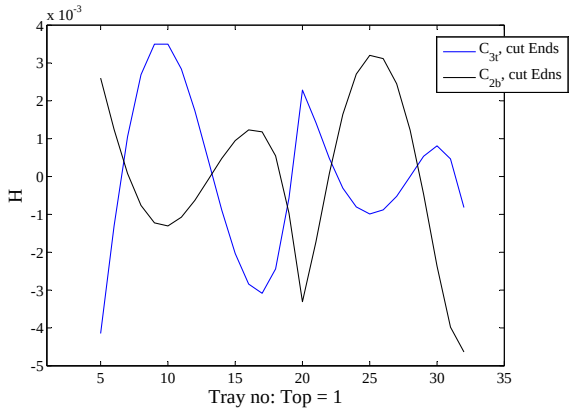

Figure 10.8: **H** values calculated for the conventional column

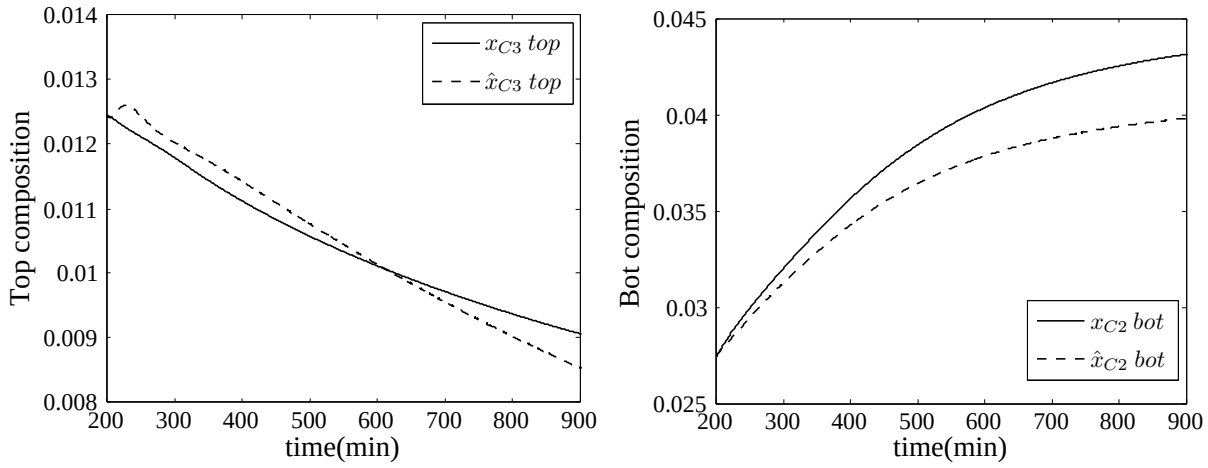

Figure 10.9: Top (right) and bottom (left) estimate with -1 percent change in boilup

As mentioned previously, the task of the column is to perform the sharp split of the second and third components in the feed. There will be a very small operation range for the prefractionator. This is because if we do not perform the sharp split, the impurities will end up in the side streams and the purity specifications of the side streams will be violated. So, we want to ensure sharp split separation in prefractionator. This can be done with 1-point temperature control, but if we want to handle feed condition changes, we will probably need to have 2-point control to be able to stay close to minimum energy consumption. This is the reason that 2-point temperature control is considered for Scenario 3. In Figure 10.10, the estimated compositions were compared to the true primary variables.

10.4.2 "Closed-loop" estimation

In Figure 10.11, the response of the primary variables and their estimates to different disturbances for the case where the estimated variables are controlled, are shown. In this case, 1 temperature loop is closed in the stabilisation layer.

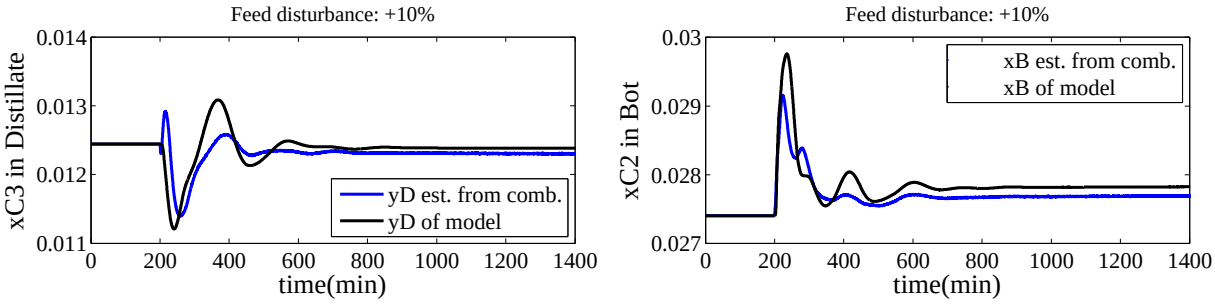

(a) Change in feed flow

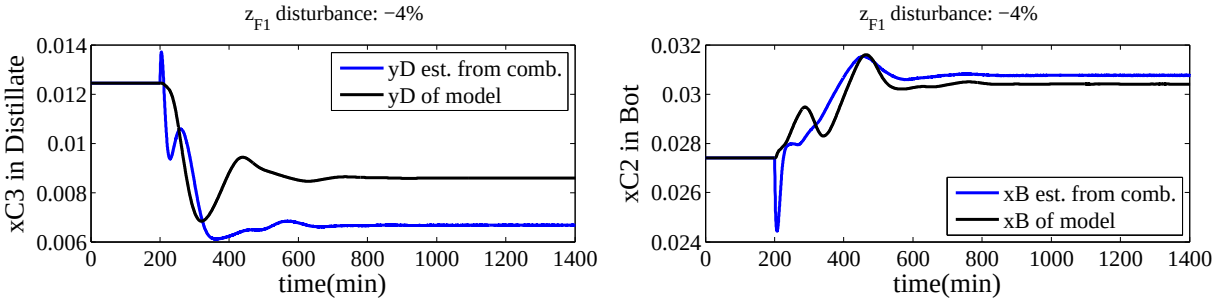

(b) Change in z_{F1}

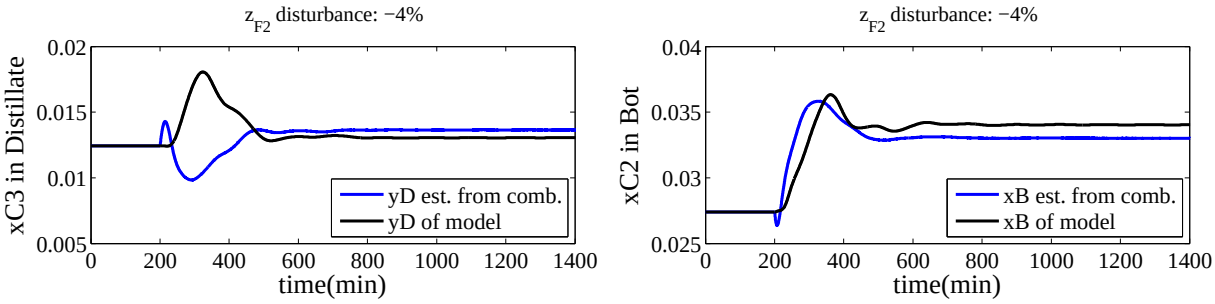

(c) Change in z_{F2}

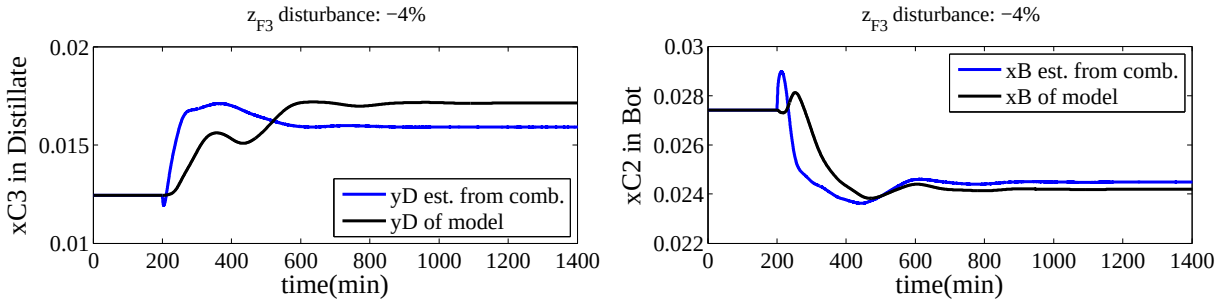

(d) Change in z_{F3}

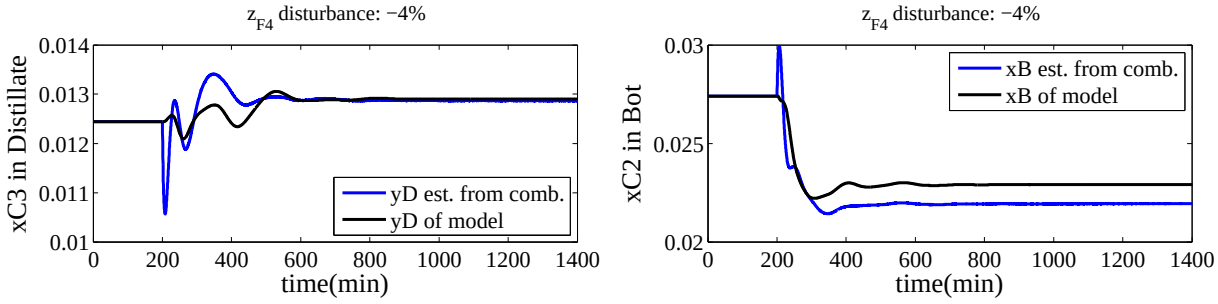

(e) Change in z_{F4}

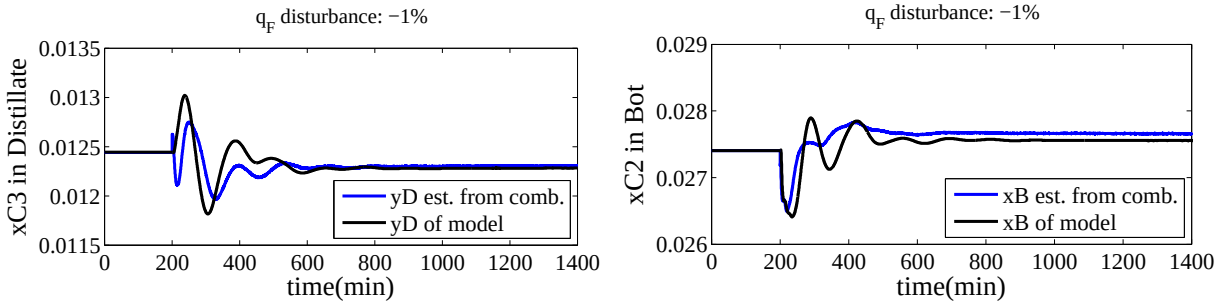

(f) Change in feed quality

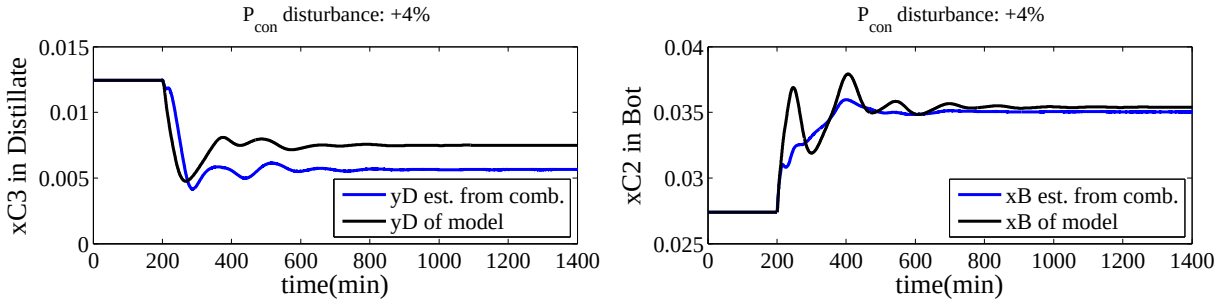

(g) Change in Condenser pressure

Figure 10.10: Composition profile for different disturbances validated for Scenario 3 (the secondary variables are controlled)

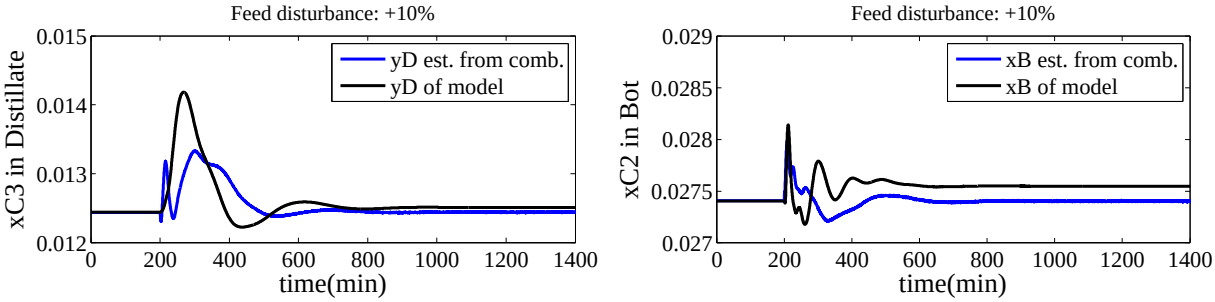

(a) Change in feed flow

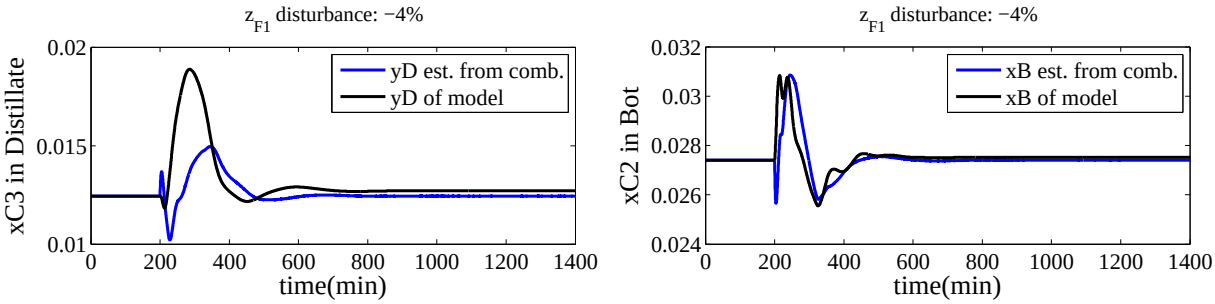

(b) Change in z_{F1}

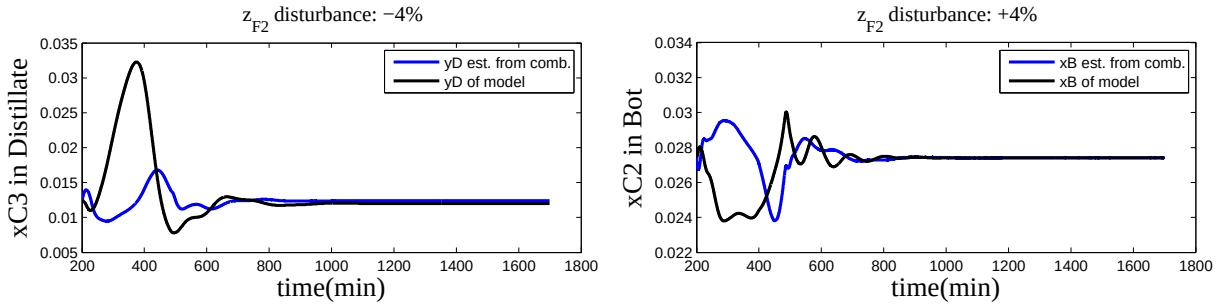

(c) Change in z_{F2}

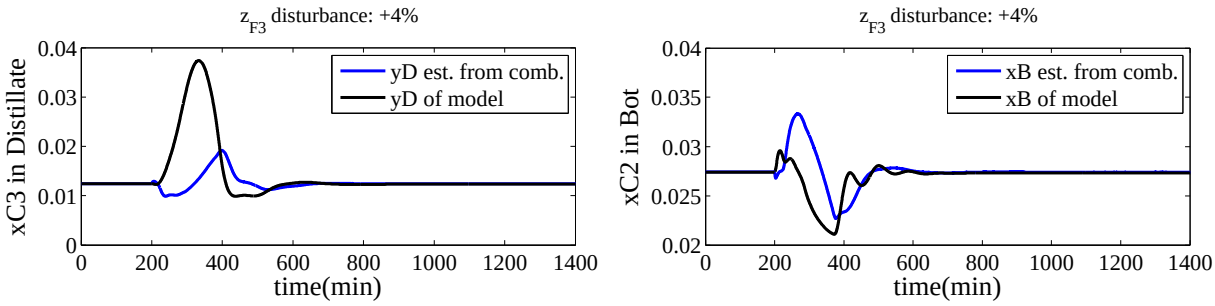

(d) Change in z_{F3}

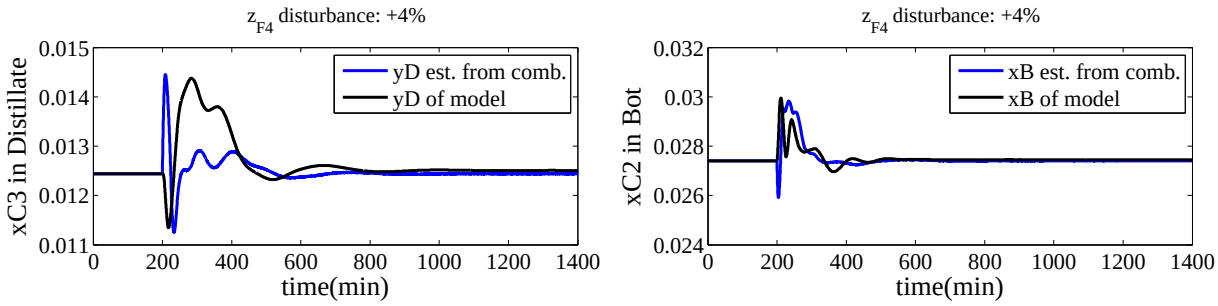

(e) Change in z_{F4}

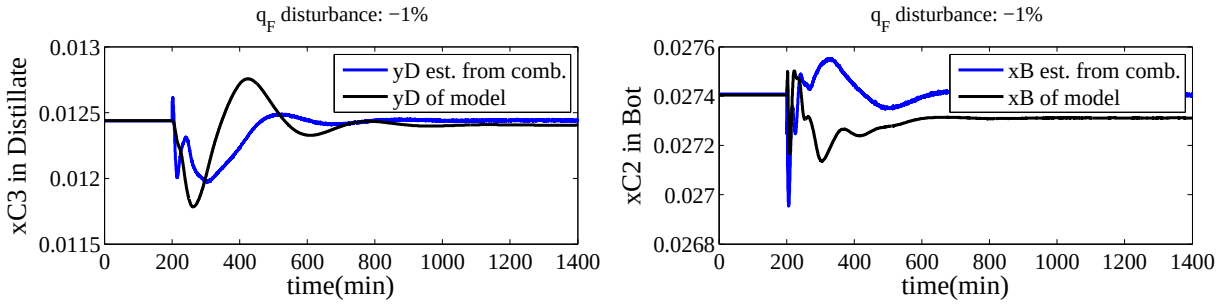

(f) Change in feed quality

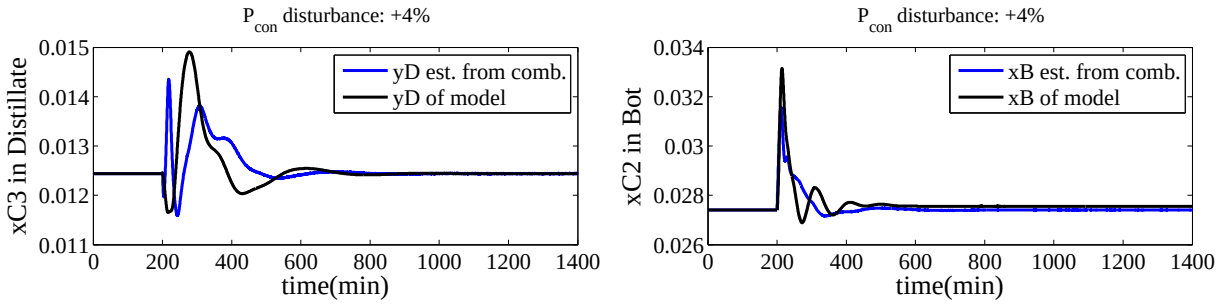

(g) Change in Condenser pressure

Figure 10.11: Composition profile for different disturbances validated for Scenario 4 (the estimated variables are controlled) with 1 stabilizing controller

Figure 10.12 shows the comparison of controlled estimated composition with the controlled true variables where there are two stabilizing loops. The figures show that the overshoots in estimated composition control responses will be much higher than those in the true composition control responses.

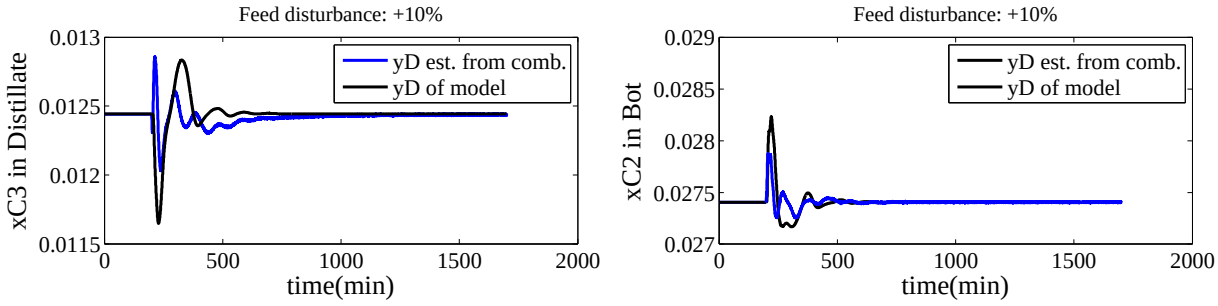

(a) Change in feed flow

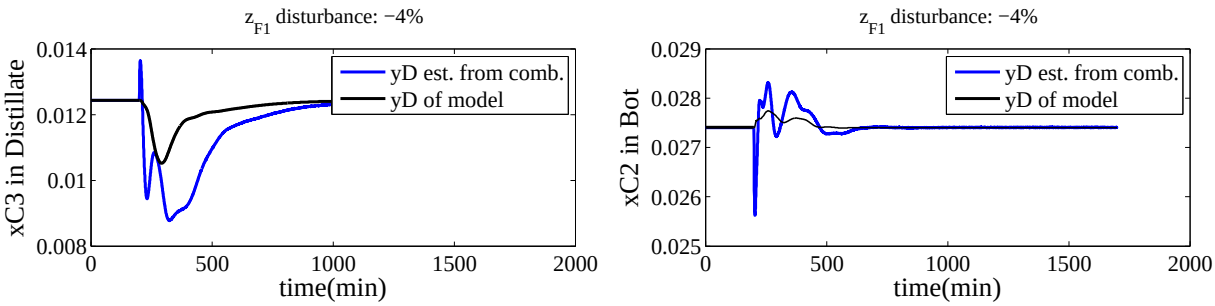

(b) Change in z_{F1}

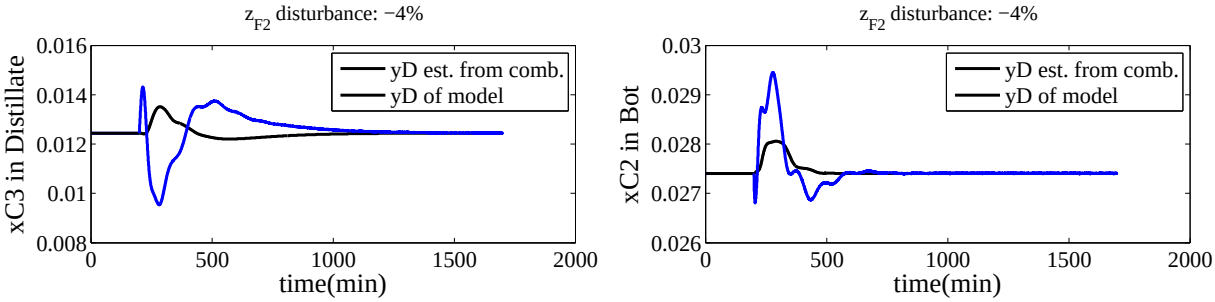

(c) Change in z_{F2}

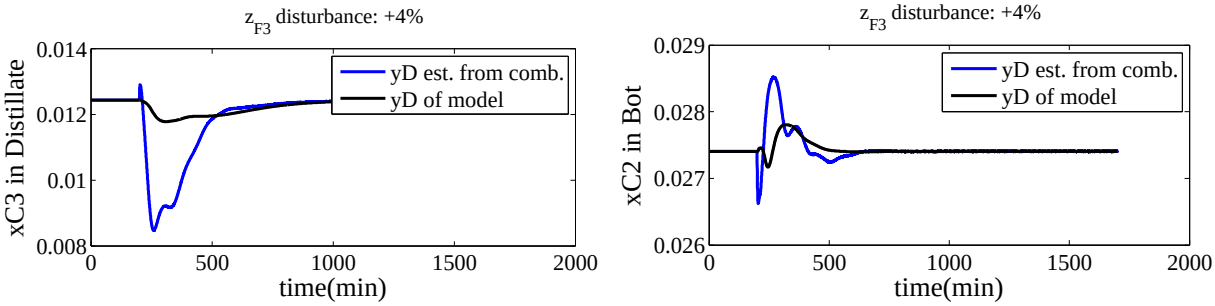

(d) Change in z_{F3}

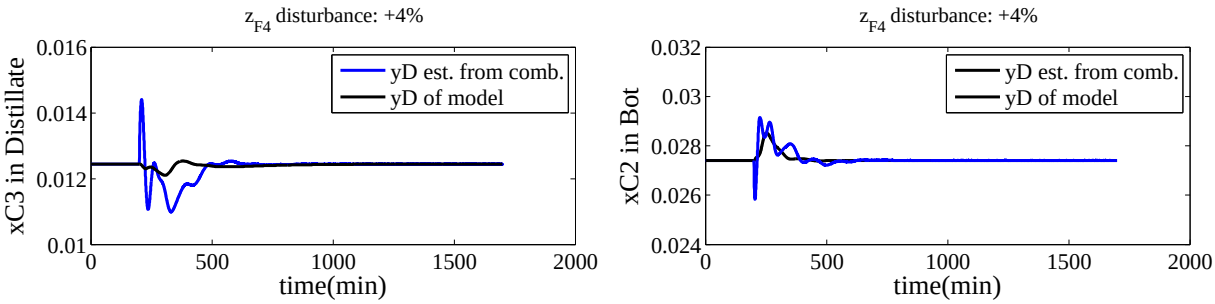

(e) Change in z_{F4}

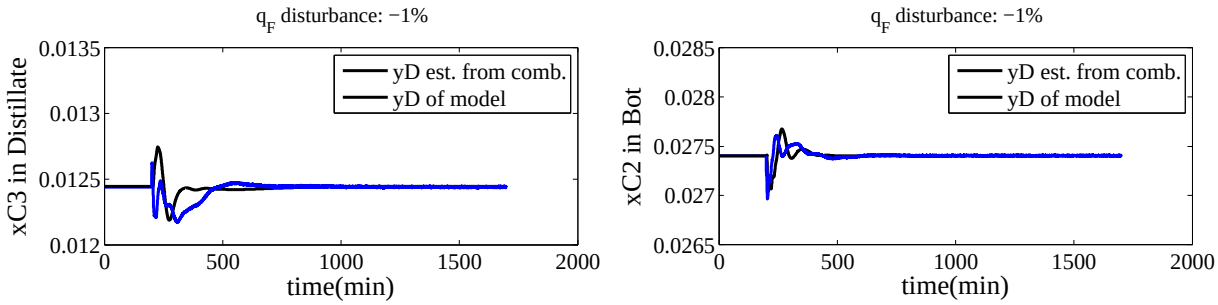

(f) Change in feed quality

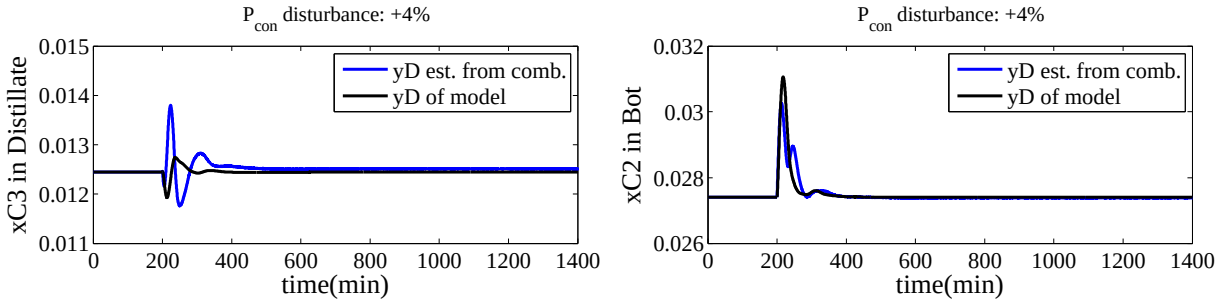

(g) Change in Condenser pressure

Figure 10.12: Composition profiles for different disturbances validated for Scenario 4; the controlled estimated variables are compared to controlled primary variables

10.4.3 Filtered variable controlled

Figure 10.13 shows the dynamic responses of the system with controlled filtered estimates of column ends' key compositions to different disturbances. The filters are first-order low-pass with τ_F = 100. They are applied to 5th, 6th, 16th, 17th and 26th measurements. These are the measurements with negative contributions to the calculated estimate.

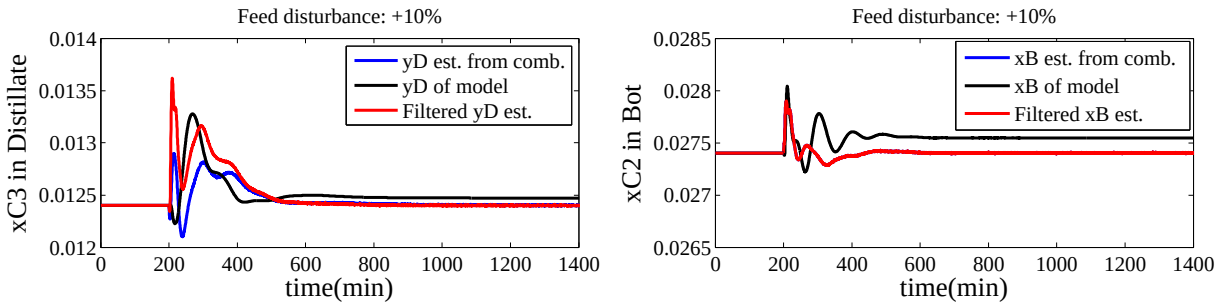

(a) Change in feed flow

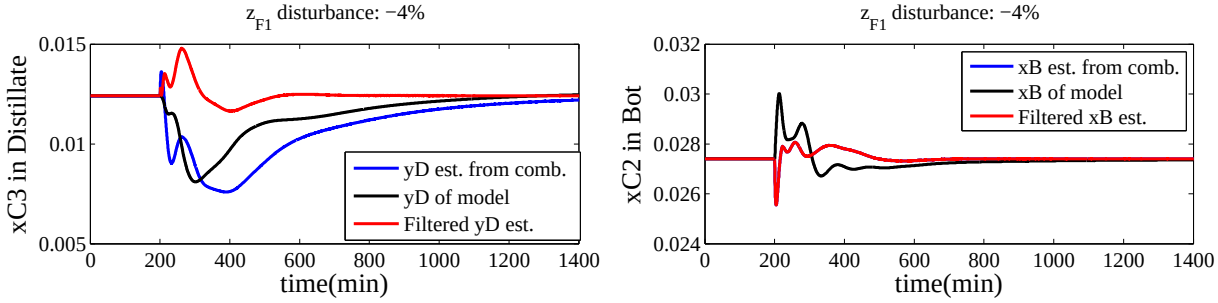

(b) Change in z_{F1}

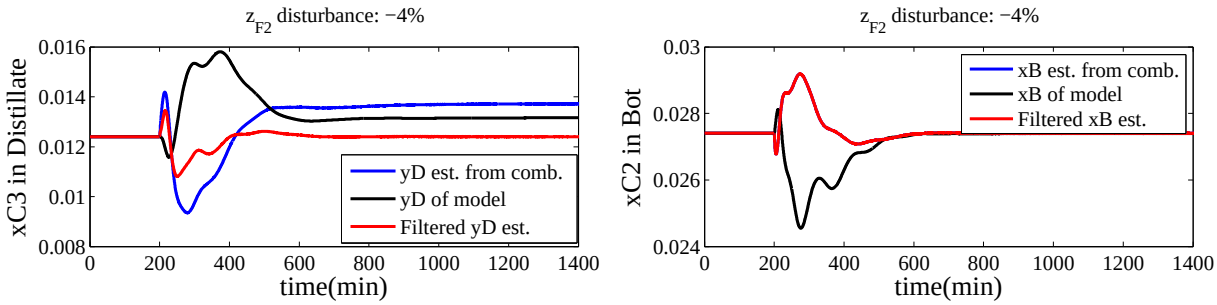

(c) Change in z_{F2}

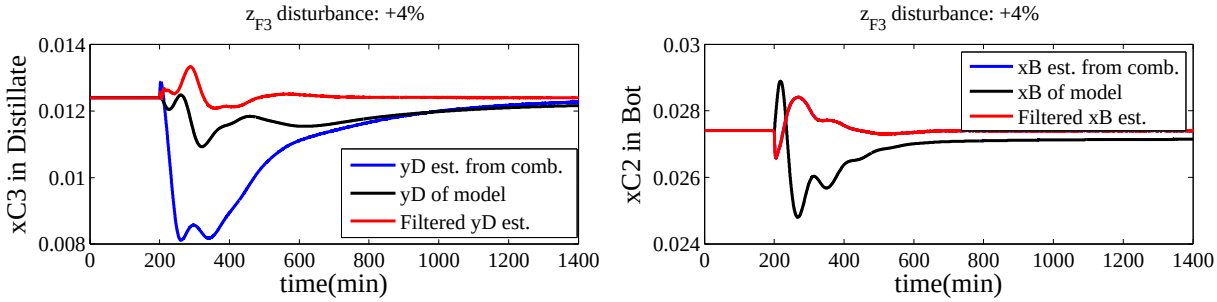

(d) Change in z_{F3}

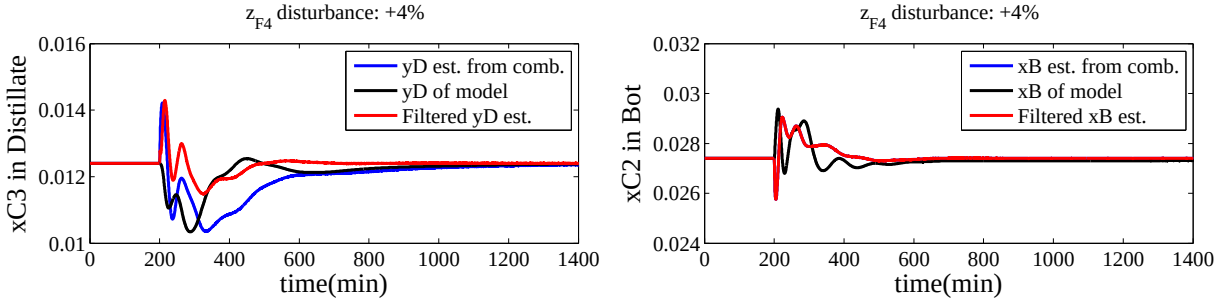

(e) Change in z_{F4}

Figure 10.13: Composition profile for different disturbances validated for Scenario 4: Filters controlled and corresponding primary variable and its estimation

10.5 Control of Kaibel column using estimates

As mentioned earlier, we have made the complex case simple by considering only the prefractionator. Here, we want to test the estimators on the Kaibel column. Figure 10.14 shows the control structure for the Kaibel column. As shown in Figure 10.1, the profiles in the main sections are binary. So, it seems that single temperature loops for each section is enough. Figures 10.15-10.16 show the product compositions in the Kaibel column for various disturbances. Figures 10.17-10.18 show the comparison of three control structures, namely the case with controlled compositions of the key components at prefractionator ends, the case with controlled estimated compositions at prefractionator ends and the case with controlling two temperatures in the prefractionator, while in all three cases have temperature controls in the main section.

10.6 Conclusion

In this chapter, control of Kaibel distillation column is studied. This is done by estimating the compositions of key components in the ends of the prefractionator. The performance of this control

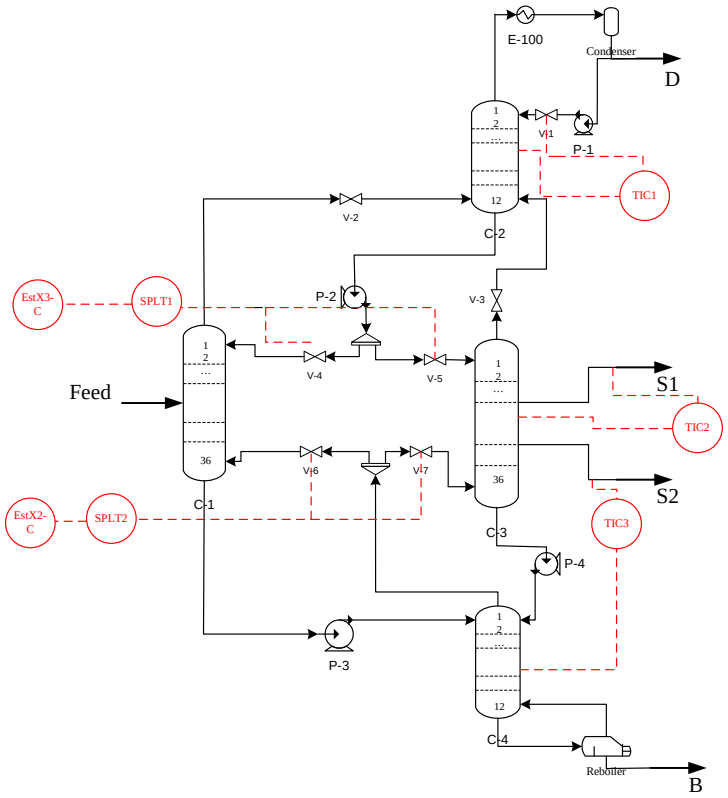

Figure 10.14: Control structure for the Kaibel distillation column

system is compared to the case where the true compositions in the ends of prefractionator are controlled and the case where two sensitive temperatures in prefractionator are controlled. The systems with composition or estimated composition control in the prefractionator perform better compared to the system with temperature control.

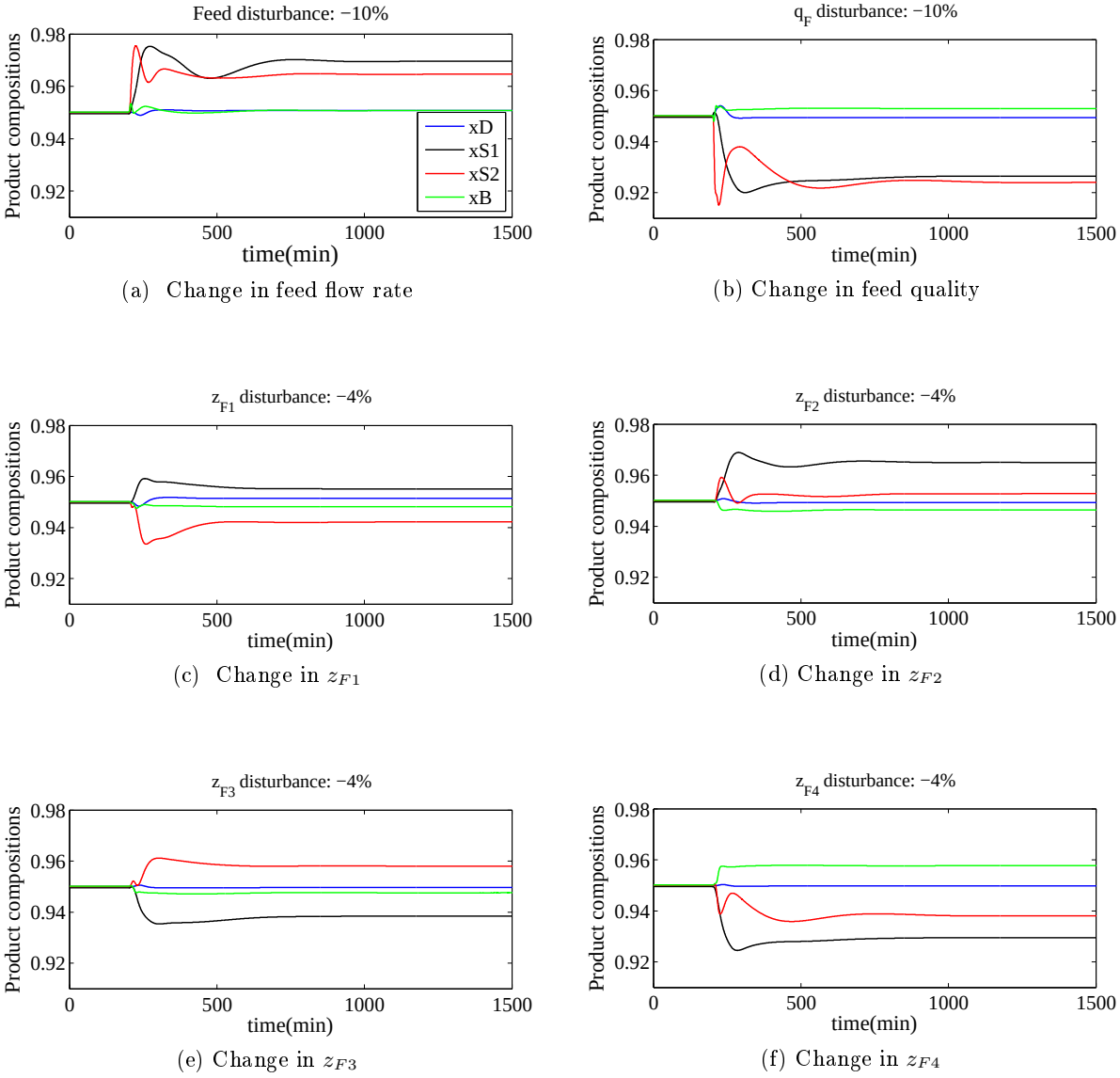

(a) Change in feed flow rate

(b) Change in feed quality

(c) Change in z_{F1}

(d) Change in z_{F2}

(e) Change in z_{F3}

(f) Change in z_{F4}

Figure 10.15: Product compositions of Kaibel column; Impurities estimation in the ends of prefractionator are controlled

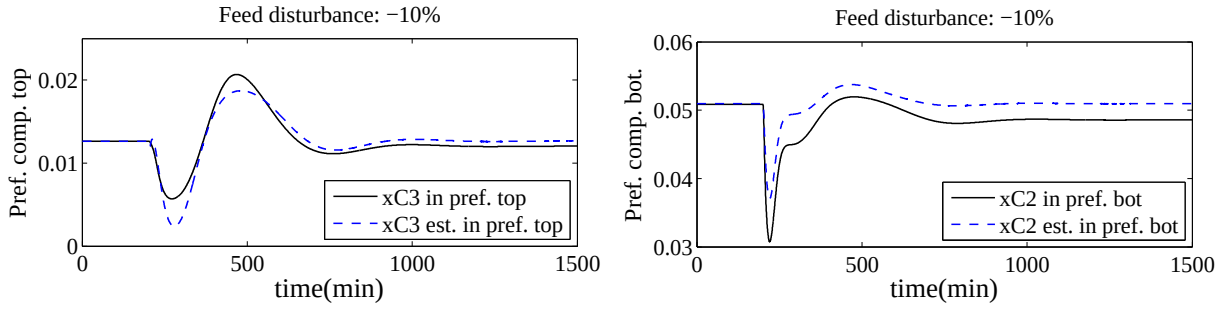

(a) Change in feed flow rate

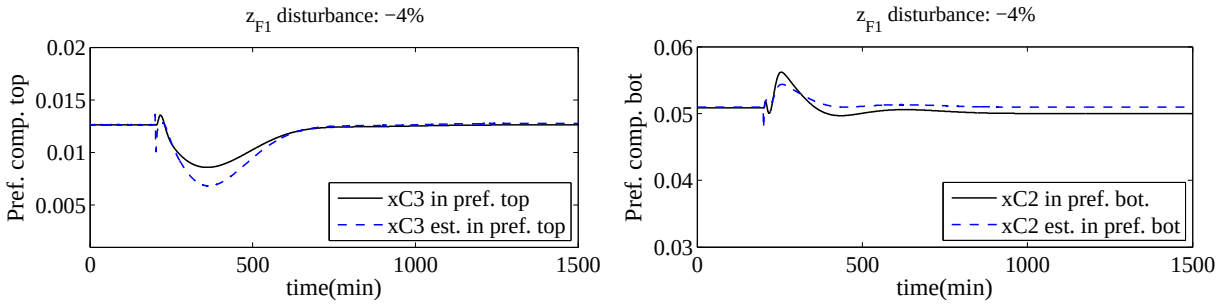

(b) Change in z_{F1}

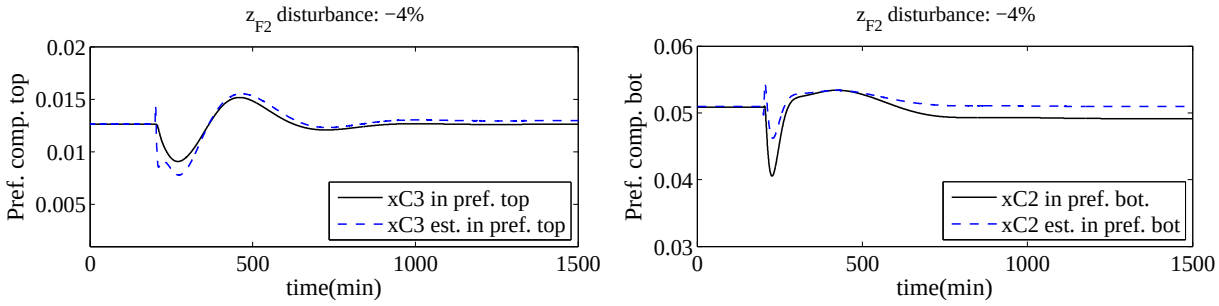

(c) Change in z_{F2}

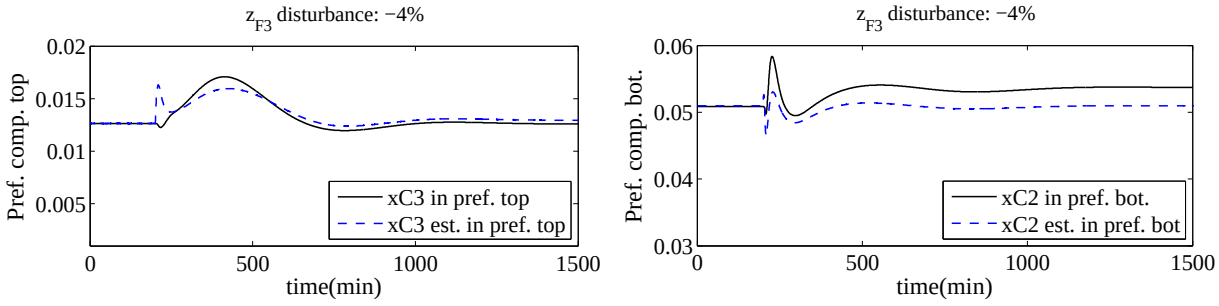

(d) Change in z_{F3}

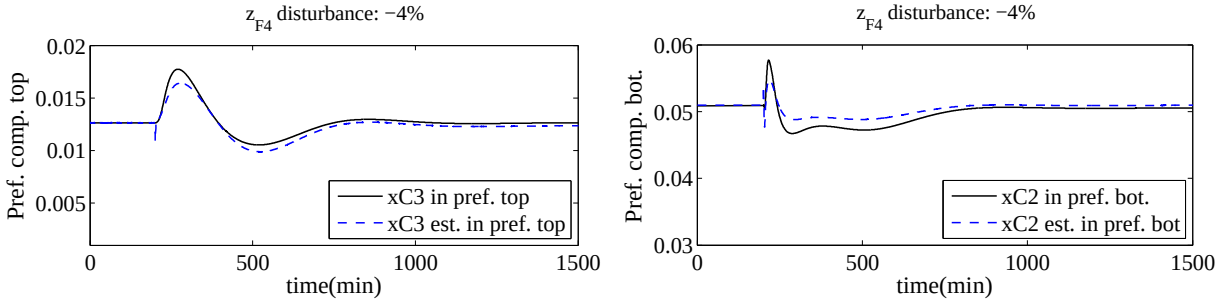

(e) Change in z_{F4}

Figure 10.16: Responses of controlled estimated compositions of prefractionator ends

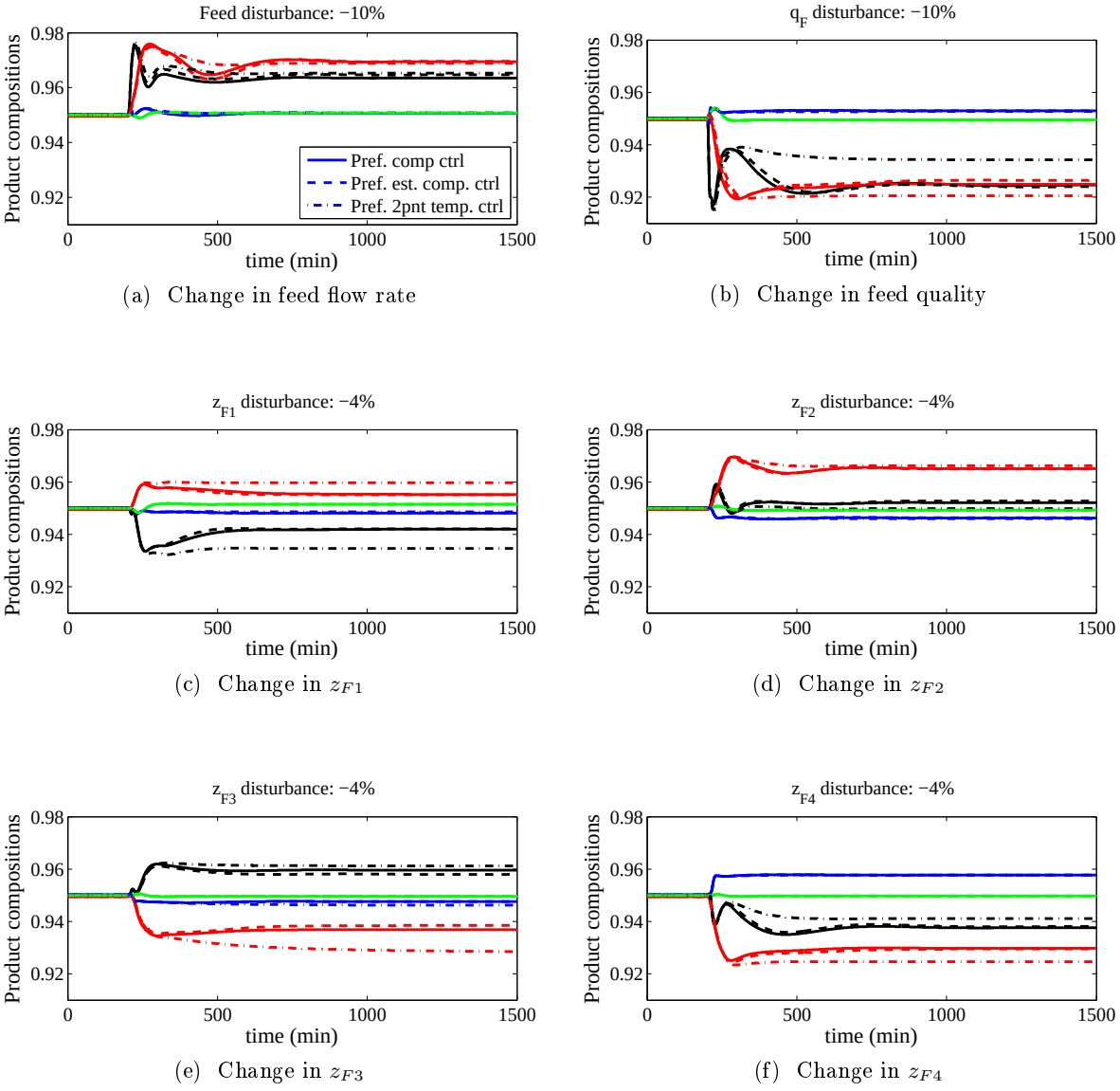

(a) Change in feed flow rate

(b) Change in feed quality

(c) Change in z_{F1}

(d) Change in z_{F2}

(e) Change in z_{F3}

(f) Change in z_{F4}

Figure 10.17: Comparison of product compositions for three control structures: Two temperature loops in prefractionator, compositions of impurities at prefractionator ends are controlled, estimated compositions of impurities at prefractionator ends are controlled

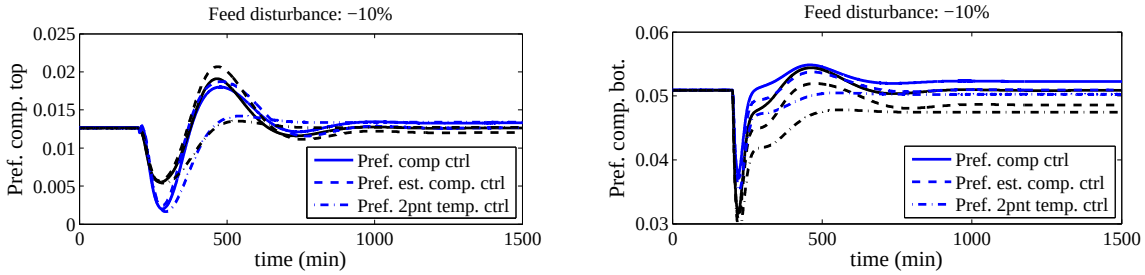

(a) Change in feed flow rate

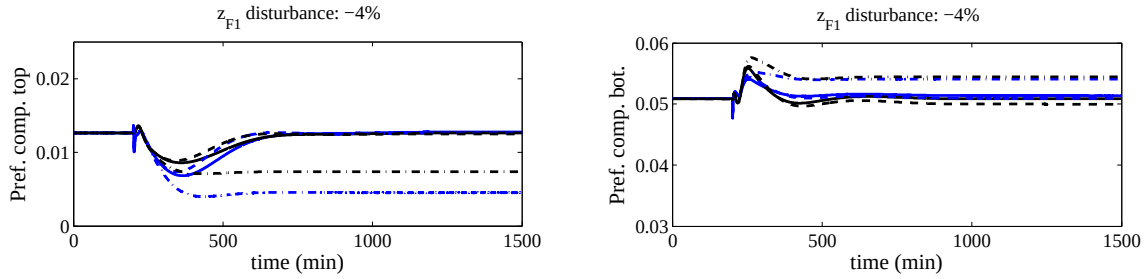

(b) Change in z_{F1}

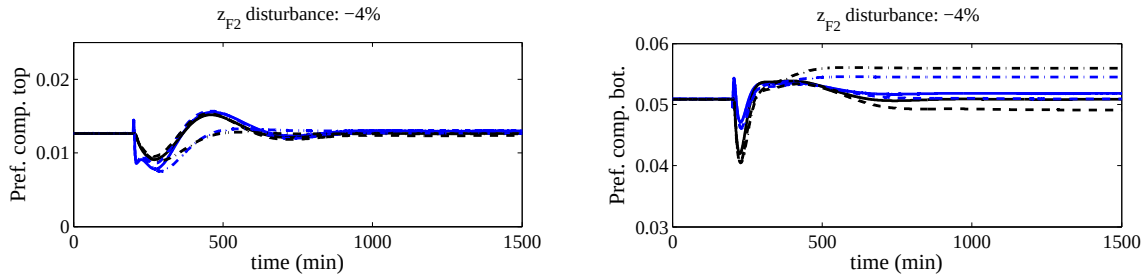

(c) Change in z_{F2}

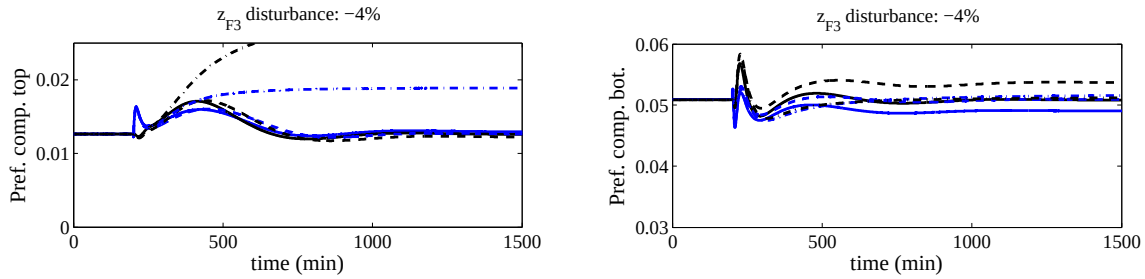

(d) Change in z_{F3}

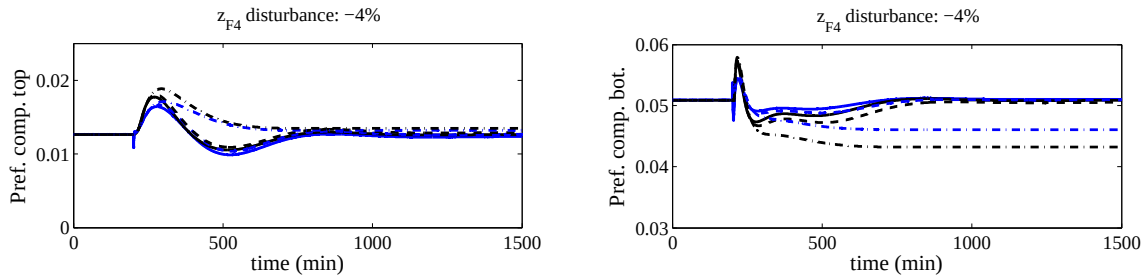

(e) Change in z_{F4}

Figure 10.18: Comparison of prefractionator end compositions and their estimated values for three control structures: Two temperature loops in prefractionator, compositions of impurities at prefractionator ends are controlled, estimated compositions of impurities at prefractionator ends are controlled; blue: true value, black: estimated value

Chapter 11

Dynamic compensation of static estimators

In this chapter, we study different possibilities to overcome the inverse response problem which is caused by combining different measurements with fast and slow dynamics to form the static estimator which was developed in Chapter 9. Our goal is to obtain a response with "No inherent limitation".

11.1 Introduction

Reliable and accurate measurement of product compositions is one of the important issues in distillation column control. Commonly, simple linear relationships, $\hat{y} = \mathbf{H}x$, are used to estimate composition (y) based on temperature measurements (x). Ghadrdan et al. [178] have presented the optimal estimators for different control applications. They are optimal in the sense that they give minimum error for the estimation of primary variables at steady-state in the presence of disturbance and noise.

Using a combination of measurements leads to a better steady-state estimate compared to single measurements. However, dynamically it may give rise to right-half plane zeros (inverse response behaviour) in the transfer function from input u to the estimate $\hat{y}$ ($\mathbf{G} = \mathbf{H}\mathbf{G}_x$), which limit the closed-loop performance for SISO systems. We have $\hat{y} = \mathbf{H}x = \mathbf{H}\mathbf{G}_x u$ (see Figure 11.1). The appearance of a RHP zero in the square transfer function $\mathbf{H}\mathbf{G}_x(s)$ from u to $\hat{y}$ is common when the measurements ($\mathbf{G}_x(s)$) have different dynamics, i.e. fast or slow, as they are located at different sections in the plant. This is noted by [181] with a simple example with two measurements and one input.

$$\hat{y}(s) = \mathbf{H}\mathbf{G}_x(s)u(s) = h_1 g_1(s)u(s) + h_2 g_2(s)u(s) \tag{11.1}$$

It is assumed that $\mathbf{G}_x$ is modeled as a rational transfer function on the form $g_i(s) = \frac{n_{g_i}(s)}{d_{g_i}(s)}$, thus the resulting plant is:

$$\begin{aligned}
\hat{y}(s) &= \left(h_1 g_1(s) + h_2 g_2(s)\right) u(s) \\
&= \left(h_1 \frac{n_{g_1}(s)}{d_{g_1}(s)} + h_2 \frac{n_{g_2}(s)}{d_{g_2}(s)}\right) u(s) \\
&= \left(\frac{h_1 n_{g_1}(s) d_{g_2}(s) + h_2 n_{g_2}(s) d_{g_1}(s)}{d_{g_1}(s) d_{g_2}(s)}\right) u(s)
\end{aligned}$$

The poles of the resulting plant are identical to the poles of the two subsystems, while the zeros are changed. For systems where $h_1 g_1$ and $h_2 g_2$ have opposing effects, this may lead to right-hand plane zeros.

We have studied three approaches to overcome this problem:

- Cascade Control:
  The idea is to close a fast inner loop based on a single measurement with no RHP-zero and adjust the setpoint on a time scale which is slower than the RHP-zero.
- Use of measurements from the same section of the process:
  If the dynamic behaviour of the selected measurements are similar, then it is less likely to get RHP-zero. However, this gives a larger steady-state error.
- Filters:
  Low-pass filters will keep the system optimal at steady state. The idea is to filter the measurements before they are combined to give the estimate. The filtered measurements are $\hat{y} = \mathbf{H}\mathbf{H}_F u$

11.2 Motivating example

We first illustrate the ideas with a simple example. Afterwards, we will give some guidelines for the case study of a distillation column.

Consider a system with two measurements x and one input u

$$\mathbf{G}_x = \begin{bmatrix} g_1 \\ g_2 \end{bmatrix} = \begin{bmatrix} \frac{1}{3s+1} \\ \frac{1}{s+1} \end{bmatrix}$$

Assume the estimator matrix $\mathbf{H}$ is

$$\mathbf{H} = \begin{bmatrix} 2 & -1 \end{bmatrix}$$

11.2.1 No dynamic compensation

The transfer function from u to $\hat{y}$ is

$$\mathbf{G} = \mathbf{H}\mathbf{G}_x = \frac{2}{3s+1} - \frac{1}{s+1} = \frac{1-s}{(3s+1)(s+1)}$$

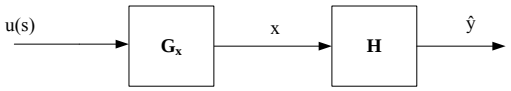

Figure 11.1: Block diagram of the estimation

The RHP zero in $\mathbf{G}(s)$ will limit the achievable closed-loop performance. Thus, we have introduced an unnecessary limitation on performance.

11.3 Cascade control

Now we consider if we can avoid the effect of the RHP zero using cascade control. We assume that we control the faster measurement x_2 ($\frac{1}{s+1}$) in an internal loop. The desired closed-loop time constant is assumed to be $\tau_c = 0.1$ (time units).

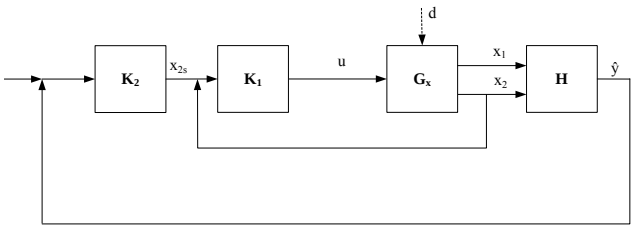

Figure 11.2: Block diagram of the estimation with a cascade loop

Using the SIMC [1] PI-tuning rules [180] with $\theta = 0$, we have

$$K_c = \frac{1}{k}\frac{\tau_1}{\tau_c + \theta} = 10$$

$$\tau_I = \min(\tau_1, 4(\tau_c + \theta)) = 0.4$$

The resulting controller and loop transfer functions become

$$K_1(s) = \frac{K_c}{\tau_I s}(\tau_I s + 1) = \frac{10}{0.4s}(0.4s + 1)$$

$$L_1(s) = K_1(s).g_2(s) = \frac{25(0.4s + 1)}{s(s + 1)}$$

and

$$\mathrm{x}_2 = \frac{L_1}{L_1 + 1}\mathrm{x}_{2s} = \frac{0.4s + 1}{(0.1283s + 1)(0.3117s + 1)}\mathrm{x}_{2s}$$

and with

$$\mathrm{u} = g_2^{-1}\mathrm{x}_2$$

we can find x_1 and then

$$\hat{\mathrm{y}} = \mathbf{H}\mathrm{x} = \frac{(0.4s + 1)(-s + 1)}{(0.1283s + 1)(0.3117s + 1)(3s + 1)}\mathrm{x}_{2s}$$

We see that the RHP zero still remains. This is explained from the following theorem.

Theorem 1. *Cascade (inner-loop) control can not move the zero of* $\mathbf{HG}_x$

Proof. The expression for the estimated primary variable is

$$\hat{\mathrm{y}} = h_1\mathrm{x}_1 + h_2\mathrm{x}_2$$

where

$$\mathrm{x}_1 = g_1\mathrm{u}$$

$$\mathrm{x}_2 = g_2\mathrm{u}$$

Assume we control x_2 in an inner cascade loop.

$$\mathrm{u} = K(s)(\mathrm{x}_{1s} - \mathrm{x}_1)$$

So,

$$\mathrm{x}_2 = \frac{K(s)g_2}{1 + K(s)g_2}\mathrm{x}_{2s}$$

$$\mathrm{x}_1 = \frac{g_1}{g_2}\mathrm{x}_2$$

The transfer function from x_{2s} to $\hat{\mathrm{y}}$ is

$$\hat{\mathrm{y}} = (h_1\frac{g_1}{g_2} + h_2)\frac{Kg_2}{1 + Kg_2}\mathrm{x}_{2s} \tag{11.2}$$

The term $(h_1g_1 + h_2g_2)$, which includes the RHP zero, is unchanged. □

[1] Skogestad's IMC

11.4 Selection of a subset of measurements

To improve the dynamic controllability, one idea is to put structural constraints on the measurements. This is done to reduce the time delay between the MVs to CVs, and also to have measurements of the same dynamics to avoid inverse response. Yelchuru et al. [148] have studied the optimal solution for measurement combinations with structural constraints. In our simple example, it means that we need to choose only the measurements which are closer to the corresponding MV. In this way, better controllability is achieved at the expense of less accurate estimation.

11.5 Filtering

Here we use individual compensators (or filters) on the measurements as illustrated by the block $\mathbf{H}_F$ in Figure 11.3 The diagonal matrix $\mathbf{H}_F$ is applied on the measurements to improve the dynamic behavior. It is required that $\mathbf{H}_F(0) = \mathbf{I}$. This means that the steady-state gain should not change, because it is already optimal. Each of the filters are simple first-order low-pass or lead-lag, e.g.

$$\mathbf{H}_F = \begin{bmatrix} \frac{1}{\tau_{F1}s+1} & 0 \\ 0 & \frac{1}{\tau_{F1}s+1} \end{bmatrix}$$

or

$$\mathbf{H}_F = \begin{bmatrix} \frac{\tau_{F1n}s+1}{\tau_{F1d}s+1} & 0 \\ 0 & \frac{\tau_{F2n}s+1}{\tau_{F2d}s+1} \end{bmatrix}$$

Different filters are used for the case-study in Table 11.1. Figure 11.4 shows the step responses of different filters introduced. We can make the transfer function from x to $\hat{y}$ as fast as we want.

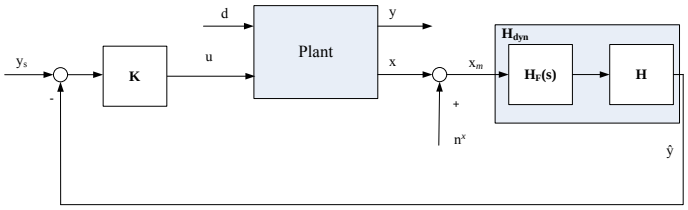

Figure 11.3: Block diagram of the estimation system including filter ($\mathbf{H}$)

Table 11.1: Different filters and the final transfer functions

Filter matrix	Transfer function from u to $\hat{y}$
$\mathbf{H}_{F1} = \begin{bmatrix} \frac{1}{s+1} & 0 \\ 0 & \frac{1}{3s+1} \end{bmatrix}$	$\mathbf{G}_1 = \mathbf{H}\mathbf{H}_{F1}\mathbf{G}_x = \frac{1}{(3s+1)(s+1)}$
$\mathbf{H}_{F2} = \begin{bmatrix} 1 & 0 \\ 0 & \frac{1}{3s+1} \end{bmatrix}$	$\mathbf{G}_2 = \mathbf{H}\mathbf{H}_{F2}\mathbf{G}_x = \frac{2s+1}{(3s+1)(s+1)}$
$\mathbf{H}_{F3} = \begin{bmatrix} 1 & 0 \\ 0 & \frac{s+1}{3s+1} \end{bmatrix}$	$\mathbf{G}_3 = \mathbf{H}\mathbf{H}_{F3}\mathbf{G}_x = \frac{1}{3s+1}$
$\mathbf{H}_{F4} = \begin{bmatrix} \frac{3s+1}{s+1} & 0 \\ 0 & 1 \end{bmatrix}$	$\mathbf{G}_4 = \mathbf{H}\mathbf{H}_{F4}\mathbf{G}_x = \frac{1}{s+1}$

From this example, it is seen that the lead-lag filters are performing better in making the response faster than the low-pass filters. One can optimize the filter parameters to get the best performance. In this particular example, it is not clear what the best performance means. The transfer function from x to $\hat{y}$ is at most second order and does not have any limitations on control performance.

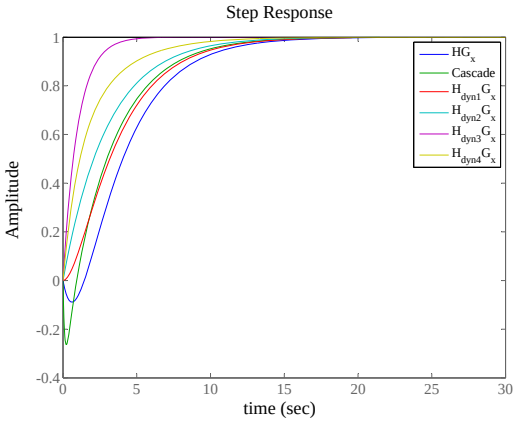

Figure 11.4: Step response of the transfer function from input to the primary variable and all alternatives

11.5.1 Distillation Case-study

We have designed a steady-state estimator **H** for a multi-component distillation column based on data from the simulator in HYSYS. Figure 11.5 shows the value of **H** from each tray in the column for the two estimated values.

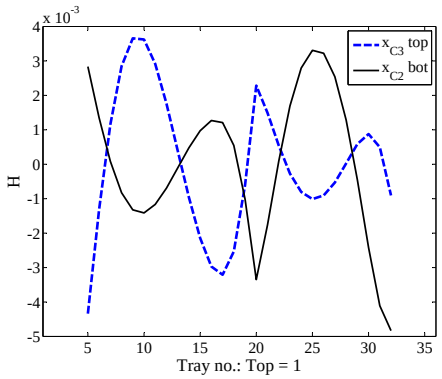

Figure 11.5: Steady-state contribution of temperatures to the estimates (**H**), Dashed: top composition estimate, Solid: bottom composition estimate

Figure 11.6 show the open-loop response of the primary variables and the estimated values to a change in boilup rate. An inverse response is seen in the estimate of the top composition. To check why this is happening, the contribution of the temperatures to the final estimate is studied. Figures 11.7-11.8 show the temperature changes as boilup rate is perturbed, and the contribution of each of the trays to the estimate of the top composition. Figure 11.8 is actually obtained by multiplying **H** to each of the time-series vectors of the measurements. The perturbation is small enough so that the results in the negative and positive directions are similar.

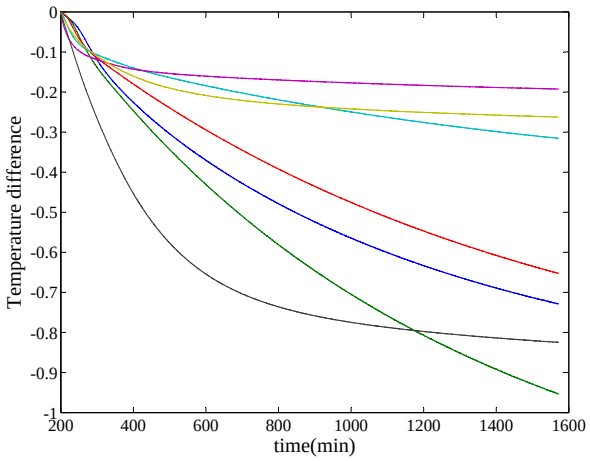

Figure 11.7: Temperature changes in the column with -1% change in boilup and constant Reflux ratio

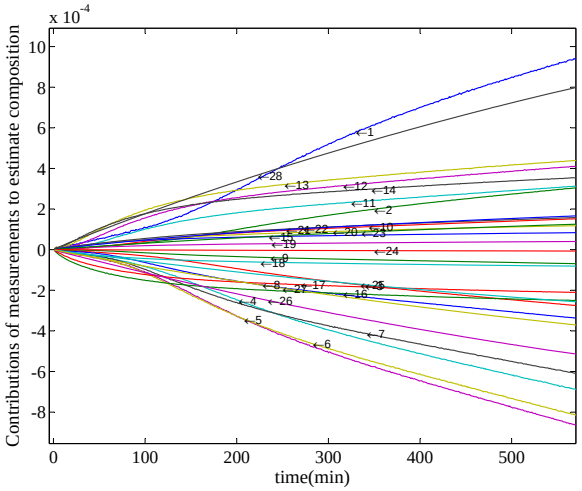

Figure 11.8: Contributions to the top composition estimate with -1% change in boilup and constant Reflux ratio

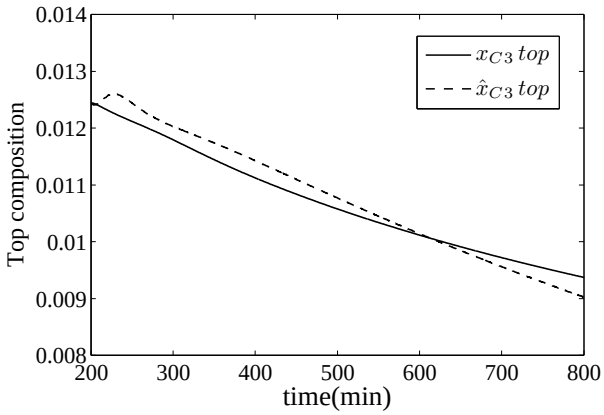

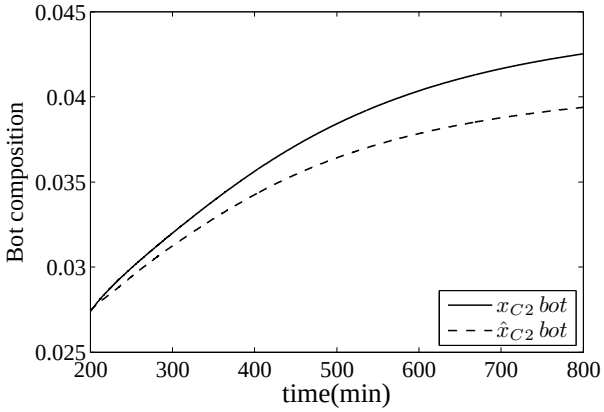

Figure 11.6: Top and bottom estimates with -1% change in boilup

As a simple trial, by adding first-order filters on the 6th, 16th and 17th stages which show fast dynamics (see the first 100 minutes in Figure 11.8) when boilup flow is perturbed, we see in Figure 11.9 that the inverse response is removed.

11.6 Optimization of the filters

The filter time constants can be optimized to give the best performance. The objective function can be defined as

$$\min_{\mathbf{H_F}} \|\mathbf{G}_{ref} - \mathbf{H}_F \mathbf{H} \mathbf{G}_x\|_\infty \tag{11.3}$$

where $\mathbf{G}_{ref}$ is the desired transfer function from input to the estimate. For monitoring purpose, the best performance means the closest response to the actual compositions. So, in this case $\mathbf{G}_{ref}$ would be the transfer function from the inputs to the real primary variables. Figure 11.10 shows the optimized filtered top estimate together with the real primary value and the unfiltered estimate which is obtained from the steady-state calculations. We have focused on the first 100 min, since we don't want to let the steady-state offset value be part of the objective function value. As it is

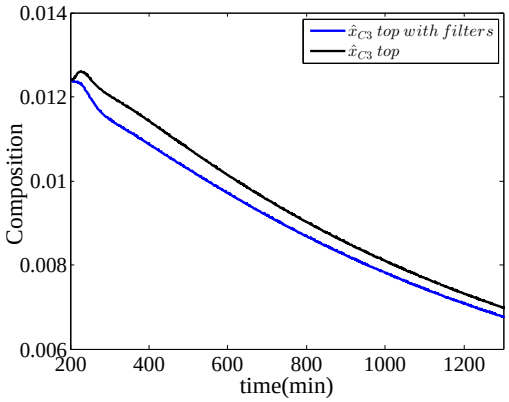

Figure 11.9: Estimated composition in the top and the filtered estimate. Filters are on 6th, 16th and 17th measurements

seen in Figure 11.10, the filtered estimate matches perfectly the real primary variable value in the first 100 minutes and it diverges to get to the steady state value of the unfiltered estimate (note that these are LP filters with no change in steady-state). Table 11.2 shows the values of the filter time constants for this optimization.

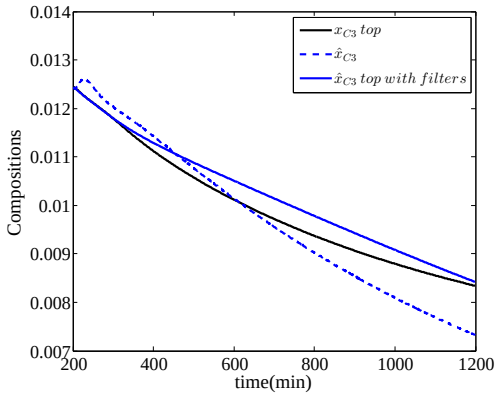

Figure 11.10: Estimated composition with optimized filters

11.6.1 Explicit solution for the optimization problem

In this section, we want to solve the optimization problem as a model-matching problem. The problem is to compute an upper bound γ and then compute a filter $\mathbf{Q}$ such that

$$\|\mathbf{T}_1 - \mathbf{T}_2\mathbf{Q}\mathbf{T}_3\|_\infty \leq \gamma$$

Here, we have $\mathbf{T}_3 = \mathbf{I}$. An optimal $\mathbf{Q}$ exists if the ranks of the two matrices $\mathbf{T}_2(j\omega)$ and $\mathbf{T}_3(j\omega)$ are constant for all $0 < \omega < \infty$ [182]. The reason to use this method is shown by the motivating example. We saw that we can not be sure about the structure of the filters, i.e. being lead-lag or LP, etc.

In the following section, the optimal filters derived for scalar and matrix-valued cases are presented from [182, 183].

Table 11.2: The time constants of the filters from optimization

Tray no.	H for top comp.	τ_F
5	-0.0043	1039.8
6	-0.0013	1338.3
7	0.0012	33.6
8	0.0028	514.1
9	0.0037	1209.1
10	0.0036	55.0
11	0.0029	1211.4
12	0.0018	1589.6
13	0.0004	554.6
14	-0.0010	1976.2
15	-0.0021	909.4
16	-0.0030	1424.3
17	-0.0032	466.6
18	-0.0025	1640.2
19	-0.0006	278.2
20	0.0023	19.8
21	0.0015	8.3
22	0.0005	1577.0
23	-0.0003	484.9
24	-0.0008	1158.8
25	-0.0010	1026.5
26	-0.0009	925.0
27	-0.0005	860.4
28	0.0000	1992.7
29	0.0006	868.7
30	0.0009	1404.7
31	0.0005	831.4
32	-0.0009	477.4

11.6.2 Nehari problem

For a model-matching problem, performing an inner-outer factorization of $\mathbf{T}_2$, we have,

$$\begin{aligned}\|\mathbf{T}_1 - \mathbf{T}_2\mathbf{Q}\|_\infty &= \|\mathbf{T}_1 - \mathbf{T}_{2i}\mathbf{T}_{2o}\mathbf{Q}\|_\infty \\ &= \|\mathbf{T}_{2i}\left(\mathbf{T}_{2i}^{-1}\mathbf{T}_1 - \mathbf{T}_{2o}\mathbf{Q}\right)\|_\infty \\ &= \|\left(\mathbf{T}_{2i}^{-1}\mathbf{T}_1 - \mathbf{T}_{2o}\mathbf{Q}\right)\|_\infty \\ &= \|\mathbf{R} - \mathbf{X}\|_\infty\end{aligned}$$

where $\mathbf{R} := \mathbf{T}_{2i}^{-1}\mathbf{T}_1$ and $\mathbf{X} := \mathbf{T}_{2o}\mathbf{Q}$

The third equality comes from the property of inner functions, $|\mathbf{T}_{2i}(j\omega)| = 1$. Nehari theorem is to find the distance between the function $\mathbf{R} \in \mathrm{RL}_\infty$ from $\mathbf{X} \in \mathrm{RH}_\infty$ [2]

$$\|\mathbf{R} - \mathbf{X}\|_\infty = \|\Gamma_{\mathbf{R}}\| \tag{11.4}$$

where $\Gamma_{\mathbf{R}}$ is the hankel operator with symbol $\mathbf{R}$. The model-matching problem can be solved by finding $\|\Gamma_{\mathbf{R}}\|$.

Calculations of the Hankel operator

Here, we study the Hankel operator with the special symbol

$$\mathbf{F}(s) = [\mathbf{A}, \mathbf{B}, \mathbf{C}, 0]$$

where $\mathbf{A}$ is antistable (all eigenvalues in Re $s > 0$). Such $\mathbf{F}$ belongs to RL_∞. The inverse bilateral Laplace transform of $\mathbf{F}(s)$ is

$$\begin{aligned}f(t) &= -\mathbf{C}e^{\mathbf{A}t}\mathbf{B}, \qquad t < 0 \\ f(t) &= 0, \qquad\qquad t \geq 0\end{aligned} \tag{11.5}$$

The time domain analog of Hankel operator (Γ_f) maps a function u in $\mathrm{L}_2[0,\infty)$ [3] to the function y in $\mathrm{L}_2(-\infty, 0]$

$$\begin{aligned}\mathrm{y}(t) &= \int_0^\infty f(t-\tau)u(\tau)d\tau, \qquad t < 0 \\ &= -\mathbf{C}e^{At}\int_0^\infty e^{-\mathbf{A}\tau}\mathbf{B}\mathrm{u}(\tau)d\tau, \qquad t < 0\end{aligned} \tag{11.6}$$

Controllability and observability operators are defined as

$$\begin{aligned}&\Psi_c : \mathrm{L}_2[0,\infty) \to \mathbf{C}^n \\ &\Psi_c\mathrm{u} = -\int_0^\infty e^{-\mathbf{A}\tau}\mathbf{B}\mathrm{u}(\tau)d\tau\end{aligned} \tag{11.7}$$

$$\begin{aligned}&\Psi_o : \mathbf{C}^n \to \mathrm{L}_2(-\infty, 0] \\ &(\Psi_o x)(t) = \mathbf{C}e^{\mathbf{A}t}\mathrm{x}, \quad t < 0\end{aligned} \tag{11.8}$$

From equation 11.6, we have

$$\Gamma_f = \Psi_o\Psi_c \tag{11.9}$$

The next theorem is about calculating $\|\Gamma_F\|$. Before that, a concept of the adjoint of an operator in Hilbert space is defined: The adjoint of an operator $\Phi : X \to Y$ is $\Phi^* : Y \to X$ satisfying

$$\langle \Phi\mathrm{x}, \mathrm{y}\rangle = \langle \mathrm{x}, \Phi^*\mathrm{y}\rangle, \ \mathrm{x} \in X, \ \mathrm{y} \in Y$$

[2] RH_∞ consists of those real-rational matrices which are stable and proper, and RL_∞ consists of those real-rational matrices which are proper with no poles on imaginary axis

[3] RL_2 consists of those real-rational vectors which are strictly proper with no poles on imaginary axis, and RH_2 consists of those real-rational vectors which are strictly proper and stable

The operator $\Phi^*\Phi$ from X to X is self-adjoint, i.e. it equals its adjoint. So,

$$\|\Phi\|^2 = \|\Phi^*\Phi\| \tag{11.10}$$

where * denotes complex-conjugate transpose.
A complex number λ is defined as an eigenvector of Φ if there is a nonzero x in $\mathbf{X}$ satisfying

$$\Phi \mathrm{x} = \lambda \mathrm{x}$$

Theorem 2. *[182] The eigenvalues of $\Gamma_F^*\Gamma_F$ are real and nonnegative and the largest of them equals $\|\Gamma_F^*\Gamma_F\|$*

Proof. This theorem together with equation 11.10 says that

$$\|\Gamma_F\| = \lambda_{max}(\Gamma_F^*\Gamma_F)^{\frac{1}{2}}$$

By defining the controllability and observability gramians

$$\mathbf{L}_c = \int_0^\infty e^{-\mathbf{A}t}\mathbf{B}\mathbf{B}^T e^{-\mathbf{A}^T t}dt \tag{11.11}$$

$$\mathbf{L}_o = \int_0^\infty e^{-\mathbf{A}^T t}\mathbf{C}^T\mathbf{C} e^{-\mathbf{A}t}dt \tag{11.12}$$

It's easy to show that $\mathbf{L}_c$ and $\mathbf{L}_o$ are the unique solutions of the Lyapunov equations

$$\mathbf{A}\mathbf{L}_c + \mathbf{L}_c\mathbf{A}^T = \mathbf{B}\mathbf{B}^T \tag{11.13}$$

$$\mathbf{A}^T\mathbf{L}_o + \mathbf{L}_o\mathbf{A} = \mathbf{C}^T\mathbf{C} \tag{11.14}$$

Also, by showing that $\mathbf{L}_c$ and $\mathbf{L}_o$ are matrix representations of $\Psi_c\Psi_c^*$ and $\Psi_o^*\Psi_o$ respectively and they have the same nonzero eigenvalues, the theorem is proved. □

11.7 Scalar problem

In this section, the model-matching problem for the scalar case is described. The following lemma and theorem describe the approach to calculate the optimal filter. We start with factorizing $\mathbf{R}$ as

$$\mathbf{R} = \mathbf{R}_1 + \mathbf{R}_2$$

with $\mathbf{R}_1$ strictly proper and $\mathbf{R}_2$ in H_∞.

$$\mathbf{R}_1(s) = \left[\begin{array}{cccc} \mathbf{A} & \mathbf{B} & \mathbf{C} & 0 \end{array}\right] \tag{11.15}$$

defining the following functions

$$f(s) = \left[\begin{array}{cccc} \mathbf{A} & w & \mathbf{C} & 0 \end{array}\right]$$

$$g(s) = \left[\begin{array}{cccc} -\mathbf{A}^T & \lambda^{-1}\mathbf{L}_o w & \mathbf{B}^T & 0 \end{array}\right]$$

where λ^2 is the largest eigenvalue of $\mathbf{L}_c\mathbf{L}_o$ and w is the corresponding eigenvector.

Lemma 1. *[182] The functions f and g satisfy the equations*

$$\Gamma_{\mathbf{R}} g = \lambda f \tag{11.16}$$

$$\Gamma_{\mathbf{R}}^* f = \lambda g \tag{11.17}$$

Proof. For the first equation, start with equation 11.13. By adding and subtracting $s\mathbf{L}_c$ on the left-hand side and then pre-multiplying by $\mathbf{C}(s-\mathbf{A})^{-1}$ and post-multiplying by $(s+\mathbf{A}^T)^{-1}v$, we have

$$-\mathbf{C}\mathbf{L}_c(s+\mathbf{A}^T)^{-1}v+\mathbf{C}(s-\mathbf{A})^{-1}\mathbf{L}_c v=\mathbf{C}(s-\mathbf{A})^{-1}\mathbf{B}\mathbf{B}^T(s+\mathbf{A}^T)^{-1}v$$

The first function in the left hand side belongs to H_2 space. The second function equals λf. From equations 11.15 and 11.14, the right hand side is equal to $\mathbf{R}_1(s)g(s)$. By projecting both sides onto $\mathrm{H}_2^\perp$ we get

$$\lambda f=\Gamma_{\mathbf{R}_1}g$$

But $\Gamma_{\mathbf{R}_1}=\Gamma_{\mathbf{R}}$, so equation 11.16 holds. Proving the second equation is similar to the first one. □

Theorem 3. *[182] The infimal model-matching problem error equals* $\|\Gamma_{\mathbf{R}}\|$*, the unique optimal* $\mathbf{X}$ *equals* $\mathbf{R}-\alpha\frac{f}{g}$.

Proof. It is claimed that

$$(\mathbf{R}-\mathbf{X})g=\Gamma_{\mathbf{R}}g \tag{11.18}$$

To prove this, define $h:=(\mathbf{R}-\mathbf{X})g$ and look at the L_2-norm of $h-\Gamma_{\mathbf{R}}g$:

$$\begin{aligned}\|h-\Gamma_{\mathbf{R}}g\|_2^2&=\langle h-\Gamma_{\mathbf{R}}g,h-\Gamma_{\mathbf{R}}g\rangle\\&=\langle h,h\rangle+\langle\Gamma_{\mathbf{R}}g,\Gamma_{\mathbf{R}}g\rangle\\&\quad-\langle h,\Gamma_{\mathbf{R}}g\rangle-\langle\Gamma_{\mathbf{R}}g,h\rangle\end{aligned}$$

Being in $\mathrm{H}_2^\perp$, $\Gamma_{\mathbf{R}}g$ is orthogonal to the H_2-component of h. Thus,

$$\langle h,\Gamma_{\mathbf{R}}g\rangle=\langle\Pi_1 h,\Gamma_{\mathbf{R}}g\rangle$$

where Π_1 is the orthogonal projection from L_2 to $\mathrm{H}_2^\perp$, and

$$\begin{aligned}\Pi_1 h&=\Pi_1(R-\mathbf{X})g\\&=\Pi_1 Rg\\&=\Gamma_{\mathbf{R}}g\end{aligned}$$

□

The methodology is summarized as below:

Step 1 Factorize $\mathbf{R}$ as

$$\mathbf{R}=\mathbf{R}_1+\mathbf{R}_2$$

with $\mathbf{R}_1$ strictly proper and $\mathbf{R}_2$ in H_∞.

$$\mathbf{R}_1(s)=\left[\begin{array}{cccc}\mathbf{A}&\mathbf{B}&\mathbf{C}&0\end{array}\right]$$

with $\mathbf{A}$ anti-stable. The controllability and observability gramians are the unique solutions of equations 11.13 and 11.14.

Step 2 Define

$$\begin{aligned}f(s)&=\left[\begin{array}{cccc}\mathbf{A}&w&\mathbf{C}&0\end{array}\right]\\g(s)&=\left[\begin{array}{cccc}-\mathbf{A}^T&\lambda^{-1}\mathbf{L}_o w&\mathbf{B}^T&0\end{array}\right]\end{aligned}$$

where w is the eigenvector corresponding to the maximum eigenvalue λ^2 of $\mathbf{L}_c\mathbf{L}_o$. Note that $f\in\mathrm{RH}_2^\perp$ and $g\in\mathrm{RH}_2$.

Step 3 $\mathbf{X}=\mathbf{R}-\alpha\frac{f}{g}$

11.7.1 Uniqueness of the solution

Theorem 4. *[184] If* $\mathbf{M}$ *is a closed convex set in a Hilbert space* H *and* $h \in \mathrm{H}$ *then there exists a unique* $\mathrm{y} \in \mathbf{M}$ *such that*

$$d(h, \mathbf{M}) = \|h - \mathrm{y}\|$$

Proof. We choose a sequence (y_n) in M such that $\delta_n \to \delta$, where $\delta_n = \|\mathrm{x} - \mathrm{y}_n\|$ (by definition of infimum). We will show that (y_n) is a Cauchy sequence and then we can make some deductions. Using the parallelogram law,

$$\begin{aligned}\|\mathrm{y}_n - \mathrm{y}_m\|^2 &= \|(\mathrm{y}_n - \mathrm{x}) - (\mathrm{y}_m - \mathrm{x})\|^2 \\ &= 2\|\mathrm{y}_n - \mathrm{x}\|^2 + 2\|\mathrm{y}_m - \mathrm{x}\|^2 - \|(\mathrm{y}_n - \mathrm{x}) + (\mathrm{y}_m - \mathrm{x})\|^2 \\ &= 2\delta_n^2 + 2\delta_m^2 - 2^2\|\frac{1}{2}(\mathrm{y}_n + \mathrm{y}_m) - \mathrm{x}\|^2\end{aligned}$$

But $\frac{1}{2}(\mathrm{y}_n + \mathrm{y}_m) \in M$ so that $\|\frac{1}{2}(\mathrm{y}_n + \mathrm{y}_m) - \mathrm{x}\|^2 \geq \delta^2$. As n and m tends to infinity, we have $\|\mathrm{y}_n - \mathrm{y}_m\| \geq 0$, which implies that (y_n) is a Cauchy sequence. Now since M is complete, the sequence (y_n) will converge to a limit say $\mathrm{y}_0 \in M$ so that $\|\mathrm{x} - \mathrm{y}_0\| \geq \delta$. Also

$$\|\mathrm{x} - \mathrm{y}_0\| = \|(\mathrm{x} - \mathrm{y}_n) - (\mathrm{y}_n - \mathrm{y}_0)\| \leq \|\mathrm{x} - \mathrm{y}_n\| + \|\mathrm{y}_n - \mathrm{y}_0\| \qquad = \delta_n + \|\mathrm{y}_n - \mathrm{y}_0\|$$

As n tends to infinity, $\|\mathrm{y}_n - \mathrm{y}_0\|$ tends to zero and δ_n tends to δ. Hence $\|\mathrm{x} - \mathrm{y}_0\| \leq \delta$ and we conclude that $\|\mathrm{x} - \mathrm{y}_0\| = \delta$

For uniqueness, we assume that $\mathrm{y}_1 \in M$ and $\mathrm{y}_2 \in M$ both satisfy $\|\mathrm{x} - \mathrm{y}_1\| = \delta$ and $\|\mathrm{x} - \mathrm{y}_2\| = \delta$. We show that $\mathrm{y}_1 = \mathrm{y}_2$. By the parallelogram equality,

$$\begin{aligned}\|\mathrm{y}_1 - \mathrm{y}_2\|^2 &= \|(\mathrm{y}_1 - \mathrm{x}) - (\mathrm{y}_2 - \mathrm{x})\|^2 \\ &= 2\|\mathrm{y}_1 - \mathrm{x}\|^2 + 2\|\mathrm{y}_2 - \mathrm{x}\|^2 - \|(\mathrm{y}_1 - \mathrm{x}) + (\mathrm{y}_2 - \mathrm{x})\|^2 \\ &= 2\delta^2 + 2\delta^2 - 2^2\|\frac{1}{2}(\mathrm{y}_1 + \mathrm{y}_2) - \mathrm{x}\|^2\end{aligned}$$

But $\frac{1}{2}(\mathrm{y}_1 + \mathrm{y}_2) \in M$ so that $\|\frac{1}{2}(\mathrm{y}_1 + \mathrm{y}_2) - \mathrm{x}\|^2 \geq \delta^2$, which implies that

$$2\delta^2 + 2\delta^2 - 2^2\|\frac{1}{2}(\mathrm{y}_1 + \mathrm{y}_2) - \mathrm{x}\|^2 \leq 4\delta^2 - 4\delta^2$$

Hence

$$\|\mathrm{y}_1 - \mathrm{y}_2\| \leq 0$$

Clearly $\|\mathrm{y}_1 - \mathrm{y}_2\| \geq 0$, which means that $\mathrm{y}_1 = \mathrm{y}_2$ □

11.7.2 Example: Scalar problem

In this case, $\mathbf{T}$ matrices are defined as below:

$\mathbf{T}_1$: Desired transfer function ($\mathbf{G}_{ref}$)
$\mathbf{T}_2$: Current transfer function ($\mathbf{HG}_x$)
$\mathbf{Q}$: Filter transfer function ($\mathbf{H}_F$)

In our example, we have the following inputs:

$$\mathbf{T}_1 = \frac{1}{0.5s + 1}$$
$$\mathbf{T}_2 = \frac{-s + 1}{3s^2 + 4s + 1}$$

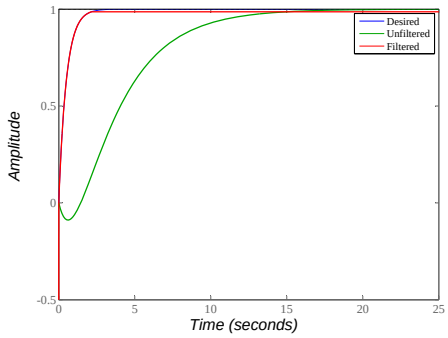

Figure 11.11: Step response of unfiltered and filtered estimates

Since the rank of $\mathbf{T}_2$ is not constant for all $0 \leq \omega \leq \infty$, a transfer function

$$\mathbf{V} = (s+1)^l$$

with l being the relative degree of $\mathbf{T}_2$, is multiplied by $\mathbf{T}_2$. So, we have

$$\gamma = \|\mathbf{T}_1 - \mathbf{T}_{p2}\mathbf{V}\mathbf{Q}\| \tag{11.19}$$

Since the steady-state values should not be affected by filtering, a weight function is multiplied to both $\mathbf{T}_1$ and $\mathbf{T}_2$. The weight function is defined as

$$\mathbf{W} = \frac{0.01\omega^{-1}s + 1}{0.1\omega^{-1}s + 1}$$

Figure 11.11 shows the desired, unfiltered and filtered responses. The resulting filter will be

$$\mathbf{Q} = \frac{19.82s^2 + 2042s + 678.5}{s^2 + 1002s + 2000} \tag{11.20}$$

11.8 Matrix-valued model matching problem

In this section, the model-matching problem for the matrix-valued case is described. In the case we have $\mathbf{R}$ as a vector/matrix, this method should be used.

Lemma 2. *Let* $\mathbf{U}$ *be an inner matrix and define*

$$\mathbf{E} = \begin{bmatrix} \mathbf{U}^{\sim} \\ \mathbf{I} - \mathbf{U}\mathbf{U}^{\sim} \end{bmatrix}$$

Then, $\|\mathbf{E}\mathbf{G}\|_\infty = \|\mathbf{G}\|_\infty$

Proof. It suffices to show that $\mathbf{E}^{\sim}\mathbf{E} = \mathbf{I}$ □

Lemma 3. *Suppose* $\mathbf{F}$ *and* $\mathbf{G}$ *are matrices with no poles on imaginary axis with equal number of columns. If*

$$\left\| \begin{bmatrix} \mathbf{F} \\ \mathbf{G} \end{bmatrix} \right\|_\infty < \gamma \tag{11.21}$$

then

$$\|\mathbf{G}\|_\infty < \gamma \tag{11.22}$$

and

$$\|\mathbf{F}\mathbf{G}_o^{-1}\|_\infty < 1 \tag{11.23}$$

Proof. Equation (11.22) follows immediately from (11.21), because

$$\|\mathbf{G}\|_\infty \le \| \begin{bmatrix} \mathbf{F} \\ \mathbf{G} \end{bmatrix} \|_\infty$$

$\gamma^2 - \mathbf{G}^\sim\mathbf{G}$ has a spectral factorization:

$$\gamma^2 - \mathbf{G}^\sim\mathbf{G} = \mathbf{G}_o^\sim\mathbf{G}_o \tag{11.24}$$

where $\mathbf{G}_o, \mathbf{G}_o^{-1} \in \mathrm{RH}_\infty$
Define

$$\epsilon := \gamma - \| \begin{bmatrix} \mathbf{F} \\ \mathbf{G} \end{bmatrix} \|_\infty \tag{11.25}$$

and

$$g := \mathbf{G}_o^{-1} f \tag{11.26}$$

where f is a $\mathbf{L}_2$-vector of unit norm. Starting from (11.25), we have

$$\begin{aligned} \| \begin{bmatrix} \mathbf{F} \\ \mathbf{G} \end{bmatrix} g\|_2 &\le (\gamma - \epsilon)\|g\|_2^2 \\ \langle \begin{bmatrix} \mathbf{F} \\ \mathbf{G} \end{bmatrix} g, \begin{bmatrix} \mathbf{F} \\ \mathbf{G} \end{bmatrix} g\rangle &\le (\gamma - \epsilon)^2\langle g, g\rangle \\ \langle g, \mathbf{F}^\sim\mathbf{F}g\rangle &\le \gamma^2\langle g, g\rangle - \epsilon(2\gamma - \epsilon)\|g\|_2^2 \\ \langle g, \mathbf{F}^\sim\mathbf{F}g\rangle &\le \langle g, (\gamma^2 - \mathbf{G}^\sim\mathbf{G})g\rangle - \epsilon(2\gamma - \epsilon)\|\mathbf{G}_o\|_\infty^{-2} \end{aligned}$$

The last step used the inequality

$$1 = \|\mathbf{G}_o g\| \le \|\mathbf{G}_o\|_\infty \|g\|_2$$

Now using (11.24) we get

$$\|\mathbf{F}g\|_2^2 \le \|\mathbf{G}_o g\|_2^2 - \epsilon(2\gamma - \epsilon)\,\|\mathbf{G}_o\|_\infty^{-2}$$

Hence,

$$\|\mathbf{F}\mathbf{G}_o^{-1} f\|_2^2 \le 1 - \epsilon(2\gamma - \epsilon)\,\|\mathbf{G}_o\|_\infty^{-2}$$

Since f was arbitrary, we find that

$$\|\mathbf{F}\mathbf{G}_o^{-1}\|_2^2 \le 1 - \epsilon(2\gamma - \epsilon)\,\|\mathbf{G}_o\|_\infty^{-2}$$

Since $\epsilon(2\gamma - \epsilon) > 0$, we arrive at equation11.23

□

Theorem 5. *[182]*

(i) $\alpha = \inf\{\gamma : \|\mathbf{Y}\|_\infty < \gamma, \mathrm{dist}\,(\mathbf{R}, \mathrm{RH}_\infty) < 1\}$

(ii) Suppose $\gamma > \alpha$, $\mathbf{G}, \mathbf{X} \in \mathrm{RH}_\infty$

$$\begin{aligned} \|\mathbf{R} - \mathbf{X}\|_\infty &\le 1 \\ \mathbf{X} &= \mathbf{T}_{2o}\mathbf{Q}\mathbf{Y}_o^{-1} \end{aligned} \tag{11.27}$$

Then $\|\mathbf{T}_1 - \mathbf{T}_2\mathbf{Q}\|_\infty \le \gamma$

Proof. (i) Let

$$\gamma_{inf} = \inf\{\gamma : \|\mathbf{Y}\|_\infty < \gamma, \mathrm{dist}\,(\mathbf{R}, \mathrm{RH}_\infty) < 1\}$$

choose $\epsilon > 0$ and then choose γ such that $\alpha + \epsilon > \gamma > \alpha$. Then there exist $\mathbf{Q}$ in RH_∞ such that

$$\|\mathbf{T}_1 - \mathbf{T}_2\mathbf{Q}\|_\infty < \gamma$$

From Lemma 2 we have:

$$\left\| \begin{bmatrix} \mathbf{T}_{2i}^{\sim} \\ \mathbf{I} - \mathbf{T}_{2i}\mathbf{T}_{2i}^{\sim} \end{bmatrix} (\mathbf{T}_1 - \mathbf{T}_2\mathbf{Q}) \right\|_\infty \leq \gamma \tag{11.28}$$

This is equivalent to

$$\left\| \begin{bmatrix} \mathbf{T}_{2i}^{\sim}\mathbf{T}_1 - \mathbf{T}_{2o}\mathbf{Q} \\ \mathbf{Y} \end{bmatrix} \right\|_\infty < \gamma \tag{11.29}$$

This implies from Lemma 3 that

$$\|\mathbf{Y}\|_\infty < \gamma \tag{11.30}$$

$$\|\mathbf{T}_{2i}^{\sim}\mathbf{T}_1\mathbf{Y}_o^{-1} - \mathbf{T}_{2o}\mathbf{Q}\mathbf{Y}_o^{-1}\|_\infty < 1 \tag{11.31}$$

The latter inequality implies

$$\operatorname{dist}\left(\mathbf{R}, \mathbf{T}_{2o}\mathrm{RH}_\infty\mathbf{Y}_o^{-1}\right) < 1 \tag{11.32}$$

$\mathbf{T}_{2o}$ is right-invertible in RH_∞ and $\mathbf{Y}_o$ is invertible in RH_∞. So, (11.33) gives

$$\operatorname{dist}(\mathbf{R}, \mathrm{RH}_\infty) < 1 \tag{11.33}$$

□

Lemma 4. *[182] For* $\mathbf{R}$ *in* RL_∞

$$\operatorname{dist}(\mathbf{R}, \mathrm{RH}_\infty) = \operatorname{dist}(\mathbf{R}, \mathrm{H}_\infty) = \|\Gamma_{\mathbf{R}}\|$$

Proof. We have

$$\operatorname{dist}(\mathbf{R}, \mathrm{RH}_\infty) \geq \operatorname{dist}(\mathbf{R}, \mathrm{H}_\infty) = \|\Gamma_{\mathbf{R}}\|$$

The latter is the Nehari's theorem. Choose $\epsilon > 0$ and set $\beta := \|\Gamma_{\mathbf{R}}\|$. Then

$$\begin{aligned} \operatorname{dist}\left[(\beta+\epsilon)^{-1}\mathbf{R}, \mathrm{H}_\infty\right] &= (\beta+\epsilon)^{-1}\|\Gamma_{\mathbf{R}}\| \\ &= \beta/(\beta+\epsilon) \\ &< 1 \end{aligned}$$

This inequality implies that there exists $\mathbf{X}$ in RH_∞ such that

$$\|(\beta+\epsilon)^{-1}\mathbf{R} - \mathbf{X}\|_\infty \leq 1$$

Thus,

$$\begin{aligned} \operatorname{dist}(\mathbf{R}, \mathrm{RH}_\infty) &\leq \beta + \epsilon \\ &= \operatorname{dist}(\mathbf{R}, \mathrm{H}_\infty) + \epsilon \end{aligned}$$

So,

$$\operatorname{dist}(\mathbf{R}, \mathrm{RH}_\infty) \leq \operatorname{dist}(\mathbf{R}, \mathrm{H}_\infty)$$

□

The general algorithm to obtain $\mathbf{Q}$ is as follows

Step 1 Compute $\mathbf{Y}$ and $\|\mathbf{Y}\|_\infty$

Step 2 Find an upper bound α_1 for α ($\|\mathbf{T}_1\|_\infty$ is the simplest choice)

Step 3 Select a trial value for γ in the interval ($\|\mathbf{Y}\|_\infty$,α_1]

Step 4 Compute $\mathbf{R}$ and $\|\Gamma_{\mathbf{R}}\|$. Then $\|\Gamma_{\mathbf{R}}\| < 1$ iff $\alpha < \gamma$. Change the value of γ correspondingly to meet this criteria

Step 5 Find a matrix $\mathbf{X}$ such that $\|\mathbf{R} - \mathbf{X}\|_\infty \leq 1$.

Step 6 Solve $\mathbf{X} = \mathbf{T}_{2o}\mathbf{Q}\mathbf{Y}_o^{-1}$ for $\mathbf{Q}$

Note that if the measurements do not have any delay or right half plane zeros, $\Gamma_{\mathbf{R}}$ will be zero.

11.9 Matrix-valued model matching problem with matrix-valued R

If $\mathbf{R}$ is matrix-valued, the algorithm will be as below. This is with the assumption of $\mathbf{R}$ being strictly proper (if not, we need to factorize it as $\mathbf{R} = \mathbf{R}_1 + \mathbf{R}_2$ where $\mathbf{R}_1$ is proper), and $\|\Gamma_{\mathbf{R}}\| < 1$ We start with some definitions.

Definition Let $\mathbf{X}$ and $\mathbf{Y}$ be two Hilbert spaces. Their *external direct sum* $\mathbf{X} \oplus \mathbf{Y}$ *consists of all such vectors as* x *ranges over* $\mathbf{X}$ *and* y *over* $\mathbf{Y}$. *Vector addition and scalar multiplication are defined component-wise, and the inner product is defined as*

$$\left\langle \begin{pmatrix} x_1 \\ y_1 \end{pmatrix} \begin{pmatrix} x_2 \\ y_2 \end{pmatrix} \right\rangle := \langle x_1, x_2 \rangle + \langle y_1, y_2 \rangle$$

Definition *Indefinite inner-product on* $\mathbf{X} \oplus \mathbf{Y}$ *is*

$$\left[\begin{pmatrix} x_1 \\ y_1 \end{pmatrix} \begin{pmatrix} x_2 \\ y_2 \end{pmatrix} \right] := \langle x_1, x_2 \rangle - \langle y_1, y_2 \rangle$$

This is indefinite because $[z, z]$ *can be negative, zero or positive. A more compact way of defining this is to introduce the operator* $\mathbf{J}$ *on* $\mathbf{X} \oplus \mathbf{Y}$

$$\mathbf{J} \begin{pmatrix} x \\ y \end{pmatrix} := \begin{pmatrix} x \\ -y \end{pmatrix}$$

The external direct sum $\mathbf{X} \oplus \mathbf{Y}$ together with indefinite inner-product is called a Krein space. Before going to the theorem, we need the following facts:

Lemma 5. *[182] Let* $\mathbf{S} \in \mathrm{RL}_\infty$. *Then* $\|\mathbf{S}\| \le 1$ *iff* $\mathbf{G}_S$ *is negative, and* $\mathbf{R} - \mathbf{S} \in \mathrm{RH}_\infty$ *iff* $\mathbf{G}_S \subset \mathbf{G}(\mathbf{H}_2 \oplus \mathbf{H}_2)$, *where* $\mathbf{G} = \begin{bmatrix} \mathbf{I} & \mathbf{R} \\ 0 & \mathbf{I} \end{bmatrix}$ *and* $\mathbf{G}_S = \begin{bmatrix} \mathbf{S} \\ \mathbf{I} \end{bmatrix} \mathbf{H}_2$

Proof. Suppose that $\|\mathbf{S}\|_\infty \le 1$. A vector in $\mathbf{G}_S$ has the form $\begin{pmatrix} \mathbf{S}f \\ f \end{pmatrix}$ for some f in $\mathbf{H}_2$. This vector is negative.

$$\begin{aligned} \left[\begin{pmatrix} \mathbf{S}f \\ f \end{pmatrix}, \begin{pmatrix} \mathbf{S}f \\ f \end{pmatrix} \right] &= \|\mathbf{S}f\|_2^2 - \|f\|_2^2 \\ &\le (\|\mathbf{S}\|_\infty^2 - 1)\|f\|_2^2 \\ &\le 0 \end{aligned}$$

Now suppose $\mathbf{R} - \mathbf{S} \in \mathrm{RH}_\infty$. So,

$$\begin{aligned} \mathbf{G}_S &= \begin{bmatrix} \mathbf{S} \\ \mathbf{I} \end{bmatrix} \mathbf{H}_2 \\ &= \begin{bmatrix} \mathbf{I} & \mathbf{R} \\ 0 & \mathbf{I} \end{bmatrix} \begin{bmatrix} \mathbf{S} - \mathbf{R} \\ \mathbf{I} \end{bmatrix} \mathbf{H}_2 \\ &\subset \begin{bmatrix} \mathbf{I} & \mathbf{R} \\ 0 & \mathbf{I} \end{bmatrix} (\mathbf{H}_2 \oplus \mathbf{H}_2) \end{aligned}$$

The converse is easy to prove. □

Definition A square matrix $\mathbf{M}$ in RL_∞ having the property $\mathbf{M}^\sim \mathbf{J} \mathbf{M} = \mathbf{J}$ [4] is said to be J-unitary, where $\mathbf{J} = \begin{bmatrix} \mathbf{I} & 0 \\ 0 & -\mathbf{I} \end{bmatrix}$

[4] $\mathbf{M}^\sim = \mathbf{M}(-s)^T$

Lemma 6. *[182] Let* $\mathbf{F} \in \mathrm{RL}_\infty$. *Then* $\mathbf{F}\mathrm{H}_2 \subset \mathrm{H}_2$ *iff* $\mathbf{F} \in \mathrm{RH}_\infty$. *If* $\mathbf{F}$ *is square and* $\mathbf{F}\mathrm{H}_2 = \mathrm{H}_2$, *then* $\mathbf{F}^{-1} \in \mathrm{RH}_\infty$

Lemma 7. *[182] Let* $\mathbf{X}$ *be a matrix in* RL_∞ *and* $\|\mathbf{X}\|_\infty \leq 1$. *Suppose* $\mathbf{M}$ *is a J-unitary matrix having the properties*

$$\mathbf{M}\mathbf{G}_X \subset \mathbf{L}_2 \oplus \mathbf{H}_2 \tag{11.34}$$
$$0 \oplus \mathbf{H}_2 \subset \mathbf{M}(\mathbf{L}_2 \oplus \mathbf{H}_2)$$

Then there exists $\mathbf{Y}$ *in* RL_∞ *such that* $\|\mathbf{Y}\|_\infty \leq 1$ *and* $\mathbf{G}_Y = \mathbf{M}\mathbf{G}_X$

Proof. see [182] □

Theorem 6. *[182] The set of all matrices* $\mathbf{S}$ *in* RL_∞ *such that* $\|\mathbf{S}\|_\infty \leq 1$ *and* $\mathbf{R} - \mathbf{S} \in \mathrm{RH}_\infty$ *is given by*

$$\mathbf{S} = \mathbf{X}_1\mathbf{X}_2^{-1}$$
$$\begin{bmatrix} \mathbf{X}_1 \\ \mathbf{X}_2 \end{bmatrix} = \mathbf{L}\begin{bmatrix} \mathbf{Y} \\ \mathbf{I} \end{bmatrix}$$
$$\mathbf{Y} \in \mathrm{RH}_\infty$$
$$\|\mathbf{Y}\|_\infty \leq 1$$

[5]

Proof. Suppose that $\mathbf{S} \in \mathrm{RL}_\infty$, $\|\mathbf{S}\|_\infty \leq 1$ and $\mathbf{R} - \mathbf{S} \in \mathrm{RH}_\infty$. From Lemma 5, $\mathbf{G}_S$ is negative and

$$\mathbf{G}_S \subset \mathbf{L}(\mathbf{H}_2 \oplus \mathbf{H}_2) \tag{11.35}$$

By defining $\mathbf{M} := \mathbf{L}^{-1}$, from equation 11.35, we will have

$$\mathbf{M}\mathbf{G}_S \subset (\mathbf{H}_2 \oplus \mathbf{H}_2)$$

So, equation 11.34 holds. Noting that $\mathbf{M}$ is J-unitary, invoke Lemma 7 to get the existence of $\mathbf{Y}$ in RL_∞ such that

$$\|\mathbf{Y}\|_\infty \leq 1, \qquad \mathbf{G}_Y = \mathbf{M}\mathbf{G}_S$$

Since $\mathbf{G}_Y \subset \mathbf{H}_2 \oplus \mathbf{H}_2$ from equation 11.34, we have by Lemma 6 that actually $\mathbf{Y} \in \mathrm{RH}_\infty$. Define

$$\begin{bmatrix} \mathbf{X}_1 \\ \mathbf{X}_2 \end{bmatrix} := \mathbf{L}\begin{bmatrix} \mathbf{Y} \\ \mathbf{I} \end{bmatrix}$$

so,

$$\begin{bmatrix} \mathbf{X}_1 \\ \mathbf{X}_2 \end{bmatrix}\mathbf{H}_2 := \mathbf{L}\mathbf{G}_Y \tag{11.36}$$
$$= \mathbf{G}_S \tag{11.37}$$
$$= \begin{bmatrix} \mathbf{S} \\ \mathbf{I} \end{bmatrix}\mathbf{H}_2 \tag{11.38}$$
$$\tag{11.39}$$

Pre-multiplying 11.9 by $\begin{bmatrix} 0 & \mathbf{I} \end{bmatrix}$, we will have $\mathbf{X}_2\mathbf{H}_2 = \mathbf{H}_2$. Thus $\mathbf{X}_2^{-1} \in \mathrm{RH}_\infty$ by Lemma 6. Pre-multiplying 11.9 by $\begin{bmatrix} \mathbf{I} & -\mathbf{S} \end{bmatrix}$, we will get $\mathbf{S} = \mathbf{X}_1\mathbf{X}_2^{-1}$. The inverse is not proved here. □

The formula is Theorem shows $\mathbf{S}$ as a linear fractional transformation of $\mathbf{Y}$. By partitioning $\mathbf{L}$ as

$$\mathbf{L} = \begin{bmatrix} \mathbf{L}_1 & \mathbf{L}_2 \\ \mathbf{L}_3 & \mathbf{L}_4 \end{bmatrix}$$

Then

$$\mathbf{S} = (\mathbf{L}_1\mathbf{Y} + \mathbf{L}_2)(\mathbf{L}_3\mathbf{Y} + \mathbf{L}_4)^{-1}$$

One possible candidate for $\mathbf{Y}$ is $\mathbf{Y} = 0$. The method to calculate the filter is summarized as below

[5] $\mathbf{L}$ is defined as $\mathbf{L} := \mathbf{G}\mathbf{G}_-^{-1}$ where $\mathbf{G}_-$ is the spectral factor.

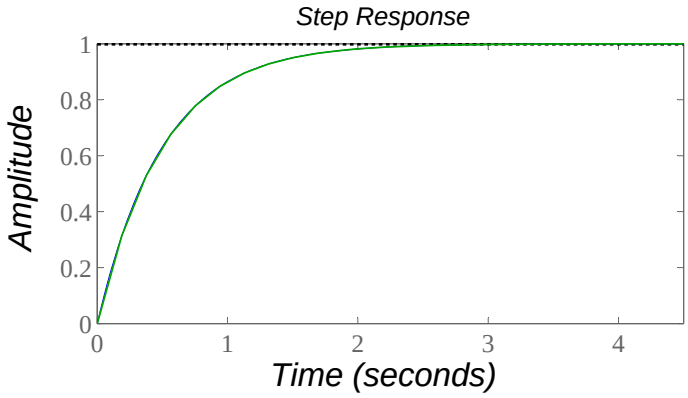

Figure 11.12: Comparison of filtered and desired responses for matrix-valued example

Step 1 Find a minimal realization of $\mathbf{R}$: $\mathbf{R}(s) = [\mathbf{A}, \mathbf{B}, \mathbf{C}, 0]$

Step 2 Solve the Lyapunov equations to find controllability and observability gramians and set $\mathbf{N} = (\mathbf{I} - \mathbf{L}_o\mathbf{L}_c)^{-1}$

Step 3 Set

$$\mathbf{L}_1(s) = \begin{bmatrix} \mathbf{A} & -\mathbf{L}_c\mathbf{N}\mathbf{C}^T & \mathbf{C} & \mathbf{I} \end{bmatrix}$$
$$\mathbf{L}_2(s) = \begin{bmatrix} \mathbf{A} & \mathbf{N}^T\mathbf{B} & \mathbf{C} & 0 \end{bmatrix}$$
$$\mathbf{L}_3(s) = \begin{bmatrix} -\mathbf{A}^T & \mathbf{N}\mathbf{C}^T & -\mathbf{B}^T & 0 \end{bmatrix}$$
$$\mathbf{L}_4(s) = \begin{bmatrix} -\mathbf{A}^T & \mathbf{N}\mathbf{L}_o\mathbf{B}^T & \mathbf{B}^T & \mathbf{I} \end{bmatrix}$$

Step 4 Select $\mathbf{Y}$ in RH_∞ with $\|\mathbf{Y}\|_\infty \leq 1$ (for example $\mathbf{Y} = 0$) and set $\mathbf{X} = \mathbf{R} - (\mathbf{L}_1\mathbf{Y} + \mathbf{L}_2)(\mathbf{L}_3\mathbf{Y} + \mathbf{L}_4)$

11.9.1 Example: Matrix valued problem

In this example, $\mathbf{T}$ matrices are defined as below:

$\mathbf{T}_1$: Desired transfer function ($\mathbf{G}_{ref}$)
$\mathbf{T}_2$: Not combined transfer function ($\mathbf{H}\mathbf{G}_x$)
$\mathbf{Q}$: Filter transfer function ($\mathbf{H}_F$)

In our example, we have the following inputs:

$$\mathbf{T}_1 = \frac{1}{0.5s + 1}$$
$$\mathbf{T}_2 = \begin{bmatrix} 2 & 0 \\ 0 & -1 \end{bmatrix} \begin{bmatrix} \frac{1}{3s+1} \\ \frac{1}{s+1} \end{bmatrix}$$

This means that we want to put filter on each of the measurements. The filter is calculated as below.

$$\mathbf{Q} = \begin{bmatrix} \frac{0.92308(s+2)^2(s+0.67)(s+0.3333)(s-0.9431)^2(s-1)}{(s+2)^3(s+0.67)(s+0.6202)(s-0.6202)(s-0.9431)^2} \\ \frac{-1.3846(s+2)^2(s+0.67)(s+0.3333)(s-0.3333)(s-0.9431)^2}{(s+2)^3(s+0.67)(s+0.6202)(s-0.6202)(s-0.9431)^2} \end{bmatrix}$$

To reduce the rank of the filters, we need to apply one of the model reduction methods on the obtained filter. The following figure shows the comparison of the desired and filtered combined measurements.

11.9.2 Distillation Example:

For the distillation case, $\mathbf{T}_1$ is the transfer function $\mathbf{G}_{ref}$ from input to the primary variables. $\mathbf{T}_2$ is the transfer function $\mathbf{G}_x$ from input to the measurements (a matrix of 28×1 matrix of transfer functions which are the temperature changes), if filters are applied to each of the measurements. It is also possible to apply filter on the estimated primary variable.In this case, $\mathbf{T} = \mathbf{H}\mathbf{G}_x$.

The inner-outer factorization of $\mathbf{T}_2$ matrix is possible if $\mathbf{D}$ in state-space representation be nonzero. This is possible if at least one of the transfer functions in $\mathbf{T}_2$ has the same degree in numerator and denominator. This is possible since some of the measurements include delay which can be interpreted as RHP zero ($e^{-\theta s} = 1 - \theta s$). The calculated $\mathbf{Q}_f$ for the scalar case, where the filter is applied on the estimated composition and the desired primary variable is calculated from 11.41, is as below

$$\mathbf{Q}_f = \frac{3.7e6s^3 + 3.8e5s^2 + 433.1s + 0.00657}{s^3 + 2.001s^2 + 1.003s + 0.00135} \tag{11.40}$$

and

$$\|\Gamma_{\mathbf{R}}\| = 0.0421$$

11.10 Discussion

Specifying $\mathbf{G}_{ref}$ for control purpose is not that easy. When the system is not only stabilizable but also controllable, one can make the closed-loop eigenvalues arbitrarily fast [185]. We need to know what is the fastest response we can get. One idea is to specify a first-order transfer function with the smallest time constant in the process as the desired transfer function from inputs to the estimates. From [186] we know that the internal time constants are smaller than the external time constants. These can be found from changing the two inputs boilup and reflux rate at the same time such that the external flows remain constant. This is very difficult to do in practice. The responses to internal flow changes, while the external flows are constant, are shown in Figure 11.13.

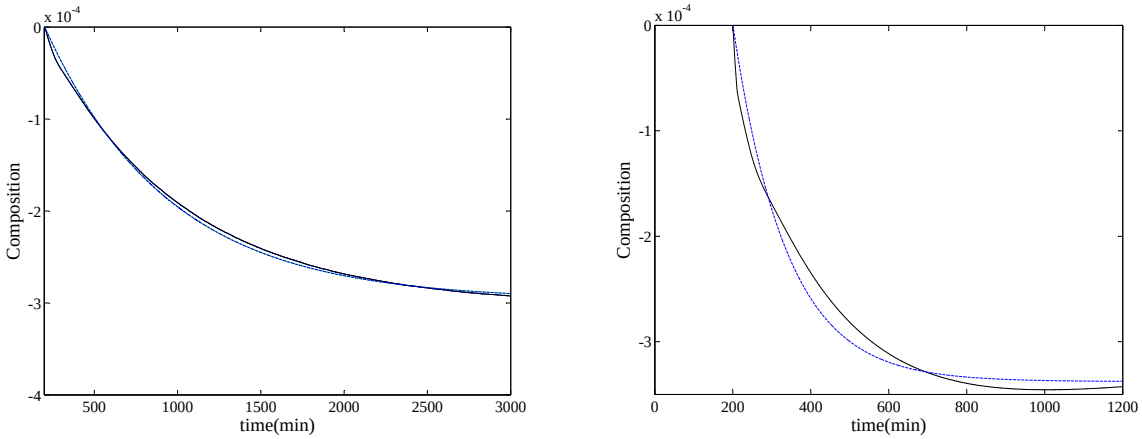

(a) Top composition, $\Delta L = \Delta V$, $\Delta D = \Delta B = 0$

(b) Bot. composition, $\Delta L = \Delta V$, $\Delta D = \Delta B = 0$

Figure 11.13: Internal time constants for our distillation example

The transfer functions of the compositions, when the internal flows are changed so that the external flows remain constant, are as below. For high purity distillation, the product compositions are sensitive to changes in external flows and the effect of internal flows may not be seen since the gain is small.

$$\Delta \mathrm{y}_D = (exp(-2s) \times \frac{-7.99e-5}{s + 0.00135})\Delta V \tag{11.41}$$

$$\Delta \mathrm{x}_B = (exp(-0.33s) \times \frac{-4.92e-4}{s + 0.0073})\Delta V \tag{11.42}$$

11.11 Conclusion

In this chapter, we have discussed different methods to overcome the band-width limitations caused by combining different measurements with different dynamics to build the static estimators. We have shown that adding filters is the best option. By using filters, we will correct the dynamic behavior while keeping the optimal steady-state estimator untouched. Two approaches were used. First, we suggested filtering some of the measurements based on the insight from the process. Then, we useed a more systematic way to construct a filter. The scalar case has been used for our distillation case-study.

Chapter 12

Concluding Remarks

12.1 Main Conclusions

This thesis reports results of the studies on control and operation of Kaibel distillation column. These arrangements are realized at industrial scale using a dividing-wall in a single columns shell. Compared the other alternatives which can be used for separating four products, Kaibel column is more energy and cost efficient. Two operational objectives are studied in this thesis.

1. maximizing the purities in the products with fixed boilup
2. minimizing energy with specified product purities

First, the optimal operation of the column is studied. This task included optimizing the process for each of the operational objectives using the remaining degrees of freedom and analysing the results in terms of ease of operation. It was shown that operating the column with the second objective is more challenging.

V_{min} diagram was used as a useful tool to give us ideas on design and operation of columns based on feed properties, namely, composition, quality and relative volatilities. It takes very little effort to get so much information about a separation system. Chapters 4 and 5 show the application of this tool in design and operation of Kaibel column.

In industrial practice, it is not common to adjust the vapour split online. It is normally given by the dividing wall placement and flow/pressure characteristics of the packing and the liquid load on each side. We have shown that manipulating the vapour split will give us more freedom to be in the optimal region and to handle feed composition disturbances.

Self-optimizing control strategy is used to find the proper control variables for the first operational objective. The dynamic performance of the system is compared to the case where impurities coming out of prefractionator, i.e. propanol in the top and ethanol in the bottom, are controlled. The structure with composition control in the prefractionator wins. This is because the impurities going out from prefractionator will end up in the side streams and make them off-spec.

One of the drawbacks of using HYSYS as the simulation tool is that the steady-state and dynamics environments are separated from each other. When converting to dynamic mode, the steady-state specifications will be deactivated and controllers should do the task of stabilization and keeping variables at their specifications. Choosing the right control structure to get to the same profiles as the steady-state model in important. This is done by closing composition loops at the ends of the prefractionator (x_{C3} in top and x_{C2} in bottom of prefractionator), the distillate product composition (x_{C1}) and ratios of impurities in side streams ($\frac{x_{C1}}{x_{C3}}$ in side stream 1 and $\frac{x_{C2}}{x_{C4}}$ in side stream 2). In the other hand, the positive points are avoiding programming and debugging and a rigorous thermodynamic package. By connecting HYSYS to MATLAB through ActiveX server, optimization is done in MATLAB in order to make use of Optimization toolbox in MATLAB.

A static estimator is made based on reformulating self-optimizing method. This estimator was derived for "open-loop" and "closed-loop" scenarios. These scenarios are when

- the system is fully open,
- the primary variables are controlled,
- the secondary variables are controlled,
- the estimate of the primary variables are controlled

The last two scenarios are more applicable. However, all of the four scenarios are presented to cover all possibilities. Frequency of updating **H** depend on how fast the system's steady-state changes. The estimators were proved to be the best for each of the scenarios. Since they are calculated based on steady-state information, it is possible that the dynamic performance is not good. The reason is that the measurements which are combined to give the estimate are from different sections and have different dynamics. They are multiplied by **H** values with positive and negative signs, which may lead to inverse response. To solve this issue, different approaches were suggested. They are as below:

- Cascade Control:
  The idea is to close a fast inner loop based on a single measurement with no RHP-zero and adjust the setpoint on a time scale which is slower than the RHP-zero.
- Use of measurements from the same section of the process:
  If the dynamic behaviour of the selected measurements are similar, then it is less likely to get RHP-zero. However, this gives a larger steady-state error.
- Filters:
  The Low-pass filters will keep the system optimal at steady state. The idea is to filter the measurements before they are combined to give the estimate. It's also possible to put filter on the obtained estimator.

It is shown by an example that one can design a filter to make the transfer function from x to $\hat{y}$ as fast as one wants. This is done by using lead-lag filters. In this work, the desired transfer function is defined based on an experiment to find the internal time constants of the system. In order to find the explicit solution, the model matching problem is converted to Nehari problem. The calculation is easy for the scalar case, but includes some iteration for the matrix-valued model-matching problem. The filter obtained by Nehari method is not necessarily low-pass. Since the steady-state values should not be affected by filtering, a weight function is multiplied to the matrices $\mathbf{T}_1$ and $\mathbf{T}_2$.

The estimator proposed in this thesis takes a different approach compared to dynamic estimators, where the calculations are started from an initial point and iterations were done through time. The positive points of our estimator are the ease and speed of calculations. Inverse response problems which might happen, can be taken care of in different ways which were discussed in the thesis. It is seen that Kalman filters is computationally intensive, and for some cases it might be impossible to implement the estimator real time. It is also not guaranteed to get a good estimate of steady-state values from Kalman filter.

12.2 Further work

The following points are suggested to be further investigated:

- The study on manipulating vapour split is done with one set of feed properties (compositions, relative volatilities) and the focus was on feed composition changes and if a column with fixed vapour split can be operated economically with regards to energy consumption. It is suggested to further study different possibilities and give a general guideline about this issue.
- There is no report of experimental work in this thesis. It is suggested to implement the estimator on the pilot column at NTNU. This was planned to be done. However, it did not come through because of the constructions in the chemistry buildings and the control experiments by other colleagues.

Joint Declaration

Chapter 3 in the doctoral thesis, "Optimal Operation of Kaibel Distillation Columns", by Maryam Ghadrdan is a joint work which has been submitted as the following article:

M. Ghadrdan, I.J. Halvorsen, S. Skogestad, "Optimal Operation of Thermally-Coupled Kaibel Distillation Columns", Chemical Engineering Research and Design, doi:10.1016/j.cherd.2011.02.007

The contribution of each co-worker is as follows:

- Maryam Ghadrdan (Author 1): Wrote model for simulation studies, performed all the simulations and wrote the manuscript.
- Ivar J. Halvorsen (Author 2): Supervised the overall work and helped in analysis of results.
- Sigurd Skogestad (Author 3): Supervised the overall work, helped in analysis of results and in revision of the manuscript.

(Maryam Ghadrdan)	(Ivar J. Halvorsen)	(Sigurd Skogestad)
PhD Candidate	Senior Scientist	Professor
NTNU	SINTEF ICT	NTNU

Chapter 5 in the doctoral thesis, "Manipulation of Vapour Split in Thermally-Coupled Distillation Arrangements", by Maryam Ghadrdan is a joint work which has been submitted as the following article:

M. Ghadrdan, S. Skogestad, I.J. Halvorsen, "Manipulation of Vapour Split in Thermally-Coupled Distillation Arrangements", Chemical Engineering and Processing 72 (2013) 10-23

The contribution of each co-worker is as follows:

- Maryam Ghadrdan (Author 1): Wrote model for simulation studies, performed all the simulations and wrote the manuscript.
- Ivar J. Halvorsen (Author 2): Supervised the overall work and helped in analysis of results.
- Sigurd Skogestad (Author 3): Supervised the overall work, helped in analysis of results and in revision of the manuscript.

(Maryam Ghadrdan)	(Ivar J. Halvorsen)	(Sigurd Skogestad)
PhD Candidate	Senior Scientist	Professor
NTNU	SINTEF ICT	NTNU

Chapter 9 in the doctoral thesis, "A New Class of Model-Based Static Estimators", by Maryam Ghadrdan is a joint work which has been submitted as the following article:

M. Ghadrdan, C. Grimholt, S. Skogestad, "A New Class of Model-Based Static Estimators", Ind. Eng. Chem. Res., 2013, 52 (35), pp 12451-12462, DOI: 10.1021/ie400542n

The contribution of each co-worker is as follows:

- Maryam Ghadrdan (Author 1): Wrote model for simulation studies, performed all the simulations and wrote the manuscript.
- Chriss Grimholt (Author 2): Wrote model for simulation studies, performed some of the simulations and wrote part of the manuscript.
- Sigurd Skogestad (Author 3): Supervised the overall work, helped in analysis of results and in revision of the manuscript.

(Maryam Ghadrdan)	(Chriss Grimholt)	(Sigurd Skogestad)
PhD Candidate	PhD Candidate	Professor
NTNU	NTNU	NTNU

Appendix A

The case-study of the thesis

A.1 Simulation of Kaibel column in HYSYS

The case-study used in this thesis is simulated in Aspen HYSYS 2006.5 using the custom column unit. This is done step by step. First, the prefractionator is simulated as a conventional column, by putting a "Tray section" unit, a condenser and reboiler. There are 4 streams going in and out of the ends of the column section. The feed stream is added in the "Optional Feeds" section in the design tab. The specifications of the column come from V_{min} diagram.

Figure A.1 shows the second step of simulation, where a column is added in the bottom of the prefractionator. The flowrate of Aux1 stream, which is an extra degree of freedom, is set to zero in the beginning and is increased gradually to reach a reasonable composition in the bottom product. The same is done for the top section and Aux2 stream (see Figure A.2). The last step is to add the middle column in the main section. This will add two degrees of freedom to the system. Changes should be done gradually. So, at each step, the new degree of freedom should be specified such that there will be no abrupt change from the previous point.

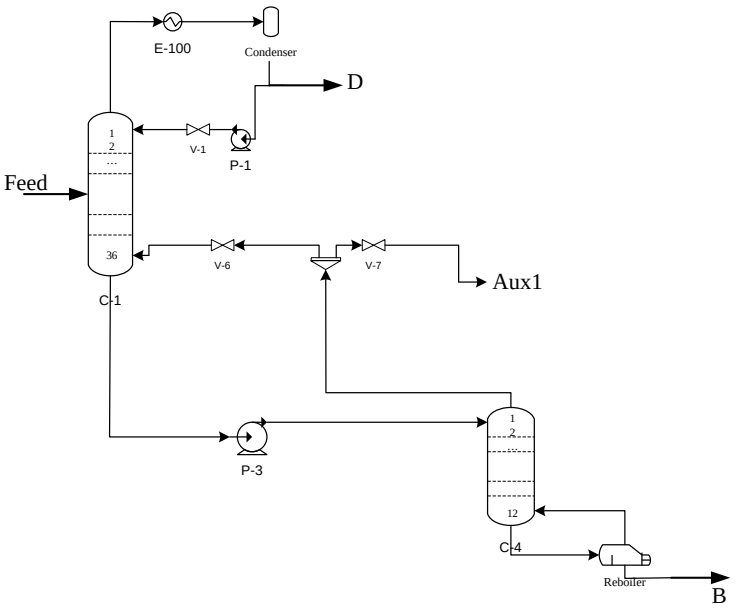

Figure A.1: Step 2 of simulating Kaibel column

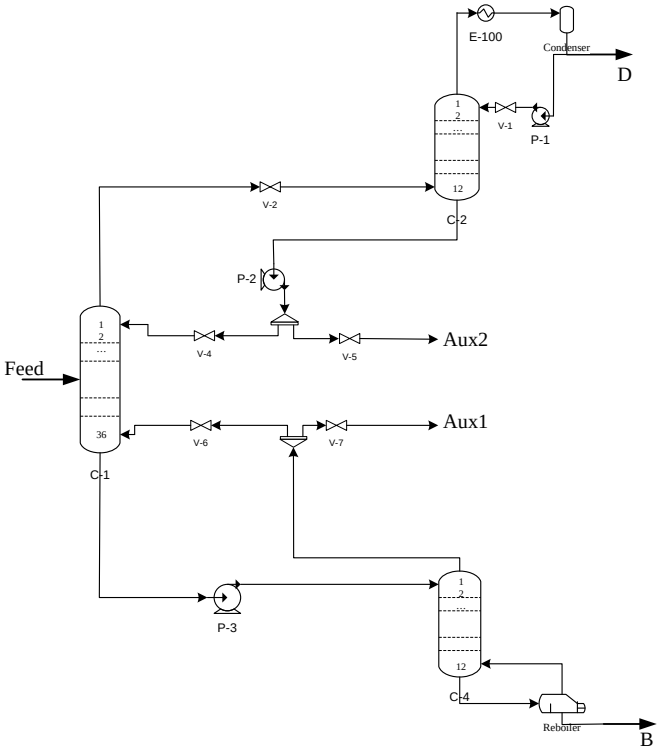

Figure A.2: Step 3 of simulating Kaibel column

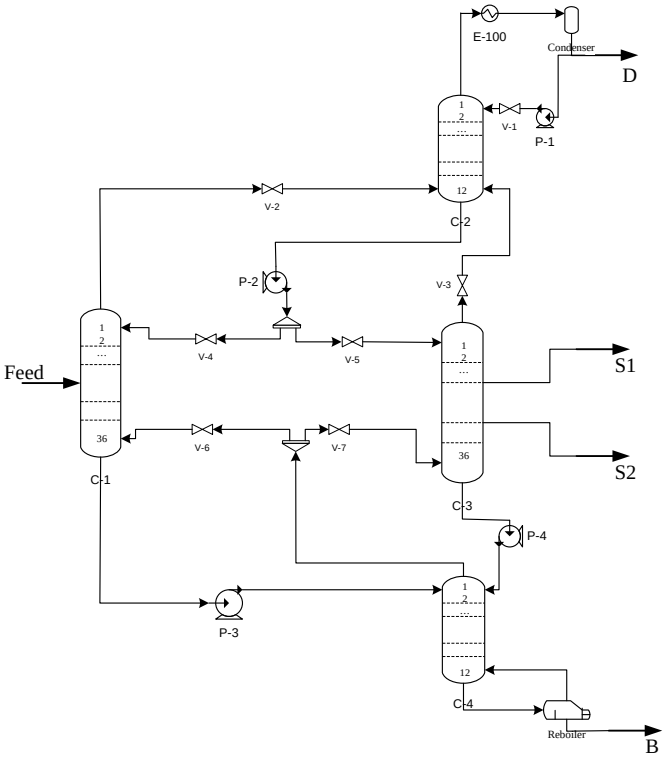

Figure A.3: Final step of simulating Kaibel column

The final model will be optimized to get to the nominal point which is the basis for the study in this thesis. Two objectives are studied:

- Maximizing product compositions with a fixed boilup
- Minimizing vapour consumption with a specified product compositions

The first optimization is done using non-gradient based optimization tools in MATLAB. However, optimizing the second case-study is not as simple as the first one. The solution surface is sketched manually in order to find the optimum. Further details are given in Appendix B.

A.2 MATLAB - HYSYS Linking

In this thesis, MATLAB is used as a tool for optimization and control structure design calculations. MATLAB is linked to HYSYS using OLE (Object Linking and Embedding). The code below shows how to link HYSYS to MATLAB and read some basic information from HYSYS.

```
serv = actxserver('Hysys.Application.2006.5');
HyCase = serv.SimulationCases.Open([pwd,filename]);
HyCase.Activate;
Col = HyCase.Flowsheet.Operations.Item('T-100');
Specs = Col.ColumnFlowsheet.Specifications;
% read compositions of Distillate and bottom streams and Feed flow rate
D     = Col.Flowsheet.MaterialStreams.Item('D');
B     = Col.Flowsheet.MaterialStreams.Item('B');
xDs = D.ComponentMolarFractionValue;
xBs = B.ComponentMolarFractionValue;
FFlowS = HyCase.Flowsheet.MaterialStreams.Item('F').MolarFlowValue;
```

This piece of code shows how to write information from MATLAB to HYSYS

```
%% temperature profile as function of Feed flow rate changes
F_Flow = HyCase.Flowsheet.MaterialStreams.Item('F').MolarFlowValue;
F_new = [0.98*F_Flow,1.02*F_Flow];
for i = 1:length(Frng)
    HyCase.Flowsheet.MaterialStreams.Item('F').MolarFlowValue = F_new;
    Col.ColumnFlowsheet.Run
    T = Col.ColumnFlowsheet.TemperaturesValue;
end
```

Changing Feed compositions is not so straightforward. This is done by recording a script first (in HYSYS: Tools → Script Manager → New). There will be an *.SCP file in the working directory which is generated by saving the script. Compositions can be changed by opening the SCP file, seeking the locations of composition values and substituting the values by desired values. The code below shows how to call, edit and play the modified script.Below is a piece of code which changes one of the 4 compositions and normalizes the compositions, so that the sum of composition become unity.

```
%% Changes in feed composition
Compfrac = ...
    HyCase.Flowsheet.MaterialStreams.Item('F').componentMolarFractionValue;
step_za = 0.02;
compositionDisturbance(Compfrac, step_za);
HyCase.Application.PlayScript([pwd,'\compChange.SCP'])

function compositionDisturbance(x, Compfrac, stp_z)
for i = 1:4
    if i ~= x
        Compfrac_d(i) = Compfrac(i) - stp_z * Compfrac(i) / ...
            (sum(Compfrac) - Compfrac(x));
    else
```

```
        Compfrac_d(i) = Compfrac(i) + stp_z;
    end
end

fid = fopen('compChange.scp', 'r+');
fseek(fid, 179, 'bof');
fprintf(fid, '%1.7e',Compfrac_d(1));
fclose(fid);

fid = fopen('compChange.scp', 'r+');
fseek(fid, 332, 'bof');
fprintf(fid, '%1.7e',Compfrac_d(2));
fclose(fid);

fid = fopen('compChange.scp', 'r+');
fseek(fid, 485, 'bof');
fprintf(fid, '%1.7e',Compfrac_d(3));
fclose(fid);

fid = fopen('compChange.scp', 'r+');
fseek(fid, 638, 'bof');
fprintf(fid, '%1.7e',Compfrac_d(4));
fclose(fid);
```

Below is the text of the SCP file saved for this purpose

```
Message "FlowSht.1/StreamObject.400(F)" "view"
Message "FlowSht.1/StreamObject.400(F)" "View EditCompositionsView"
Specify "FlowSht.1/StreamObject.400(F)" ":ExtraData.520.0.0"  ...
    2.6333341e-001
Specify "FlowSht.1/StreamObject.400(F)" ":Index.500"  1.000000000000e+000
Specify "FlowSht.1/StreamObject.400(F)" ":ExtraData.520.0.1"  ...
    2.6333335e-001
Specify "FlowSht.1/StreamObject.400(F)" ":Index.500"  2.000000000000e+000
Specify "FlowSht.1/StreamObject.400(F)" ":ExtraData.520.0.2"  ...
    2.6333330e-001
Specify "FlowSht.1/StreamObject.400(F)" ":Index.500"  3.000000000000e+000
Specify "FlowSht.1/StreamObject.400(F)" ":ExtraData.520.0.3"  ...
    2.0999994e-001
Message "FlowSht.1/StreamObject.400(F)" "Normalize"
Message "FlowSht.1/StreamObject.400(F)" "AcceptComp"
SpecWhileSolving Message "FlowSht.1/StreamObject.400(F)" "CloseView"
SpecWhileSolving Message "FlowSht.1/StreamObject.400(F)" "CancelComp"
```

Feed quality is set by the feed temperature. The reason is that we can not set values below zero or over one.

```
% temperature profile of the column as function of feed quality

vrng = [-0.02,0.02];
for i = 1:length(vrng)
    temptoset = fsolve(@reachq,100,[],HyCase,1+vrng(i));
    HyCase.Flowsheet.MaterialStreams.Item('F').VapourFraction.Erase
    HyCase.Flowsheet.MaterialStreams.Item('F').Temperature.Value = ...
        temptoset;
    Col.ColumnFlowsheet.Run
    T = Col.ColumnFlowsheet.TemperaturesValue;
    riteTofile
    HyCase.Flowsheet.MaterialStreams.Item('F').Temperature.Erase
    HyCase.Flowsheet.MaterialStreams.Item('F').VapourFraction.value = 0;
end
```

```
function q = calcq(HyCase,temperature)
    % This function calculates 'q' for a stream with the specified temperature
    % and Pressure and composition as stream 'F'
    HyCase.Application.PlayScript([pwd,'\definefromother.SCP'])
    HyCase.Flowsheet.MaterialStreams.Item('7').TemperatureValue = temperature;
    HyCase.Solver.CanSolve = 1;
    hf = HyCase.Flowsheet.MaterialStreams.Item('7').MolarEnthalpyValue;

    HyCase.Flowsheet.MaterialStreams.Item('7').Temperature.Erase

    HyCase.Flowsheet.MaterialStreams.Item('7').vapourFractionValue = 1;
    HyCase.Solver.CanSolve = 1;
    hv_sat = HyCase.Flowsheet.MaterialStreams.Item('7').MolarEnthalpyValue;

    HyCase.Flowsheet.MaterialStreams.Item('7').vapourFractionValue = 0;
    HyCase.Solver.CanSolve = 1;
    hl_sat = HyCase.Flowsheet.MaterialStreams.Item('7').MolarEnthalpyValue;

    q = (hv_sat - hf)/(hv_sat - hl_sat);

    HyCase.Flowsheet.MaterialStreams.Item('7').vapourFraction.Erase
```

Appendix B

Contour plots

In this appendix, the idea of how to sketch the contours of boilup as a function of vapour and liquid split using HYSYS is discussed.

B.1 Contour plots with R_V manipulated

For a Kaibel column with a fixed feed, there are 6 degrees of freedom. Four degrees of freedom are used to satisfy the four product purities specifications. The remaining two degrees of freedom, here selected as vapour and liquid splits, are used to minimize energy requirement. So, contours of boilup with vapour and liquid splits show the solution surface.

We start from one of the end points. In HYSYS, the four main product composition plus the vapour boilup and one of the splits are set as specifications. Let's assume we have R_L as a specification and we have found the bottom point as the starting point. The next step is to increase the value of R_L stepwise, till it reaches the other end, above which there is no feasible solution. Since there is multiplicity in the solution, we have two different ways to reach the other end. There is no guarantee which one is obtained in this procedure. The column "current values" in the specifications tab in HYSYS is actually the initial points. So, when a specification is changed, the operating point is also affected by the current values, specifically when there is multiplicity in the solution. We will elaborate more in our case-study. Consider Figure B.1, which shows one of the curves in the boilup contour. Note that if we decrease R_V, The closest value of R_L which is on the contour plot, will be on the bottom curve, which is the desired curve to obtain. So, to continue on the bottom line, we decrease R_V by a step size and then continue decreasing it till the other end point.

The same strategy is used for the cases we have the starting point in the top of the contour plots (see Figures B.3 and B.4).

B.2 Solution plots with fixed R_V

In this case, R_V is fixed. We need to plot the boilup flow as a function of the liquid split R_L. There is multiplicity in the solutions because of different paths that the impurities take to get to the side-streams. In HYSYS, we use this aspect to find the two curves of the solution plots. We start with a high value of boilup and then the value of R_L is decreased till it gets to the minimum feasible value. Note that one of the impurity specifications in the prefractionator ends has a very small value in the beginning. Figure B.5 shows the solution for R_V = 0.5968 and nominal feed conditions (equimolar feed at boiling point). Assume that we get the dotted curve in the first round. This is obtained with very little ethanol in the bottom of the prefractionator as the initial point. In order to get the other curve, we first move the operating point to a relatively high value of boilup and then specify a very little value of propanol in the top of prefractionator, say $1e-5$ and activate the specified variable as one of the specifications in HYSYS. With this initial point, if

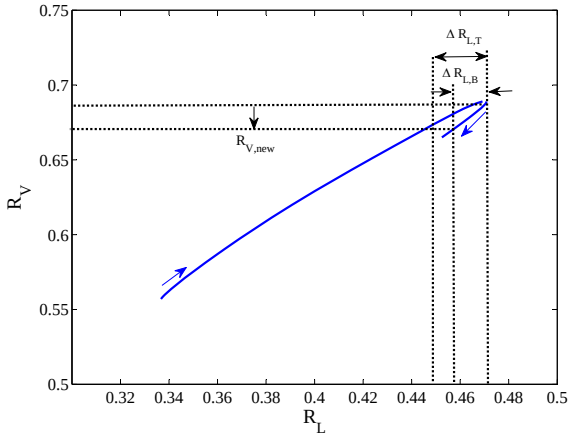

Figure B.1: A contour plot

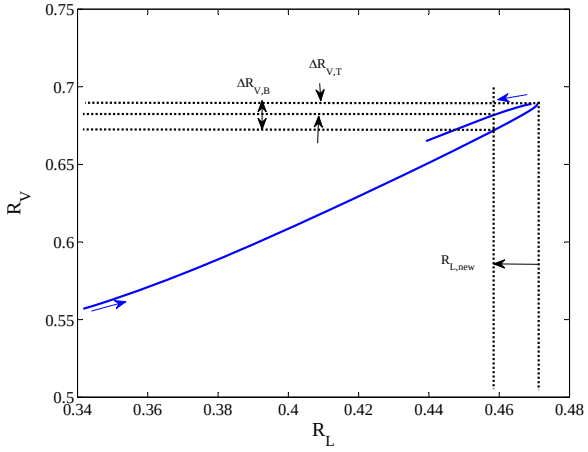

Figure B.2: A contour plot

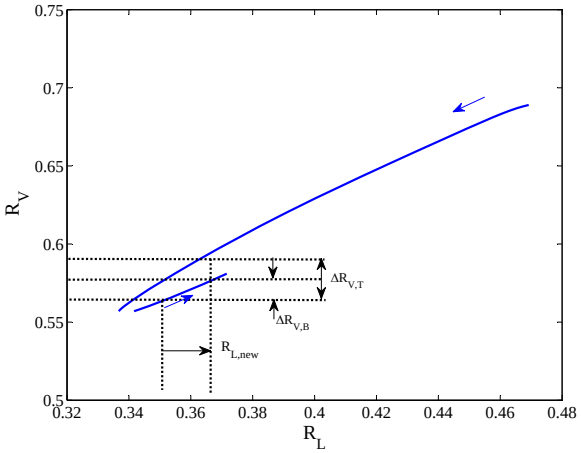

Figure B.3: A contour plot

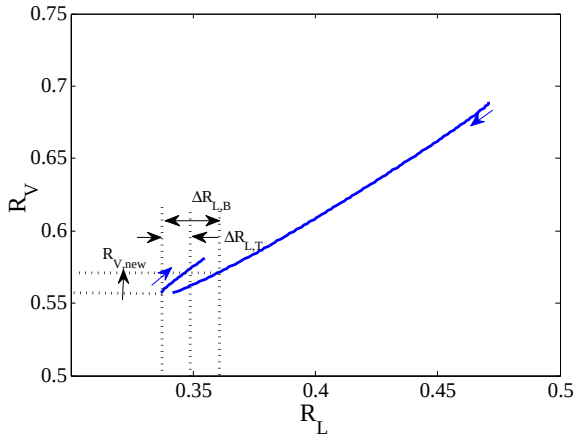

Figure B.4: A contour plot

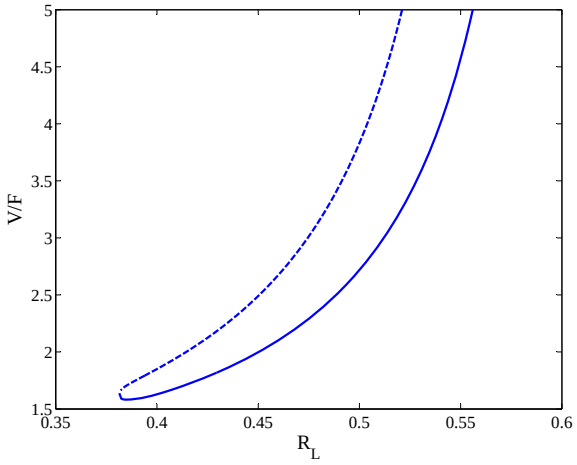

Figure B.5: A contour plot

we start iterating on R_L we will get the operating points corresponding to the other curve in the solution plot.

Appendix C

Unscented Kalman Filter

The Unscented Transformation (UT) is founded on the intuition that it is easier to approximate a probability distribution than to approximate an arbitrary nonlinear function [187]. A set of sigma points are chosen. Then, the nonlinear function is applied to each sigma point. An estimate of the nonlinearly transformed mean and covariance are calculated. The procedure is summarized as below:

1. Choosing the sigma points and propagation through the nonlinear function:
   Some weights are defined as

$$\begin{aligned} W_m^{(0)} &= \frac{\lambda}{\lambda + n} \\ W_c^{(0)} &= \frac{\lambda}{\lambda + n} + (1 - \alpha^2 + \beta) \\ W_m^{(i)} &= \frac{\lambda}{2(\lambda + n)}, \; i = 1, ..., 2n \\ W_c^{(i)} &= \frac{\lambda}{2(\lambda + n)}, \; i = 1, ..., 2n \end{aligned} \tag{C.1}$$

   A set of $2n + 1$ sigma points is computed

$$x_{k-1} = \begin{bmatrix} \hat{x}_{k-1} & \hat{x}_{k-1} + \left[\sqrt{(n+\lambda)\,P_{k-1}}\right]_{i=1:n} & \hat{x}_{k-1} - \left[\sqrt{(n+\lambda)\,P_{k-1}}\right]_{i=n+1:2n} \end{bmatrix} \tag{C.2}$$

   The initial estimates are set to be 10% higher than the initial points for the simulation. These points are transferred through the nonlinear model $f(.)$

$$\hat{\mathrm{x}}_k^{(i)} = f(\mathrm{x}_{k-1}^{(i)}) \tag{C.3}$$

   So,

$$\hat{\mathrm{x}}_k^- = \sum_{i=0}^{2n+1} W_m^{(i)} \hat{\mathrm{x}}_k^{(i)} \tag{C.4}$$

$$P_k^- = (\hat{\mathrm{x}}_k - \hat{\mathrm{x}}_k^-) w_c (\hat{\mathrm{x}}_k - \hat{\mathrm{x}}_k^-)^T + Q \tag{C.5}$$

   where

$$w_c = diag\left(\begin{bmatrix} W_c^{(0)} & ... & W_c^{2n} \end{bmatrix}\right)$$

2. Measurement update
   The following initial points is transformed through the nonlinear measurement function $g(.)$ to give the updated measurements.

$$X_k = \begin{bmatrix} \hat{\mathrm{x}}_k^- & \hat{\mathrm{x}}_k^- + \left[\sqrt{(n+\lambda)\,P_k^-}\right]_{i=1:n} & \hat{\mathrm{x}}_k^- - \left[\sqrt{(n+\lambda)\,P_k^-}\right]_{i=n+1:2n} \end{bmatrix}$$

$$\mathrm{y}_k^{(i)} = g(X_k^{(i)}) \tag{C.6}$$

So,

$$\hat{\mathrm{y}}_k^- = \sum_{i=0}^{2n+1} W_m^{(i)} \mathrm{y}_k^{(i)} \tag{C.7}$$

$$P_{\mathrm{x}_k\mathrm{y}_k} = (X_k - \hat{\mathrm{x}}_k) w_c (Y_k - \hat{\mathrm{y}}_k)^T$$
$$P_{\mathrm{y}_k^-\mathrm{y}_k^-} = (Y_k - \hat{\mathrm{y}}_k) w_c (Y_k - \hat{\mathrm{y}}_k)^T + R$$

The observer gain will be calculated by

$$K_k = \frac{P_{\mathrm{x}_k\mathrm{y}_k}}{P_{\mathrm{y}_k^-\mathrm{y}_k^-}} \tag{C.8}$$

So the estimated state in each iteration will be

$$\hat{\mathrm{x}}_k = \hat{\mathrm{x}}_k^- + K_k(\mathrm{y}_k - \hat{\mathrm{y}}_k^-) \tag{C.9}$$

Note that the size of y_k is equal to the number of sensors in the process.

$$P_k = P_k^- - K_k P_{\mathrm{y}_k^-\mathrm{y}_k^-} K_k^T \tag{C.10}$$

No linearization is needed in this method. However, many samples are required. This means that as the number of states increases, the computational burden will be more. This leads to the question of whether the samples can be chosen wisely and thus much fewer samples are required. This is the concept of the sigma point filter. You pick $2n+1$ points and weights for an n dimensional distribution. For example, a two dimensional Gaussian would require 5 points (one being the mean). The points would be chosen to preserve the covariance and mean of the distribution. If f is linear or quadratic, this sampling yields the exact moment of the distribution.

The following figures show the dynamic trends of compositions and temperatures and their estimates. The initial values of the estimated states are set to be 10% higher than the initial values of the states. It is observed that all the estimates are tracking the states very nicely. The computational time is almost 5 times the simulation time, e.g. 4.63 hours for 1 hour of simulation. This is due to the high number of states (164 states). The functions for state and measurement calculations are called 658 times for each iteration.

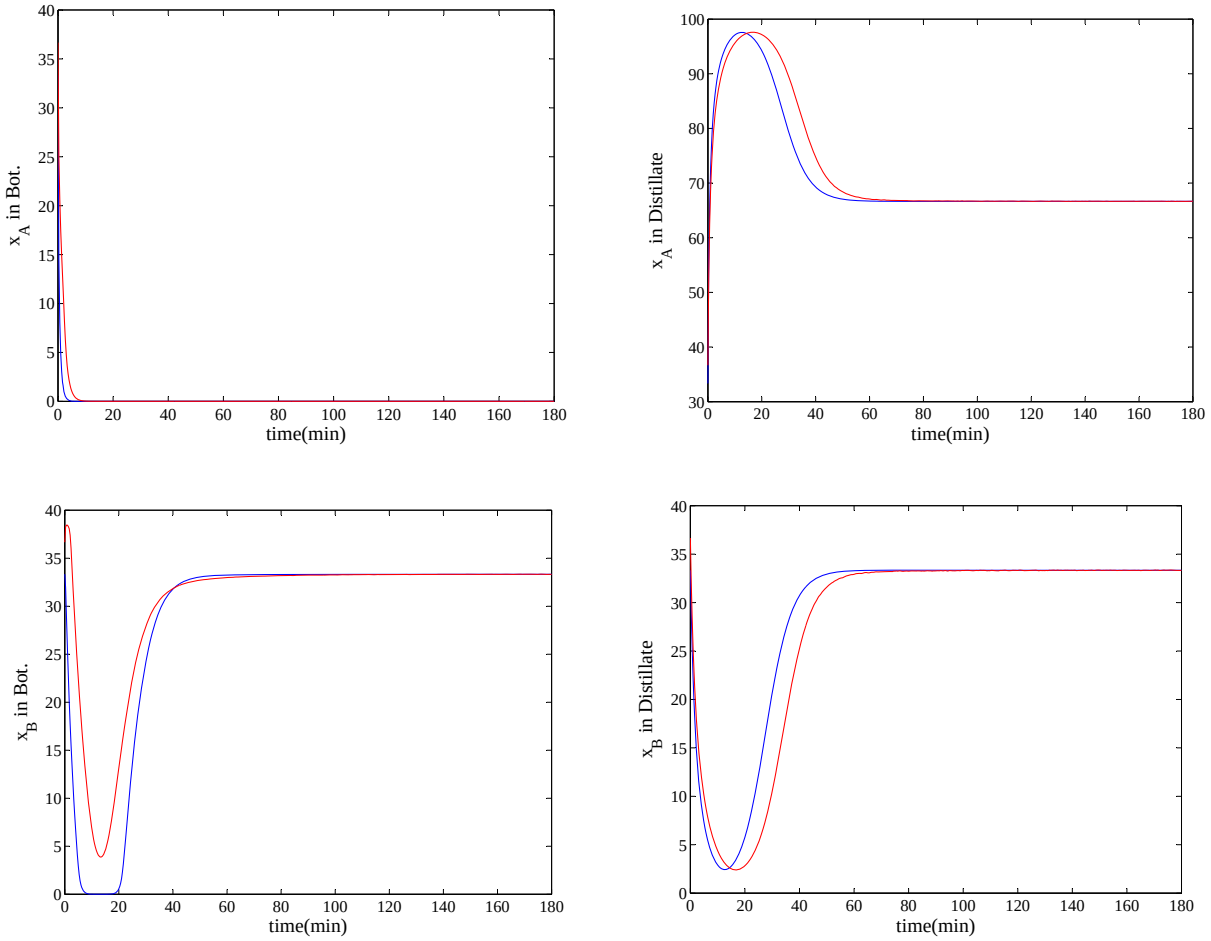

Figure C.1: Compositions in the product streams and their estimates; blue: true values, red: estimated values

Bibliography

[1] I. J. Halvorsen, S. Skogestad, Minimum energy consumption in multicomponent distillation. 1. v_{min} diagram for a two-product column, Journal of Industrial Engineering and Chemistry Research 42 (2003) 596–604.

[2] S. Skogestad, Plantwide control: the search for the selfoptimizing control structure, Journal of Process Control 10 (2000) 487–507.

[3] M. A. Schultz, D. G. Stewart, J. M. Harris, S. P. Rosenblum, M. S. Shakur, D. E. O'Brien, Reduce costs with dividing-wall columns, Journal of Chemical Engineering Progress 98 (5) (2008) 64–71.

[4] I. Dejanović, L. Matijašević, Z. Olujić, Dividing wall column - a breakthrough towards sustainable distilling, Journal of Chemical Engineering and Processing: Process Intensification 49 (6) (2010) 559–580.

[5] J. Humphrey, A. Siebert, Separation technologies: an opportunity for energy savings, Journal of Chemical Engineering Progress 92.

[6] M. Schaller, Numerically optimized diabatic distillation columns, Ph.D. thesis, Technische Universität Chemnitz, Fakultät für Naturwissenschaften (2007).

[7] A. Brugma, Fractional distillation of liquid mixtures, especially petroleum, Dutch Patent, Number 41.850 1937. (1937).

[8] R. Wright, Fractionation apparatus, US Patent 2,471,134 (1949).

[9] F. Petlyuk, V. Platonov, D. Slavinskii, Thermodynamically optimal method for separating multicomponent mixtures, International Journal of Chemical Engineering (1965) 555–561.

[10] A. J. Finn, Rapid assessment of thermally coupled side columns, Journal of Gas Separation & Purification 10 (3) (1996) 169–175.

[11] R. P. Cahn, E. Di Micelli, A. G. Di Micelli, Separation of multicomponent mixture in single tower, US Patent, Number 3,058,893 (1962).

[12] K. Aso, T. Nakanishi, M. Nakaiwa, T. Takamatsu, Heat integrated distillation column, European Patent, Number EP1380328 (2007).

[13] H. Rust, G. Kaibel, Dividing wall column, US Patent 20010052453 A1 (2005).

[14] P. C. Steacy, Dividing wall fractionation column control system and apparatus, US Patent, Number 6558515 B1 (2001).

[15] Z. Fidkowski, L. Krolikowski, Minimum energy requirements of thermally coupled distillation systems, AIChE Journal 33 (1987) 643–653.

[16] P. B. Shah, Squeeze more out of complex columns, Journal of Chemical Engineering Progress (2002) 46–55.

[17] A. Al-Elg, A. Palazoglu, Modeling and control of a high-purity double-effect distillation column, Journal of Computers and Chemical Engineering 13 (1989) 1183–1187.

[18] M. Han, S. Park, Multivariable control of double-effect distillation configurations, Journal of Process Control 6 (1996) 247–253.

[19] D. Freshwater, The heat pump in multicomponent distillation, British Chemical Engineering Journal 6 (1961) 388–391.

[20] T. Takamatsu, M. Nakaiwa, T. Nananishi, The concept of an ideal heat integrated distillation column (HIDiC) and its fundamental properties, Kagaku Kogaku Ronbunshu 22 (1996) 985–990.

[21] T. Takamatsu, M. Nakaiwa, T. Nananishi, K. Aso, Possibility of energy saving in the ideal heat integrated distillation column (HIDiC), Kagaku Kogaku Ronbunshu 23 (1997) 28–36.

[22] M. Nakaiwa, K. Huang, A. Endo, T. Ohmori, T. Akiya, T. Takamatsu, Internally heat

integrated distillation columns: A review, Trans IChemE 81 (2003) 162–177.
[23] D. Tedder, D. Rudd, Parametric studies in industrial distillation (part i): Design comparisons, AIChE Journal 24 (1978) 303.
[24] E. Wolff, S. Skogestad, Operation of integrated three-product (petlyuk) distillation columns, Journal of Industrial Engineering and Chemistry Research 34 (1995) 2094–2103.
[25] G. Kaibel, Distillation columns with vertical partitions, Journal of Chemical Engineering and Technology 10 (1987) 92–98.
[26] C. Triantafyllou, R. Smith, The design and optimisation of fully thermally coupled distillation columns, Trans. IChemE 70 (1992) 118–132.
[27] B. Kolbe, S. Wenzel, Novel distillation concepts using one-shell columns, Journal of Chemical Engineering and Processing: Process Intensification 43 (2004) 339–346.
[28] R. Premkumar, G. Rangaiah, Retrofitting conventional column systems to dividing-wall columns, Journal of Chemical Engineering Research and Design 87 (2009) 47–60.
[29] R. Agrawal, Multicomponent distillation columns with partitions and multiple reboilers and condensers, Journal of Industrial Engineering and Chemistry Research 40 (2001) 4258–4266.
[30] T. Adrian, H. Schoenmakers, M. Boll, Model predictive control of integrated unit operations: control of a divided wall column, Journal of Chemical Engineering and Processing. 43 (2004) 347–355.
[31] Z. Fidkowski, L. Krolikowski, Thermally coupled system of distillation columns: Optimization procedure, AIChE Journal 32 (4) (1986) 537–546.
[32] A. Underwood, Fractional distillation of ternary mixtures, part 1, Journal of the Institute of Petroleum 31 (1945) 111.
[33] A. Underwood, Fractional distillation of ternary mixtures, part 2, Journal of the Institute of Petroleum 32 (1946) 598.
[34] A. J. V. Underwood, Fractional distillation of multicomponent mixturesscalculation of minimum reflux ratio, Journal of the Institute of Petroleum 32 (1946) 614.
[35] H. Z. Kister, Distillation Design, McGraw-Hill, New York, 1992.
[36] C. J. King, Separation Processes, McGraw-Hill, New York, 1980.
[37] J. Cerda, A. Westerberg, Shortcut methods for complex distillation columns. 1. minimum reflux, Journal of Industrial & Engineering Chemistry Process Design and Development 20 (1981) 546–557.
[38] I. Malinen, J. Tanskanen, A rigorous minimum energy calculation method for a fully thermally coupled distillation system, IChemE 85 (A4) (2007) 502–509.
[39] P. B. Shah, Conceptual programming: A new approach for the optimisation, analysis and novel development of simple and complex separation systems, Ph.D. thesis, University of Manchester Institute of Science and Technology (1999).
[40] I. J. Halvorsen, S. Skogestad, Minimum energy consumption in multicomponent distillation. 2. three-product petlyuk arrangements, Journal of Industrial Engineering and Chemistry Research 42 (2003) 605–615.
[41] I. J. Halvorsen, S. Skogestad, Minimum energy consumption in multicomponent distillation. 3. more than three products and generalized petlyuk arrangements, Journal of Industrial Engineering and Chemistry Research 42 (2003) 616–629.
[42] I. J. Halvorsen, S. Skogestad, Optimizing control of petlyuk distillation: Understanding the steady-state behavior, Journal of Computers and Chemical Engineering 21 (1997) S249–S254.
[43] I. J. Halvorsen, S. Skogestad, Minimum energy for the four-product kaibel-column, AIChE Annual Meeting (2006).
[44] Y. H. Kim, Structural design and operation of a fully thermally coupled distillation column, Chemical Engineering Journal 85 (2002) 289–301.
[45] R. Agrawal, Z. Fidkowski, Preliminary screening of column configurations for ternary distillation, AIChE Spring Meeting (2002).
[46] I. J. Halvorsen, S. Skogestad, Shortcut analysis of optimal operation of petlyuk distillation, Journal of Industrial Engineering and Chemistry Research 43 (2004) 3994–3999.
[47] M. Abdul-Mutalib, R. Smith, Operation and control of dividing wall distillation columns. part 1. degrees of freedom and dynamic simulation, Trans. IChemE Part A (76) (1998) 308–318.
[48] R. Agrawal, Z. T. Fidkowski, More operable arrangements of fully thermally coupled distillation columns, AIChE Journal 44 (11) (1998) 2565–2568.
[49] R. Agrawal, More operable fully thermally coupled distillation column configurations for

multicomponent distillation, Trans IChemE 77 (Part A) (1999) 543–553.
[50] R. Agrawal, A method to draw fully thermally coupled distillation column configurations for multicomponent distillation, Trans IChemE 78 (Part A).
[51] B.-G. Rong, I. Turunen, New heat-integrated distillation configurations for petlyuk arrangements, Chemical Engineering Research and Design 84 (A12) (2006) 1095–1116.
[52] B.-G. Rong, A. Kraslawski, L. Nyström, The synthesis of thermally coupled distillation flowsheets for separations of five-component mixtures, Journal of Computers and Chemical Engineering 24 (2000) 247–252.
[53] S. Hernández, J. G. Segovia-Hernández, V. Rico-Ramírez, Thermodynamically equivalent distillation schemes to the petlyuk column for ternary mixtures, Journal of Energy 31 (2006) 2176–2183.
[54] A. Jiménez, N. Ramírez, A. Castro, S. Hernández, Design and energy performance of alternative schemes to the petlyuk distillation system, Trans IChemE 81 (Part A).
[55] R. Agrawal, Z. Fidkowski, New thermally coupled schemes for ternary distillation, AIChE Journal 45 (1999) 485–496.
[56] R. Agrawal, Thermally coupled distillation with reduced number of intercolumn vapor transfers, AIChE Journal 46 (2000b) 2198–2210.
[57] R. Agrawal, Synthesis of distillation column configurations for a multicomponent separation, Journal of Industrial Engineering and Chemistry Research 35 (4) (1996) 1059–1071.
[58] A. C. Christiansen, S. Skogestad, K. Lien, Complex distillation arrangements: Extending the petlyuk ideas, Journal of Computers and Chemical Engineering 21 (1997) S237–S242.
[59] R. W. H. Sargent, K. Gaminibandara, Optimum Design of Plate Distillation Columns. In: Optimization in Action, Academic Press, London, 1976.
[60] Y. H. Kim, A new fully thermally coupled distillation column with postfractionator, Journal of Chemical Engineering and Processing 45 (2006) 254–263.
[61] Y. Kim, W. Luyben, Effect of recycle on chemical reactor controllability, Chemical Engineering Communications 128 (1994) 65–94.
[62] I. Grossmann, Review of nonlinear mixed-integer and disjunctive programming techniques, Optimization and Engineering 3 (2002) 227.
[63] J. Caballero, I. Grossmann, Logic based methods for generating and optimizing thermally coupled distillation systems, Journal of Computer Aided Chemical Engineering 10 (2002) 169–174.
[64] J. Caballero, I. Grossmann, Thermodynamically equivalent configurations for thermally-coupled distillation, AIChE Journal 49 (11) (2003) 2864–2884.
[65] J. A. Caballero, I. E. Grossmann, Design of distillation sequences: from conventional to fully thermally coupled distillation systems, Journal of Computers and Chemical Engineering 28 (2004) 2307–2329.
[66] I. Grossmann, P. Aguirre, M. Barttfeld, Optimal synthesis of complex distillation columns using rigorous models, Journal of Computers and Chemical Engineering 29 (2005) 1203–1215.
[67] J. Caballero, I. Grossmann, Structural considerations and modeling in the synthesis of heat-integrated thermally-coupled distillation sequences, Journal of Industrial Engineering and Chemistry Research 45 (25) (2006) 8454–8474.
[68] X.-H. Wang, Y.-G. Li, Y.-D. Hu, Y.-L. Wang, Synthesis of heat-integrated complex distillation systems via genetic programming, Journal of Computers and Chemical Engineering 32 (12) (2008) 1908–1917.
[69] S. Hernández, A. Jiménez, Design of energy-efficient petlyuk systems, Journal of Computers and Chemical Engineering 23 (1999) 1005–1010.
[70] S. Hernández, A. Jiménez, Design of optimal thermally-coupled distillation systems using a dynamic model, IChemE Trans. 74 (1996) 357–362.
[71] J. Tanskanen, V. Pohjola, Minimum internal recycle in homogeneous multicomponent distillation, Journal of Chemical Engineering Science 55 (2000) 2713–2726.
[72] J. L. Blancarte-Palacios, M. N. Bautista-Valdés, S. Hernández, V. Rico-Ramírez, A. Jiménez, Energy-efficient designs of thermally coupled distillation sequences for four-component mixtures., Journal of Industrial Engineering and Chemistry Research 42 (2003) 5157.
[73] O. Annakou, Rigorous comparative study of energy integrated distillation schemes, Ph.D. thesis, Technical University of Budapest, Hungary (1996).
[74] M. Emtir, E. Rev, Z. Fonyo, Rigorous simulation of energy integrated and thermally coupled

distillation schemes for ternary mixture, Journal of Applied Thermal Engineering 21 (2001) 1299–1317.

[75] P. Mizsey, N. T. Hau, N. Benko, I. Kalmar, Z. Fonyo, Process control for energy integrated distillation schemes, Journal of Computers and Chemical Engineering 22 (1998) S427–S434.

[76] E. R. v, M. Emtir, Z. Szitkai, P. Mizsey, Z. Fonyó, Energy savings of integrated and coupled distillation systems, Journal of Computers and Chemical Engineering 25 (2001) 119–140.

[77] B. Suphanita, A. Bischertb, P. Narataruksa, Exergy loss analysis of heat transfer across the wall of the dividing-wall distillation column, Journal of Energy 32 (2007) 2121–2134.

[78] T. E. Güttinger, M. Morari, Multiple steady states in homogeneous separation sequences, Journal of Industrial Engineering and Chemistry Research 35 (1996) 4597–4611.

[79] C. Chavez, J. Seader, T. Wayburn, Multiple steady-state solutions for interlinked separation systems, Journal of Industrial & Engineering Chemistry Fundamentals 25 (1986) 566–576.

[80] J. Douglas, Conceptual Design of Chemical Processes, McGraw-Hill, New York, 1988.

[81] J. Viswanathan, I. Grossmann, Optimal feed locations and number of trays for distillation columns with multiple feeds, Journal of Industrial Engineering and Chemistry Research 32 (1993) 2942–2949.

[82] P. Mizsey, Z. Fonyo, Toward a more realistic process synthesiss, the combined approach, Journal of Computers and Chemical Engineering 14 (11) (1990) 1213–1236.

[83] O. Annakou, P. Mizsey, Rigorous comparative study of energy-integrated distillation schemes, Journal of Industrial Engineering and Chemistry Research 35 (1996) 1877–1885.

[84] R. Treybal, Mass Transfer Operations, McGraw-Hill, New York, 1986.

[85] E. Wolff, S. Skogestad, M. Hovd, K. W. Mathisen, A procedure for controllability analysis, IFAC Workshop on Interations between Process Design and Process Control (1992).

[86] H. Rosenbrock, State-space and multivariable theory, Nelson, London (1970).

[87] S. Skogestad, M. Morari, Implications of large rga elements on control performance, Journal of Industrial and Engineering Chemistry Research 26 (1987) 2223–2230.

[88] E. Bristol, On a new measure of interactions for multi variable process control, IEEE Transactions on Automatic Control 11 (1966) 133–134.

[89] J. G. Balchen, K. Mumme, Process Control, Structures and Applications, Van Nostrand Reinhold, New York, 1988.

[90] H. S. Papastathopoulou, W. L. Luyben, Control of a binary sidestream distillation column, Journal of Industrial Engineering and Chemistry Research 30 (4) (1991) 705–713.

[91] M.-J. He, W.-J. Cai, New criterion for control-loop configuration of multivariable processes, Journal of Industrial Engineering and Chemistry Research 43 (2004) 7057–7064.

[92] M.-J. He, W.-J. Cai, New criterion for control-loop configuration of multivariable processes, Journal of Industrial and Engineering Chemistry Research 43 (2004) 7057–7064.

[93] M.-J. He, W. B. F. Cai, W.-J., Block control structure selection based on relative interaction decomposition, 9th International Conference on Control, Automation, Robotics and Vision, Singapore (2006).

[94] S. Hernández, A. Jiménez, Controllability analysis of thermally coupled distillation systems, Journal of Industrial Engineering and Chemistry Research 38 (1999) 3957–3963.

[95] J. G. Segovia-Hernández, S. Hernández, A. Jiménez, Control behavior of thermally coupled distillation sequences, Trans IChemE 80 (Part A).

[96] J. C. Cárdenas, S. Hernández, I. R. Gudiño-Mares, F. Esparza-Hernández, C. Y. Irianda-Araujo, L. M. Domínguez-Lira, Analysis of control properties of thermally coupled distillation sequences for four-component mixtures, Journal of Industrial Engineering and Chemistry Research 44 (2005) 391–399.

[97] J. G. Segovia-Hernández, S. Hernández, A. Jiménez, Analysis of dynamic properties of alternative sequences to the petlyuk column, Journal of Computers and Chemical Engineering 29 (2005) 1389–1399.

[98] J. G. Segovia-Hernández, E. A. Hernández-Vargas, J. A. Márquez-Muñoz, Control properties of thermally coupled distillation sequences for different operating conditions, Journal of Computers and Chemical Engineering 31 (2007) 867–874.

[99] V. E. Tamayo-Galván, J. G. Segovia-Hernández, S. Hernández, J. Cabrera-Ruiz, J. R. Alcántara-Ávila, Controllability analysis of alternate schemes to complex column arrangements with thermal coupling for the separation of ternary mixtures, Journal of Computers and Chemical Engineering 32 (12) (2008) 3057–3066.

[100] S. J. Wang, D. S. H. Wong, Controllability and energy efficiency of a high-purity divided wall column, Chem. Eng. Sci. 62 (2007) 1010–1025.
[101] S. Skogestad, I. Postlethwaite, Multi-variable Feedback Control, Analysis and Design (2nd Edition), Wiley, 2007.
[102] M. S. Govatsmark, S. Skogestad, Optimal number of stages in distillation with respect to controllability, Journal of Computer Aided Chemical Engineering 10 (2002) 499–504.
[103] M. Serra, M. Perrier, A. Espuna, L. Puigjaner, Study of the divided wall column controllability: influence of design and operation, Journal of Computers and Chemical Engineering 24 (2000) 901–907.
[104] M. Serra, A. Espuna, L. Puigjaner, Controllability of different multicomponent distillation arrangements, Journal of Industrial Engineering and Chemistry Research 42 (2003) 1773–1782.
[105] Y. Cao, D. Rossiter, D. W. Edwards, J. Knechtel, D. Owens, Modelling issues for control structure selection in a chemical process, Journal of Computers and Chemical Engineering 22 (Supplement 1) (1998) S411–S418.
[106] E. A. Wolff, S. Skogestad, K. Havre, Dynamics and control of integrated three-product (petlyuk) distillation columns, AIChE Annual Meeting (1993).
[107] M. I. Abdul Mutalib, A. O. Zeglam, R. Smith, Operation and control of dividing wall distillation columns, part 2: Simulation and pilot plant studies using temperature control, Trans IChemE 76 (Part A) (1998) 319–334.
[108] J. G. Segovia-Hernández, S. Hernández, V. Rico-Ramírez, A. Jiménez, A comparison of the feedback control behavior between thermally coupled and conventional distillation schemes, Journal of Computers and Chemical Engineering 28 (2004) 811–819.
[109] M. Serra, A. Espuna, L. Puigjaner, Control and optimization of the divided wall column, Journal of Chemical Engineering and Processing 38 (1999) 549–562.
[110] H. Ling, W. L. Luyben, New control structure for divided-wall columns, Journal of Industrial Engineering and Chemistry Research 48 (13) (2009) 6034–6049.
[111] H. Ling, W. L. Luyben, Temperature control of the btx divided-wall column, Journal of Industrial Engineering and Chemistry Research 49 (1) (2010) 189–203.
[112] M. Morari, G. Stephanopoulos, Y. Arkun, Studies in the synthesis of control structures for chemical processes. part i: formulation of the problem, process decomposition and the classification of the controller task. analysis of the optimizing control structures, AIChE Journal 26 (2) (1980) 220–232.
[113] S. Skogestad, Self-optimizing control: A distillation case study, Symposium of Advanced Control of Chemical Processes (ADCHEM) (2000).
[114] H. K. Engelien, S. Skogestad, Selecting appropriate control variables for a heat integrated distillation system with prefractionator, Journal of Computers and Chemical Engineering 28 (2004) 683–691.
[115] I. J. Halvorsen, S. Skogestad, Use of feedback for indirect optimizing control: Application to petlyuk distillation, DYCOPS-5 Symposium (1998).
[116] I. J. Halvorsen, M. Serra, S. Skogestad, Evaluation of self-optimizing control structures for an integrated petlyuk distillation column, Hungarian Journal of Industrial Chemistry 28 (1) (1999) 11–15.
[117] I. J. Halvorsen, S. Skogestad, Optimal operation of petlyuk distillation: steady-state behavior, Journal of Process Control 9 (1999) 407–424.
[118] L. Narraway, J. Perkins, Selection of process control structure based on linear dynamic economics, Journal of Industrial Engineering and Chemistry Research 32 (1993) 2681–2692.
[119] C. Schweiger, C. Floudas, Interactions of design and control .In W.W. Hager, P.M. Pardalos, Optimization with dynamic models. Optimal control: theory, algorithms and applications, 1997.
[120] V. Kariwala, Optimal measurement combination for local self-optimizing control, Journal of Industrial Engineering and Chemistry Research 46 (2007) 3629–3634.
[121] V. Alstad, S. Skogestad, E. Hori, Optimal measurement combinations as controlled variables, Journal of Process Control 19 (1) (2009) 138–148.
[122] J. Strandberg, S. Skogestad, Stabilizing control of an integrated 4-product kaibel column, Symposium of Advanced Control of Chemical Processes (ADCHEM) (2006).
[123] I. J. Halvorsen, Minimum energy requirements in complex distillation arrangements, Ph.D.

thesis, Norwegian University of Science and Technology, Department of Chemical Engineering (Available from homepage of S. Skogestad) (2001).

[124] I. J. Halvorsen, S. Skogestad, Energy efficient distillation, Journal of Natural Gas Science and Engineering 3 (4) (2011) 571–580.

[125] I. J. Halvorsen, S. Skogestad, I. Dejanovic, L. Matijac, Z. Olujic, Multi-product dividing wall columns: A simple and effective assessment and conceptual design procedure, Chemical Engineering Transactions 25 (2011) 611–616.

[126] J. Stichlmair, Distillation and Rectification, Ullmann's Encyclopedia of Industrial Chemistry, Wiley-VCH, 1988.

[127] A. J. V. Underwood, Fractional distillation of multi-component mixtures, Journal of Chemical Engineering Progress 44 (8) (1948) 603–614.

[128] A. H. 2006, Aspen Engineering Suite (2006).

[129] R. C. v. Diggelen, A. A. Kiss, A. W. Heemink, Comparison of control strategies for dividing-wall columns, Journal of Industrial Engineering and Chemistry Research 49 (2010) 288–307.

[130] J. P. Strandberg, Optimal operation of dividing wall columns, Ph.D. thesis, Norwegian University of Science and Technology, Department of Chemical Engineering (available from homepage of S. Skogestad) (2011).

[131] J. Strandberg, S. Skogestad, Basic control of dividing-wall columns, Conference on Distillation and Absorption (2010).

[132] N. Sotudeh, B. Hashemi Shahraki, A method for the design of divided wall columns, Journal of Chemical Engineering and Technology 30 (9) (2007) 1–9.

[133] V. Alstad, I. J. Halvorsen, S. Skogestad, Optimal operation of petlyuk distillation column: Energy savings by over-fractionating, Journal of Computer Aided Chemical Engineering 18 (2004) 547–552.

[134] M. Abdul Mutalib, R. Smith, Operation and control of dividing wall distillation columns. part 1. degrees of freedom and dynamic simulation, Trans. IChemE Part A (76) (1998) 308–318.

[135] M. Ghadrdan, I. J. Halvorsen, S. Skogestad, Optimal operation of kaibel distillation columns, Journal of Chemical Engineering Research and Design 89 (8) (2011) 1382–1391.

[136] D. Dwivedi, J. Strandberg, I. J. Halvorsen, S. Skogestad, Steady state and dynamic operation of four-product dividing-wall (kaibel) columns: Experimental verification, Journal of Industrial Engineering and Chemistry Research 51 (48) (2012) 15696–15709.

[137] M. Ghadrdan, I. J. Halvorsen, S. Skogestad, A shortcut design for kaibel columns based on minimum energy diagrams, Journal of Computer Aided Chemical Engineering 3 (4) (2011) 571–580.

[138] S. Skogestad, Near-optimal operation by self-optimizing control: from process control to marathon running and business systems, Journal of Computers and Chemical Engineering 29 (1) (2004) 127–137.

[139] M. van de Wal, B. de Gager, A reveiw of methods for input/output selection, Automatica 37 (2001) 487–510.

[140] T. Marlin, A. N. Hrymak, Real-time operations optimization of continuous processes, in: Proceedings of International Conference in Process Control; Tahoe City, Nevada, USA, 1996.

[141] I. J. Halvorsen, S. Skogestad, J. Morud, V. Alstad, Optimal selection of controlled variables, Journal of Industrial Engineering and Chemistry Research 42 (2003) 3273–3284.

[142] V. Alstad, S. Skogestad, Null space method for selecting optimal measurement combinations as controlled variables, Journal of Industrial Engineering and Chemistry Research 46 (3) 846–853.

[143] E. S. Hori, S. Skogestad, A. V., Perfect steady-state indirect control, Journal of Industrial Engineering and Chemistry Research 44 (2005) 863–867.

[144] M. Serra, M. Perrier, A. Espuna, L. Puigjaner, Analysis of different control possibilities for the divided wall column: feedback diagonal and dynamic matrix control, Journal of Computers and Chemical Engineering 25 (2001) 859–866.

[145] C. Buck, C. Hiller, G. Fieg, Decentralized temperature control of a pilot dividing wall column, Journal of Chemical Engineering and Processing: Process Intensification 50 (2) (2011) 167–180.

[146] M. Ghadrdan, I. J. Halvorsen, S. Skogestad, Manipulation of vapour split in kaibel distillation arrangements, Journal of Chemical Engineering and Processing 72 (2013) 10–23.

[147] E. M. B. Aske, S. Skogestad, Consistent inventory control, Journal of Industrial Engineering

and Chemistry Research 48 (24) (2009) 10892–10902.
[148] R. Yelchuru, Quantitative methods for controlled variables selection, Ph.D. thesis, Norwegian University of Science and Technology (2012).
[149] S. Khatibisepehr, B. Huang, S. Khare, Design of inferential sensors in the proess industry: A review of bayesian methods, Journal of Process Control 23 (2013) 1575–1596.
[150] T. Mejdell, S. Skogestad, Estimation of distillation compositions from multiple temperature measurements using partial-least-squares regression, Journal of Industrial Engineering and Chemistry Research 30 (1991a) 2543–2555.
[151] J. Zhang, Inferential feedback control of distillation composition based on PCR and PLS models, American Control Conference.
[152] S. Bhartiya, J. R. Whiteley, Development of inferential measurements using neural networks, ISA Transactions 40 (2001) 307–323.
[153] W. Yan, H. Shao, X. Wang, Soft sensing modeling based on support vector machine and bayesian model selection, Journal of Computers and Chemical Engineering 28 (2004) 1489–1498.
[154] W. F. Massy, Principal component regression in exploratory statistical research, Journal of American Statistical Association 60 (1965) 234–246.
[155] H. Wold, Path Models with Latent Variables: The NIPALS Approach, Academic Press, 1975.
[156] R. Rosipal, N. Kramer, Overview and recent advances in partial least squares, Lecture Notes in Computer Science (2006).
[157] H. Wold, Soft Modelling by Latent Variables; the Nonlinear Iterative Partial Least Squares Approach, Academic Press, London, 1975.
[158] R. Ergon, Noise handling capabilities of multivariate calibration methods, Modeling, identification and control 23 (2002) 259–273.
[159] S. de Jong, SIMPLS: An alternative approach to partial least squares regression, Chemometrics and Intelligent Laboratory Systems 18 (3) (1993) 251–263.
[160] A. Höskuldsson, PLS regression methods, Journal of Chemometrics 2 (1988) 211–228.
[161] P. Kadlec, B. Gabrys, S. Strandt, Data-driven soft sensors in the process industry, Journal of Computers and Chemical Engineering 33 (795-814).
[162] D. Di Ruscio, A weighted view on the partial least-squares algorithm, Automatica 36 (2000) 831–850.
[163] L. Elden, Partial least-squares vs. lanczos bidiagonalization - i: Analysis of a projection method for multiple regression, Computational Statistics & Data Analysis 46 (2004) 11–31.
[164] P. D. Wentzell, V. Montoto, Comparison of principal components regression and partial least squares regression through generic simulations of complex mixtures, Chemometrics and Intelligent Laboratory Systems 65 (2003) 257–279.
[165] B. Joseph, C. B. Brosilow, Inferential control of processes: Part i. steady state analysis and design, AIChE Journal 24 (3) (1978) 485–492.
[166] G. Pannocchia, A. Brambilla, How auxiliary variables and plant data collection affect closed-loop performance of inferential control, Journal of Process Control 17 (2007) 653–663.
[167] S. Tronci, F. Bezzo, M. Barolo, R. Baratti, Geometric observer for a distillation column: Development and experimental testing., Journal of Industrial Engineering and Chemistry Research 44 (2005) 9884–9893.
[168] M. Nakamura, Relationship between steady state kalman filter gain and noise variances, Journal of Systems Science 13 (1982) 1153–1163.
[169] T. Mejdell, S. Skogestad, Output estimation using multiple secondary measurements: High-purity distillation, AIChE Journal 39 (10) (1993) 1641–1653.
[170] R. G. Brown, P. Y. C. Hwang, Introduction to Random Signals and Applied Kalman Filtering, John Wiley & Sons, 1997.
[171] S. Skogestad, R. Yelchuru, J. Jäschke, Optimal use of measurements for control, optimization and estimation using loss method: Summary of existing results and some new (2011).
[172] S. Skogestad, Dynamics and control of distillation columns: A critical survey, Journal of Modeling, Identification and Control 18 (3) (1997) 177–217.
[173] V. Kariwala, Y. Cao, S. Janardhanan, Local self-optimizing control with average loss minimization, Journal of Industrial Engineering and Chemistry Research 47 (4) (2008) 1150–1158.
[174] D. Di Ruscio, The partial least squares algorithm: A truncated cayley-hamilton series approximation used to solve the regression problem, Journal of Modeling, Identification and

Control 19 (3) (1998) 117–140.
[175] N. A. Butler, M. C. Denham, The peculiar shrinkage properties of partial least squares regression, Journal of Royal Statistical Society B 62 (2000) 585–593.
[176] O. C. Lingjæ rde, N. Christophersen, Shrinkage structure of partial least squares, Scandinavian J.ournal of Statistics 27 (2000) 459–473.
[177] I. S. Helland, Some theoretical aspects of partial squares regression, Chemometrics and Intelligent Laboratory Systems 58 (2001) 97–107.
[178] M. Ghadrdan, C. Grimholt, S. Skogestad, A new class of model-based static estimators, Journal of Industrial Engineering and Chemistry Research 52 (35) 12451–12462.
[179] T. Mejdell, Estimators for product composition in distillation columns, Ph.D. thesis, Norwegian University of Science and Technology (1990).
[180] S. Skogestad, Simple analytic rules for model reduction and pid controller tuning, Journal of Process Control 13 (2003) 291–309.
[181] V. Alstad, Studies on selection of controlled variables, Ph.D. thesis, Norwegian University of Science and Technology (2005).
[182] B. Francis, Lecture Notes in Control and Information Sciences: A Course in $H\infty$ Control Theory, Springer-Verlag, 1987.
[183] B. Francis, Notes on $H\infty$ optimal linear feedback systems, Lectures given at Linköping Universtiy, 1983.
[184] E. Kreyszig, Introductory functional analysis with applications, John Wiley & Sons, 1978.
[185] P. Antsaklis, A. Michel, Linear Systems, McGraw-Hill Series in Electrical and Computer Engineering, 1997.
[186] S. Skogestad, Studies on robust control of distillation columns, Ph.D. thesis, California Institute of Technology (1987).
[187] S. J. Julier, J. K. Uhlmann, A new extension of the kalman filter to nonlinear systems, In Proc. of AeroSense: The 11th International Symposium on Aerospace/Defence Sensing, Simulation and Controls.